HEAVY QUARKS AT FIXED TARGET

FRASCATI PHYSICS SERIES

Series Editor
Vincenzo Valente

Technical Editor
Luigina Invidia

Cover illustration based on drawing by *Claudio Federici*

This volume is the first of a new series – the "Frascati Physics Series" – edited and published by the Scientific Information Service (SIS) of the Laboratori Nazionali di Frascati (LNF). The series will include conference proceedings, collections of articles on the Laboratory research activity, and monographs on different subjects. The SIS Publication Office sees to the technical preparation and the distribution of the volumes.

Volume I Anno I

Istituto Nazionale di Fisica Nucleare – Laboratori Nazionali di Frascati
Divisione Ricerca – SIS – Ufficio Pubblicazioni
P.O. Box 13, I–00044 Frascati (Roma) Italy
email: sispub@vaxlnf.lnf.infn.it

WELCOME ADDRESS

Before the meeting starts, let me welcome you to our laboratory and to the First Workshop on Heavy Quarks at Fixed Target. For those of you visiting us for the first time, I would like to give some information about our Laboratory tradition and present and future activities.

The Workshop is taking place at a special time for the Laboratory. A month ago the Adone storage ring was shut down after 25 years of operation. We must go back to the beginning of the '60's, when our Laboratory housed the 1–Gev electrosynchrotron, at that time the second most energetic machine in the world. The construction of the electrosynchrotron was the motivating factor in the birth of the Laboratory. Without a new idea and a new project, the great concentration of skill that the electrosynchrotron had gathered would have been wasted. The new idea came from Bruno Touschek, to make electrons and positrons collide.

This was the time when there were short delays between ideas, projects, and their achievement. Actually, ADA, the first electron–positron accumulation ring (ADA is an Italian acronym for "storage ring") was built in 1961. ADA first worked in Frascati, then it was transported to Orsay. For the first time, beam–beam collisions were obtained and studied at the energy of 250 MeV per beam.

After the success of ADA, at the beginning of 1961, INFN started the design for the construction at LNF of an electron–positron storage ring with 1.5–GeV energy per beam. The construction began in 1963 and the new machine was operational in 1969.

From 1969 to the 26th of April, 1993, when it was finally shut down, ADONE provided beams for 7.5×10^4 hours. Three generations of physicists have worked at ADONE in the fields of subnuclear physics, nuclear physics, and condensed matter.

During the seventies, physicists at ADONE obtained exciting results, among which the discovery of multihadron production,whose ratio with two–muon production provided the first experimental evidence of the color quantum number of hadrons; and the discovery of the ρ' resonance, which was the first evidence of the existence of the vector meson family.

Searches for narrow resonances were made at ADONE by many experimental groups; unfortunately, the J/Ψ mass lay just few MeV's above the maximum allowed energy of ADONE.

After a phone call by S. Ting, however, enthusiasm outweighed prudence: the radiofrequency was pushed to its extreme and the physicists working at Adone

confirmed the J/Ψ discovery. In the following years the community of physicists working at ADONE contributed intensively to the study of the J/Ψ nature until 1979, when the two–beam mode operation was stopped.

During the '80's Adone worked with only one beam circulating, and pursued the use of the nuclear and synchrotron radiation machine facilities already established. Two tagged–photon beams, one obtained via inverse Compton scattering of laser light off ADONE electrons, the other from electron bremsstrahlung on a nitrogen jet target, have allowed the study of photonuclear reactions over a wide energy domain. With the ADONE synchrotron radiation facilities, fundamental studies on condensed matter were performed, together with important applications like mammography and lithography.

In 1990 the two–beam operation was re–established to achieve the first experimental determination of the neutron form factor. The name given to this experiment was FENICE, the mythological Phoenix rising from its own ashes. It is obvious why the experiment was so baptized.

With the shutdown of ADONE now we are not at an end, but rather at a turning point in our Laboratory's scientific history. A new machine, DAΦNE — a high – luminosity ϕ–factory — will be assembled in the same building that housed ADONE.

DAΦNE will be operational starting at beginning of '96. Two experiments have been approved in the two intersection regions of the new machine: the KLOE detector dedicated to the fundamental study of CP and CPT violation in the K meson system and the FINUDA experiment which will study, with high–energy resolution, the physics of hypernuclei.

To the milestones that mark the scientific history of our Laboratory from the electrosynchrotron to ADA, ADONE and DAΦNE, we must add the LEALE linear accelerator, which provided electron and pion beams for nuclear studies, and the Gravitational Wave Experiment NAUTILUS now operating, whose cryogenic antenna has reached the lowest temperature in the world — 100 m°K.

Apart from the activities regarding the on–site machines, our Laboratory has participated and is active in many other experiments at various institutions, at the collider, in underground laboratories, in the sky, and, of course, at fixed target.

The idea of organizing a workshop on fixed target heavy–quarks physics was proposed by some of us in Milan last January, during a meeting of the E687 collaboration. The workshop was defined and formalized in March. Nowadays, a never–ending list of meetings, conferences, congresses, and workshops is offered each

year to us high–energy physicists. However, in this list are often lacking very specialized meetings addressed to a relatively small but well qualified attendance. The format of this meeting, as conceived by the Scientific Committee, is essentially based on invited talks with only a few relevant communications condensed in a short time.

Unfortunately, the scientific aspects do not leave sufficient time for the touristic necessities, as generally conceived nowadays in conference organization.

These are the reasons why this workshop, in spite of the short time available for organizing and calling it, received a very positive response that encourages the idea of making a fixed target meeting a periodical appointment for our community. INFN and Fermilab have assured their sponsorship of the workshop series. The University of Virginia has already presented its candidature for the organization in '94.

I am sure you will find it worthwhile participating in this first fixed target workshop and I hope you will enjoy your stay with us in Frascati, even if it is so short.

Franco L. Fabbri
Director, LNF Research Division

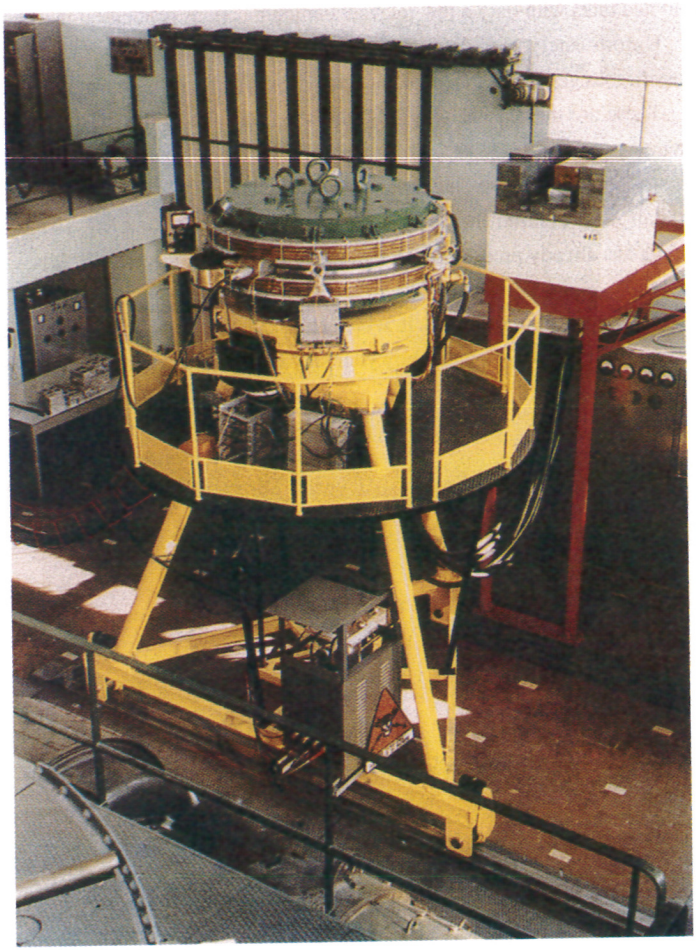

FIG. 1 — The ADA electron–positron storage ring in operation at Frascati in 1961.

FIG. 2 — The ADONE electron–positron storage ring in the '80's.

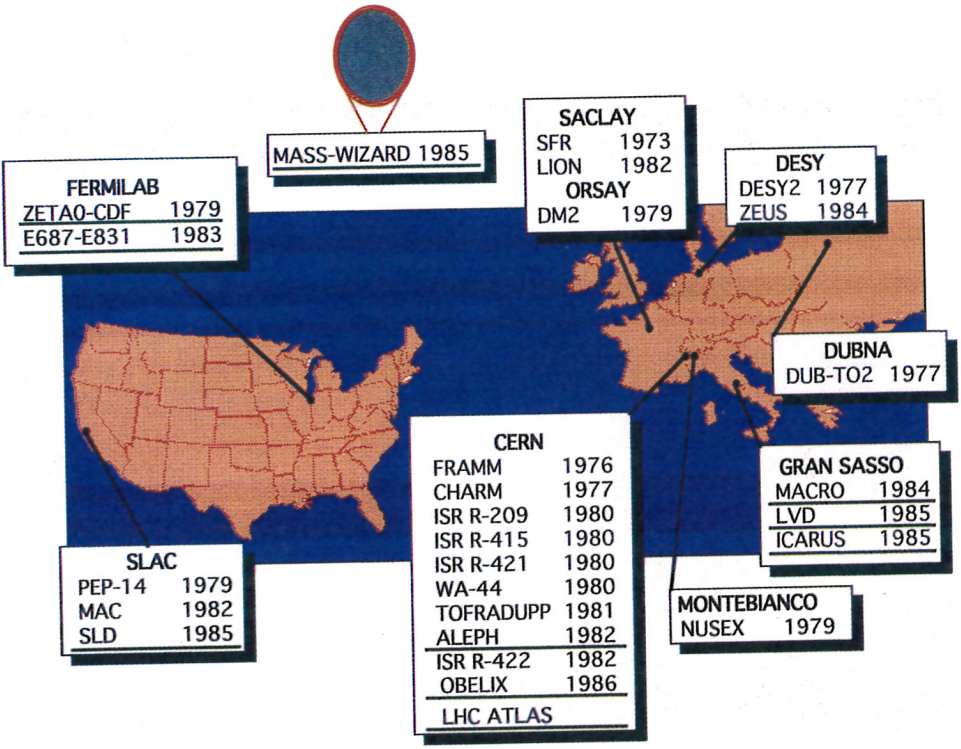

FIG. 3 — Chart showing experiments around the world with participation of groups from LNF. Experiments underlined in red are ongoing.

TABLE of CONTENTS

SESSION I

HEAVY QUARKS AT FIXED TARGET: INTRODUCTORY THEORETICAL CONSIDERATIONS

M. Lusignoli

Università di Roma I, "La Sapienza", Dipartimento di Fisica G. Marconi
Sezione INFN, Piazzale Aldo Moro, 2, I-00185 Roma, (ITALIA)

No written contribution received

Frascati Physics Series, Vol. 1 (1993)
HEAVY QUARKS AT FIXED TARGET
Frascati, May 31st – June 2nd 1993
(pp. 5–18)

CHARMONIUM FORMATION AT FIXED TARGET

D. Bettoni
Università di Ferrara, Dipartimento di Fisica,
Via Paradiso 12, I-44100 Ferrara, (ITALIA)

for the E760 Collaboration[19]

Abstract

In this paper we review recent results on charmonium spectroscopy in proton-antiproton interactions.

1 Introduction

The charmonium system was discovered in 1974, when two experimental groups at SLAC and Brookhaven announced almost simultaneously the observation of a new narrow resonance, called J/ψ [1]. This was followed very shortly by the discovery by the SLAC group of another narrow state, which was called ψ' [2]. These two resonances were interpreted as bound states of a new quark, called charm or c quark, and its antiquark ($\bar{c}$), whose existence had been predicted several years before to account for the non-existence of strangeness changing neutral currents [3]. The high mass of the c quark ($m_c \sim 1.5 GeV/c^2$) makes it plausible to attempt a description of the dynamical properties of the ($c\bar{c}$) system in terms of non-relativistic potential models, in which the functional form of the potential is chosen to reproduce the asymptotic properties of the strong interaction. The free parameters in these models are determined from a comparison with the experimental data. The study of the charmonium (and bottomonium) spectrum is thus thought to be a powerful tool for the understanding of the strong interaction and this is the reason why this system has often been called *the hydrogen atom of QCD.*

Experimentally a large amount of data on the charmonium spectrum came originally from e^+e^- experiments. In this kind of experiment only the states with the quantum numbers of the photon, $J^{PC} = 1^{--}$, namely the J/ψ and the ψ', can be formed directly. The parameters of these resonances

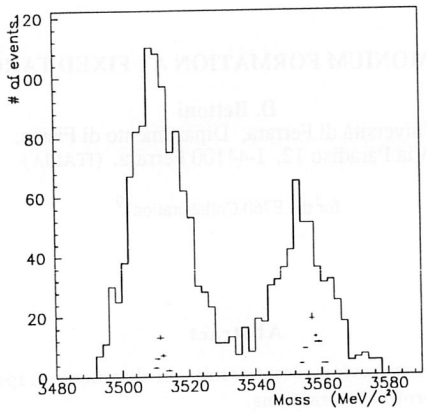

Figure 1: χ_1 and χ_2 data from R704 (points) and e^+e^- (solid line)

(masses and widths) have been measured very accurately by the e^+e^- experiments, because the initial state was known with good precision. All other states have been studied by measuring the inclusive photon spectrum from the radiative decay of the ψ' (e.g. $\psi' \to \chi + \gamma$); in this case the measurement of masses and widths is limited by the resolution of the detector and is therefore far less accurate.

On the other hand, all $(c\bar{c})$ states can be directly formed in $\bar{p}p$ annihilations, through the coherent annihilation of the three quarks of the proton and the three antiquarks of the antiproton. This makes the direct study of the χ_c states and the search for previously unobserved states, such as the $h_c(^1P_1)$, possible. This technique, proposed in 1979 [4], was first exploited at the CERN ISR by experiment R704, which took data for a few months before the ring was eventually shut down in 1984. The experiment used the $\bar{p}$ beam from the ISR and an internal gas jet target and identified the charmonium states via their electromagnetic decays. As an example, we show in fig. 1 a comparison between the χ_1 and χ_2 data from R704 (identified from $\chi \to J/\psi + \gamma$) and from an e^+e^- experiment. The (low statistics) ISR data yielded a measurement of the total width for these states far better than the (high statistics) e^+e^- data [5]. In spite of the limited running time, R704 was very successful in proving the feasibility of the technique and in setting

the stage for its successor, E760 at Fermilab, to which the remainder of this review will be devoted.

2 The E760 Experiment

The resonant formation of charmonium states in $\overline{p}p$ annihilations has been studied at Fermilab by the E760 experiment, which has completed a five month data taking period in January 1992. A high-luminosity, nearly point-like annihilation source was obtained by intersecting the $\overline{p}$ beam circulating in the Fermilab antiproton accumulator (up to 4×10^{11} antiprotons) with a hydrogen gas jet target. With this arrangement peak luminosities up to $8 \times 10^{30} cm^{-2} s^{-1}$ have been reached. This experiment has represented a substantial improvement over its predecessor in beam quality, luminosity and detector equipment.

2.1 Experimental Method

The cross section for the process:

$$\overline{p}p \rightarrow (\overline{c}c) \rightarrow \text{final state} \tag{1}$$

is given by the well known Breit-Wigner formula:

$$\sigma_{BW}(E) = \frac{2J+1}{4} \frac{\pi}{k^2} \frac{B_{in} B_{out} \Gamma_R^2}{(E - M_R)^2 + \Gamma_R^2/4} \tag{2}$$

where E and k are the center of mass (c.m.) energy and momentum; J, M_R and Γ_R are the resonance spin, mass and total width and B_{in} and B_{out} are the branching ratios into the initial ($\overline{p}p$) and final states. Due to the finite energy spread of the beam, the measured cross section is a convolution of the Breit-Wigner cross section eq.(2) and the beam energy distribution function $f(E, \Delta E_B)$; the effective production rate ν is given by:

$$\nu = L_0 \left\{ \epsilon \int dE f(E, \Delta E_B) \sigma_{BW}(E) + \sigma_b \right\} \tag{3}$$

where L_0 is the instanteneous luminosity, ϵ an overall efficiency $\times$ acceptance factor and σ_b a background term.

The parameters of a given resonance can be extracted by measuring the formation rate for that resonance as a function of the c.m. energy E. In the experimental arrangement of E760, where the $\overline{p}$ beam collides with an

effectively stationary target, the c.m. energy depends only on the beam energy E_B. An accurate determination of masses and widths depends then crucially on the precise knowledge of the absolute energy scale and on the beam energy spectrum.

The beam energy can be determined by measuring the $\overline{p}$ revolution frequency in the accumulator and the orbit length. As the frequency can be measured to a very good precision (1 part in 10^7), the error on the beam energy is dominated by the error on the orbit length. Conventional surveying techniques do not yield the necessary precision to improve on the existing mass measurements, thus it was decided to calibrate the beam energy by performing an energy scan at the ψ', whose mass is known to ± 100 keV from e^+e^- experiments [6]. This corresponds to an error in the orbit length $\Delta L = \pm 0.67mm$, and this in turn translates into an error in the mass measurements of $\pm 33keV$ at the J/ψ and ± 80 keV at the χ states.

The beam momentum spectrum was determined by E760 using a technique, called double scan, which gave a very precise measurement of the beam energy spread, thus allowing the collaboration to obtain the first direct measurement of the total width of the ψ' and even the J/ψ. A detailed description of the double scan technique can be found in [7].

Essential to the success of the experiment is the stochastic cooling system, which keeps the momentum spread of the beam at $\Delta p/p \sim 2 \times 10^{-4}$, thus allowing the measurement of resonance widths in the sub-MeV region.

2.2 The E760 Detector

At the formation energies of charmonium the $\overline{p}p$ total cross section is several orders of magnitude larger than the formation cross sections of the $\overline{c}c$ resonances, which makes it impractical to extract a signal searching for the hadronic decay modes of the charmonium states. A much better signal to noise ratio can be obtained by looking at electromagnetic decay modes such as $\chi_{1,2} \rightarrow J/\psi\gamma \rightarrow e^+e^-\gamma$ or $\chi_2 \rightarrow \gamma\gamma$. For this reason the E760 detector has been designed to detect final states containing electrons and photons.

E760 is a non magnetic spectrometer with full azimuthal (ϕ) coverage and polar angle acceptance $2° < \theta < 70°$. The central detector ($12° < \theta < 70°$) has cylindrical symmetry around the beam axis and consists of scintillator hodoscopes, wire chambers, a threshold Čerenkov counter for e/π

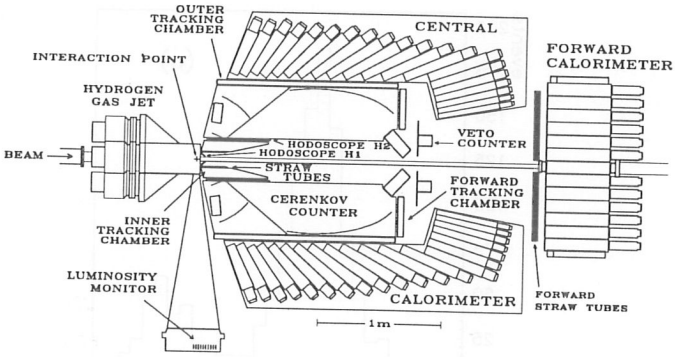

Figure 2: The E760 detector

separation and a very finely segmented lead-glass calorimeter. The forward region (down to $\theta = 2°$) is instrumented with a scintillator hodoscope, a straw-tube drift chamber and a calorimeter consisting of 144 lead/scintillator sandwich towers. An absolute measurement of the luminosity is provided by a silicon detector at 86.5° to the $\overline{p}$ beam direction, measuring the yield of elastic recoil protons. A detailed description of the detector and its performance can be found in [8, 9]

3 Charmonium decays to $J/\psi + X$

3.1 Masses and widths of χ_1, χ_2, J/ψ and ψ'

The technique described in the previous section has been used by E760 to study the $c\bar{c}$ resonance parameters via the formation processes:

$$\overline{p}p \to J/\psi \to e^+e^- \tag{4}$$

$$\overline{p}p \to \psi' \to e^+e^- \tag{5}$$

$$\overline{p}p \to \psi' \to J/\psi + X \to e^+e^- + X \tag{6}$$

$$\overline{p}p \to \chi_{1,2} \to J/\psi + \gamma \to e^+e^- + \gamma \tag{7}$$

These processes are tagged by the decay of the J/ψ to e^+e^- and are characterized by a high-mass e^+e^- pair in the final state. Fig. 3 shows the reconstructed invariant mass of identified e^+e^- pairs for data taken at the formation energy of the ψ'. The large peak centered on the J/ψ mass is due

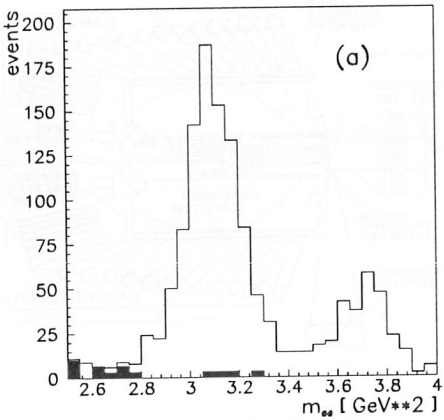

Figure 3: e^+e^- invariant mass spectrum (ψ' scan)

Table 1: χ_1, χ_2, J/ψ and ψ' parameters

	Mass (MeV)	Width (MeV)	BR to $p\bar{p} \times 10^4$
χ_1	$3510.53 \pm 0.04 \pm 0.12$	$0.88 \pm 0.11 \pm 0.08$	$0.78 \pm 0.10 \pm 0.11$
χ_2	$3556.15 \pm 0.07 \pm 0.12$	$1.98 \pm 0.17 \pm 0.07$	$0.91 \pm 0.08 \pm 0.14$
ψ	$3096.87 \pm 0.03 \pm 0.03$	$0.099 \pm 0.012 \pm 0.006$	$18.2^{+2.6}_{-1.9} \pm 1.6 \pm 0.6$
ψ'	$3686.0(input)$	$0.306 \pm 0.036 \pm 0.016$	$2.61^{+0.31}_{-0.27} \pm 0.17 \pm 0.17$

to events from reaction (6), whereas the smaller peak on the right, centered on the ψ' mass, arises from the direct decay of the ψ' to e^+e^-. The shaded area in the histogram represents an estimation of the background, performed by applying the same analysis to a sample of data taken off-resonance; it can be seen that the background contamination is extremely low (less than 5%).

Fig. 4 shows the measured formation cross section as a function of the center-of-mass energy for the χ_1 and χ_2 states. By fitting this data to the convolution of a Breit-Wigner with a Gaussian (representing the beam energy spectrum, see eq. (3)) one can extract, for each resonance, the value of the mass, total width and product of branching ratios into the initial and final states. The results obtained by E760 [7, 8, 9] are reported in table 1. The values of the branching ratios to $\bar{p}p$ have been determined by using the

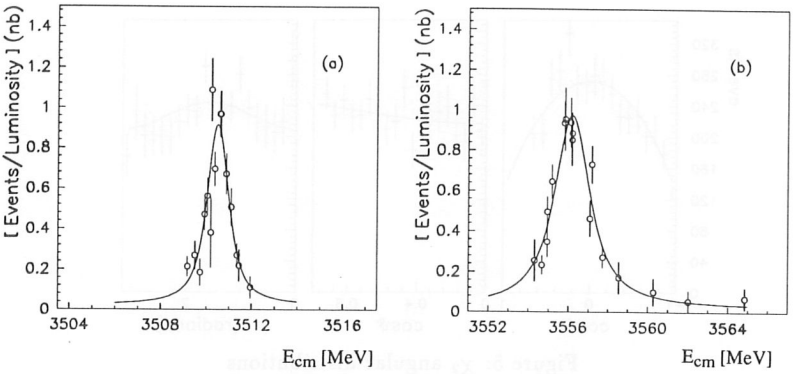

Figure 4: Measured cross section for χ_1 (a) and χ_2 (b) resonance formation

published values of the branching ratios into the final states [6]. All these measurements represent substantial improvements over previous world averages; in some cases (χ_1 total width and decay rate to $\overline{p}p$) only upper limits existed before the E760 results became available. It should also be noted that the very good determination of the beam shape has allowed E760 to produce the first determination, based on line shape analysis, of the total width for the narrow states J/ψ and ψ' [7].

3.2 Angular distributions in the radiative decay of the χ_2

The angular distributions for the process:

$$\overline{p}p \rightarrow \chi_2 \rightarrow J/\psi + \gamma \rightarrow e^+e^- + \gamma \qquad (8)$$

are sensitive to the helicity amplitudes in the formation process, to the properties of the $c\bar{c}$ bound state and to the multipole structure of the radiative decay. The angular distributions for reaction (8) are determined by three independent parameters, which are conventionally chosen to be: B_0^2, the helicity zero amplitude in the formation process, a_2 and a_3, the quadrupole and octupole amplitudes for the decay channel.

Using a sample of $\sim$ 2000 χ_2 decays E760 has carried out an angular distribution analysis for process (8). The angular distribution is a function of three angles: θ, the polar angle of the J/ψ with respect to antiproton in the c.m. system; θ' and ϕ', the polar and azimuthal angles of the positron in the J/ψ rest frame. Fig. 5 shows the E760 data on one-dimensional plots in

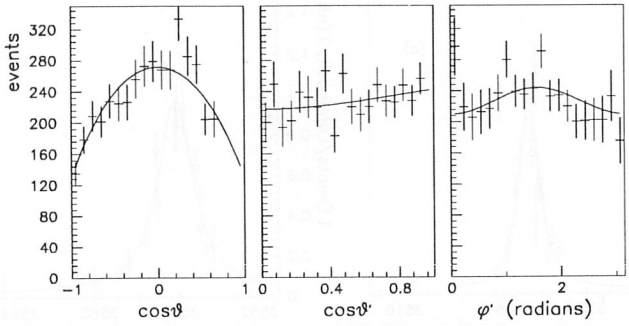

Figure 5: χ_2 angular distributions

$\cos\theta$, $\cos\theta'$ and ϕ', together with the best fit (solid line).

The E760 results for B_0^2, a_2 and a_3 are:

$$a_2 = -0.14^{+0.08}_{-0.07} \tag{9}$$

$$a_3 = 0.00^{+0.06}_{-0.05} \tag{10}$$

$$B_0^2 = 0.05^{+0.14}_{-0.13} \tag{11}$$

These measurements significantly improve the experimental knowledge of the angular distribution parameters. The statistical errors on a_2 and a_3 are reduced by a factor of 5 with respect to previous measurements. The result for B_0^2 is strong evidence that the contribution of helicity zero in the formation process is small. The measured value of a_2 is consistent with a vanishing anomalous magnetic moment of the c quark.

3.3 The $^1P_1$ state of charmonium

The $^1P_1$ state of charmonium (h_c) is of particular importance, because a comparison of its mass with the mass of the χ states is a measurement of the deviation of the vector part of the $c\bar{c}$ interaction from pure *one gluon exchange*. The $^1P_1$ has quantum numbers $J^{PC} = 1^{+-}$; its mass is predicted to be within a few MeV of the center of gravity of the χ states defined as:

$$m_{cog} = \frac{m(\chi_0) + 5m(\chi_1) + 9m(\chi_2)}{9} = (3525.27 \pm 0.12)MeV \tag{12}$$

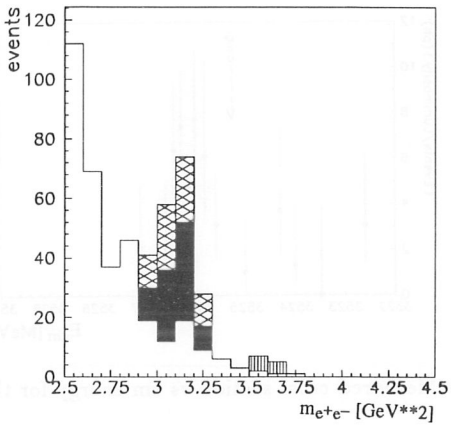

Figure 6: e^+e^- invariant mass distribution ($^1P_1$ scan)

Its width is expected to be small ($\leq 1MeV$). E760 has searched for this state in the following channels:

$$^1P_1 \rightarrow \eta_c + \gamma \rightarrow \gamma\gamma + \gamma \tag{13}$$

$$^1P_1 \rightarrow J/\psi + \pi^0 \rightarrow e^+e^- + \pi^0 \tag{14}$$

$$^1P_1 \rightarrow J/\psi + \pi\pi \rightarrow e^+e^- + \pi\pi \tag{15}$$

The dominant decay mode is expected to be $\eta_c + \gamma$, but the small branching ratio $\eta_c \rightarrow \gamma\gamma$ strongly suppresses the 3γ final state and makes its rate comparable to (14) and (15). The branching ratios for the decays (14) and (15) are expected to be small, because (14) does not conserve isospin and (15) is suppressed by phase space and angular momentum barrier effects. E760 confined its search for the $^1P_1$ to the immediate vicinity of the χ states center of gravity and took data in small energy steps to allow observation of a narrow resonance.

The data analysis relative to the $\eta_c\gamma$ decay mode is still in progress, so we will limit our discussion to the decays (14) and (15). The e^+e^- invariant mass distribution for all data taken during the $^1P_1$ scan is shown in fig. 6, in which the peak due to events of the type $\overline{p}p \rightarrow J/\psi + X$ is clear. The shaded areas in the histogram represent events which could be kinematically fitted to

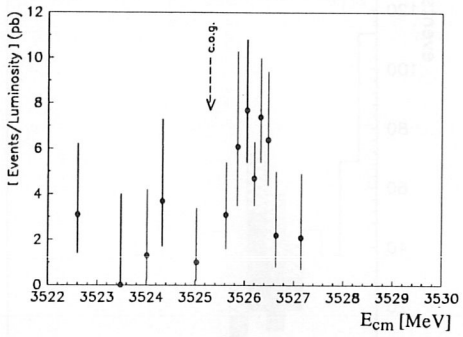

Figure 7: Measured cross section vs cm energy for the ${}^1P_1$ scan

$J/\psi + \pi^0$ (black solid), $J/\psi + \gamma$ (cross hatched) and e^+e^- (vertical stripes). The residual events in the J/ψ region are compatible with the expected background. No events were found which could be fitted to reaction (15). The $J/\psi + \gamma$ events were attributed to the tails of the nearby χ_1 and χ_2 states, and the e^+e^- events were used to measure the proton electromagnetic form factor in the time-like region [12].

The results for the $J/\psi + \pi^0$ channel are shown in fig. 7. The uniform level below m_{cog} is consistent with a prediction for the continuum production $\overline{p}p \rightarrow J/\psi + \pi^0$ [13]. The data above m_{cog} show a consistently higher cross section and could be fitted to the convolution of a Breit-Wigner resonance shape with the known beam energy distribution function (with a constant background term added). These data represent the first evidence of the ${}^1P_1$ state of charmonium, with a mass of $3526 \pm 0.15 \pm 0.2 MeV$. Because of the low statistics, E760 could only set an upper limit on the resonance width of $\Gamma_R \leq 1.1 MeV$ at the 90 % confidence level [11].

4 Charmonium decays to $\gamma\gamma$

A detector like E760, with excellent calorimetry, is ideally suited for the study of the decays of the C-even charmonium states to two photons through the process:

$$\overline{p}p \rightarrow (\overline{c}c) \rightarrow \gamma\gamma \qquad (16)$$

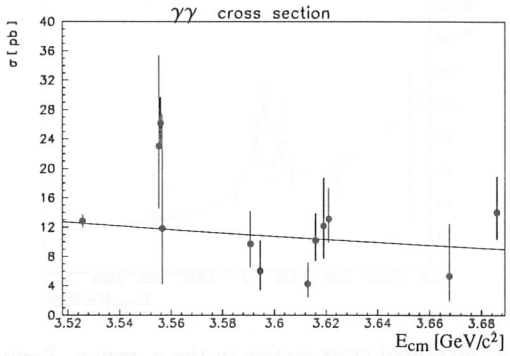

Figure 8: Measured $\gamma\gamma$ cross section

It should be pointed out that the study of these reactions is difficult, because the decay rates to $\gamma\gamma$ are small and the backgrounds from the hadronic production of π^0 and η are very large. The measured $\gamma\gamma$ cross section for all data taken at $\sqrt{s} > 3.5\ GeV$ is shown in fig. 8. The only high point in this figure corresponds to the formation of the χ_2 state and its subsequent decay to $\gamma\gamma$. From these data the E760 collaboration has extracted the value of the partial decay width [14]:

$$\Gamma(\chi_2 \to \gamma\gamma) = 321 \pm 78 \pm 54\ eV \tag{17}$$

This result, which, is in agreement with the upper limit of 1 keV reported by the CLEO collaboration [15], represents the most precise measurement of this quantity to date.

E760 has also carried out a preliminary scan in the η_c region. Background rejection is a severe problem at these lower energies. The results of a preliminary analysis of the E760 data are shown in fig. 9. When completed, this analysis will yield a $\sim$ 30 % measurement of the branching fraction $\eta_c \to \gamma\gamma$ and an even less precise measurement of the total width.

E760 also performed a limited search for the η_c' resonance in the interval $\sqrt{s} = 3595 - 3621 MeV$. The data, shown in fig. 8, present no evidence of a signal. Based on this negative result and assuming a total width of 5 MeV one can set upper limits [16] on the product $BR(\eta_c' \to \overline{p}p) \times BR(\eta_c \to \gamma\gamma)$ of 8×10^{-8} for $3588 < \sqrt{s} < 3598$ and $3608 < \sqrt{s} < 3623$, and of 3×10^{-8} for $3592 < \sqrt{s} < 3596$. A previous claim for the η_c' resonance [17] remains

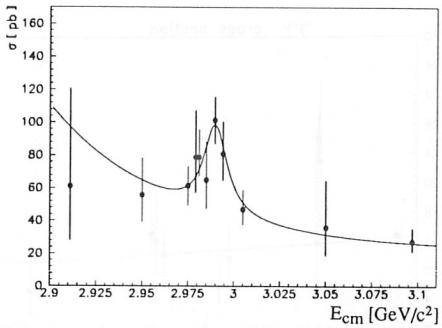

Figure 9: Measured cross section in the η_c region. Preliminary

thus unconfirmed. This negative result, however, is of limited statistical significance, because the scan has not been completed.

5 Conclusions

The use of $\overline{p}p$ annihilations has led to a significant progress in the knowledge of the charmonium system. This has been shown by R704 at the CERN ISR, which pioneered the technique, and by E760 at Fermilab, which has produced a wealth of new and exciting measurements, including the observation of the $^1P_1$, which had so far escaped detection. Despite this progress there is still a lot to be done, and for this reason the E760 detector is being upgraded and will take data as experiment E835 during the next Fermilab fixed target run, which at present is expected to start in late 1995. The plan is to increase the instantenous luminosity by a factor of about five and to collect data for $\sim 200pb^{-1}$. The physics program of E835 includes a high statistics study of the $^1P_1$, a new scan of the η_c (adding the $\phi\phi$ decay mode to the $\gamma\gamma$ channel), a search for the η_c', a scan at the χ_0 and a search for the D states [18].

References

[1] J.E. Augustin et al., Phys. Rev. Lett. **33**,1406(1974).
J.J. Aubert et al., Phys. Rev. Lett. **33**,1404(1974).

[2] G.S. Abrams et al., Phys. Rev. Lett. **33**,1453(1974).

[3] S.L. Glashow, J.Iliopoulos, L.Maiani, Phys. Rev. **D2**,1285(1970).

[4] P.Dalpiaz, Proceedings of the first LEAR workshop, Karlsruhe, Germany, edited by H. Poth (1979).

[5] C.Baglin et al., Phys. Lett. **B 172**,455(1986).

[6] Particle Data Group, K.Hikasa et al., Phys. Rev. **D 45**,S1(1992).

[7] T.A.Armstrong et al., Phys. Rev. **D 47**,772(1993).

[8] T.A.Armstrong et al., Phys. Rev. Lett. **68**,1468(1992).

[9] T.A.Armstrong et al., Nucl. Phys., **B 373**,35(1992).

[10] T.A.Armstrong et al., Fermilab-Pub-93/037-E, February 1993, to be published in Phys. Rev. D.

[11] T.A.Armstrong et al., Phys. Rev. Lett. **69**,2337(1992).

[12] T.A.Armstrong et al., Phys. Rev. Lett., **70**,1212(1993).

[13] M.K.Gaillard et al., Phys. Lett., **110 B**,489(1992).

[14] T.A.Armstrong et al., Phys. Rev. Lett., **70**,2988,(1993).

[15] W.Chen et al., Phys. Lett. **B 243**,169(1990).

[16] James E. Fast, Ph.D. thesis, University of California, Irvine, 1992.

[17] C.Edwards et al., Phys. Rev. Lett. **48**,70(1982).

[18] Proposal to extend E760 activities in the next fixed target run (E760 Collaboration) Fermilab Proposal P835.

[19] T.A.Armstrong[6], D. Bettoni[2], V. Bharadwaj[1], C. Biino[7], G. Borreani[2], D. Broemmelsiek[4], A. Buzzo[3], R. Calabrese[2], A. Ceccucci[7], R. Cester[7], M. Church[1], P. Dalpiaz[2], P.F. Dalpiaz[2], R. Dibenedetto[7], D. Dimitroyannis[5], M.G. Fabbri[2], J. Fast[4], A. Gianoli[2], C.M. Ginsburg[5], K. Gollwitzer[4], A. Hahn[1], M. Hasan[6], S. Hsueh[1], R. Lewis[6], E. Luppi[2],

M. Macrí[3], A.M. Majewska[6], M. Mandelkern[4], F. Marchetto[7], M. Marinelli[3], J. Marques[4], W. Marsh[1], M. Martini[2], M. Masuzawa[5], E. Menichetti[7], A. Migliori[7], R. Mussa[7], M. Pallavicini[3], S. Palestini[7], N. Pastrone[7], C. Patrignani[3], J. Peoples Jr.[1], L. Pesando[7], F. Petrucci[2], M.G. Pia[3], S. Pordes[1], P. Rapidis[1], R. Ray[5,1], J. Reid[6], G. Rinaudo[7], B. Roccuzzo[7], J. Rosen[5], A. Santroni[3], M. Sarmiento[5], M. Savrie'[2], A. Scalisi[3], J. Schultz[4], K.K. Seth[5], A. Smith[4], G.A. Smith[6], M. Sozzi[7], S. Trokenheim[5], M.F. Weber[4], S. Werkema[1], Y. Zhang[6], J. Zhao[5], G. Zioulas[4].

[1] *Fermi National Accelerator Laboratory, Batavia, Illinois 60510, U.S.A.*

[2] *I.N.F.N. and University of Ferrara, 44100 Ferrara, Italy*

[3] *I.N.F.N. and University of Genoa, 16146 Genoa, Italy*

[4] *University of California at Irvine, California 92717, U.S.A.*

[5] *Northwestern University, Evanston, Illinois 60208, U.S.A.*

[6] *Pennsylvania State University, University Park, Pennsylvania 16802, U.S.A.*

[7] *I.N.F.N. and University of Turin, 10125 Turin, Italy.*

Frascati Physics Series, Vol. 1 (1993)
HEAVY QUARKS AT FIXED TARGET
Frascati, May 31st – June 2nd 1993
(pp. 19–28)

RECENT RESULTS ON CHARMONIUM PRODUCTION AT HIGH ENERGY

S. Conetti
University of Virginia, Institute of Nuclear and Particle Physics
McCormick Road, Charlottesville VA 22901, (USA)

for the E705 Collaboration*

Abstract

Twenty years after the observation of charmonium production in proton-nucleus interactions, a consistent picture of the mechanism for the formation of a $c\bar{c}$ bound state is still missing. Recent results from Fermilab experiment E-705 address such a question and also provide some evidence for the possible observation of new states of charmonium.

1 Models of J/ψ production.

The, now historical, observation[1] of a sharp resonance, at a mass of 3.1 GeV/c^2, in both e^+e^- annihilations and proton-nucleus interactions, shortly after interpreted[2] as the formation of a bound charm-anticharm quark pair, led to a considerable amount of speculation about the exact mechanism responsible for the hadronic production of "charmonium". A quick overview[3]

*L.Antoniazzi,M.Arenton,Z.Cao,T.Chen,S.Conetti,G.Corti,B.Cox,S.Delchamps, L.Fortney,K.Guffey,M.Haire,P.Ioannou,C.M.Jenkins,D.Judd,C.Kourkoumelis, A.Manousakis,J.Kuzminski,T.LeCompte,A.Marchionni,M.He,P.O.Mazur,C.T.Murphy, P.Pramantiotis,R.Rameika,L.K.Resvanis,M.Rosati,J.Rosen,C.Shen,Q.Shen,A.Simard, R.P.Smith,L.Spiegel,D.G.Stairs,Y.Tan,R.Tesarek,T.Turkington,L.Turnbull,F.Turkot, S.Tzamarias,G.Voulgaris,D.E.Wagoner,C.Wang,W.Yang,N.Yao,N.Zhang,X.Zhang, G.Zioulas,B.Zou Athens-Duke-Fermilab-McGill-Nanjing-Northwestern-PrairieView-Shandong-Virginia.

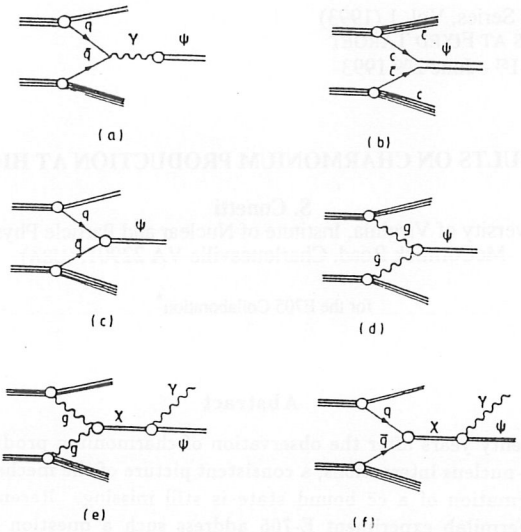

Figure 1: Parton diagrams of charmonium production mechanisms

of the theoretical developments is contained in Fig.1, where various postulated mechanisms for the production of J/ψ and other charmonium states are presented in the form of QCD parton diagrams. Starting from Fig. 1a, the early hypothesis seeing the J/ψ as produced by a Drell-Yan-like process was soon discarded, since many of its predictions (unequal production by π^+ vs. π^-, shape of the angular distribution, etc.) were disproved by the experimental results. Another suggestion is shown in Fig. 1b, where the charmonium is being produced by the $c\bar{c}$ quarks from the sea. Such a model, introduced in part to explain the relatively copious J/ψ production in proton-nucleon reactions, where no valence antiquarks are present, was soon abandoned since it predicted that charmonium should be produced in conjunction with a further $D\overline{D}$ pair, a fact not borne out by experimental observation.

The process of Fig. 1c, the direct annihilation of a $q\bar{q}$ pair, could obviously

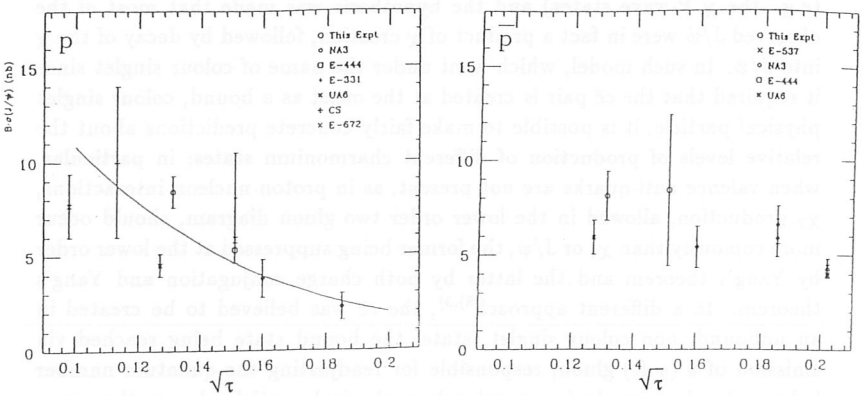

Figure 2: σ x BR for $J/\psi \rightarrow \mu\mu$, proton and antiproton beams.

be expected to be relevant, but its relative importance can be assessed by comparing the cross-section for J/ψ production by protons vs. antiprotons. The most recent results for such a comparison are from Fermilab E-705[4], which took data with 300 Gev/c $\pi^{\pm}$, p and $\overline{p}$ on a ^{7}Li target. The results are shown in Fig. 2a,b[5] as a function of energy (or, more specifically, of the scaling variable $\sqrt{\tau} = M_{\psi}/\sqrt{s}$). It can be seen that, while at lower energies the J/ψ production is in fact smaller for protons than for antiprotons, as the energy increases the difference between the two decreases, indicating that processes other than $q\overline{q}$ annihilation become dominant.

After these first unsuccesful attempts at describing J/ψ hadroproduction, it became clear, in line with the refining of QCD, that gluons should play a major part in the process of charmonium production. The introduction of gluons nevertheless opened a whole new set of questions. Fig. 1d shows what would be the lowest order process of J/ψ production via gluon fusion, but it was recognized very early that such a process is forbidden because of charge-conjugation (which is negative for the J/ψ and positive for a two gluon system). Moreover, a theorem attributed to Yang[6] disallows the transition from a symmetric state of two spin 1 particles to an odd-spin state. Such a realization led to the formation of two major schools of thought describing the process of charmonium creation: on the one side, it was recognized[7),3)] that the above selection rules do not apply to different states of charmonium

(e.g. the χ P-wave states) and the hypothesis was made that most of the observed J/ψ were in fact a product of χ creation, followed by decay of the χ into J/ψ. In such model, which went under the name of colour singlet since it required that the $c\bar{c}$ pair is created at the onset as a bound, colour singlet physical particle, it is possible to make fairly concrete predictions about the relative levels of production of different charmonium states; in particular, when valence anti-quarks are not present, as in proton-nucleon interactions, χ_2 production, allowed in the lower order two gluon diagram, should occur more copiously than χ_1 or J/ψ, the former being suppressed at the lower order by Yang's theorem and the latter by both charge conjugation and Yang's theorem. In a different approach[8),3)], the $c\bar{c}$ was believed to be created in an unbound, non colour singlet, state, the bound state being reached via emission of a (soft) gluon, responsible for readjusting the quantum number balance (and so producing a colourless physical particle, hence the name of "colour bleaching" or "colour evaporation" for such a class of models). In this approach, all charmonium states could be thought as occurring at comparable levels (or possibly in the ratio of their 2J+1 states, suggesting e.g. a 1:3:5 production ratio for the three χ states).

In spite of the outstanding lack of knowledge of the production mechanism(s), it has been customary to analyze the J/ψ x_F differential cross sections to extract the gluon structure function in a model dependent way (typically under the simplifying assumption that J/ψ production is dominated by two gluon fusion). As an example, a recent study[9]) was performed by Fermilab E-789, a high rate experiment that measured J/ψ production by 800 Gev/c protons for very large values of x_F. Fig. 3 shows the data together with the estimated contributions due to gluon fusion (seemingly not enough to reproduce the highest x_F data points) as well as the contributions of $q\bar{q}$ annihilation, the antiquark being originated from the sea. In the same spirit of trying to disentangle glue-glue vs. quark-antiquark contributions, Fig. 4a,b show the E-705 comparison of $d\sigma/dx_F$ for π^+ vs. π^- or π vs. proton respectively. As it should be, the ratio of π^+/π^- is consistent with unity over the whole measured range (E-705 was run with positive and negative beams over a ^{7}Li target, a quasi-isoscalar), while the pion over proton comparison shows a relative increase in the pion cross-section at large x_F, a possible indication of contributions from $q\bar{q}$ annihilations.

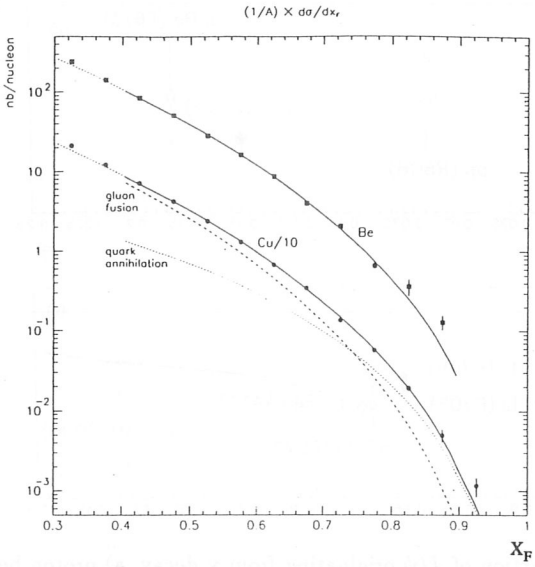

Figure 3: E789 $d\sigma/dx_F$ for J/ψ production by 800 GeV/c protons.

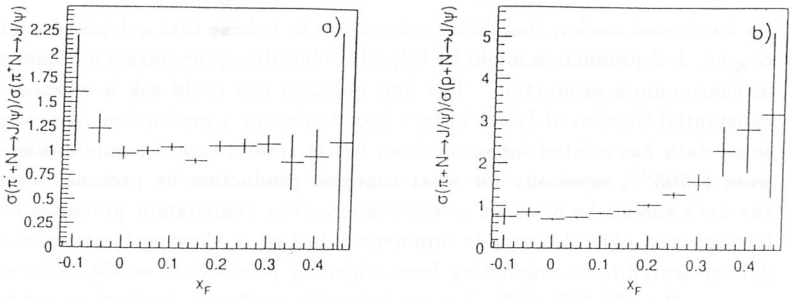

Figure 4: Comparison of x_F differential cross-section. a) π^-/π^+ b)π/p

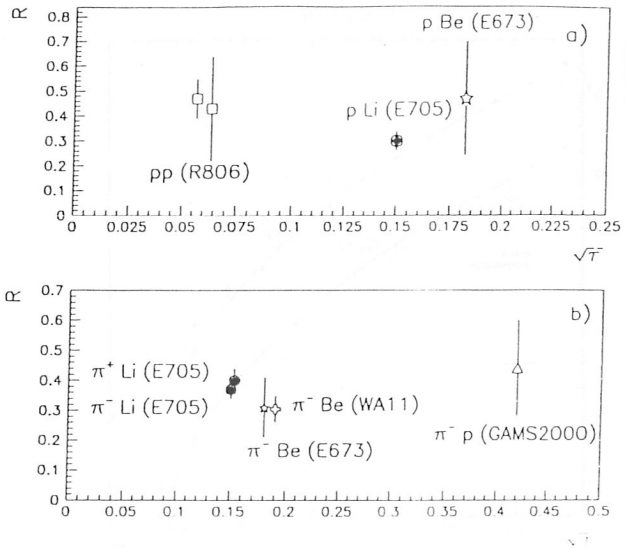

Figure 5: Fraction of J/ψ originating from χ decay. a) proton beam b) pion beam

2 Production of χ states

As mentioned earlier, there are good reasons to believe that a detailed study of χ vs. J/ψ production might be helpful in identifying the correct mechanism of charmonium production. The first question one could ask is whether a substantial fraction of J/ψ is in fact due to primary χ production. Although some data has existed for some time, better results have become available from E-705[10], especially for what concerns production by protons, where the data should be of easier interpretation since annihilation processes can be neglected. The situation is summarized in Fig. 5, showing the fraction of J/ψ measured to be originating from original χ production: as Fig. 5 shows, no more than 30-40% of the J/ψ are indirectly produced , leaving room for a large contribution due to direct production. Even more to the point, E-705 estimated the actual cross-section for direct J/ψ production (i.e. removing contributions due to χ as well as to ψ' decays) with the results:[10]

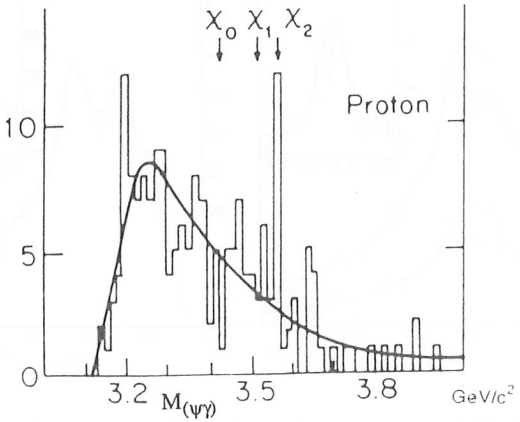

Figure 6: $J/\psi - \gamma$ mass spectrum from E673 proton data

$$\sigma(\pi^+ N \to J/\psi + x) = 97. \pm 14. nb/nucleon$$

$$\sigma(\pi^- N \to J/\psi + x) = 102. \pm 14. nb/nucleon$$

$$\sigma(pN \to J/\psi + x) = 89. \pm 12. nb/nucleon,$$

to be compared with cross sections for χ_1 and χ_2 productions of 131.±23. and 188.±36. nb/nucleon respectively. In other words, direct J/ψ production, even in the absence of annihilation processes, takes place at roughly the same level as χ production, favouring the interpretation suggested by the colour evaporation model. As a consequence, one would be led to expect that χ_1 production by proton should follow the same trend. Unluckily the existing data, albeit limited in statistics, seem to contradict such a simple deduction. An early experiment[11] had hinted at a lack of χ_1 production by proton (Fig.6) and recent results from E-705[12] seem to confirm such an observation. Fig. 7 shows the, statistically resolved, χ_1 and χ_2 signals for pion and proton production respectively: while the two states seem to be produced in comparable amounts by pions, only χ_2 production seem to be present for the proton beam. While waiting for a confirmation[13], the present result

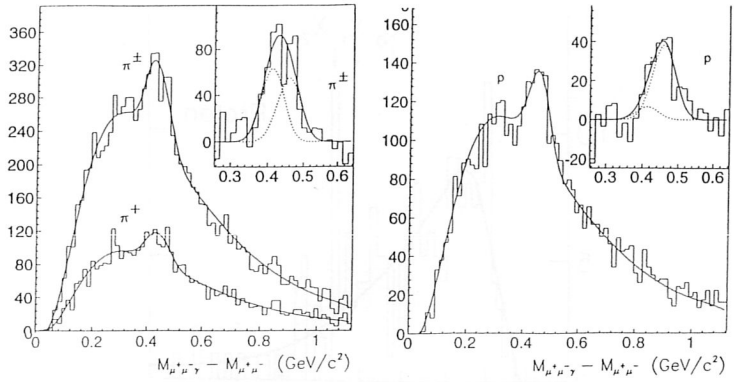

Figure 7: $J/\psi - \gamma$ mass spectrum from E705, pion and proton beams

taken at face value raises the intriguing question of what is the mechanism that allows relatively copious J/ψ production by protons, while suppressing the production of χ_1.

3 Production of other charmonium states

Another new result from the E-705 experiment is the tentative observation of some new levels of charmonium[14]. Such signals were observed in the mass spectrum of the J/ψ plus one or two pions. In Fig. 8 the J/$\psi\pi^0$ spectrum shows an enhancement at a mass of 3.527 GeV/c^2, which appears to confirm the recent observation of the $^1P_1$ state recently reported by Fermilab E-760[15]. Another enhancement, corresponding to a heretofore unobserved state, is seen in the J/$\psi\pi^+\pi^-$ spectrum (Fig. 9). Together with the expected signal from the ψ', known to decay into J/$\psi\pi^+\pi^-$ with a branching ratio of 16.2%, another peak appears at a mass of 3.836 GeV/c^2. A likely interpretation for such a signal would be a charmonium $^3D_2$ level ($J^{PC} = 2^{--}$), which is above the open charm threshold, but is forbidden from decaying into $D\overline{D}$. A confirmation of such observations carrying a stronger statistical significance would be the welcome outcome of new experiments[13].

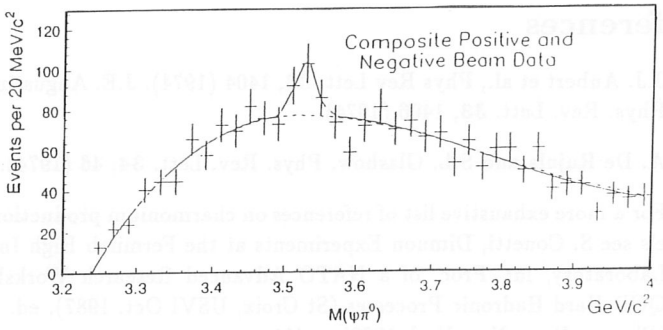

Figure 8: $J/\psi\pi^0$ invariant mass spectrum from E705

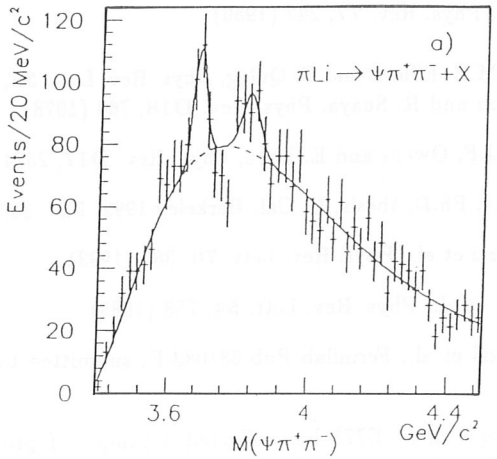

Figure 9: $J/\psi\pi^+\pi^-$ invariant mass spectrum from E705

References

[1] J.J. Aubert et al., Phys Rev Lett. **33**, 1404 (1974). J.E. Augustin et al., Phys. Rev. Lett. **33**, 1406 (1974).

[2] A. De Rujula and S.L. Glashow, Phys. Rev. Lett. **34**, 46 (1974).

[3] For a more exhaustive list of references on charmonium production models see S. Conetti, Dimuon Experiments at the Fermilab High Intensity Laboratory, in: Proc. of a NATO Advanced Research Workshop on QCD Hard Hadronic Processes (St Croix, USVI Oct. 1987), ed. B. Cox (Plenum Press New York 1988) p. 411.

[4] L. Antoniazzi et al., Phys. Rev **D46**, 4828 (1992)

[5] See Ref. 4 for the complete list of references to the data points appearing in Fig. 2.

[6] C.N. Yang, Phys. Rev. **77**, 242 (1950)

[7] S.D. Ellis, M.B. Eihorn and C. Quigg, Phys. Rev. Lett. **36**, 1263 (1976). C.E. Carlson and R. Suaya, Phys. Rev. **D18**, 760 (1978).

[8] M. Gluck, J.F. Owens and E. Reya, Phys. Rev. **D17**, 2324 (1978).

[9] M.S. Kowitt, Ph.D. thesis, U. Cal. Berkeley 1992, LBL-33331/UC-414.

[10] L. Antoniazzi et al., Phys. Rev. Lett. **70**, 383 (1993).

[11] D.A. Bauer et al., Phys. Rev. Lett. **54**, 753 (1985).

[12] L. Antoniazzi et al., Fermilab Pub-93/083-E, submitted to Phys. Rev. Lett.

[13] Fermilab experiment E771 has collected a sample of proton induced J/ψ about five times larger than the E705 sample. Another proposed experiment, P867, would increase the statistics by a factor of 20 or more.

[14] L. Antoniazzi et al., Fermilab-Pub-92/265-E, April 1993, submitted to Phys. Rev. D.

[15] T.A. Armstrong et al., Phys. Rev. Lett. **69**, 2337 (1992). See also D. Bettoni, these Proceedings.

SESSION II

- G. Pancheri
  An Introduction to CP Violation
- Y.W. Wah
  K–Meson Rare Decays
- S. Palestini
  Search for Direct CP–Violation in Neutral Kaons
- M. Purohit
  The Status of D^0–$\overline{D^0}$ Mixing

Frascati Physics Series, Vol. 1 (1993)
HEAVY QUARKS AT FIXED TARGET
Frascati, May 31st – June 2nd 1993
(pp. 31–45)

AN INTRODUCTION TO CP–VIOLATION

G. Pancheri
INFN – Laboratori Nazionali di Frascati
P.O.Box 13, I–00044 - Frascati (Roma), (ITALIA)

ABSTRACT

We briefly review the main properties of CP-violation in the Kaon system and illustrate its origin in the Standard Model through the Cabibbo-Kobayashi-Maskawa matrix. Forthcoming experiments at DAΦNE, the Frascati ϕ-factory, are reviewed. A short discussion of the top system is presented.

1 – Introduction

CP-Violation has been observed in hadronic systems through decay and oscillations between states corresponding to different CP-eigenvalues. The best studied case is that of oscillations between K^0 and $\bar{K}^0$, through the observation of Kaon decay modes into the 2π and 3π systems. If CP were conserved, the physical states in the CP-invariant limit would be

$$K_1 = \frac{K^0 + \bar{K}^0}{\sqrt{2}} \quad \text{with } CP = 1 \quad \text{and} \quad K_2 = \frac{K^0 - \bar{K}^0}{\sqrt{2}} \quad \text{with } CP = -1$$

with dominant hadronic decays into 2π and 3π respectively. The observation in 1964 [1] of the 2π (CP-even) decay mode of K_2, showed the existence of a CP-violating interaction.

These violations are allowed in the Standard Model, where the Cabibbo-Kobayashi- Maskawa (CKM) matrix provides for intergeneration mixing[2] . Typically this takes place via box diagrams like the ones shown in Fig. 1, where the quark pair $q_i\bar{q}_j$ of meson M^0, with i and j being flavour indices, can make a transition to the pair $q_j\bar{q}_i$ of meson $\bar{M}^0$. For the K^0 and $\bar{K}^0$ system, this transition is

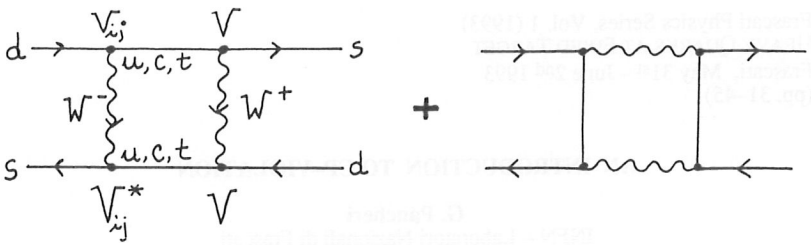

Figure 1: Typical electroweak loop diagram for the transition $K^0 - \bar{K}^0$

characterized by a change of strangeness of two units, i.e. it is a $\Delta S = 2$ transition. Let us first examine the Standard Model mechanism through which there arise mass differences and CP-violation effects. In the Standard Model, the mass difference between K^0 and $\bar{K}^0$ can be obtained from the real part of the amplitude for the graphs shown in Fig. 1. The weak matrix element is written as

$$H_{wk}^{(2)} = 2\left(\frac{-ig}{\sqrt{2}}\right)^4 \sum_{i,j} (V_{id}^* V_{is}) \left(V_{jd}^* V_{js}\right) \int \frac{d^4p}{(2\pi)^4} \left(\frac{-i}{p^2 - M_W^2}\right)^2 \cdot$$

$$\left(\bar{d}_L \gamma^\mu \frac{i(\not{p} + m_i)}{p^2 - m_i^2} \gamma^\nu s_L\right) \left(\bar{d}_L \gamma_\nu \frac{i(\not{p} + m_j)}{p^2 - m_j^2} \gamma_\mu s_L\right)$$

where V_{ij} are the elements of the Cabibbo-Kobayashi-Maskawa matrix and all three flavours of the up-quark type contribute. In the large W-limit, the contribution of individual graphs is divergent, but cancellations[3] occur between uu,cc type contributions and the interference terms, of the uc and cu type. The final result can be written as

$$\Delta m = V_{us}^2 V_{ud}^2 m_c^2 \frac{G_F^2}{16\pi^2} \left(\bar{d}\gamma_\mu(1-\gamma_5)s\right) \left(\bar{d}\gamma^\mu(1-\gamma_5)s\right)$$

Evaluating the above between the physical hadronic states for $< \bar{K}^0|$ and $|K^0 >$ and saturating with all possible intermediate states, one obtains the expression

$$\Delta m_{12} = m_2 - m_1 \approx 4m_c^2 \frac{cos\theta_c^2}{3\pi m_\mu^2} \Gamma(K^+ \to \mu^+ \nu)$$

which contains the K-decay constant f_K defined through

$$\Gamma(K^+ \to \mu^+ \nu) = \frac{8}{3} m_K^2 f_K^2 B_K$$

and B_K is a quantity containing all the uncertainties due to the confinement scale.

One now defines as physical states the two linear combinations

$$|K_L >= \frac{|K_2 > + \epsilon |K_1 >}{\sqrt{1+\epsilon^2}} \approx |K_2 > + \epsilon |K_1 >$$

and

$$|K_S>=\frac{|K_1>+\epsilon|K_2>}{\sqrt{1+\epsilon^2}}\approx|K_1>+\epsilon|K_2>$$

where ϵ is a small ($\approx 10^{-3}$) quantity, and the dominant decay modes of K_L and K_S are into 3 and 2 pions respectively.

The question which one may ask is if the observed CP-violation is due to a direct $K_2 \to K_1$ transition, as in the so called superweak interaction[4], or if there is some other mechanism which contributes the observed CP-violation, and how could one distinguish it from standard model effects. Let us suppose the existence of a direct $K_2 \to K_1$ transition, for which one can define a CP-violating parameter ϵ_{SW} such that

$$\epsilon_{SW}=\frac{A(K_2\to\pi\pi)}{A(K_1\to\pi\pi)}\approx-\frac{<K_1|H_{SW}|K_2>}{m_2^2-m_1^2+im_K\gamma_1}$$

Assuming CPT invariance, one then has

$$\epsilon_{SW}\approx\frac{<\bar{K}^o|H_{SW}|K^o>-<K^o|H_{SW}|\bar{K}^o>}{(2m_K)(2\Delta m+i\gamma_s)}$$

where $\gamma_1 \approx \gamma_s \approx \Gamma(K_S \to \pi\pi)$ and $\Delta m = m_L - m_S$ is the mass difference for the physical states. For the Kaon-system, the mass difference is exceedingly small (thus enhancing CP-violating effects), and very close to the decay width γ_s. In fact, $\Delta m = 3.5\ 10^{-6}\ eV = 0.535\ 10^{10}\hbar\ sec^{-1}$ and $\tau_s = 0.89\ 10^{-10}\ sec$, so that one has

$$2\Delta m \approx \gamma_s \tag{1}$$

Then, writing

$$\epsilon_{SW}=e^{i\Phi_{SW}}\frac{\Im<\bar{K}^0|H_{SW}|K^0>}{\Delta m}\frac{1}{2m_K\sqrt{2}}$$

we see that relation (1) implies for the superweak phase

$$\Phi_{SW}=tan^{-1}\frac{2\Delta m}{\gamma_S}\approx 45^o$$

Thus the parameter ϵ which is a measure of CP-violations must have a non-zero phase, in fact close to 45^o.

Another observed[5] effect which violates CP-invariance, is the charge asymmetry in the semileptonic decay of K_L, i.e.

$$A=\frac{\bar{\Gamma}(K_L\to\pi^-l^+\nu)-\Gamma(K_L\to\pi^+l^-\bar{\nu})}{\bar{\Gamma}(K_L\to\pi^-l^+\nu)+\Gamma(K_L\to\pi^+l^-\bar{\nu})}\approx 2\Re\epsilon$$

Thus both the Superweak hypothesis, which corresponds to no CP-violation in decays, but only in the transition matrix element, and the CKM model are compatible

with the observed value of the CP-violating parameter ϵ. But, is it possible to discriminate further ? The available tests can be divided into three cathegories :
(a) CP-asymmetries in K- or B-decays which are accompanied by final state rescattering as in the case of K^o decays or charmless B-decays
(b) Direct CP-violation in rare decays so as to avoid the $\Delta I = 1/2$ rule (see later), as in the case of leptonic and semileptonic decays. A case at hand is the branching ratio for $K_L \to \pi^o e^+ e^-$ for which estimates for direct and indirect CP-violation mechanisms[6] may differ by as much as one order of magnitude (with the indirect smaller than the direct one, contrary to what happens with $K_L \to \pi\pi$).
(c) non-zero dipole moments for elementary particles like the electron, the neutron, the τ and the Z. Unfortunately, so far, there is no evidence for such effects.

2 – CP-Violation in the Standard Model

If CPT holds, then CP-violation implies T-violation, and we can examine some of the consequences of T-violation as possible signals of CP-violation. In quantum mechanics, a c-number transforms under Time Reversal as

$$TcT^{-1} = c^*$$

For a T-violating interaction, one then needs complex numbers. In the Standard Model, complex numbers appear through the Yukawa coupling of the quark fields to the Higgs scalars. Through these couplings, which are then resposible for generating the masses, one constructs the quark mass matrices $M^{u(d)}$, which in the most general way, can be written as the product of a unitary matrix $V^{u(d)}$ times a hermitian matrix $H^{u(d)}$. There are then two possible ways to get a non-zero phase :

- from the Unitary matrices, through a chiral transformation, one can rotate away all but one of the phases[7]. This remaining non-zero phase is called θ_{strong}. Strong CP-violation brings around a modification of the effective lagrangian, such that there appear new interactions of the type $\eta\pi\pi, \bar{K}K\pi, ...$, whose strength in the Lagrangian is proportional to θ_{strong}. As an example, we show in Fig. 2 two diagrams where the CP-violating contribution to $K \to \pi\pi$ decay arises i) from an allowed $\Delta S = 1$ transition $K^o \to \eta$ followed by the decay $\eta \to \pi\pi$ proportional to the parameter θ_{strong}, or ii) from the θ_{strong} induced decay $K^o \to K\pi$ followed by the allowed $\Delta S = 1$ $K \to \pi$ conversion. However[8], this leads to a purely real CP-violating parameter ϵ and thus cannot be the sole origin of the observed violations. There still remains the possibility to study these effects in the dipole moments.

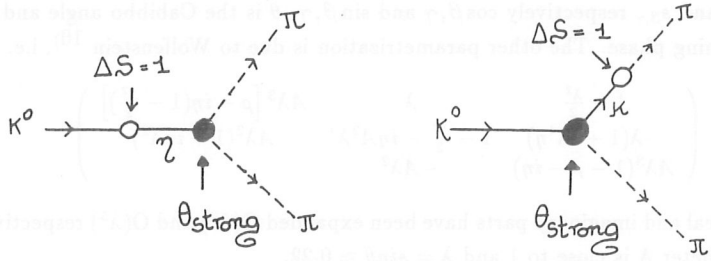

Figure 2: $K \to \pi\pi$ decays induced by strong CP-violation . Empty circle indicates $\Delta S = 1$ transitions, black dot is for new interactions proportional to the parameter θ_{strong}.

- from the Hermitian matrices $H^{u(d)}$, one can see that with three quark generations, it is not possible to write a transformation matrix with purely real elements. Let us call this remaining phase δ. We shall discuss this contribution in the following section.

3 – The CKM Matrix

In the Standard Model, CP-violation appears naturally in the Cabibbo-Kobayashi-Maskawa matrix which allows for mixing of the quark flavours in the charged weak vector current. In terms of of the general mixing matrix, these currents read

$$J^{\dagger}_{L\mu} = (\bar{u}, \bar{c}, \bar{t})_L \gamma_\mu \begin{pmatrix} V_{ud} & V_{us} & V_{ub} \\ V_{cd} & V_{cs} & V_{cb} \\ V_{td} & V_{ts} & V_{tb} \end{pmatrix} \begin{pmatrix} d \\ s \\ b \end{pmatrix}_L$$

V is a 3x3 unitary matrix, i.e. $VV^{\dagger} = V^{\dagger}V = 1$, which can be specified in general by 9 independent parameters, since the 18 complex numbers are reduced to 9 by the unitarity constraints $V^{\dagger}_{\alpha\beta}V_{\beta\gamma} = \delta_{\alpha\gamma}$. Of the remaining 9 parameters, one has the freedom to absorb a phase into each left handed field, so that 6 phases could be absorbed by the spinors, except that, since V is unchanged by a common phase transformation of all the q_L, one phase cannot be rotated away. Thus one remains with 4 independent parameters and the matrix can be parametrized in terms of three real numbers and one phase. Two complementary parametrizations have been proposed, one due to Maiani et al.[9)]

$$\begin{pmatrix} c_\beta c_\theta & c_\beta s_\theta & s_\beta e^{-i\delta} \\ -c_\gamma s_\theta - s_\beta c_\theta s_\gamma e^{+i\delta} & c_\gamma c_\theta - s_\beta s_\theta s_\gamma e^{+i\delta} & c_\beta s_\gamma \\ s_\gamma s_\theta - s_\beta c_\theta c_\gamma e^{i\delta} & -s_\gamma c_\theta - s_\beta s_\theta c_\gamma e^{i\delta} & c_\beta c_\gamma \end{pmatrix}$$

with $c_{\beta,\gamma}$ and $s_{\beta,\gamma}$ respectively $\cos\beta,\gamma$ and $\sin\beta,\gamma$. θ is the Cabibbo angle and δ is the remaining phase. The other parametrization is due to Wolfenstein [10], i.e.

$$\begin{pmatrix} 1-\frac{\lambda^2}{2} & \lambda & A\lambda^3\left[\rho - i\eta(1-\frac{\lambda^2}{2})\right] \\ -\lambda(1+i\lambda^4\eta) & 1-\frac{\lambda^2}{2}-i\eta A^2\lambda^4 & A\lambda^2(1+i\eta\lambda^2) \\ A\lambda^3(1-\rho-i\eta) & -A\lambda^2 & 1 \end{pmatrix}$$

in which real and imaginary parts have been expanded $O(\lambda^3)$ and $O(\lambda^5)$ respectively. The parameter A is close to 1 and $\lambda = sin\theta \approx 0.22$.

Until now CP-violation has been well established in the $K^o - \bar{K}^o$ system. The $B - \bar{B}$ system is the next candidate[11] in which one can test CP-violation, the validity of the CKM description and also the search for other non standard CKM effects. A graphical representation of such effects and the CKM matrix is obtained through the so-called unitarity triangle, which follows from satisfaction of the unitarity relation

$$V_{ub}V_{ud}^* + V_{cb}V_{cd}^* + V_{tb}V_{td}^* = 0$$

The above is just one out of six such relations, which can be represented by a triangle in the complex plane. Thus one can relate specific measurements to each side of the triangle and the satisfaction of the unitarity relation can be tested. In particular, for the b-quark case, $b \to u$ transitions are related to the first term of the above equation, the second term, proportional to $-\lambda V_{cb}$, is related to B-meson lifetime and $B^0 - \bar{B}^0$-mixing to the third term. In addition, one also introduces three angles, which can be measured through observation of CP-asymmetries in various B-decays. Since the Standard Model for the CKM matrix predicts a non-degenerate triangle, one can see that any difference with planar geometry can be considered a measure of non-Standard Model physics.

Using the Wolfenstein parametrization, the unitarity triangle can be represented in the complex plane, as in Fig.3, where ρ and η are respectively real and imaginary part of the position of the vertex A. The CKM phase is the angle with the real axes. One has the relation

$$\delta \approx tan^{-1}\frac{\eta}{\rho}$$

Then a number of constraints can be placed on the triangle. From charmless semileptonic B-decays, one obtains $|\frac{V_{ub}}{V_{cb}}| \approx 0.1$ from whence the relation

$$\rho^2 + \eta^2 \approx 0.2$$

follows. Further contraints come from the CP-violating parameter ϵ and $B_d^0 - \bar{B}_d^0$ mixing[12], related to the ratio $\left(\frac{\Delta m}{\Gamma}\right)_{B_d}$. This quantity, calculable through graphs

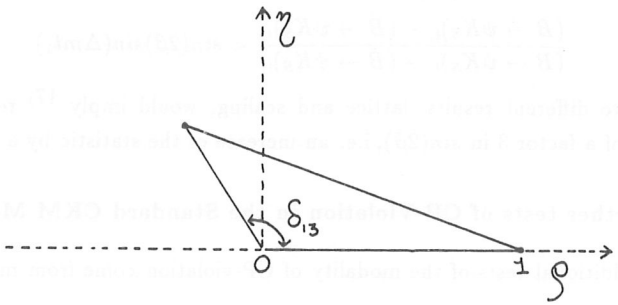

Figure 3: Rescaled unitarity triangle in the $\rho - \eta$ plane

like the ones in Fig.1, is proportional to $|V_{tb}^* V_{td}|^2$. These are the same graphs, which contribute to the parameter ϵ when the quark b is substituted by an s-type quark. In the latter case, the contribution is related to the imaginary part of $|V_{ts}^* V_{td}|^2$. In addition to the dependence from the CKM matrix elements, there is an additional dependence upon the top quark mass.

From the $K^0 - \bar{K}^0$ transitions, the $\Delta S = 2$ contribution shows that one can write [14]

$$\epsilon \propto m_t^2 f_K^2 B_K (1 - \rho)\eta$$

where f_K and B_K have already been mentioned in the introduction. We then see that, since ρ and η must have modulus less then one, η must be positive. An additional constraint comes from the value of the top mass. Choosing $m_t = 140 GeV/c^2$ [13] and $B_K \geq 0$, one obtains two possible solutions to all the constraints, one with positive and the other with negative ρ values. One has thus two possible triangles, one with the vertex in the second quadrant and the angle $\delta_{CKM}^{13} \approx 8\pi/9$ and the other with the vertex in the first quadrant and the angle is acute and close to $\pi/4$. To further determine the triangle, and establish as to whether ρ is positive or negative, one can use $B_d^0 - \bar{B}_d^0$ mixing . The mixing parameter x_d is proportional to $m_t^2 f_B^2 B_B \left[(1-\rho)^2 + \eta^2\right]$. While, in principle, this relation should allow for a determination of the sign of ρ, together with all the other constraints, in practice this is not so since f_B is not as well known as f_K. As for B_B there are two different ways to evaluate it, one through lattice calculations and the other through a naive scaling approach from D-mesons. Unfortunately, this ambiguity is not yet solved[16], due to the large hadronic uncertainties : lattice calculations indicate a positive value, while naive scaling a negative one. It must be noticed that a positive ρ value would be very interesting since it implies large CP-asymmetries in the B-system. In fact, if β is the angle from the Maiani representation of the CKM matrix, one can see that there is the following relation between this angle and the time asymmetry in

B-decays :

$$\frac{(B \to \psi K_S)_{t_1} - (\bar{B} \to \psi K_S)_{t_1}}{(B \to \psi K_S)_{t_1} + (\bar{B} \to \psi K_S)_{t_1}} \approx sin(2\beta) sin(\Delta m t_1)$$

and the two different results, lattice and scaling, would imply [17] respectively a difference of a factor 3 in $sin(2\beta)$, i.e. an increase of the statistic by a factor 10.

4 – Further tests of CP-Violation in the Standard CKM Model

Possible additional tests of the modality of CP-violation come from measuring the two ratios

$$\eta_{+-} = \frac{A(K_L \to \pi^+\pi^-)}{A(K_S \to \pi^+\pi^-)} = \epsilon + \epsilon' \quad ; \eta_{00} = \frac{A(K_L \to \pi^o\pi^o)}{A(K_S \to \pi^o\pi^o)} = \epsilon - 2\epsilon'$$

According to the Superweak hypothesis, CP-violations arise from the direct $K_2 \to K_1$ transition and thus one should have $\epsilon'_{SW} = 0$. Therefore a measurement of the quantities ϵ and ϵ' (four real numbers) can in principle lead to a discrimination among models. On the other hand, the situation is far from being this simple, since one can see that the magnitude of ϵ' could be small for reasons which have nothing to do with CP-violation. In fact, from the Standard Model, one has

$$\epsilon' \approx \frac{1}{\sqrt{2}} \frac{\Im A_2}{A_0} e^{i(\pi/2 - \delta_0 + \delta_2)}$$

where A_0 and A_2 are the transition amplitudes $< K|H_W|\pi\pi >$ for $I_{\pi\pi} = 0, 2$ values and δ's are the relative phaseshifts. It is well known that in strong interactions there is an empirical, but well observed, selection rule, which favours transition between states with $\Delta I = 1/2$ and thus suppresses the transition $K \to I = 2$ relative to $K \to I = 0$. We can therefore remain uncertain as to whether $\epsilon' = 0$ because of some superweak interaction or simply because of the $\Delta I = 1/2$ rule.

Published results of measurements by NA31 [18] and E731 [19] Collaborations yield the following values:

- (NA31) $\Re\frac{\epsilon'}{\epsilon} = [33 \pm (statistical)7 \pm (systematic)8] \times 10^{-4}$
- (E731) $\Re\frac{\epsilon'}{\epsilon} = [7.4 \pm (statistical)5.2 \pm (systematic)2.9] \times 10^{-4}$

5 – CP-Asymmetries

Observations of the time evolution of Kaon and B-meson systems have led to measurements of asymmetries in the particle decays due to CP-violation, as well as to the observation of oscillations between the different CP-states. If one introduces

the decay widths $\Gamma \propto |A|^2$ and $\bar{\Gamma} \propto |\bar{A}|^2$ relative to the two CP-conjugate processes $K^0 \to \pi\pi$ and $\bar{K}^0 \to \pi\pi$, the quantity

$$\Delta\Gamma = \frac{\bar{\Gamma} - \Gamma}{\bar{\Gamma} + \Gamma}$$

can measure CP-violations, with $\Delta\Gamma \neq 0$. Let the above amplitudes be written as

$$A(K^0 \to \pi^+\pi^-) = A_1 e^{i\alpha_1} + A_2 e^{i\alpha_2}$$

$$\bar{A}(\bar{K}^0 \to \pi^+\pi^-) = A_1^* e^{i\alpha_1} + A_2^* e^{i\alpha_2}$$

where α_1 and α_2 are CP-conserving phases, we have

$$\Delta\Gamma \propto \Im(A_1 A_2^*) sin(\alpha_1 - \alpha_2)$$

then, in order to observe a CP-asymmetry, one needs the following conditions to be fulfilled :

- relative CP-violating phases from the CKM matrix;
- relative dynamical CP-conserving phases.

Of possible effects to be observed, there are oscillations of unstable neutral pseudoscalar mesons provided there is mass difference $\Delta m \propto \alpha_1 - \alpha_2$, final state interaction (FSI) effects in different decay channels and time dependent decays.

5.1 Time evolution of the $K^0 - \bar{K}^0$ System

Let us consider the time dependent asymmetry

$$\Delta\Gamma^K_{\pi\pi}(t) = \frac{\bar{\Gamma}(\bar{K}^0 \to \pi^+\pi^-) - \Gamma(K^0 \to \pi^+\pi^-)}{\bar{\Gamma}(\bar{K}^0 \to \pi^+\pi^-) + \Gamma(K^0 \to \pi^+\pi^-)}$$

For the physical states K_S, K_L, the time evolution can be written as

$$K_S(t) = e^{-im_S t} e^{-\frac{\gamma_S}{2}t} K_S(0)$$

$$K_L(t) = e^{-im_L t} e^{-\frac{\gamma_L}{2}t} K_L(0)$$

One can distinguish between three different time periods :

- very large observation times such that $t >> \tau_S$: only the K_L component will survive and one has

$$\Delta\Gamma(t >> \tau_S) \simeq 2\Re(\epsilon)$$

- $t \leq 10\tau_S$: both K_S and K_L are present at the same time and the time asymmetry can be written as

$$\Delta\Gamma(t \leq 10\tau_S) \simeq -2e^{-\frac{\gamma_S t}{2}} \left[\Re(\epsilon+\epsilon')\cos(\Delta m t) + \Im(\epsilon+\epsilon')\sin(\Delta m t)\right] + 2\Re\epsilon$$

and we see that
(i)$\Delta\Gamma(t=0) = -2\Re\epsilon'$
(ii) $\Delta\Gamma(t = 3\pi\tau_S) \simeq 2e^{\frac{3\pi}{2}}\Im(\epsilon+\epsilon')$

Thus, a measurement of the complete time evolution could in principle allow for a determination of all the four quantities : $\Re\epsilon'$ near $t = 0$, $\Im(\epsilon+\epsilon')$ and $\Re(\epsilon+\epsilon')$ in intermediate times and $\Re(\epsilon)$ at large times. The observation of CP-asymmetries for the Kaon system has been done by the CP-LEAR experiment[20], through the time evolution of the oscillation between K^0 and $\bar{K}^0$, in one single given final state decay. Of course, due to limited statistics, only the small time region was well studied, but improvements are expected.

6 – CP-Violation at DAΦNE

In this section we shall briefly discuss plans to measure CP-violation at a symmetric ϕ-factory like the one under construction at Frascati, DAΦNE. Observation of ϕ-decays into a $K\bar{K}$ pair at e^+e^- colliders selects a special state, odd under charge conjugation, because of the photon quantum numbers. Thus one of the reactions under scrutiny is

$$e^+e^- \to \phi \to \bar{K}^0K^0 \to \frac{K_SK_L - K_LK_S}{\sqrt{2}} \to \pi^+\pi^-, \pi^0\pi^0$$

and what one can study is

- (i) time evolution of $K^0\bar{K}^0$
- (ii) time asymmetries in the decays $\pi^+\pi^-$ and $\pi^0\pi^0$
- (iii) magnitude of the double ratio

$$\frac{\Gamma(K_L \to \pi^+\pi^-)}{\Gamma(K_S \to \pi^+\pi^-)} \Big/ \frac{\Gamma(K_L \to \pi^0\pi^0)}{\Gamma(K_S \to \pi^0\pi^0)} = 1 + 6\Re\frac{\epsilon'}{\epsilon}$$

- (iv) Branching ratios for different charge configurations

In one particular set up, described by Patera and Pugliese [21], the quantities ϵ and ϵ' are measured through the distance travelled by K-mesons decaying into the neutral and charged pair. Let us define

$$d_+ = \text{distance travelled by K before decaying into } \pi^+\pi^-$$

$$d_0 = \text{distance travelled by K before decaying into } \pi^0\pi^0$$

and $d = d_+ - d_0$. Then for a given $K - \bar{K}$ pair, the number of events corresponding to a given $\{d_+, d_0\}$ pair will be a function of $|\eta_{+-}|^2, |\eta_{00}|^2$, and of the interference between the amplitudes, i.e. $\Re\frac{\epsilon'}{\epsilon}$ and $\Im\frac{\epsilon'}{\epsilon}$. Integration over the symmetric variable $d_+ + d_0$ defines the quantity

$$N(d) = \int N(d_+, d_0) d(d_+ + d_0)$$

from whence one can obtain the time asymmetry

$$A(d) = \frac{N(|d|) - N(-|d|)}{N(|d|) + N(-|d|)} = A_R(d)\Re\frac{\epsilon'}{\epsilon} - A_I\Im\frac{\epsilon'}{\epsilon}$$

with the functions $A_R(d)$ and $A_I(d)$ such that at large d/d_s values, with d_s the distance covered by the decaying K_S during one life time, only the first terms of the above right hand side survives, allowing for a determination of $\Re\frac{\epsilon'}{\epsilon}$. Both the real and the imaginary parts of $\frac{\epsilon'}{\epsilon}$ can in principle be measured through a precise determination of the function N(d) for a set of values of the distance d. If the space resolution is good enough, one can measure the expected dip in this function at d=0 and the asymmetrical behaviour at large positive d-values relative to the negative ones. The study in [21] indicates that an estimated accuracy $\sigma = 5mm$ could allow for a determination of $\Re\frac{\epsilon'}{\epsilon}$ with a precision of $\sim 10^{-4}$ and of $\Im\frac{\epsilon'}{\epsilon}$ with a precision of $\sim 10^{-3}$.

At present, the KLOE experiment under preparation[22] is geared to measure $\frac{\epsilon'}{\epsilon}$ with the double ratio method and to obtain a 10^{-4} precision for $\Re\frac{\epsilon'}{\epsilon}$.

7 – A Digression on the top-quark systems

CP-Violation and other CKM-allowed effects are observed in the hadronic systems formed by the 5 different quark flavours experimentally discovered. How about the top quark ? Concerning the top system, the present lower limits on the top mass established by CDF and recently also by the D0 Collaboration[23], exclude the possibility of T- meson formation and almost but all exclude the formation of toponium bound states. This can be understood in a rather simple and intuitive way, by comparing the revolution time of the bound state with the top quark decay

probability. The limits on the top mass, in fact have established that the top can openly decay into a real W and a b-quark. This decay probability is a rapidly varying function of the top mass and, for sufficiently large values, it can be written as

$$\Gamma_t \approx \left(\frac{m_t}{246\ GeV}\right)^2 \frac{m_t}{16\pi}$$

showing that the decay width increases like the cubic power of the quark mass. This width is close to hundred Mev for a 100 GeV top, i.e. it is comparable and even larger that the hadronic widths. Thus the life-time of T-hadrons, toponium type or other, are dominated by single quark decay. For a bound state on the other hand, the typical formation time of a hadron is characterized by a revolution time dictated by strong interactions. Clearly no bound state can exist if the revolution time is longer than the life time of the rotating quarks[24]. A physical criterion can be used[25], which states that formation of a hadron can take place only if the bound state spectrum is such that the splitting between the lowest lying levels is larger than the natural width of the state. Using a hydrogenic model, with a Coulombic potential

$$V = -\frac{4}{3}\frac{\alpha_s(r_B)}{r}$$

with α_s evaluated at the Bohr radius, $r_B \approx 0.02\ fm$ for a 100 GeV top quark, one can write for the splitting 2S-1S

$$\Delta E_{2S-1S} = \frac{1}{3}\alpha_s^2 m_t$$

where we have used the reduced mass $\mu_{red} = m_t/2$. We show in Fig.4 a comparison of the width $\Gamma_{toponium} \approx 2\Gamma_t$ with ΔE_{2S-1S}, as a function of the top quark mass, where we have used the one loop expression for α_s, $N_f = 5$ and $\Lambda = 0.2\ GeV$. One can see that for top quark masses around 130-150 GeV the splitting will become smaller than the decay width and therefore toponium bound states become more and more unlikely.

One may apply a similar criterion for the case of a T-meson, i.e. a meson formed with one light and one top quark. In this case, the decay width of the state is the single quark decay width Γ_t, which we may compare with a splitting proportional to the reduced mass of the light-heavy quark system,

$$\Delta E = \frac{2}{3}\hat{\alpha_s}^2 m_{light}$$

where now $\hat{\alpha}_s$ is the effective coupling strength between the top and the light quark of mass m_{light}. For an estimate, we can consider that for very light quarks, u, d and s, $\hat{\alpha_s}(m_{light})$ cannot be larger than 1 and thus $\frac{2}{3}\hat{\alpha_s}^2 m_{light} \approx \frac{2m_{light}}{3} \leq 100\ MeV$,

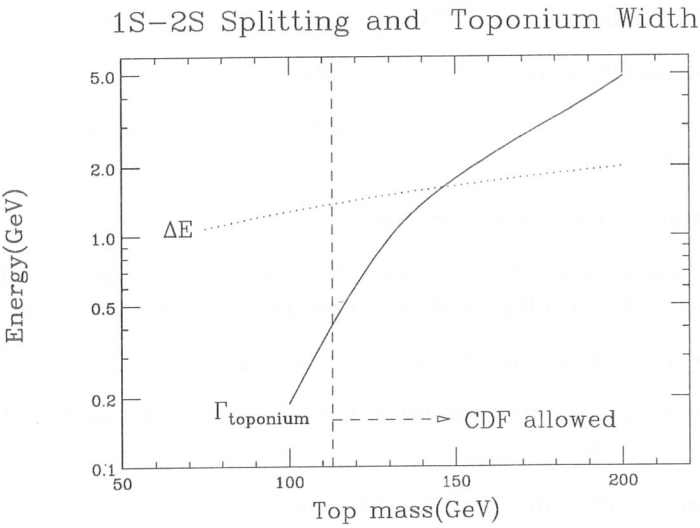

Figure 4: Comparison between toponium width and 1S-2S level splitting from a hydrogen-like bound state model with Coulombic potential.

while for the b-quark case, $\hat{\alpha_s} \approx 0.3$ and $\frac{2}{3}\hat{\alpha_s}^2 m_b \approx 0.06 m_b \leq 300\ MeV$. This value equals the top width for a top mass of 120 GeV. For larger values, the splitting is smaller than the width and no light-heavy quark states are possible. Thus, we see that a top quark of mass $\geq 120 \div 130\ GeV$ will be too heavy, and its decay width too large, to allow for hadronic bound states and thus for CP- violating effects of the type discussed in the previous sections.

These are rather imprecise estimates, but sufficient for the present illustrative purpose. Notice however that this analysis is based on a Born approximation to the top width and on a Coulombic potential with a one-loop expression for α_s. Using the two loop expression, ΔE will be smaller and the critical mass for toponium formation will be $\approx 130\ GeV$ rather than 150. Including also other higher order QCD effects will non substantially change the picture, but non-perturbative effects can obviously modify part of this scenario[26].

References

1. J.H.Christenson, J.W.Cronin, V.L. Fitch and R.Turlay, Phys. Rev. Lett. 13 (1964) 138.

2. N.Cabibbo, Phys. Rev. Lett. 10 (1963) 531 ; M.Kobayashi and K.Maskawa, Progr. Theor. Phys. 49 (1973) 652.

3. S. Glashow, J.Iliopoulos and L.Maiani, Phys. Rev. D2 (1970) 1285.

4. L.Wolfenstein, Phys. Rev. Lett. 13 (1964) 562.

5. J. Dorfan et al., Phys.Rev.Lett. 19 (1967) 987 ; S.Bennet et al., Phys. Rev. Lett. 19 (1967) 993.

6. L.M.Sehgal, Phys.Rev. D38 (1988) 808.

7. J.S. Bell and R. Jackiw, Nuovo Cimento 60A (1969) 47 ; S.L.Adler, Phys. Rev. 182 (1969) 2426; S.L.Adler and W.A.Bardeen, Phys.Rev. 182 (1969) 1517.

8. R.Peccei, DESY Report 88-109 (1988) and references therein.

9. L.Maiani, Phys. Lett. 62B (1976) 183. L.-L. Chau and W.-Y. Keung, Phys. Rev. Lett. 53 (1984) 1802.

10. L. Wolfenstein, Phys. Rev. Lett. 51 (1983) 1945.

11. For a review, see A. Le Yaouanc, L.Oliver, O.Pene and J.-C. Raynal, "CP Violation in B-Mesons", Monographs on Fundamental Physics, Proceedings of Capri Symposia 1990-1991. Ed. F.Buccella, Bibliopolis, Napoli 1992.

12. UA1 Collaboration, C.Albajar et al., Phys. Lett. B 186 (1987)247; ibidem 262 (1991) 171; CD Collaboration, F. Abe et al., Phys. Rev. 67 (1991) 3357.

13. The value chosen here is within one standard deviation from the most recent value extracted from all the electroweak constraints as reported by J.Ellis, at XXVII ICHEP Cornell, Ithaca, 10-17 August 1993.

14. M.K. Gaillard and B.W.Lee, Phys. Rev. D10 (1974) 897.

15. A.J.Buras and J.-M.Gerard, Phys. Lett. 192B (1987) 156. J.M.Flynn and L.Randall, Phys. Lett. 224B (1989) 221;235B (1990)412(E). G.Buchalla, A.J.Buras and M.K.Harlander, Nucl.Phys.B 337 (1990) 313; E.A.Paschos and Y.L.Wu, Mod. Phys. Lett. A6 (1991) 93.

16. J.-.M.Gerard, Joint International Lepton Photon Symposium and Europhysics Conference on High Energy Physics, Geneva 25 July - 1 August 1991.

17. M.Lusignoli, L.Maiani, G.Martinelli and L.Reina, Nucl. Phys. B369 (1992) 139; M.Ciuchini, E.Franco, G.Martinelli, L.Reina, Phys. Lett. B 301 (1993) 263.

18. CERN NA31 Collaboration, H.Burkhardt et al., Phys.Lett. B 206 (1988) 169.

19. E731 Collaboration, L.K.Gibbons et al., Phys. Rev. Lett. 70 (1993) 1203.

20. CP-LEAR Collaboration, R.Adler et al., Phys.Lett.B286 (1992) 180.

21. V.Patera and A.Pugliese, "Asymmetries and Time Evolution in the $\bar{K}^0 - K^0$ System", DaΦNE Physics Handbook, Ed. L.Maiani et al., Frascati 1992.

22. KLOE Collaboration, "The KLOE Detector Technnical Proposal", LNF-93/002.

23. CDF Collaboration, A.Caner, 28th Rencontres de Moriond, Les Arcs 20-26 March 1993; ibidem D0 Collaboration, M.Narain.

24. I.Bigi, Y. Dokshitzer, V. Khoze, J. Kuhn and P. Zerwas, Phys. Lett. B181 (1986) 157; V.S. Fadin and V.A. Khoze, JEPT Lett. 46 (1987) 525.

25. G.Pancheri, J.-P. Revol and C.Rubbia, Phys.Lett. B277 (1992) 518; A. Grau, N.Fabiano and G.Pancheri, "Toponium Bound States at LHC/SSC", Proceedings of the VIII Corso Invernale di Fisica Adronica, Folgaria 31 January - 6 February 1993.

26. P.Jain, D.McKay and H.J.Munczek, "Infrared Corrections to the Top Quark Width", Proceedings of the 7th Meeting of APS/DPF, Batavia, Illinois 10-14 November 1992, pag. 436.

K–MESON RARE DECAY

Yau W. Wah

University of Chicago
5630 South Ellis Ave., Chicago, IL 60637, (USA)

No written contribution received

Frascati Physics Series, Vol. 1 (1993)
HEAVY QUARKS AT FIXED TARGET
Frascati, May 31st – June 2nd 1993
(pp. 49–61)

SEARCH FOR DIRECT CP VIOLATION IN NEUTRAL KAONS DECAYS

S. Palestini
INFN, Sezione di Torino,
Via Pietro Giuria 1, I–10125 Torino, (ITALIA)

ABSTRACT

The search for direct CP violation in the decays of K_L into neutral and charged pion pairs is reviewed. Experiments which have recently presented results are discussed, together with projects for new measurements.

1 Introduction

Almost thirty years have passed since the first observation[1)] of violation of the symmetry *Charge conjugation* × *Parity* in the decays of K_L to two pions, and still the neutral kaons remain the only system in which violation of *CP* has been observed.

All the available measurements concern either the decay $K_L \to \pi\pi$ (branching ratio BR=0.29 %), or the asymmetry in the semileptonic decays $K_L \to \pi^- l^+ \nu_l$ vs. $\pi^+ l^- \bar{\nu}_l$ (asymmetry $\delta = 0.33\,\%$).[1]

These CP violating effects can be described saying that the eigenstates of mass (and lifetime) K_L, K_S are not eigenstates of CP, and beyond a dominant component with CP=−1, +1 respectively, they contain a combination of K°, $\overline{K}^\circ$ with opposite CP eigenvalue[3)]. In this way the violation of CP is related to the off-diagonal element in the mass matrix:

$$< K_L | \mathcal{H}_{CPV} | K_S >$$

which is determined by the element:

$$< K^\circ | \mathcal{H}_{CPV\ \Delta S=2} | \overline{K}^\circ >$$

[1]To these processes, we should add a recent observation[2)] of the related asymmetry between K° and $\overline{K}^\circ \to \pi\pi$.

This is referred to as *indirect* violation of CP , and is described by the complex parameter ε which specifies the mixing between the two components:

$$|\mathrm{K_L}>=[\,|CP=-1>+\varepsilon\,|CP=+1>]/\sqrt{1+|\varepsilon|^2}$$

$$|\mathrm{K_S}>=[\,|CP=+1>+\varepsilon\,|CP=-1>]/\sqrt{1+|\varepsilon|^2}$$

The natural question to ask now is whether is there any form of *direct* CP violation, due to transitions associated to matrix elements of the form:

$$< X_{S=0}|\mathcal{H}_{CPV\ |\Delta S|=1}|\mathrm{K^o}>$$

The Standard Model naturally allows the existence of direct CP violation, through the presence of the complex phase in the Cabibbo-Kobayashi-Maskawa (CKM) matrix[4], and the interference of different decay amplitudes. In the case of $\mathrm{K_L}\to\pi\pi$ the interference is between the amplitudes of the transitions to the two final states of definite Isospin: $I_{\pi\pi}=0,2$. Since the states $\pi^o\pi^o$ and $\pi^+\pi^-$ select different combinations of isospin, direct CP violation will determine different amplitudes (A) for the two channels:

$$\begin{aligned} A(\mathrm{K_L}\to\pi^o\pi^o)/A(\mathrm{K_S}\to\pi^o\pi^o) &\equiv \eta_{00} = \varepsilon-2\,\varepsilon' \\ A(\mathrm{K_L}\to\pi^+\pi^-)/A(\mathrm{K_S}\to\pi^+\pi^-) &\equiv \eta_{+-} = \varepsilon+\varepsilon' \end{aligned}$$

where ε' is given by[5]:

$$\varepsilon'=\frac{i}{\sqrt{2}}e^{i(\delta_2-\delta_0)}\frac{\mathcal{I}(A_2)}{A_0}$$

where δ_0, δ_2 are the final state interaction phases, and A_0 (chosen to be real), A_2 are the decay amplitudes for the two states of definite $I_{\pi\pi}$. The parameter ε determines a CP violating amplitude independent of Isospin, and indeed is equivalent to the parameter of indirect CP violation described above. Instead, the parameter ε' causes direct violation.

We know that the direct CP violating component of the amplitude is much smaller than indirect one[2], in agreement with the $\Delta I=1/2$ rule, implying $|A_2|\ll|A_0|$ and therefore $|\varepsilon'/\varepsilon|\ll 1$. The Standard Model[6] relates the value of ε' to the coefficients of the CKM matrix, to the mass of the quark top, and to matrix elements of strong interactions. Recent computations predict $|\varepsilon'/\varepsilon|\approx 0.001$[7].

The quantity which can be experimentally measured is the *double ratio*

$$R=\frac{\Gamma(\mathrm{K_L}\to\pi^o\pi^o)/\Gamma(\mathrm{K_S}\to\pi^o\pi^o)}{\Gamma(\mathrm{K_L}\to\pi^+\pi^-)/\Gamma(\mathrm{K_S}\to\pi^+\pi^-)}=\left|\frac{\eta_{00}}{\eta_{+-}}\right|^2\simeq 1-6\,\mathcal{R}(\varepsilon'/\varepsilon)$$

[2]This is true for the $\mathrm{K^o}$ system only, and in the $\mathrm{B^o}$ system the situation may be opposite, as discussed by other contributors to this conference.

Notice that the phase of ε' is determined by $(\delta_0 - \delta_2)$ and is equal to $(47. \pm 5.)^o$, while the phase of ε is measured in K_L-K_S interference, and found equal to $(43.68 \pm 0.14)^o$. Therefore, the ratio ε'/ε is real to good approximation[8].

Concluding this introduction, notice again that the search for direct violation is a test of the Standard Model of highest relevance. An accurate measurement of ε'/ε would constrain fundamental parameters of the Standard Model, while a tight limit on the presence of direct CP violation would imply that an interaction outside the Standard Model exists(the *superweak* interaction[3]), in order to allow for the observed indirect violation.

2 The measurement of direct CP violation

In this section, we shall discuss some relevant aspects of the measurement of the double ratio (R). Following the title of this workshop, we shall consider experiments performed at fixed target facilities, studying the decays of beams of neutral kaons with energy $\sim$100 GeV. Here we shall discuss the most general problems typical of this technique, and in the following sections we shall examine the solutions chosen by experiments recently completed, or in preparation.

First of all notice that the measurement of R requires counting events in the four processes of K_L, K_S decaying to neutral and charged pion pairs. Since for K_S's these are dominant decay channels, and since most K_S's decay in the fiducial volume of the detector, the statistical sensitivity is normally determined by the sample of collected K_L decays, in particular for the channel $K_L \to \pi^o\pi^o$, which has a branching ratio one half of the charged decay. In order to reach a statistical accuracy of about ± 0.001 in R, one needs about 1,200,000 $K_L \to \pi^o\pi^o$ neutral decays. This requires a total sample of 1.3×10^9 K_L decays, to be collected together with $> 4 \times 10^6$ K_S decays.

Systematic uncertainties represent a delicate aspect of this measurement. Since the same final states are detected for both K_L and K_S, to first order systematic uncertainties related to detector performance cancel in the double ratio. However, the cancellation cannot be total, because of differences in the geometry and momentum spectrum of the two beams, and particularly because the lifetime difference $\tau_S \ll \tau_L$ generates very different decay distributions in the fiducial volume.

Other sources of systematic uncertainty, related to time dependent detector inefficiencies, dead time, and overlay of accidental events, cancel in the double ratio, if at least some of the processes involved are measured simultaneously. Again, one has to worry about the degree of accuracy in the cancellation. As an example, inefficiencies due to accidental activity in the detector, which tend to affect differently neutral and charged decays, may have a significant component different

between K_L and K_S, which tends to bias the measurement of the double ratio.

Another critical systematics is the accuracy in the fiducial volume. This is related to the measurement of the longitudinal decay coordinate z. While for charged decays the value of z can be reconstructed directly with tracking chambers, for neutral decays the decay vertex is obtained from the energies E_i and the transverse coordinates $r_i = \sqrt{x_i^2 + y_i^2}$ of the four photons measured by a shower detector. Assuming that the photons originate from a neutral kaon with mass M_K, directed toward the center of the calorimeter, the distance between the decay vertex and the detector satisfies to good approximation the relation:

$$\Delta z \cong \frac{\sum E_i}{M_K} \sqrt{\frac{\sum r_j^2 E_j}{\sum E_k}}$$

The scale of z is proportional to the scale of the energy measurement, and the accuracy required in the definition of the fiducial volume reflects into accuracy in the energy calibration of the calorimeter.

Finally, another source of systematic uncertainty is the subtraction of background. The dominant background processes are $K_L \to \pi^o\pi^o\pi^o$ and $K_L \to \pi^\pm l^\mp \nu$, which affect K_L decays to $\pi^o\pi^o$ and $\pi^+\pi^-$ respectively. The rejection factor achieved in the experiments discussed below are at least as good as 1/10,000, with the relative uncertainty smaller by a factor 20. Finally, particular techniques may involve a characteristic background due to misidentification between K_L and K_S, as shown below in two cases.

3 Experiments recently concluded

Two experiments have recently produced results on ε'/ε. As discussed below, the results are placed at the boundary of the interval predicted in the framework of the Standard Model, and do not allow to establish the existence of direct CP violation. In the following sections, we shall review experimental techniques, uncertainties of measurements, and results.

3.1 Experiment CERN/NA31

This experiment[9] has shown the first evidence for direct CP violation[10]. The data was collected with short, alternated periods of K_L and K_S data taking. The K_S beam is produced from the attenuated primary proton beam, hitting on a movable target–collimator system. This technique allows to shift the decay volume of the K_S beam, $\sim$ 6 m long, along the entire fiducial volume for the K_L beam, 50 m long. This reduces systematic effects related to detector acceptance and efficiency, maintaining a good level of symmetry between K_L and K_S decays to the same final states. The

detector is 40 to 60 m downstream of the end of the fiducial volume, and consists of drift chambers, an e.m. calorimeter made of liquid Argon–lead sandwich, a hadron calorimeter, a muon detector, and is complemented by iron–scintillator veto counters placed along the decay volume.

The experiment took data in 1986, 1988, and 1989. The sum of the samples collected in 1986 and 1988 are shown in Table 1. About the same amount of data

Table 1: Statistical samples for NA31 1986 and 1988 data.

	$\pi^o\pi^o$	$\pi^+\pi^-$
K_L	220,000	590,000
K_S	1,490,000	3,680,000

was collected in 1989. The analysis of the data collected in the last period is only preliminary, and is based on 80 % of the data samples[11].

The major corrections applied to the directly measured double ratio are shown in Table 2. When a statistical component of the error can be identified, statistical and systematic errors are quoted separately. Notice that NA31 requires little corrections for acceptance, while the biases due to accidentals and background subtraction are relatively large. The background to $K_L \to \pi^o\pi^o$ is due do $K_L \to 3\,\pi^o$,

Table 2: Corrections (%) and uncertainties applied to R for NA31 1988 data.

Acceptance (Monte Carlo)	$0.23 \pm 0.09 \pm 0.01$
Accidentals	$0.5 \pm 0.12 \pm 0.2$
Background to $K_L \to \pi^o\pi^o$	3.2 ± 0.16
Background to $K_L \to \pi^+\pi^-$	0.9 ± 0.15
Inefficiencies and trigger losses	0.15 ± 0.16
Energy calibration and stability	± 0.14
Statistical error on data samples	± 0.4

and is removed imposing that the four γ's can be paired to provide the π^o invariant mass. The background to $K_L \to \pi^+\pi^-$ is mainly due to $K_L \to \pi\, e\, \nu$ and $\pi\, \mu\, \nu$, and is rejected by particle identification, and by verifying that the $\pi^+\pi^-$ pair is coplanar with the K_L beam. The overall average of all the data collected by NA31, which is still preliminary, is equal to[11]:

$$\mathcal{R}(\varepsilon'/\varepsilon) \;=\; (2.3 \pm 0.35 \pm 0.6) \times 10^{-3} \;=\; (2.3 \pm 0.7) \times 10^{-3}$$

which favours the existence of direct CP violation, at a level compatible with predictions based on the Standard Model.

3.2 Experiment FNAL/E731

This experiment makes use of two identical neutral beams, nearly parallel, about 20 cm apart. A regenerator target is switched between the two beams at any machine cycle. The regenerator acts as source of K_S. The detector, 35 to 65 m downstream of the regenerator, consists of a magnetic spectrometer equipped with drift chambers, scintillator trigger planes and vetoes, a lead glass electromagnetic calorimeter, and muon counters. Two pion decays from both beams are collected simultaneously.

Since the coherent regeneration cross section depends on the kaon momentum P as $1/P^{1.2}$, the momentum spectrum of the K_S beam is similar to the spectrum of *decaying* K_L's, reducing systematic differences between the measurements of K_L and K_S decays. The fiducial decay volume is equal to ≈ 10 m for K_S, and chosen equal to 42 m for $K_L \to \pi^o\pi^o$ and 27 m for $K_L \to \pi^+\pi^-$.

About 60 % of the $\pi^o\pi^o$ sample was collected in data taking periods which alternated $\pi^o\pi^o$ and $\pi^+\pi^-$ modes. In the neutral mode, a 9 % X_o converter was placed near the center of the fiducial volume, at the *trigger plane*. Neutral decays are assigned to the K_L or K_S beams selecting events where one photon converts and the tracking chambers determine the origin of the e^+e^- pair. For the remaining part of the data taking, the converter was removed, and the four decay processes were collected simultaneously. In this case, the identification of the decaying particle is made from the measurement of the transverse coordinates of the *center of energy* measured by the electromagnetic calorimeter.

The statistical sample collected by E731 is shown in Table 3.

Table 3: Statistical samples for E731.

	$\pi^o\pi^o$	$\pi^+\pi^-$
K_L	410,000	330,000
K_S	800,000	1,060,000

The major systematic uncertainties are shown in Table 4[12]. The overall acceptance correction computed by Monte Carlo is at the level of several percent. The accuracy of the correction has been tested with large samples of $\pi\, e\, \nu$ and $\pi^o\pi^o\pi^o$ decays. Notice the characteristic uncertainties due to non-coherent regeneration and incoherent or diffractive scattering at the trigger plane, which may cause misidentification between K_L and K_S (*cross-over*). The former effect produces a background to the neutral channels of 2–3 %, and the latter a background to $K_L \to \pi^o\pi^o$ of about 0.8 %.

The final result of E731 is[12]:

$$\mathcal{R}(\varepsilon'/\varepsilon) = (0.74 \pm 0.52 \pm 0.29)\times 10^{-3} = (0.74 \pm 0.59)\times 10^{-3}$$

Table 4: Systematic uncertainties (%) in R for E731 data.

Acceptance	± 0.071
Accidentals	± 0.064
Background to $\pi^o\pi^o$	± 0.036
Background to $\pi^+\pi^-$	± 0.018
Regenerator scattering	± 0.050
Regenerator anti-counter position	± 0.031
Trigger plane effects	± 0.073
Beam scattering	± 0.018
Energy calibration	± 0.096
Statistical error on data samples	± 0.28

The combined uncertainty is similar to the one of NA31, and the two results differ by 1.7σ. Furthermore, E731 is well compatible with absence of direct CP violation.

4 Experiments in preparation

From the results discussed above, we see that despite the high accuracy obtained by two experimental groups during the last five years, still there is no clear evidence about the existence of direct violation at the level predicted by the Standard Model.

New measurements are now in preparations. In the following sections, we shall discuss the main characteristics of two projects at fixed target facilities which represent upgrades of the programs discussed above. We shall also review the basic aspects of a novel technique which will be applied here in Frascati.

4.1 Experiment FNAL/KTEV–E832

This project[13] will continue the activity at Fermilab, maintaining several characteristics of E731. New beams will be used, with higher flux and lower background. A new calorimeter made with bars of CsI crystals will improve the resolution of the energy measurement. This will allow a better decay vertex resolution and a reduction in background. The new detector will be capable of running at intensity five times larger than E731 with improved lifetime ratio. Simultaneous data collection in the four channels is planned.

Table 5[13] shows the expected corrections and uncertainties in the double ratio, compared to those of E731, at a preliminary stage of the analysis. The combination of statistical and systematic error should provide a total uncertainty of $\pm 1 \times 10^{-4}$ in $\mathcal{R}(\varepsilon'/\varepsilon)$.

Table 5: Corrections (%) and uncertainties in R estimated for E832.

	E731	E832
Background $\pi\, e\, \nu$	0.32 ± 0.014	0.03 ± 0.005
Background $\pi^o\pi^o\pi^o$	0.45 ± 0.03	0.02 ± 0.01
Cross-over	4.66 ± 0.07	0.35 ± 0.01
Incoherent regeneration $(\pi^o\pi^o)$	2.58 ± 0.05	1.0 ± 0.01
Accidental effects $(\pi^o\pi^o)$	0.07 ± 0.05	± 0.01
Accidental effects $(\pi^+\pi^-)$	± 0.04	± 0.01
Energy scale	± 0.10	± 0.02
Acceptance charged	± 0.05	± 0.02
Acceptance neutral	± 0.05	± 0.02
Total	± 0.17	± 0.04

4.2 Experiment CERN/NA48

The program of NA31 at CERN is continued by NA48[14]. The experiment will make use of new beams, with 10 times higher intensity in K_L's. The production angle of the two beams will be different in order to minimize the difference in the momentum spectrum of the decays. At the upstream end of the decay volume, the two beams will be 7 cm apart, and they will converge to the same point at the electromagnetic calorimeter. Data collection will be simultaneous in the four channels. This will prevent from the use of a movable K_S station as in NA31. In order to maintain a good cancellation of the difference in acceptance due to the different decay regions, this experiment plans to apply a statistical weight to the K_L decays, defined as:

$$w_L(z,P) = \exp\left[-\frac{z\, M_K}{P}\left(\frac{1}{\tau_S} - \frac{1}{\tau_L}\right)\right]$$

where P is the kaon momentum.

Higher rates will be handled, with reduced sensitivity to accidentals, by improving the time response and the granularity of the apparatus. In particular, the electromagnetic calorimeter will be a new device, made with liquid Krypton, and read-out with longitudinal electrode structure and initial current technique.

The assignment of K_L or K_S tag to each decay will be made by means of two sets of small scintillator counters (*tagger*), placed on the primary (K_S) beam line, which will identify a decay as K_S if a proton signal is in coincidence, within a few ns, with the event measured by the main detector. Tagger inefficiency and accidental coincidences will not represent a serious systematic uncertainty, since they can be accurately monitored, and they can only dilute the value of $|\mathcal{R}(\varepsilon'/\varepsilon)|$. However, great care must be taken in controlling possible differences in the time response of the main detector between charged and neutral decays.

Table 6 shows the expected corrections and uncertainties in the double ratio, compared to those of NA31. Notice the large improvements in the background.

Table 6: Corrections (%) and uncertainties in R estimated for NA48.

	NA31	NA48
Background $Ke3$	0.9 ± 0.15	$(0.2\text{–}0.3) \pm 0.03$
Background $\pi^o\pi^o\pi^o$	3.2 ± 0.16	$(0.02\text{–}0.03) \pm 0.03$
Accidental effects	± 0.23	± 0.02
Energy scale	± 0.14	± 0.07

For $\pi^+\pi^-$ decays, the background is reduced mainly because of the use of a magnetic spectrometer; for $\pi^o\pi^o$, the improvement is due to the better energy resolution, and to the choice of a smaller decay fiducial volume. In fact, the large majority of $K_L \to \pi^o\pi^o\pi^o$ events simulating a $\pi^o\pi^o$ decay will be apparently shifted downstream of the fiducial volume.

The statistical accuracy should be three times better than in NA31, and the combined uncertainty expected for $\mathcal{R}(\varepsilon'/\varepsilon)$ is $(1\text{–}2)\times 10^{-4}$.

4.3 Experiment KLOE at LNF/DAΦNE

In DAΦNE[15] the electrons and positrons of a double–ring accumulator annihilate at the formation energy of the Φ. The very high design luminosity of $1\times 10^{33}\mathrm{cm}^{-2}\mathrm{s}^{-1}$ allows the study of monochromatic K^+–K^- and K_L–K_S pairs with statistical samples as large as 1×10^{10} per year. The search for direct violation of CP is considered as the major physics goal of the project. In the following, we shall review some aspects concerning the measurement of ε'/ε, and some characteristics of the experiment KLOE.

At a *Φ–factory*, kaons are produced with 110 MeV/c momentum, and the average decay pathlengths are 0.6 cm for K_S, and 350 cm for K_L. The most straightforward technique to measure direct violation is to collect samples of K_L and K_S decays, and to measure the fractions $\mathrm{BR}(K_L \to \pi^o\pi^o)/\mathrm{BR}(K_L \to \pi^+\pi^-)$, $\mathrm{BR}(K_S \to \pi^o\pi^o)/\mathrm{BR}(K_S \to \pi^+\pi^-)$, before combining them in the double ratio. The decaying particles are properly identified by the partner. For K_L, this is done choosing events with a $\pi^+\pi^-$ decay with pathlength <2 cm, which selects K_S's in a frequent decay. Conversely, a K_S is tagged by a K_L decay to $\pi^+\pi^-\pi^o$, $\pi\mu\nu$ or $\pi e\nu$ with pathlength >20 cm.

The statistical accuracy in measuring $\mathcal{R}(\varepsilon'/\varepsilon)$ is determined by the size of the fiducial volume for K_L decays. If pathlengths as long as 150 cm are used, a

resolution of about $\pm 1 \times 10^{-4}$ can be achieved in 1×10^7s of data collection at full luminosity.

Concerning systematic uncertainties, notice that tagging inefficiencies cancel out in the ratios defined above. The major systematic uncertainties are due to limited space resolution in the decay vertex reconstruction and loss of events outside the fiducial volume. This inefficiency is different for the four processes entering the double ratio. The problem should be solved with a vertex resolution of ≈ 1 cm, and by studying the response of the detector to $K^{\pm} \to \pi^{\pm}\pi^o$ events[16].

It is remarkable that a Φ–factory is suited for other studies in the K^o–$\overline{K}^o$ system, which exploit the correlation between kaons, due the well defined quantum numbers of the initial state[17]. At formation, the two kaons, with momentum $\vec{p}$ and $-\vec{p}$, are described by:

$$\frac{1}{\sqrt{2}} \left[K^o(\vec{p}) \overline{K}^o(-\vec{p}) - \overline{K}^o(\vec{p}) K^o(-\vec{p}) \right] =$$

$$= \frac{1 + |\varepsilon|^2}{\sqrt{2}(1 - \varepsilon^2)} \left[K_L(\vec{p}) K_S(-\vec{p}) - K_S(\vec{p}) K_L(-\vec{p}) \right]$$

Consider the decay into $\pi^o\pi^o$ of the kaon with momentum $\vec{p}$, occurring at time t_1, together with the decay of the recoiling kaon, at time t_2, into a $\pi^+\pi^-$ final state. The amplitude of the double process is given by:

$$A(t_1^{00}, t_2^{+-}) = \frac{1 + |\varepsilon|^2}{\sqrt{2}(1 - \varepsilon^2)} < \pi^o\pi^o | K_S > < \pi^+\pi^- | K_S > \times$$

$$\times \exp\left(-i\frac{\mu\, t}{2}\right) \left[\eta_{00} \exp\left(-i\frac{\Delta\mu\, \Delta t}{2}\right) - \eta_{+-} \exp\left(+i\frac{\Delta\mu\, \Delta t}{2}\right) \right]$$

where the notation is: $\Delta\mu = \Delta M - i\Delta\Gamma/2 = \mu_S - \mu_L$, $\mu = \mu_S + \mu_L$, $\Delta t = t_2 - t_1$, $t = t_1 + t_2$.

For vanishing $\Delta t \to 0$, the amplitude is proportional to $\eta_{00} - \eta_{+-} = -3\varepsilon'$; for large, positive Δt (implying $t_2 \gg 1/\Gamma_S$) the amplitude is proportional to $-\eta_{+-} = -\varepsilon - \varepsilon'$, and for large negative Δt ($t_1 \gg 1/\Gamma_S$) the amplitude is proportional to $\eta_{00} = \varepsilon - 2\varepsilon'$. In the first case, the process is purely due to direct CP violation, but unfortunately its smallness makes it practically undetectable. In the other two cases, direct violation is enhanced by interference with indirect violation, and $\mathcal{R}(\varepsilon'/\varepsilon)$ can be measured.

In the region $|\Delta t| = (1\text{–}10)\tau_S$, interference between the two components of the amplitude allows to extract $\mathcal{I}(\varepsilon'/\varepsilon)$[17], although the relatively narrow range in Δt implies a statistical error much larger than the one for the real part.

In order to factorize the $|\varepsilon|^2$ coefficient in the decay probability, one must normalize the observed rate to that of a similar process. For instance, one may

compare the sample observed in a given interval in t, Δt with the one collected in the same interval in t but opposite in Δt, *i.e.* choosing the case with inverted time relation between neutral and charged decays. But one could also normalize the events counted in the process $\pi^o\pi^o - \pi^+\pi^-$ with those observed in $\pi^+\pi^- - \pi^+\pi^-$ or in $\pi^o\pi^o - \pi^o\pi^o$. For each choice, a different combination of $\mathcal{R}(\varepsilon'/\varepsilon)$ and $\mathcal{I}(\varepsilon'/\varepsilon)$ can be extracted, which depends on the integration interval in t and Δt[17].

Clearly these different possibilities will be statistically correlated, and the ultimate statistical sensitivity in $\mathcal{R}(\varepsilon'/\varepsilon)$ will not be better than the one obtained with approach based on tagged decays, described above. However, the systematic uncertainties will affect differently the various observable quantities, and this will facilitate the delicate process of understanding the detector performance.

Tight requirements on the accuracy of pathlength reconstruction and in background rejection are placed on the detector. The KLOE collaboration[16] will study K_S decays and K_S–K_L interference inside the beam pipe (8 cm radius), and study the decays of K_L's in a fiducial volume with outer radius equal to 150 cm. This is inside the main drift chamber, with radius of 200 cm, located in a magnetic field of 0.6 T. The calorimeter will be a sampling device made of scintillating fibers and lead. The main requirements placed on photon detection are efficiency down to 20 MeV, full geometrical acceptance, and measurement of the conversion with space resolution of ≈ 1 cm and timing resolution of ≈ 0.1 ns. The spatial information will be used in a global fit to compute the coordinates of the decay vertex with the required resolution of ≈ 1 cm, which will be independently confirmed by the timing information.

5 Conclusion

At the end of this review, I shall recall the status of our knowledge on CP violation. Over thirty years, several generations of experiments have studied the K_S–K_L system, obtaining accurate measurements of the mixing parameter ε. However, even the latest results, which have reached accuracy of ± 0.004 in the double ratio, have not bee able to answer the question about the existence of direct violation of CP symmetry.

The situation is not satisfactory for two reasons. On one side, the two most accurate experiments have presented results which are barely compatible one to the other: NA31 with $\mathcal{R}(\varepsilon'/\varepsilon) = (2.3 \pm 0.7) \times 10^{-3}$ still favours the existence of direct violation, while E731 with $(0.74 \pm 0.59) \times 10^{-3}$ still casts some doubts on it. On the other side, the weighted upper limit $\mathcal{R}(\varepsilon'/\varepsilon) < 3 \times 10^{-3}$ at 95 % C.L. is not satisfactory, because it does not rule out the possibility that direct violation may exist at a level in agreement with the Standard Model. It must be recalled that

during the last dozen of years, while the experimental uncertainty was decreasing because of better techniques, the prediction of the effect was decreasing too, due to higher expectations for the mass of the quark top.

The new measurements being prepared now may overcome this situation. This is because the interval between the lower and the upper, model dependent, bound in the top mass is becoming smaller[18], and because the new experimental projects described above promise significant improvements over the accuracy reached so far. The CERN result suggests that direct CP violation may be just at the current experimental limit. If this is the case, by the end of this decade its discovery should be clearly established. And we really hope that the next years will be successful for kaon experiments, because the next decade may be the one for studying CP violation in the heavier B^o system.

References

1. J.H. Christenson, J.W. Cronin, V.L. Fitch and R. Turlay, Phys. Rev. Lett. **13**, 138 (1964).
2. CPLEAR Collaboration, R. Adler *et al.*, Phys. Lett. **B286**, 180 (1992).
3. L. Wolfenstein, Phys. Rev. Lett. **13**, 562 (1964).
4. M. Kobayashi and K. Maskawa, Progr. Theor. Physics **49**, 652 (1973).
5. T.T. Wu and C.N. Yang, Phys. Rev. Lett. **13**, 380 (1964).
6. J.F. Donoghue, E. Golowich and B. Holstein, Phys. Reports **131**, 320 (1986).
7. M. Ciuchini, E. Franco, G. Martinelli and L. Reina, Phys. Lett. **B301**, 263 (1993) J. Heinrich, E.A. Paschos,J.-M. Schwarz and Y.L. Wu, Phys. Lett. **B279**, 140 (1992); A.J. Buras, M. Jamin, M.E. Lautenbacher and P.H. Weisz, Nucl. Phys. **B370**, 69 (1992); M. Lusignoli, L. Maiani, G. Martinelli and L. Reina, Nucl. Phys. **B369**, 139 (1992);
8. Particle Data Group, *Review of Particle Properties*, Phys. Rev. **D45**, p. VII.97 (1992).
9. H. Burkhardt *et al.*, Nucl. Instrum. Methods **A268**, 116 (1988).
10. H. Burkhardt *et al.*, Phys. Lett. **B206**, 169 (1988).
11. G. Barr,*New Results on CP Violation from the NA31 Experiment at CERN*, in Proc. Joint Int. Lepton-Photon Symp. and Europhys. Conf. on H.E.P., eds. S. Hegarty *et al.*, World Scientific, Singapore, 1992, Vol. I, p. 179.

12. L.K. Gibbons *et al.*, Phys. Rev. Lett. **70**, 1203 (1993).

13. K. Arisaka *et al.*, Fermilab, Illinois, UCLA, Chicago, Elmhurst, Osaka and Rutgers Collaboration, *KTeV Design Report*, Fermilab FN-580 (1992).

14. G.D. Barr *et al.*, Cagliari, Cambridge, CERN, Dubna, Edinburgh, Ferrara, Mainz, Perugia, Pisa, Saclay, Siegen, Torino and Vienna Collaboration, *Proposal for a Precision Measurement of* ε'/ε *in CP Violating* $K^\circ \to 2\pi$ *Decays*, CERN/SPSC/90-22 (1990).

15. G. Vignola *et al.*, *DAΦNE - Design Criteria and Project Overview*, in Proc. Workshop on Physics and Detectors for DAΦNE, ed. G. Pancheri, INFN-LNF, Frascati, 1991, p. 11.

16. The KLOE Collaboration: Bari, Frascati, Karlsruhe, Lecce, Napoli, Columbia, Perugia, Pisa, Roma I, Roma II, ISS-Roma, Stony Brook, Trieste/Udine, A. Aloisio *et al.*, *KLOE, A General Purpose Detector for DAΦNE*, INFN-Frascati, LNF-92/019(IR) (1992); *The KLOE Detector - Technical Proposal*, INFN-Frascati, (1993).

17. F.J. Botella, J. Roldán and J. Bernabéu, ε'/ε *at a* Φ*–Factory: the Double Ratio and Time Integrated Methods*, in Proc. Workshop on Physics and Detectors for DAΦNE, *ibid.*, p. 325; see also: *The DAΦNE Physics Handbook*, eds. L. Maiani, G. Pancheri and N. Paver, INFN-LNF, Frascati, 1992.

18. Particle Data Group, *ibid.*, p. VII.159.

Frascati Physics Series, Vol. 1 (1993)
HEAVY QUARKS AT FIXED TARGET
Frascati, May 31st – June 2nd 1993
(pp. 63–78)

THE STATUS OF D^0–$\overline{D^0}$ MIXING

M.V. Purohit
Princeton University, Department of Physics Joseph Henry Labs.,
Jadwin Hall P.O.Box 708, Princeton NJ 08544, (USA)

ABSTRACT

The experimental status of $D^0 - \overline{D^0}$ mixing is presented. Presently, the best limit comes from Fermilab experiment E691. The wrong sign signal $D^0 \to K^+\pi^-$ observed by CLEO II is presented along with its implications for E687 and the high-statistics charm experiment E791. The introduction covers recent developments in theoretical estimates of the mixing rate.

1 – Introduction

Second-order weak diagrams lead to mixing of K^0 and $\overline{K^0}$. This mixing has been observed and is well known. Similarly, with the discovery of new flavors the standard model allows for the mixing of the D^0 meson with the $\overline{D^0}$, of the $B^0{}_d$ with the $\overline{B^0}_d$ and of the $B^0{}_s$ with the $\overline{B^0}_s$. Mixing between the D^0 and the $\overline{D^0}$ is expected to be very small because of the close cancellation of the s and d quark masses. Assuming that the mixing is entirely due to a mass difference in the CP-eigenstates of the mesons, i.e., due to Δm as opposed to $\Delta\Gamma$, the rate for mixing can be expressed as

$$r \equiv \frac{\Gamma(D^0 \to \overline{D}^0 \to \overline{f})}{\Gamma(D^0 \to f)} = \frac{x^2}{2+x^2} \approx \frac{x^2}{2} \tag{1}$$

where

$$x \equiv \frac{\Delta m}{\Gamma} \tag{2}$$

The difference between the Kaon and D-meson cases is very striking[1]:

$$\frac{\Delta m_K}{m_K} \approx 7 \times 10^{-15} \qquad \frac{\Delta m_K}{\Gamma_K} \approx 1.0$$

$$\frac{\Delta m_D}{m_D} \approx 1.3 \times 10^{-17} \qquad \frac{\Delta m_D}{\Gamma_D} \approx 1.6 \times 10^{-5}$$

Thus, in the K^0- $\overline{K^0}$ system, mixing is large and can be used as a tool to probe CP violation. Also, because of phase space differences, $\Gamma_S >> \Gamma_L$ for neutral kaons which allows one to study mixing in greater detail. However the CP-eigenstates are a small fraction of the decays of the D^0 and hence $\Delta\Gamma$ is expected to be very small. $\Delta\Gamma$ may not be smaller than Δm though. Thus, in the standard model we expect that[1)]

$$r_{\text{mix}} \sim 10^{-7}$$

The extremely small rate of mixing expected in the D^0- $\overline{D^0}$ system can be exploited to probe physics beyond the standard model. For instance, models with a 4^{th} $-\frac{1}{3}$ quark (b') and reasonable mixing angles, e.g., $|V_{ub'}V_{cb'}| > 0.01$, predict significant mixing above $m_{b'} = 100\text{GeV}$. Of course, if such a scenario exists, mixing would be a sensitive probe of $m_{b'}$. These models also predict[2)]

$$FCNC \sim 10^{-9}(\text{B.R.}) \text{ for } D \to \mu^+\mu^-, \pi e^+ e^- etc.$$

and

$$\text{B.R.}\,(D^0 \to \rho\gamma) \quad \sim 10^{-8}$$

Similarly, Left-Right Supersymmetric models[3)] have large values of

$$\Delta m_D \sim 1 - 3 \times 10^{-12} \quad \text{GeV}$$

which is 4 – 5 orders of magnitude larger than the standard model and within the range of present experiments. These arguments lead to a great interest in studying D^0- $\overline{D^0}$ mixing.

However, a few years ago Wolfenstein[4)] and later Donoghue, Golowich, Holstein and Trampetić[5)] suggested that hadronic intermediate states such as K^+K^- and $\pi^+\pi^-$ common to both the D^0 and the $\overline{D^0}$ could induce mixing. Donoghue, Golowich, Holstein and Trampetić suggested that Δm_D could be as large as $\sim 10^{-15}$ GeV. Thus, mixing could be present at the $r = 10^{-4} - 10^{-3}$ level. If true, this mundane possibility would make observation or limits on D^0- $\overline{D^0}$ mixing less interesting.

This question was recently re-visited by Georgi[6)] who suggested that certain cancellations must occur among competing hadronic-intermediate-state diagrams. Using Heavy Quark Effective Theory (HQET) he suggested that the enhancement of the Standard Model r_{mix} is actually very modest.

More recently, Ohl, Ricciardi and Simmons[7)] worked out QCD corrections to the diagrams arising from the short distance physics. They found that Δm is enhanced by only a factor of 2 – 3 (using Georgi's approach). They conclude that

$$(\Delta m)_{\text{HQET}} \approx (0.9 - 3.5) \times 10^{-17} \quad \text{GeV}$$

for

$$m_s = 200 \quad \text{MeV}$$

This work renews the interest in D^0- $\overline{D^0}$ mixing as a probe of physics beyond the standard model.

2 – Early Limits on $D^0 - \overline{D^0}$ Mixing

2.1 BCDMS

CERN experiment BCDMS[8] used a 200 GeV muon beam incident on Carbon and looked for trimuon events where the two extra muons were both of the same sign. Two extra same sign muons would most likely arise from the semileptonic decay of a D-meson (either D^0 or D^+) followed by the semileptonic decay of a D^0 which had arisen from a $\overline{D^0}$ after mixing. 17 events were observed and 15.5±2.8 background events were expected from decays of hadrons produced in the shower. They concluded that

$$r_{\text{mix}} < 1.2\% \text{ at the } 90\% \text{ C.L.}$$

2.2 ARGUS

The e^+e^- experiment ARGUS[9] searched for events with 2 D^0's or with two $\overline{D^0}$'s. They used dE/dx and time-of-flight information for particle identification. Kinematic cuts and a mass constraint were applied to reduce backgrounds. They found 162 Right Sign (RS) events and No Wrong Sign (WS) events which implies that

$$r < \frac{2.3}{162} = 1.4\% \text{ at the } 90\% \text{ C.L.}$$

Of course, because of a lack of decay time information they could not state whether this was a limit on r_{mix} or on r_{DCSD}.

2.3 E615

The Fermilab experiment E615[10] used a 255 GeV pion beam on a tungsten target. Again, they looked for same-sign, high-mass ($m > 2.0$ GeV) $\mu^\pm\mu^\pm$ pairs. Assuming $\sigma_{c\bar{c}} \sim A^1$ they obtained

$$r_{\text{mix}} < 0.56\%$$

However, this limit could be substantially worse if $\sigma_{c\bar{c}}$ rises more slowly with A.

3 – e^+e^- vs. Fixed Target experiments

In the early days, e^+e^- experiments such as the ARGUS experiment just described and Mark III searched for decays of 2 D^0's or of 2 $\overline{D^0}$'s in the same event. Mark III[11] had 224 events with D^0 $\overline{D^0}$ and 3 events with $\overline{D^0}$ $\overline{D^0}$, D^0D^0. These three events involved decays to $K^+\pi^-$ with $K^+\pi^-\pi^0$ and to $K\pi\pi^0$ with $K\pi\pi^0$.

$$\Rightarrow \frac{\Gamma(\text{DCSD, Mixing})}{\Gamma(\text{Cabibbo Favored})} \approx 1.3\%$$

When the D^0- $\overline{D^0}$ pair is produced from ψ'' decays, as in the Mark III detector, coherence of the wavefunction prevents both D-mesons to decay into identical two-body final states if one decays via a DCSD decay. Whether two of the Mark III events are due to decay into three particles via a resonance is not clear. Combining the MARK III results with ARGUS's results would lead to a 0.75% rate for wrong sign decays due either to mixing or Doubly Cabibbo Suppressed Decays (DCSD's).

Although e^+e^- events are very clean due to the high signal to background ratio, the lack of luminosity and of precise lifetime information makes these experiments unsuitable for studies of D^0- $\overline{D^0}$ mixing. In contrast, fixed target experiments (such as E691, E687 and E791) produce charm copiously, and have a lifetime resolution of about 0.04ps, which is a factor of ten smaller than the D^0 lifetime. The low reconstruction efficiency is a problem however and D^0- $\overline{D^0}$'s are not always produced in pairs. Hence fixed target experiments use D^0's from D^{*+} decays and use the charge of the D^* decay pion to determine the flavor of the D^0 at birth. The flavor of the D^0 when it decays is determined from the charge of the Kaon:

$$\begin{aligned} D^{*+} \rightarrow D^0\,\pi^+ \quad & \text{Charge of pion} \\ K^-\pi^+ \quad & \text{tags flavor of D} \\ \cdot & \\ \cdot & \\ \cdot & \\ \overline{D^0} \rightarrow K^+\pi^- & \end{aligned}$$

This technique allows experiments to do away with the double-tagging requirement and is now used by the e^+e^- experiment CLEO II as well.

The major advantage of fixed target experiments lies in their ability to use lifetime information to classify wrong-sign events as due to DCSD decays, which have a normal exponential survival probability and due to mixing, which has a component which goes approximately as $t^2\exp(-t/\tau)$: If at $t = 0$ a D^0 is produced, the intensity of $\overline{D^0}$ as a function of time is given by

$$|<\overline{D}^0|D^0(t)>|^2 = \frac{\exp(-\Gamma t)}{4}\left\{(\Delta m)^2t^2 + \left(\frac{\Delta\Gamma}{2}\right)^2 t^2\right\} \qquad (3)$$

The $t^2 \exp(-t/\tau)$ nature of the time-dependence is unique and is used to separate the mixing signal from DCSD decays. In the more general case of interference with mixing one gets

$$| < \overline{D}^0 | D^0(t) > |^2 = \frac{\exp(-\Gamma t)}{4} \left[\left\{ (\Delta m)^2 t^2 + \left(\frac{\Delta\Gamma}{2} \right)^2 t^2 \right\} + (4 - 2\Delta\Gamma t)|\rho|^2 + 2\rho\Delta\Gamma t \right] \quad (4)$$

where ρ is the ratio of the DCSD amplitude to the Cabibbo-favored amplitude. Figure 1 illustrates the difference in time dependence due to mixing and DCSDs in the simplest case of no interference.

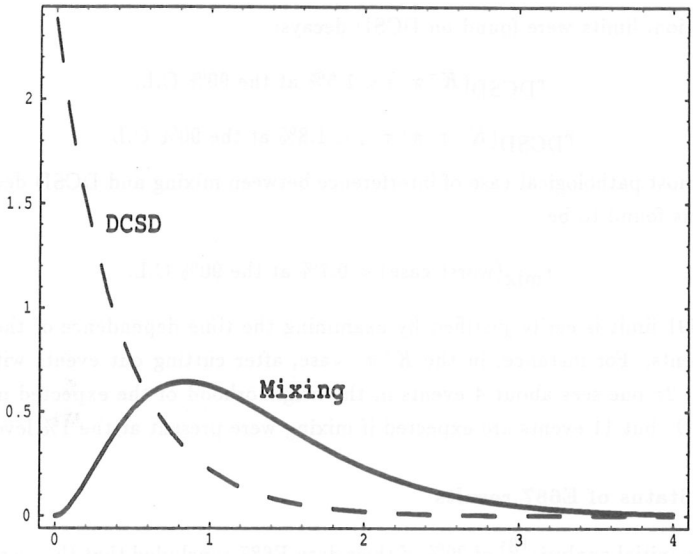

Figure 1: D-meson survival probability for wrong sign decays. Note that the mixed signal peaks at 2 lifetimes.

4 – The E691 limit

Experiment E691 at the Tagged Photon Lab. at Fermilab collected about 1800 clean D^0 decays where the D^0's were observed to come from D^{*+} decays. Of these 1800,

about 1100 were in the $K^-\pi^+$ mode and about 700 were in the $K^+\pi^-\pi^+\pi^-$ mode. We fit our right sign data to components including a signal component, D^0 mesons combining with random pions, D^* events where the D^0 decays to other modes such as the $K^-\pi^+\pi^0$ and a random combinatoric background. The wrong sign sample also has a signal component (with DCSD and mixing subcomponents), random combinatorics and a component in which D^0-mesons combine with random pions. The fits were unbinned maximum-likelihood fits and were done simultaneously to mass and lifetime. The result[12] in the simplest case of no interference was:

$$r_{\text{mix}} < 0.37\% \text{ at the } 90\% \text{ C.L.}$$

In addition, limits were found on DCSD decays:

$$r_{\text{DCSD}}(K^+\pi^-) < 1.5\% \text{ at the } 90\% \text{ C.L.}$$

$$r_{\text{DCSD}}(K^+\pi^-\pi^+\pi^-) < 1.8\% \text{ at the } 90\% \text{ C.L.}$$

In the most pathological case of interference between mixing and DCSD decays, the limit was found to be

$$r_{\text{mix}}(\text{worst case}) < 0.7\% \text{ at the } 90\% \text{ C.L.}$$

The E691 limit is easily justified by examining the time dependence of the wrong-sign events. For instance, in the $K^+\pi^-$ case, after cutting out events with decay times $< 2\tau$ one sees about 4 events in the neighborhood of the expected masses of the D, D^* but 11 events are expected if mixing were present at the 1% level.

5 – Status of E687 results

After an initial analysis[13] of 20% of their data E687 concluded that they would have $\sim$ 2500 very clean D^*'s from their full sample in the $K^-\pi^+$ mode (and a similar number in the $K^-\pi^+\pi^+\pi^-$ mode). At that point there was essentially no background in their data and therefore they expected their sensistivity to decrease as 1/n and reach a limit of 0.05%. However, they have since discovered the presence of backgrounds and choose to present results from only 10% of their sample pending completion of their analysis.[14] Figure 2 shows their data in the $K^+\pi^-$ and $K^+\pi^-\pi^+\pi^-$ modes and figure 3 shows the limit obtained. The limit from this subset is 0.6% at the 90% C.L. In the absence of mixing, this limit should improve as $1/\sqrt{n}$. At present they guess that their backgrounds consist of D^0's combining with random pions, charm remnants and secondary interactions. Paradoxically, the very low background makes it hard to conduct studies of the backgrounds in order to help reduce them. E687's data set must also contend with the wrong-sign signal seen by CLEO II (see below).

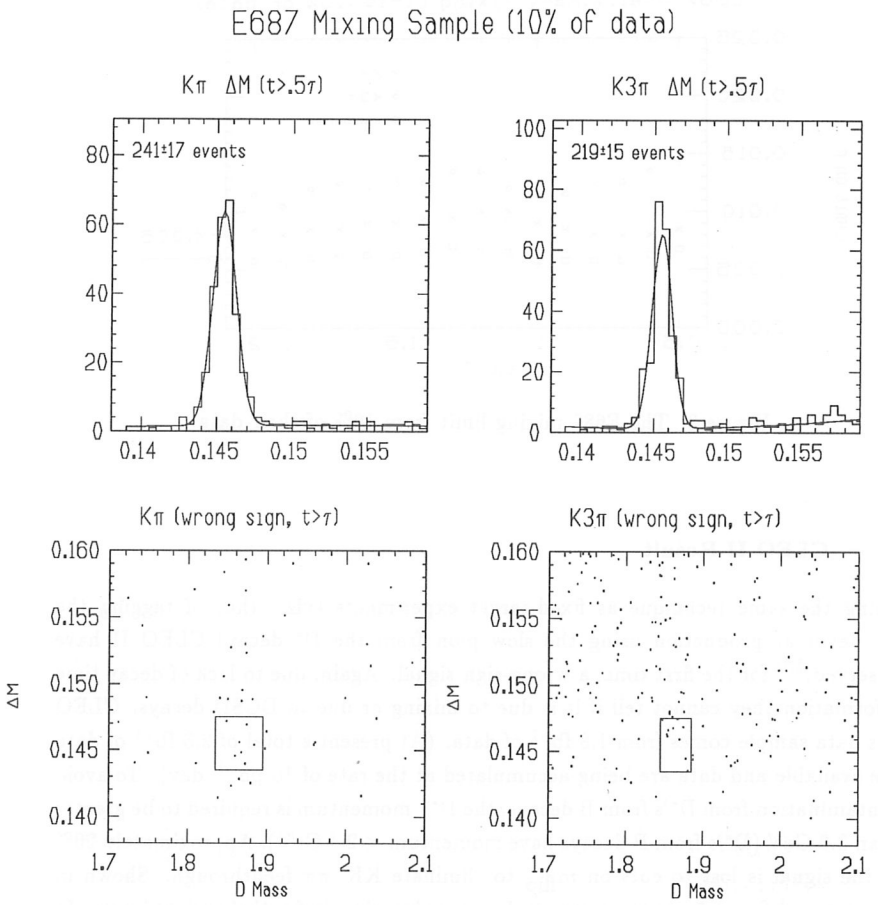

Figure 2: The E687 wrong-sign signals in the $K^+\pi^-$ and $K^+\pi^-\pi^+\pi^-$ modes from 10% of their data.

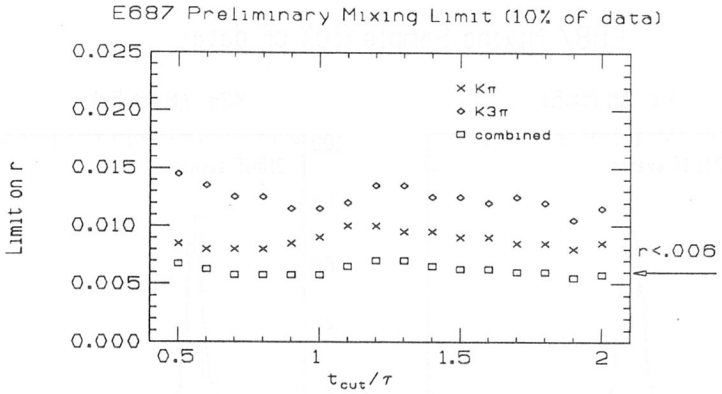

Figure 3: The E687 mixing limit from 10% of their data.

6 – CLEO II Result

Using the same technique as fixed-target experiments (viz. that of tagging the D^0 flavor at production using the slow pion from the D^* decay) CLEO II have observed,[15] for the first time, a wrong-sign signal. Again, due to lack of decay time information they cannot tell if it is due to mixing or due to DCSD decays. CLEO II's data sample comes from 1.8 fb^{-1} of data. (At present a total of 2.3 fb^{-1} of data are available and data are being accumulated at the rate of 10 pb^{-1}/day). To avoid contamination from D^*'s from B decays, the D^{*+} momentum is required to be greater than 3.0 GeV (D^*'s from B decays have momentum < 2.4 GeV). Approximately 20% of the signal is lost to cuts on m_{flip} to eliminate KK, $\pi\pi$ feedthrough. Shown in figure 4 and figure 5 are the right- and wrong-sign signals for their "tight" cuts. In figure 6 one sees that a sideband of the D^* Q-value histogram shows no peak at the D^0 mass. CLEO II concludes that

$$\frac{\Gamma(D^0 \to K^+\pi^-, D^0 \to \overline{D}^0 \to K^+\pi^-)}{\Gamma(D^0 \to K^-\pi^+)} = 0.77 \pm 0.25 \pm 0.25\%$$

When rewritten as a factor times $\tan^4\theta_c$, one obtains a rate of $(2.92 \pm 0.95 \pm 0.95) \times \tan^4\theta_c$. Earlier, E691 had obtained the limit $r_{\text{DCSD}} < 1.5\%$ @90% C.L. in the $K^+\pi^-$ mode.

7 – The Future for $D^0 - \overline{D^0}$ Mixing

The CLEO II result makes the entire subject of $D^0 - \overline{D^0}$ mixing very interesting. It really calls for a fixed target experiment to use its decay time resolution to decide whether the signal is

a) real and

b) due to DCSD or mixing.

What are the prospects for the fixed target experiments E687 and E791 deciding the issue? Without backgrounds E791, for instance, would achieve

$$r_{\text{mix}} < \frac{2.3}{6000} = 0.04\% \text{ @ } 90\% \text{ C.L.}$$

However, there are many backgrounds to these decays. Real backgrounds include:

- a) Combinatoric backgrounds
- b) Real D^0's with fake pions
- c) Real D^0's with real random pions
- d) DCSD decays
- e) Misidentified K^+K^-, $\pi^+\pi^-$ decays
- f) Doubly misidentified $K^-\pi^+$ decays

Of these known backgrounds a) and b) can be reduced by better tracking while e) and f) can be eliminated by a cut on m_{flip}. While backgrounds c) and d) are irreducible they have a $\exp(-t/\tau)$ time dependence compared to the $t^2\exp(-t/\tau)$ time dependence expected of a mixing signal. The experiments are working on these techniques.

One very interesting question can be asked: what is the gain in background reduction due to knowledge of the lifetimes? Of course, if mixing is present, such information will lead to a definite observation. However, if mixing is absent, how much does one gain from lifetime information? This question can be posed in statistics as follows:

If n wrong sign events are distributed according to an exponential density (due to DCSDs/Random pions) but are fit to DCSD + Mixing, i.e., to

$$(1 - r')\frac{\exp(-t/\tau)}{\tau} + r'\frac{t^2\exp(-t/\tau)}{2\tau^3} \tag{5}$$

what is the error on r'?

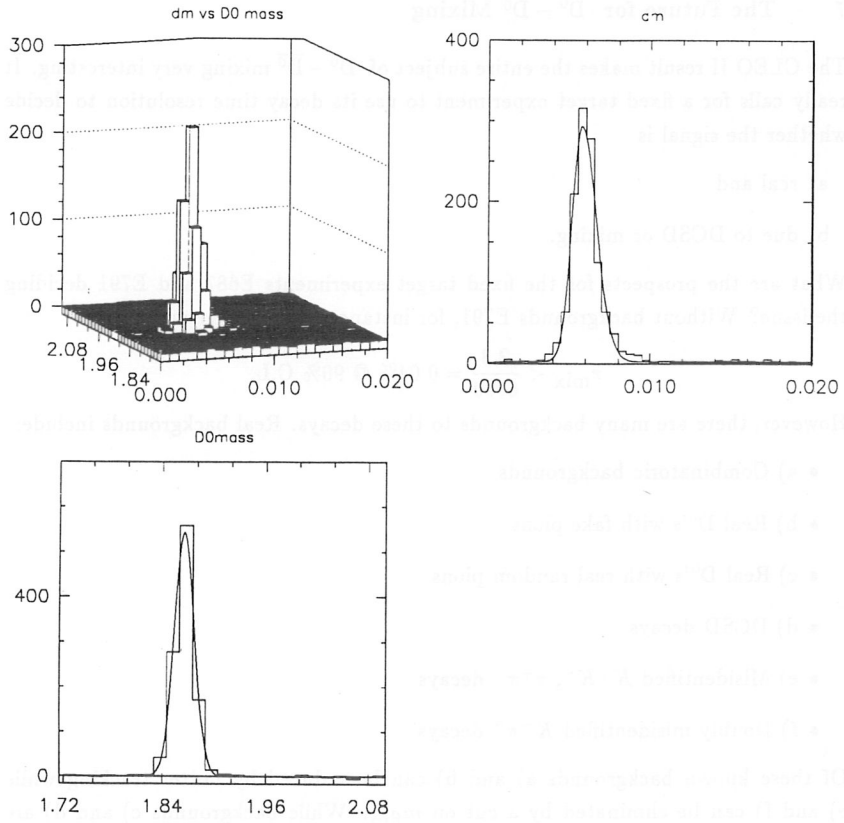

Figure 4: The CLEO II right-sign signal displayed as a function of the $K\pi$ mass and the Q-value in the D^* decay (called dm by CLEO II).

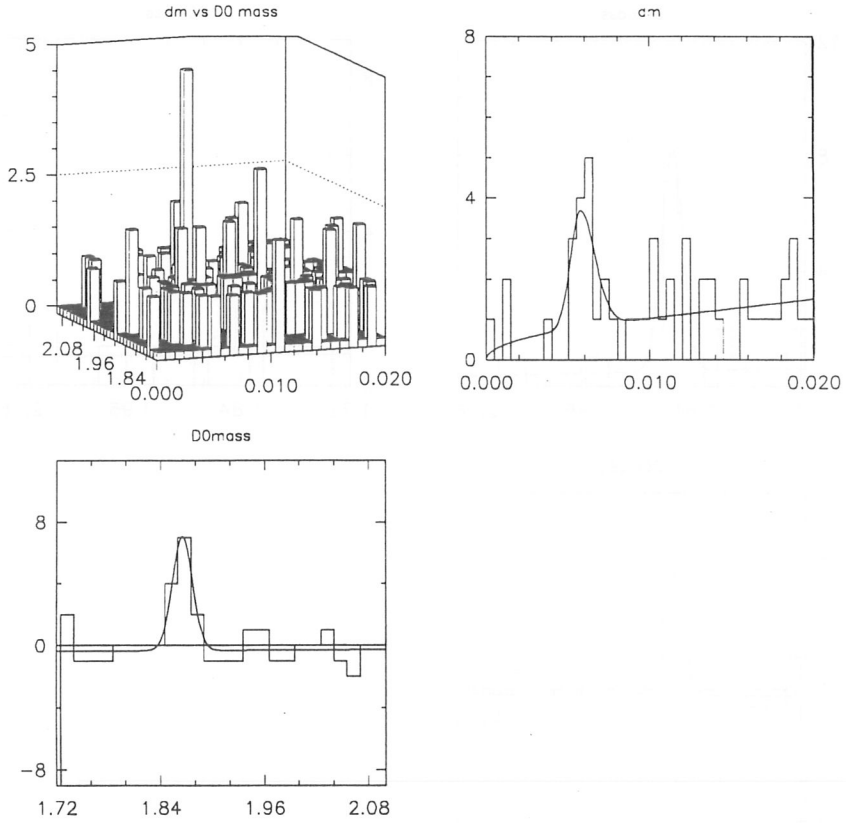

Figure 5: The CLEO II wrong-sign signal displayed as a function of the $K\pi$ mass and the Q-value in the D^* decay (called dm by CLEO II).

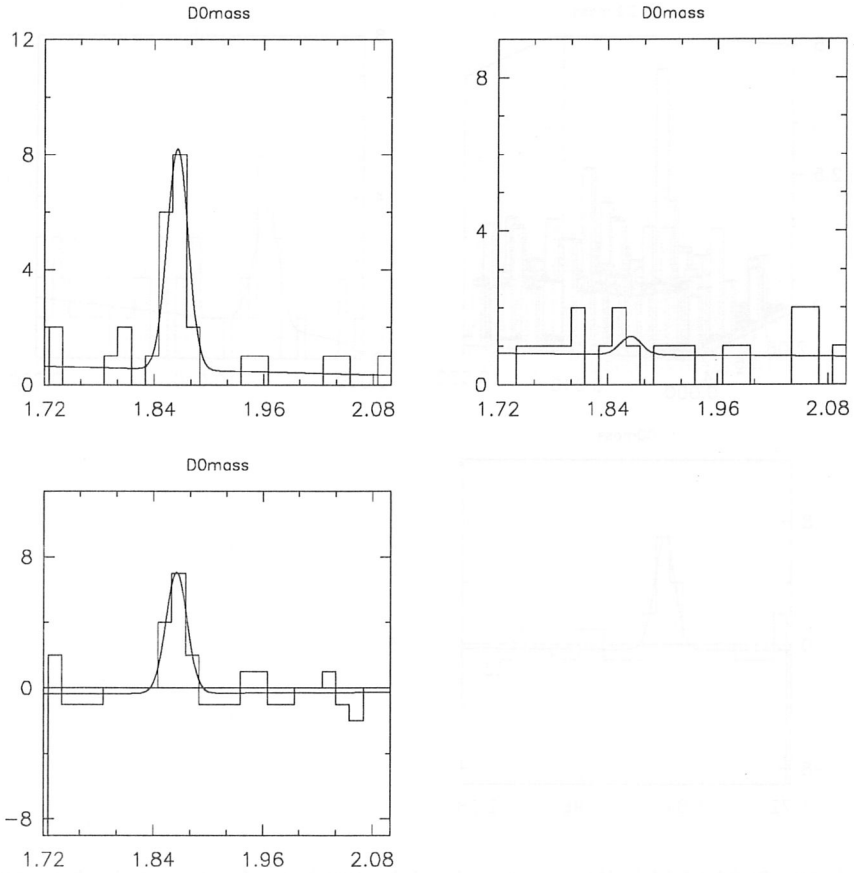

Figure 6: The CLEO II wrong-sign signal displayed as a function of the $K\pi$ mass. The top-left and top-right plots are slices at the expected Q-value and in a sideband. The bottom plot is the same as the top-left except for background subtraction.

A straight-forward maximum likelihood analysis reveals that with no time information,

$$n\Delta r' \approx \sqrt{n} \qquad \text{(n large)} \tag{6}$$

while with decay time information,

$$n\Delta r' \approx \sqrt{n/5} \qquad \text{(n large)} \tag{7}$$

Thus we may conclude that fixed target experiments are sensitive to fluctuations in the tail of DCSD and random pion backgrounds but can use the time dependence to reduce such backgrounds by a factor of 5. We can now project the sensitivity of various experiments. Using the known amounts of right-sign signals expected for E691, E687 and E791, we can project that

E791	can do no better than	0.1%
E687		0.2%
E691		0.24%

(This assumes 1800 events in the right-sign from E691, 2500 from E687 and 6000 from E791: see figure 7).

The limits actually obtained will depend on control of other backgrounds ($\Rightarrow$ slightly worse) and/or on luck ($\Rightarrow$ fluctuations in DCSD bkgd. for $t > \tau$ can make the limit better or worse). E691, for instance, had an actual limit of

$$r_{\text{mix}} < 0.37\%$$

which is about 50% worse than the limit due to fluctuations in the DCSD signal alone. E687 might suffer more from fluctuations in the DCSD signal, while E791 should have sufficient statistics to be able to cleanly separate a mixing component, if any.

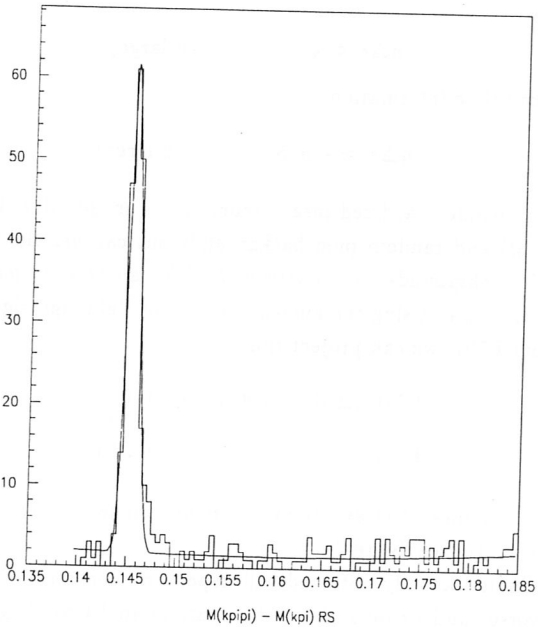

Figure 7: The E791 right-sign signal displayed as a function of the Q-value in the D^* decay from a small sample (about 5%) of our data set.

8 – Using Semileptonic Decays

As is well known, the semileptonic decays $D^0 \to K^- e^+ \nu_e$ etc. cannot be faked by DCSD decays. This leads to the possibility of a "background-free" observation or search for mixing and would lead to a $1/n$ dependence of the mixing limit. Unfortunately, even in the absence of a physics background, experimental limitations imply that there will be backgrounds. For instance, the D^0 + random pion background will presist. For comparison, E691 had serious backgrounds[16] in this mode. E691 observed $\sim$ 70 "clean" events and $\sim$ 190 "dirty" events on a background of 57 events. E791 would need $\sim$ 1500 very clean events to achieve as good performance as the $K^+\pi^-$ mode. One expects E791 to have no more than 500 such "clean" events, but perhaps more refined analysis techniques will improve this outlook.

9 – Conclusions

The current best limit on $D^0 - \overline{D^0}$ mixing remains the one from E691 ($r_{\rm mix} < 0.37\%$) which is still several orders of magnitude (in $r_{\rm mix}$) from the Standard Model prediction ($r_{\rm mix} \sim 10^{-7}$). This implies a big discovery window for new physics and requires us to pursue $D^0 - \overline{D^0}$ mixing studies assiduously. The new CLEO II observation of wrong-sign decays calls for fixed-target experiments to decide whether the signal is due to DCSD decays or due to mixing. Assuming that it is due to DCSD decays, one gets an irreducible background to mixing. The implications of this background are that E791 should be able to set a limit on $r_{\rm M}$ at the 0.1 – 0.15% level, depending on backgrounds, while E687 should get to the 0.2 – 0.3% level.

References

1. See, for instance, E. D. Commins and P. H. Bucksbaum "Weak Interactions of leptons and quarks", Cambridge University Press, New York, 1983.
2. K. S. Babu et al., Phys. Lett. **B205**, 540 (1988).
3. E. Ma, Mod. Phys. Lett. **A3**, 319 (1988).
4. L. Wolfenstein, Phys. Lett. **B164**, 170 (1985).
5. J. F. Donoghue et al., Phys. Rev. **D33**, 179 (1986).
6. H. Georgi, Phys. Lett. **B297**, 353 (1992).
7. T. Ohl, G. Ricciardi and E. H. Simmons, Nucl. Phys. **B403**, 605 (1993).
8. BCDMS: A. Benvenuti et al., Phys. Lett. **B158**, 531 (1985).
9. ARGUS: H. Albrecht et al., Phys. Lett. **B199**, 447 (1987).
10. E615: W. C. Louis et al., Phys. Rev. Lett. **56**, 1027 (1986).
11. Mark III: G. Galdding in the "Proceedings of the International Symposium on Production and Decay of Heavy Flavors, Stanford, CA 1987".
12. E691: J. C. Anjos et al., Phys. Rev. Lett. **60**, 1239 (1988).
13. Paul Sheldon in "Proceedings of the Physics in Collision Conference, 1992".
14. Ray Culbertson, Univ. of Illinois, private communication.
15. T. Browder, Cornell University, private communication.
16. J. C. Anjos et al., Phys. Rev. Lett. **62**, 1587 (1989).

SESSION III

- G. Ridolfi et al.
  Heavy–Quark Hadroproduction and Photoproduction: Theoretical Progress
- A.P. McManus
  Fixed Target Beauty Physics at FNAL
- D.M. Kaplan
  E789 and P865: High–Rate Fixed–Target Studies of Charm and Beauty
- G. Martellotti and M. Verzocchi
  Beauty Hadroproduction at CERN in Fixed Target Experiments

Frascati Physics Series, Vol. 1 (1993)
HEAVY QUARKS AT FIXED TARGET
Frascati, May 31st – June 2nd 1993
(pp. 81–97)

HEAVY-QUARK HADROPRODUCTION AND PHOTOPRODUCTION: THEORETICAL PROGRESS

Giovanni Ridolfi*
CERN TH–Division
CH-1211 Genève 23, (SWITZERLAND)

Stefano Frixione
Università di Genova, Dipartimento di Fisica, Sezione INFN
Via Dodecaneso 33, I-16136 Genova (ITALIA)

Michelangelo L. Mangano
INFN, Scuola Normale Superiore and Dipartimento di Fisica
P.za dei Cavalieri 7, I–56100 Pisa (ITALIA)

Paolo Nason†
CERN TH–Division
CH-1211 Genève 23, (SWITZERLAND)

Abstract

We present an analysis of charm and bottom production in fixed-target experimental configurations. We discuss inclusive distributions and correlations in the context of perturbative QCD at next-to-leading order, and we comment about additional higher order and non-perturbative effects.

1. Introduction

Heavy-quark production at high energies is a good testing ground for perturbative Quantum Chromodynamics, since the energy scale typical of the process is set by the heavy-quark mass m_Q, and therefore lies in a region where perturbation theory may be reliable. This is certainly true for the (yet undetected) top quark, whose mass is known to be above a hundred GeV. In fact, the search for the top depends on reliable estimated from perturbative calculations. Also for bottom production, perturbative QCD predictions are expected to give a reasonable description of experimental data. Next-to-leading order QCD cross sections have been compared to bottom production data collected by UA1 at CERN and by CDF at FNAL. The

*On leave of absence from INFN, Sezione di Genova, Genoa, Italy.
†On leave of absence from INFN, Sezione di Milano, Milan, Italy.

agreement is good for UA1 data, while there are some (as yet unexplained) discrepancies at the CDF energy (see ref. [1] for details and bibliography). The situation is more involved for charm production. Here, the mass of the heavy quark is not much larger than Λ_{QCD}, and therefore non-perturbative and higher-order effects are known to be important. On the other hand, a huge amount of experimental information is now available for charm production, especially from fixed-target experiments. Knowledge of the predictions of perturbation theory, together with the relevant theoretical uncertainties, can provide also in this case useful indications.

Inclusive distribution for heavy-quark hadroproduction at next-to-leading order have been computed by two different groups[2], whose results are in full agreement. In ref. [3] a calculation of fully exclusive distributions for heavy-quark hadroproduction at next-to-leading order was performed. The results of ref. [3] were then applied to fixed-target experimental configuration of current interest in ref. [4]. Photoproduction of heavy quarks has been first studied in ref. [5]. The same techniques of ref. [3] have then been applied to the photoproduction case[6,7], in order to obtain fully exclusive distributions. For details about the calculation, we refer the reader to refs. [3] and [7]. Here we will present and comment some of the results of refs. [4] and [6], with a particular accent on the theoretical uncertainties that affect QCD predictions in heavy-quark production.

2. Hadroproduction

We start with heavy-quark hadroproduction. According to the factorization theorem, the cross section for this process can be calculated in perturbative QCD by the formula

$$\begin{aligned} d\sigma_{H_1 H_2} &= \sum_{i,j} \int dx_1 dx_2 f_i^{H_1}(x_1,\mu_F) f_j^{H_2}(x_2,\mu_F) \\ &\quad d\hat{\sigma}_{ij}(x_1 P_1, x_2 P_2, k_1, k_2, m_Q, \mu_F, \mu_R, \alpha_S(\mu_R)), \end{aligned} \tag{2.1}$$

where H_1 and H_2 are the incoming hadrons with momenta P_1 and P_2 respectively, k_1 and k_2 are the momenta of the heavy quark and antiquark respectively, m_Q is the heavy-quark mass, and μ_R and μ_F are energy scales that refer to the subtraction of ultraviolet and collinear divergences respectively. Perturbative QCD gives a prescription for the computation of the partonic cross sections $d\hat{\sigma}_{ij}$ at any fixed order in perturbation theory. The parton densities $f_i^{H_{1,2}}$ are universal function, they can be

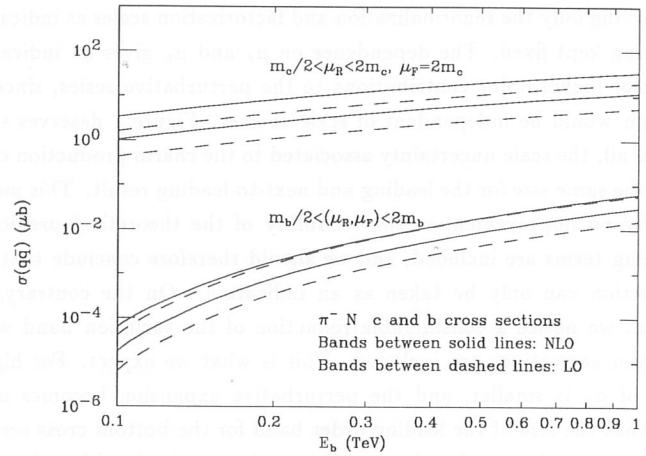

Figure 1: Total cross section at leading and next-to-leading order for charm and bottom production in $\pi^- N$ collisions as a function of the beam energy. We plot the range of variation for the scale changes indicated in the figure, for $m_c = 1.5$ GeV and $m_b = 4.75$ GeV and SMRS2-HMRS parton distribution sets.

extracted from one process and used to predict rates for another one. Equation (2.1) displays the major sources of uncertainty that affect the calculation: the knowledge of parton density function, the value of α_S (or equivalently of Λ_{QCD}, the value of the heavy-quark mass and the uncertainty connected to the truncation of the perturbative series. Furthermore, one has to take into account the uncertainty originating from non-perturbative phenomena like the formation of hadrons in the final state.

2.1. Total cross sections

We begin with total cross sections for charm and bottom production in pion-nucleon collisions (total cross sections for proton-nucleon collisions display very similar features). The cross sections have been computed using the parton distribution set HMRSB[8] for the nucleon and the central set SMRS[9] for the pion (see ref. [4] for a complete discussion of parton distribution dependence).

As an illustration of the reliability of the theoretical prediction we present in fig. 1 the leading (order α_S^2) and next-to-leading (order α_S^3) results for the total charm and bottom cross sections in pion-nucleon collisions. The bands in the figure

are obtained by varying only the renormalization and factorization scales as indicated, everything else being kept fixed. The dependence on μ_F and μ_R gives an indication of the importance of higher-order contributions to the perturbative series, since an all-order calculation would be independent of scale choices. Figure 1 deserves some comments. First of all, the scale uncertainty associated to the charm production cross section has about the same size for the leading and next-to-leading result. This means that there is nearly no improvement in the reliability of the theoretical prediction when next-to-leading terms are included, and we should therefore conclude that the predicted cross section can only be taken as an indication. On the contrary, for bottom production, we notice a considerable reduction of the variation band when next-to-leading order corrections are included. This is what we expect. For higher masses the value of α_S is smaller, and the perturbative expansion becomes more reliable. Observe that the size of the leading order band for the bottom cross section is not much smaller than the one for charm. This is due to the fact that, because of practical reasons, we did not try to study the factorization scale dependence in the case of charm production. The reader should therefore remember that a further uncertainty should be added to the charm result, and that the band shown in the figure is only an underestimate of the uncertainties involved in the computation of charm production cross sections.

In fig. 2 we summarize the effect of all the other sources of uncertainties, such as the structure function choice, the value of Λ_{QCD} and the mass of the heavy quarks. The bands shown in the figure refer to three different choices for the heavy-quark masses, and are obtained by varying the other parameters as follows. Factorization scales have been varied as in fig. 1. The value of Λ_{QCD} has been chosen in the range[10] $100 < \Lambda_4 < 300$ MeV, corresponding to $60 < \Lambda_5 < 204$ MeV, and the structure function have been varied among those of ref. [11].

For the charm cross section, as one can see, the value of the charm quark mass is a major source of uncertainty, with a factor of $8 - 10$ between the two extreme values of m_c. The corresponding variation in the bottom case are much more moderate.

Most of the considerations made in the case of the pion beam also apply to the case of protons. This is certainly the case for the large overall range of values allowed by the uncertainties of the calculation.

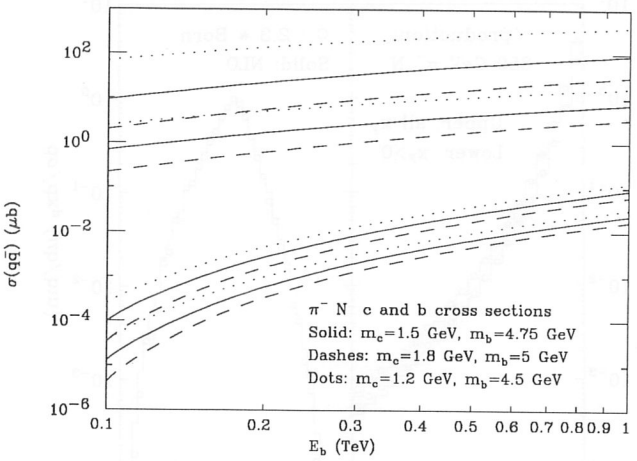

Figure 2: Total cross section for charm and bottom production in $\pi^- N$ collisions as a function of the beam energy. We plot the overall range of variation for changes in the parameters as discussed in the text, each band representing the result for a specified value of the quark mass.

2.2. Differential distributions

We now turn to single- and double-differential distributions for charm and bottom hadroproduction. All the distributions presented here have been computed using the parton distribution set HMRSB[8] for the proton and the nucleon and the central set SMRS[9] for the pion. The default values of the masses are $m_c = 1.5$ GeV and $m_b = 4.75$ GeV. The default values of the factorization and renormalization scales μ_F and μ_R are

$$\mu_F = 2\mu_0, \quad \mu_R = \mu_0 \tag{2.2}$$

for charm, and

$$\mu_F = \mu_0, \quad \mu_R = \mu_0 \tag{2.3}$$

for bottom, where

$$\mu_0 = \sqrt{m^2 + p_T^2} \tag{2.4}$$

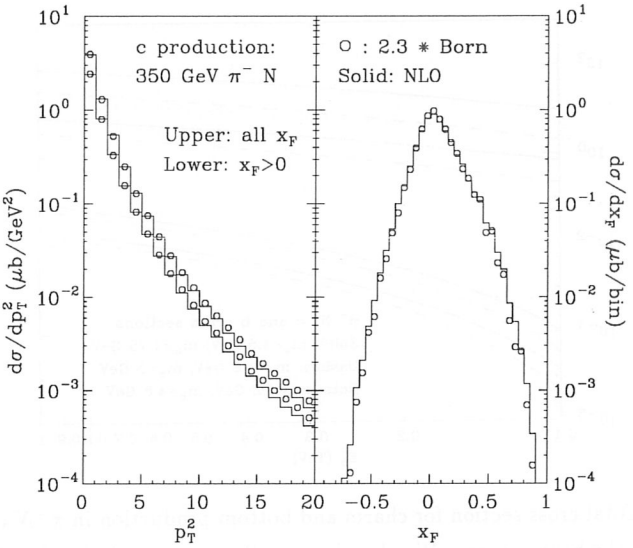

Figure 3: Charm inclusive $p_{\rm T}$ and x_F distributions in $\pi^- N$ collisions at 350 GeV.

for the one particle distributions, and

$$\mu_0 = \sqrt{m^2 + \frac{p_T^2 + \bar{p}_T^2}{2}} \tag{2.5}$$

for correlations.

1. Charm production with π^- Beam

We begin with one-particle inclusive rates. On the left side of fig. 3 we show the inclusive $p_{\rm T}$ distribution of c quarks in the case of 350 GeV π^- beams. The upper histogram represents the full NLO result. The lower histogram is obtained by imposing an $x_F > 0$ cut on the produced quark. The dots give the LO Born contribution (with or without the x_F cut) rescaled by a factor equal to the ratio of the integral of the NLO result to the integral of the Born result.

On the right hand side of fig. 3 we show the inclusive x_F distribution for the full NLO calculation, superimposed to the rescaled Born result. For both distributions in fig. 3 the higher order terms do not change significantly the shape of the curves.

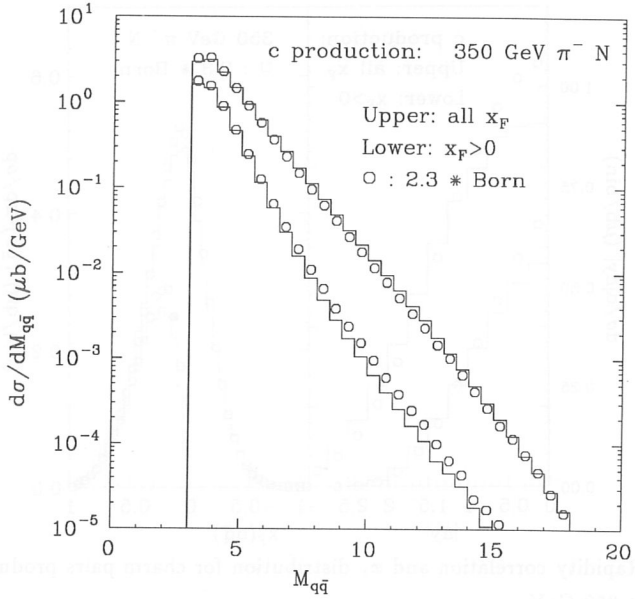

Figure 4: Invariant mass distribution of charm pairs produced in $\pi^- N$ collisions at 350 GeV.

Next we consider $c\bar{c}$ correlations. We start with distributions which are already non-trivial at the LO, namely the invariant mass of the heavy quark pair, the difference in rapidity between the quark and the antiquark and the x_F of the pair. These distributions are shown in figs. 4 and 5 for the case $E_b = 350$ GeV. As before, the upper lines represent the full result of the NLO calculation, while the dots are the rescaled Born results. The lower lines are obtained by imposing $x_F > 0$ for both quarks. As in the case of the inclusive distributions, no significant change in shape is noticed between the LO and the NLO results, but for the rapidity correlation, which is slightly broader at the NLO.

We now consider correlations which are trivial at the leading order, namely the difference in azimuth and total transverse momentum of the quark pair, $p_T^{Q\overline{Q}}$. At leading order these distributions are delta functions centered respectively at $\Delta\phi = \pi$ and $p_T^{Q\overline{Q}} = 0$. Higher order real corrections such as gluon radiation or gluon splitting processes smear them. We plot these distributions for $E_b = 350$ GeV in fig. 6. Even after the inclusion of higher order effects, the azimuthal correlation shows a strong

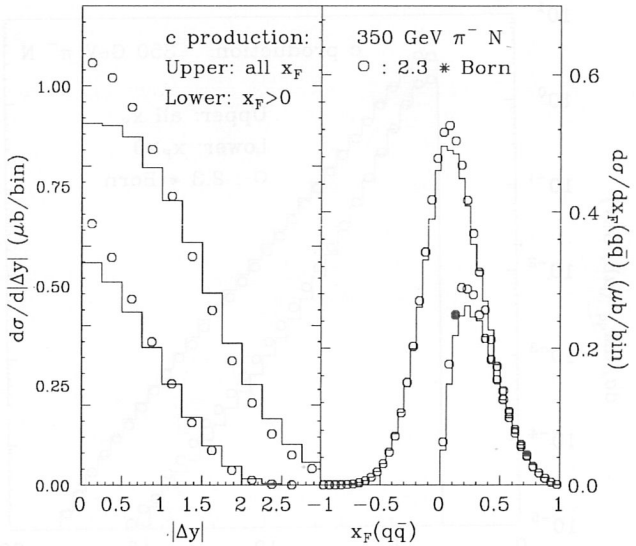

Figure 5: Rapidity correlation and x_F distribution for charm pairs produced in $\pi^- N$ collisions at 350 GeV.

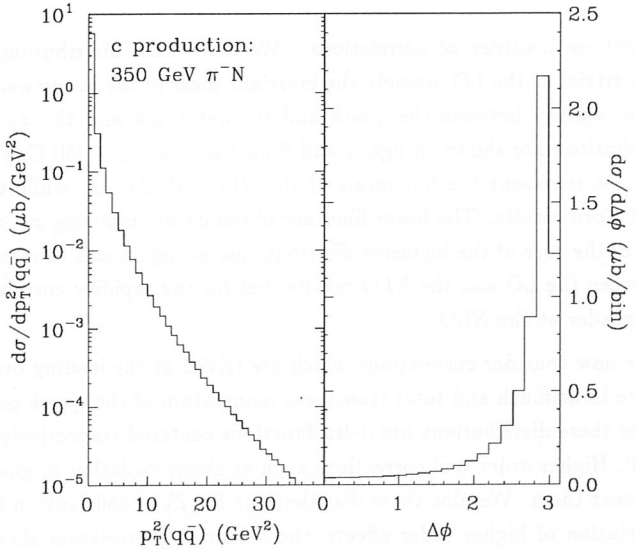

Figure 6: Charm pair $p_T^{Q\overline{Q}}$ and azimuthal correlation for $\pi^- N$ collisions at 350 GeV.

peaking for $\Delta\phi \approx \pi$. Likewise, the $p_T^{Q\overline{Q}}$ distribution is dominated by configurations with $p_T^{Q\overline{Q}}$ smaller than 1 GeV.

We verified that changing the PDF set among the three SMRS fits only affects the overall normalization but not the shape of either of the previous curves. The change in normalization is within 10%. Changing the values of the charm mass and renormalization scale μ_R results in small and easily predictable shape modifications.

In ref. [4] a comparison was made between charm production in pion-nucleon and in proton-nucleon collisions. It was found that total cross sections are similar at similar energies, but a comparison between distributions should rather be made at $E_\pi/E_p \approx 2/3$, a ratio consistent with the valence contents of pions and protons.

2. *Bottom production*

The differential distributions for bottom production in pion nucleon collisions are shown in figs. 7-9. The p_T^2 (single inclusive) and the $M_{Q\overline{Q}}$ distributions are broader than the corresponding distributions for charm production. They are however nar-

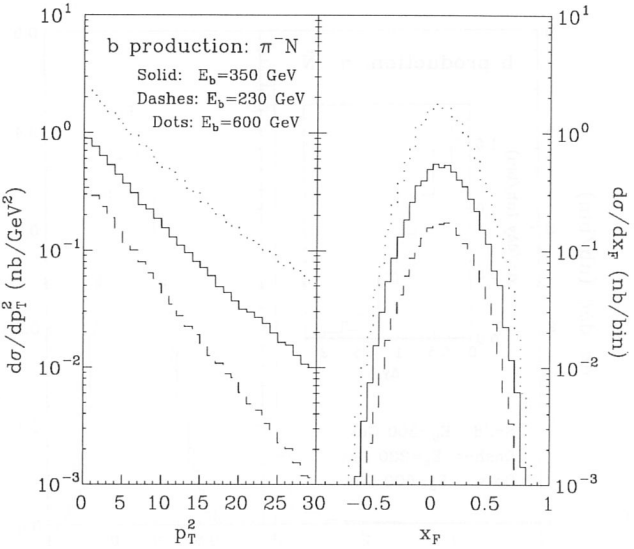

Figure 7: Bottom inclusive distributions in $\pi^- N$ collisions.

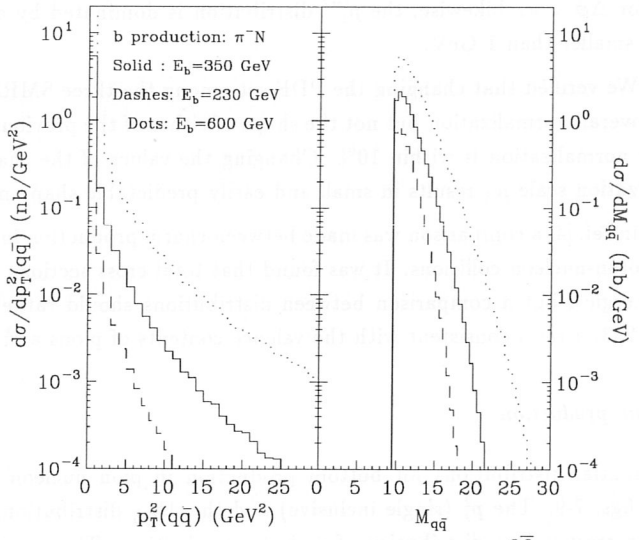

Figure 8: Bottom correlations in $\pi^- N$ collisions: $p_T^{Q\overline{Q}}$ and $M_{Q\overline{Q}}$.

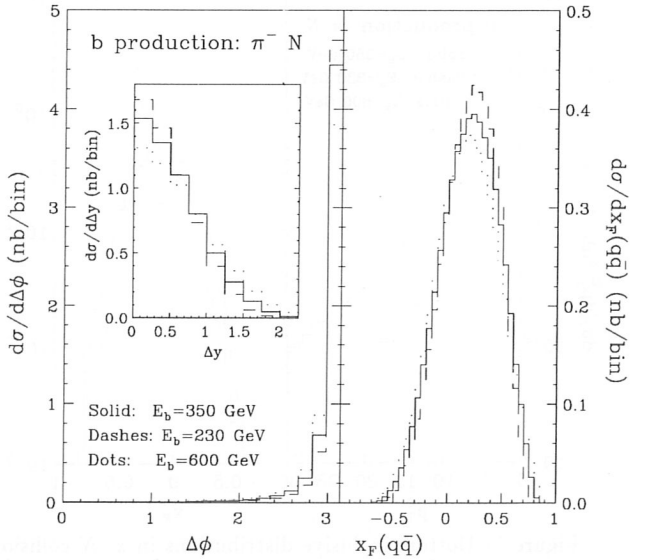

Figure 9: Bottom correlations in $\pi^- N$ collisions: $\Delta\phi$, Δy and $x_F^{q\bar{q}}$.

rower than one would expect on the basis of simple scaling arguments. This is because b production at fixed target energies is still too close to the threshold, and thus constrained by phase space effects (this can also be noticed from the strong energy dependence of the shape of the curves). For the same reason, the Δy distribution is narrower than in the charm case. The $p_T^{Q\overline{Q}}$ and the $\Delta\phi$ distributions are much narrower, which is a consequence of the smaller value of α_S at the b mass, and of the previously mentioned phase space constraints. The x_F distributions is harder for bottom than for charm, as appropriate for the production of a heavier object.

2.3. Higher Order Corrections and Hadronization

The results we have presented were obtained using an exact calculation of the heavy-quark production matrix elements up to the order α_S^3 in perturbation theory. No exact calculation beyond this order is available at present. In this section, we will discuss the effect of higher-order terms on the distributions shown previously. To do this, we will use an approach alternative to the calculation of matrix elements in fixed order perturbation theory, namely the shower Monte Carlo approach[12]. In this approach the partons from a hard collision process are evolved via emission of gluon and quark radiation until some small momentum scale is reached, where confinement forces take over and give rise to the formation of hadrons. We will use the Monte Carlo program HERWIG[13]. In HERWIG, the spectrum of radiation is governed by perturbative QCD and incorporates emission probabilities calculated resumming to all orders leading and next-to-leading collinear and soft logarithms[14]. This perturbative evolution stops when the virtuality of the partons has decreased to a value of the order of one GeV. At this scale QCD interactions become strong and a cluster hadronization model is used to form the hadrons.

We will consider charm production in 800 GeV pN collisions. Since the generation of the hard process is done in HERWIG using the leading order matrix elements, the K factor which we find between the LO and full NLO cross sections have been put in by hand. All of the distributions presented will therefore have the HERWIG curves rescaled to the partonic NLO result.

In fig. 10 we show the inclusive p_T and x_F distributions. The p_T distribution of charmed quarks is harder in HERWIG's case (dotted curve). After the hadronization of the charm quark and the strong decay of the resonant state which might have formed (*e.g.* a D^*), one would expect a softening of the p_T spectrum due to the energy lost during the process. This is indeed the case, as illustrated by the dashed line in fig. 10 which represents the p_T spectrum of the stable hadrons. The result-

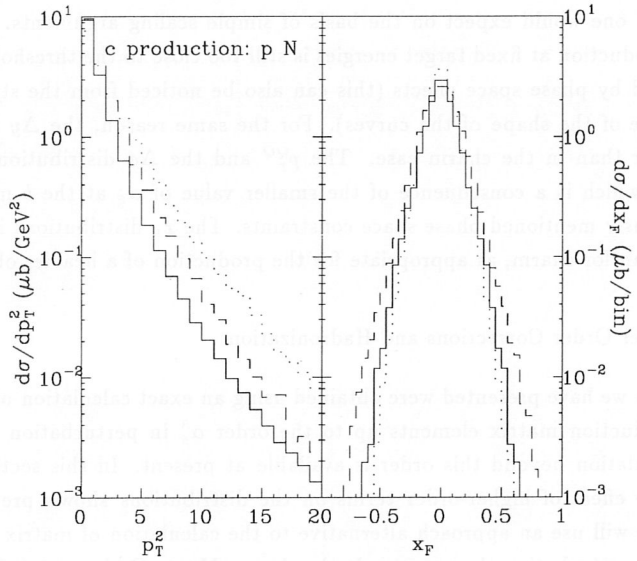

Figure 10: Comparison between HERWIG and the $\mathcal{O}(\alpha_s^3)$ result (solid) for inclusive distributions of charm in pN collisions at 800 GeV. For HERWIG we plot the variables relative to the charm quark before hadronization (dotted line) and relative to stable charm hadrons (dashed line).

ing distribution, nevertheless, is still slightly harder than the one predicted by the $\mathcal{O}(\alpha_s^3)$ calculation. Therefore, contrary to naive expectations, the non-perturbative and higher order effects incorporated in the Monte Carlo do not necessarily soften the p_T spectrum. The intrinsic transverse momentum of the incoming partons may compensate the effects of fragmentation at moderate p_T. Ultimately, at very large p_T the effect of fragmentation prevails (otherwise the factorization theorem would be violated). In fact, fragmentation effects rescale the p_T by a factor, while the intrinsic p_T of the partons simply smears the distribution uniformly. We have examined the effect of an intrinsic p_T on the LO parton distributions by giving the incoming partons a random p_T distributed according to

$$\frac{dN}{dp_T^2} \approx e^{-p_T^2/\langle p_T^2 \rangle}. \tag{2.6}$$

We find that with an intrinsic $\langle p_T^2 \rangle \approx 2 - 3$ GeV^2 we can reproduce the p_T spectrum of the charm quark given by HERWIG. We have verified that the origin of this high intrinsic p_T in HERWIG is the following. Heavy quark production always has a very

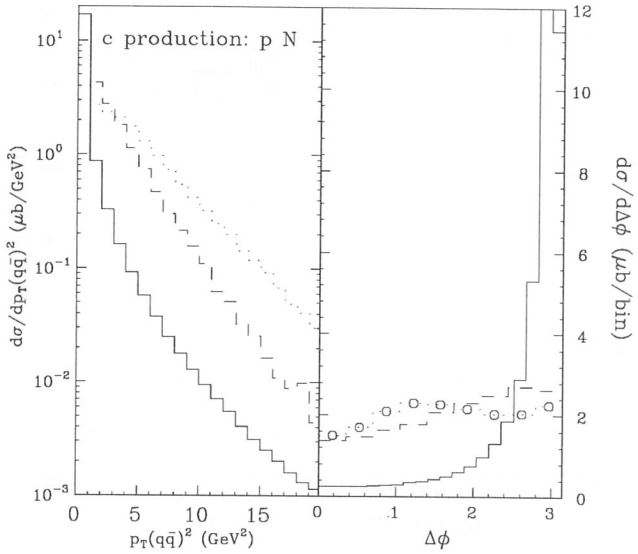

Figure 11: Comparison between HERWIG and the $\mathcal{O}(\alpha_s^3)$ result (solid) for inclusive distributions of charm in pN collisions at 800 GeV: $p_T^{Q\overline{Q}}$ and $\Delta\phi$ distributions. Different line patterns are explained in the previous figure's caption.

large gluon fusion component. In HERWIG an initial state space-like gluon is forced to originate from radiation off a valence quark. The radiation process has an infrared cut-off of the order of 1 GeV, and therefore the p_T of the initial state gluon is generally larger than 1 GeV. Because of the tail of this distribution, the average p_T turns out to be about 1.7 GeV, which is consistent with the number given above. Of course, this mechanism in HERWIG should just be viewed as a model for the intrinsic p_T of initial state gluons, and the 1 GeV cut-off is and adjustable parameter. Furthermore, since HERWIG was not tuned in this kind of processes, the 1 GeV value should just be taken as an indication.

In fig. 11 we show the $\Delta\phi$ and p_T distributions for the complete α_S^3 perturbative calculation, the HERWIG partonic result and the HERWIG result for the stable charmed hadrons. The HERWIG partonic results are much broader than the order α_S^3 ones. As in the case of the inclusive p_T distribution, we have verified that this effect is due to the previoulsly-mentioned gluon intrinsic p_T in HERWIG. In fact, we could reproduce similar effects by using the leading order production mechanism

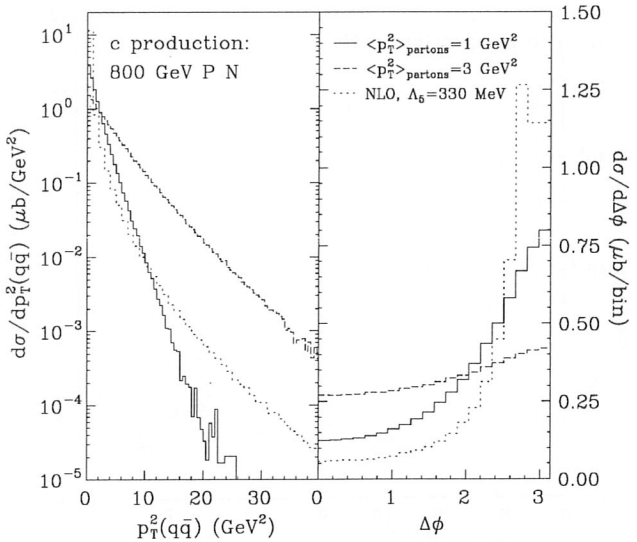

Figure 12: Effect of a non-perturbative p_T kick on the incoming partons compared with the $\mathcal{O}(\alpha_s^3)$ effect. The curves with a p_T kick are obtained with the Born cross section with HMRSB structure functions and $\Lambda_5 = 120\,\text{MeV}$, supplemented by a random p_T kick on the incoming partons. The NLO curves are obtained with the HMRSB structure functions and $\Lambda_5 = 330\,\text{MeV}$, and they were rescaled to the same normalization of the other curves.

supplemented with an intrinsic p_T of the incoming partons distributed as in eq. (2.6), with $\langle p_T^2 \rangle \approx 2 - 3\ \text{GeV}^2$. This is presented in fig. 12. The curves with an intrinsic $\langle p_T^2 \rangle = 3\ \text{GeV}^2$ match very well the HERWIG parton level result. For comparison, we also show curves with the more moderate value $\langle p_T^2 \rangle = 1\ \text{GeV}^2$, and curves with NLO effects (but no p_T kick) included. The value of $\langle p_T^2 \rangle = 3\,\text{GeV}^2$ seems rather high. As mentioned earlier, the cause of this large value is not physical, but it is rather a tunable feature of the Monte Carlo program. In view of the fact that the Monte Carlo program was not tuned in this region, we conclude that such a large intrinsic p_T does not have a sound justification. Theoretically, one would expect the p_T of the pair to arise from the combined effect of gluon radiation (the dotted lines of fig. 12) and of an intrinsic p_T of the incoming partons of the order of 1 GeV (dashed lines in the figure). From the figure we see that even with the most extreme choice for Λ, the

combination of these effects is still much more moderate than the effect of an average intrinsic p_T^2 of the order of 3 GeV^2 (solid line in the figure). We therefore expect that the data should be more peaked in the back-to-back region than predicted by Monte Carlo programs. If such a large intrinsic p_T was instead found to be consistent with the experimental data, we would have to conclude that in processes initiated by gluons (like heavy quark production), the intrinsic p_T is much higher than in processes initiated by quarks (like for example the Drell-Yan processes).

3. Photoproduction

The same technique of ref. [3] has been applied to compute distributions for photoproduction of heavy quarks[7]. In this case, one has to take into account two contributions to the cross section. In the first one, the photon is considered to be a pointlike object, while the second one accounts for the fact that the photon can behave as an hadron itself, with its own parton density fuctions. The parton density functions of the photon are very poorly known, and therefore sufficiently precise predictions in perturbative QCD can be made only in those kinematical regions where the hadronic component of the photon is negligible.

As an example of an application of double-differential formulae for heavy-quark photoproduction, we consider the possibility of extracting the gluon density of the proton from heavy-quark production at HERA. The details of the procedure are described in ref. [6]. Here we just present in fig. 13 a comparison between the pointlike and the hadronic contribution (computed with two extreme parametrizations of the photon parton densities) to a particular distribution, which is proportional to the gluon density in the photon. It can be seen that the hadronic component is indeed negligible in a wide range for the fraction x_g of the proton momentum carried by the incoming gluon.

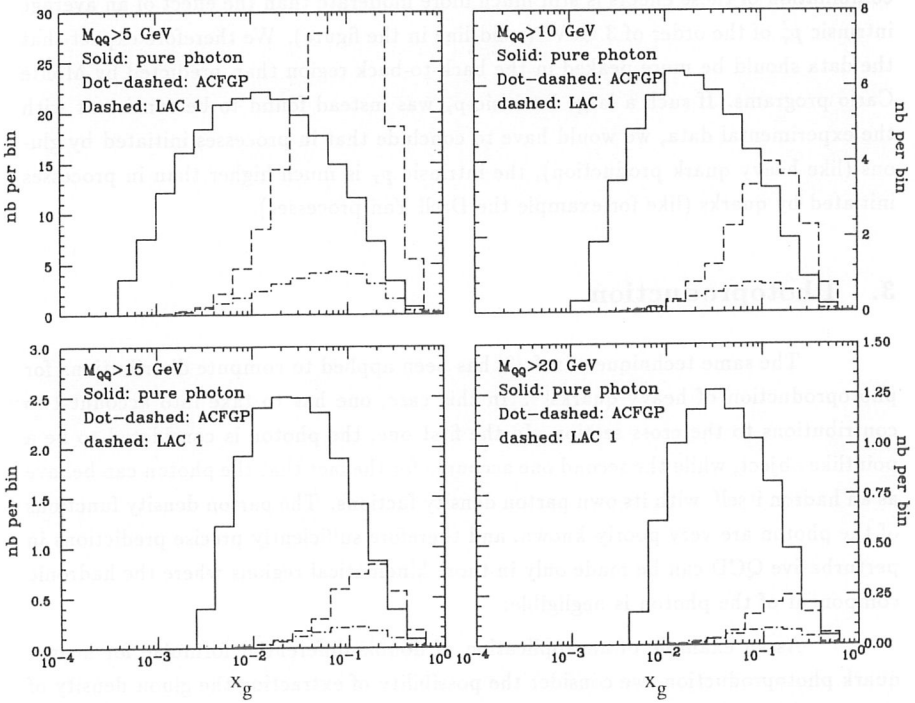

Figure 13: Contribution of the hadronic component of the photon, compared with the pure photon component, for two extreme choices of the photon structure functions.

References

[1] J.E. Huth and M.L. Mangano, preprint FERMILAB-PUB-93/19-E, to appear in Annu. Rev. Nucl. Part. Sci., vol. 43 (1993).

[2] P. Nason, S. Dawson and R. K. Ellis, *Nucl. Phys.* **B303**(1988)607; P. Nason, S. Dawson and R. K. Ellis, *Nucl. Phys.* **B327**(1988)49; W. Beenakker et al., *Phys. Rev.* **D40**(1989)54.

[3] M. Mangano, P. Nason and G. Ridolfi, *Nucl. Phys.* **B373**(1992)295.

[4] M. Mangano, P. Nason and G. Ridolfi, to appear in Nucl. Phys. B.

[5] R.K. Ellis and P. Nason, *Nucl. Phys.* **B312**(1989)551.

[6] S. Frixione, M.L. Mangano, P. Nason and G. Ridolfi, *Phys. Lett.* **B308**(1993)307;

[7] S. Frixione, M.L. Mangano, P. Nason and G. Ridolfi, preprint CERN-TH.6921/93 (1993).

[8] P.N. Harriman, A.D. Martin, R.G. Roberts and W.J. Stirling, *Phys. Rev.* **D42**(1990)798.

[9] P.J. Sutton, A.D. Martin, R.G. Roberts and W.J. Stirling, *Phys. Rev.* **D45**(1992)2349.

[10] G. Altarelli, CERN-TH. 6623/92.

[11] A.D. Martin, R.G. Roberts and W.J. Stirling, *Phys. Rev.* **D43**(1991)3648.

[12] B.R. Webber, *Annu. Rev. Nucl. Part. Sci.* **36**(1986)253.

[13] G. Marchesini and B.R. Webber, *Nucl. Phys.* **B310**(1988)461.

[14] See A. Bassetto, M. Ciafaloni and G. Marchesini, *Phys. Rep.* **100**(1983)201, and references therein.

Frascati Physics Series, Vol. 1 (1993)
HEAVY QUARKS AT FIXED TARGET
Frascati, May 31st – June 2nd 1993
(pp. 99–109)

FIXED TARGET BEAUTY PHYSICS AT FNAL

A.P. McManus
University of Virginia, Physics Department, Institute of Nuclear and Particle Physics, McCormick Road, Charlottesville VA 22901, (USA)

Abstract

A review of beauty (B) physics results from fixed target experiments at the Fermilab National Accelerator Laboratory (FNAL) using published papers and other sources. B meson lifetimes from E653 and B cross sections at 600 GeV/c and 530 GeV/c from E653 and E672 are included with some preliminary results from E771 and E789 as well as expectations from future experiments at FNAL.

1 Introduction

At this time, few beauty (B) physics results have been presented by hadronic fixed target experiments primarily because the cross section for B production is low at current fixed target energies. The only published results from the FNAL fixed target program are from experiment E653 which operated in the 1988 FNAL fixed target run and collected 9 partially reconstructed B particle pairs[1,2] from an expected few hundred $b\bar{b}$ pairs produced during the run using a 600 GeV/c pion beam on an emulsion target and a one muon trigger. The relatively high percentage (~1-2%) of $b\bar{b}$ pairs reconstructed from the total number of $b\bar{b}$ pairs produced shows the promise of fixed target experiments and that an active target, which is unique to the fixed target environment, can be used to reconstruct complicated decay topologies. From the 1990 FNAL fixed target run E672 has collected 26 $B \rightarrow J/\Psi + X$ with some exclusive decays reconstructed[3,4]. In the 1991 fixed target run, E771 and E789, which are dedicated B experiments, took data for a portion of the total fixed target run and these data are now being analyzed. A clear progression of fixed target experiments with experience in extracting B physics is beginning to emerge and the results from E771[5] and E789[6,7] should be able to guide future experiments at FNAL.

The strength of fixed target experiments is the large Lorenz boost that the B particles have in the lab frame allowing determination of the B lifetime with good precision using silicon microstrip detectors. In addition, B baryons, B_S mesons and B_C mesons are created in hadronic interactions and can be observed and lifetimes measured. Fixed target experiments should give complimentary information to electron and Hadron colliders with strengths in B lifetime measurements and the ability to observe complicated B meson or B baryon decay topologies because of the Lorenz

boost. The ability of fixed target to distinguish complicated topologies will also aid in tagging B's for use in CP violation measurements.

Table 1: Fixed target B experiments

	E653	E672	E687 [8,9]
primary Experimental goals	Charm and Beauty decays	J/Ψ, χ	Charm
Beam energy	600 GeV	530,800* GeV	⟨221 GeV⟩
Beam/target	π^- / Emulsion	π^-,p* / Be,Cu,H*	γ / Be
Target (λ_I)	0.056 λ_I	0.136 λ_I	0.10 λ_I
Triggers	1μ	2μ	n_C>4 • E_{tot}>35 GeV
Interaction rate	6×10^2	4×10^5	2×10^2 hadronic
Geometry	open	open	open
total interactions	2.5×10^8	2×10^{11}	5×10^8
b pair produced	6×10^2	(Be targ) 2×10^5	10^3 -10^4
Run date	1988	1990,1991	1990,1991

	E771	E789	E791 [10]
primary Experimental goals	B decays into J/Ψ and μ	B decays into 2 body states	Charm
Beam energy	800 GeV	800 GeV	500 GeV
Beam/target	p / Si	p / Au	p^- / C,Pt
Target (λ_I)	0.041 λ_I	0.03 λ_I	0.072 λ_I
Triggers	1μ • P_t>0.8 GeV or 2μ	2μ or 2e or 2h or any 2 μ,e,h	n_C>4 Σ E_t>X**
Interaction rate	2×10^6	4×10^7	1×10^5
Geometry	open	**2 arm**, 20-60mR	open
total interactions	1×10^{12}	4×10^{13}	5×10^{10}
b pair produced	2×10^6	1×10^8	1×10^5
Run date	1991(1 month)	1991(2.5 month)	1990,1991

* except for these conditions, all conditions are for the 1990 run.
** Very loose trigger, cuts are made off-line.
b pair estimation made using A dependence of $A^{1.0}$ and b pair cross sections per nucleon of[11]: σ_{pN}=17nb at 800 GeV/c, $\sigma_{\pi N}$=28 nb at 600 GeV/c, $\sigma_{\pi N}$=23 nb at 530, $\sigma_{\pi N}$=20 nb at 500.

A summary of fixed target experiments that may be able to provide some B physics results and have taken data in the period of time from 1988 to 1991 is listed in table 1. Note that the interaction rates and number of $b\bar{b}$ pairs produced as a function of time is

increasing, particularly in the dedicated B physics (E771 and E789) experiments. An interesting observation about fixed target B physics is that in general the experiments attempt to trigger on either one muon to observe the semi-leptonic decay of the B or on two muons to observe the decay of the B into J/Ψ. The advantages of triggering on one muons are sensitivity to ~ 20% of the total number of B events, while the two muon trigger gives sensitivity to the J/Ψ decays of the B which is a clean B signal when the J/Ψ decays into two muons outside of material. An exception to the rule of muon triggering is the E791 experiment which uses a very loose E_t trigger that should retain most of the B signal coupled with a very High rate data acquisition system.

2 Results from the first round of experiments (E653, E672)

To date, two experiments from the previous fixed target runs (before the 1991 run) have presented some results either in journal papers or in conference proceedings.

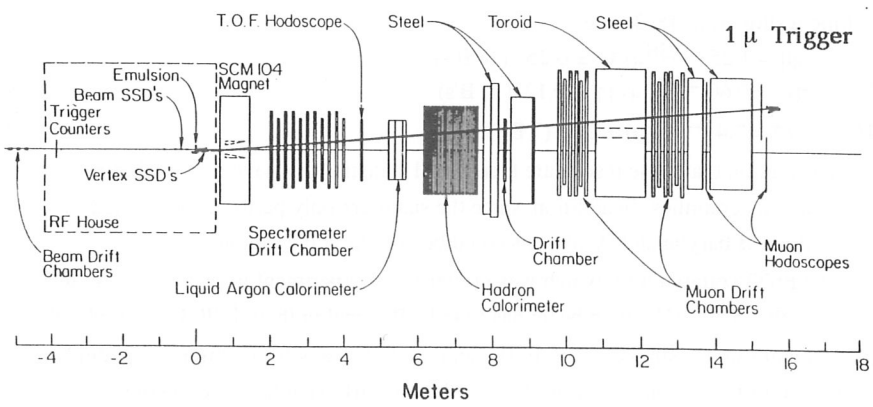

Figure 1: E653 spectrometer

The first FNAL fixed target experiment to present B physics results was E653 (figure 1) which used a 600 GeV/c negative pion beam on an emulsion target integrated with downstream silicon microstrip tracking planes. The experiment used a single muon

trigger with an off-line cut of 1.5 GeV/c on the P_t of the trigger muon to improve rejection of charm decays. Nine B pairs were identified using topology and visible mass cuts on visible secondary vertices. They defined a vertex as either heavy (H) or very heavy (VH), visible mass > 2.0 GeV/c^2, when the visible mass was consistent with a D or a B meson respectively. The B pairs all passed the test that there must be either 3 vertices of any combination H+VH or 2 VH vertices. The trigger muon must also have come from one of the secondary vertices.

The E653 collaboration reports that the cross section for 600 GeV/c pions on a nucleus is

[1] $\sigma_{b\bar{b}} = 33 \pm 11$ (statistical) $\pm$ 6 (systematic) nb/nucleon

(all x_f; A^1 assumed)

which is fairly consistent with theoretical predictions. They also find that the B's are produced preferentially back to back with an average center of mass angle of 148 degrees between the produced B particles. The angle between the produced B's is peaked near 180 degrees. This is in contrast to charm production were they find the average angle to be 113 degrees[12]. Unlike results from colliders, the E653 collaboration also finds a difference in the charged vs. neutral B lifetimes. The B lifetime results from 18 B's are

[2] $\tau_{all} = 1.25\ ^{+0.38}_{-0.32} \pm 0.25$ (18 B's)

[3] $\tau_{B^\circ} = 0.60\ ^{+0.23}_{-0.17} \pm 0.12$ (11 B's)

[4] $\tau_{B^\pm} = 2.4\ ^{+1.3}_{-0.9} \pm 0.6$ (7 B's)

with the caution that these results are from small statistics and have only preliminary systematic uncertainties. In addition, since the states are only partly reconstructed, some admixture of B baryon and B_c mesons could be present in the sample.

The E672 collaboration which was primarily an experiment to measure J/Ψ and χ decays with a 530 GeV/c pion beam has found a B signal in their J/Ψ data sample. The E672 apparatus is shared with E706 and includes a silicon microstrip detector downstream of a Be and Cu target followed by a fairly standard open geometry fixed target spectrometer consisting of a dipole magnet and set of PWC's downstream of the target with a muon detector in the rear. The experiment triggered on dimuon events to enhance the sample of J/Ψ on tape. Using 11.2×10^3 original J/Ψ events they find 73 events in which the J/Ψ vertex is detached from the primary vertex. Taking the ratio of detached J/Ψ events observed inside vs. outside their target material they calculate that they have obtained a sample of 26 $\pm$ 10 $B \rightarrow J/\Psi + X$ with 10 of these events clearly outside of the targets (figure 2). In addition they have fully reconstructed five events (one of these events is outside of the target) of the types $B^\pm \rightarrow J/\Psi + K^\pm$ (2 events) and

$B^{\circ} \rightarrow J/\Psi + K^{\circ}$ (3 events).The E672 collaboration reports that the **preliminary** cross section for 530 GeV/c pions on a nucleus is

[5] $\sigma_{b\bar{b}} = 28 \pm 9$ (statistical) $\pm$ 8 (systematic) nb/nucleon
($x_f > 0.1$)

or

[6] $\sigma_{b\bar{b}} = 42 \pm 13$ (statistical) $^{+16}_{-13}$ (systematic) nb/nucleon
(all x_f)

with the results from E672 being somewhat higher than the E653 results but still in agreement when the large errors are considered.

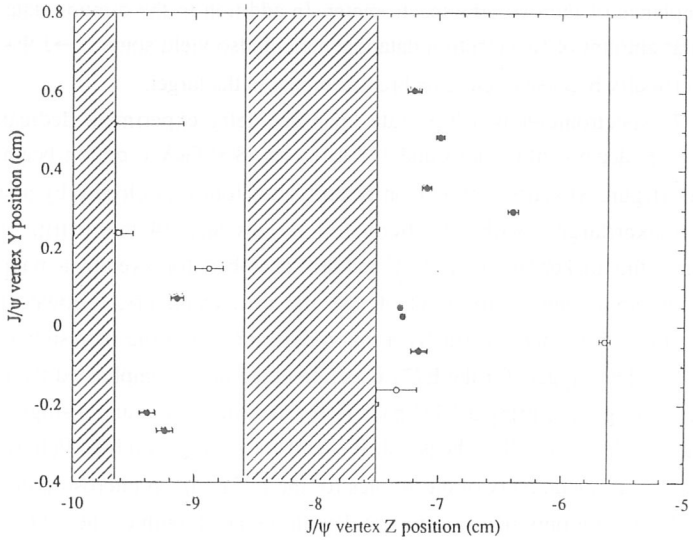

Figure 2: E672 J/Ψ vertices outside of target material

3 Results from current fixed target B experiments (E771 , E789)

Some preliminary results are available from the dedicated fixed target B experiments at FNAL, E771 and E789.

The E789 spectrometer is a 2 arm very high rate spectrometer which is mass focusing. At a given magnet current only the 2 oppositely charged particles that make a small range of invariant mass are accepted into the spectrometer. The spectrometer has silicon microstrip detectors near the target (in 2 arms) as well as PWC's, an electron

calorimeter, a hadronic calorimeter, a RICH, a muon detector and the mass focusing magnet. The experiment used a primary proton beam (800 GeV/c) on a gold wire (0.2 mm x 3.0 mm thick). The principle goal of the E789 experiment was to look for rare two body decays of the B. Unfortunately because of rate constraints imposed by radiation safety at FNAL the experiment ran with the magnet set to the J/Ψ mass at a lower than expected rate instead. With about 2.5 months of running at the J/Ψ mass they accumulated approximately 10^5 J/Ψ→μμ decay and expect to reconstruct about 40 decays of the type B→J/Ψ+X→μμ+X. At this time they have analyzed about 50% of their two muon trigger data and have found about 20 J/Ψ from vertices outside the target. Unfortunately E789 can not fully reconstruct exclusive states because of the limited acceptance of the two arm spectrometer. In addition to the dimuon data, they have a similar amount of two electron data that should also yield some B→J/Ψ+X but with more difficulty because of electron bremstrahlung in the target.

The E771 spectrometer is a high rate open geometry experiment dedicated to triggering on B decays into muons and J/Ψ using an 800 GeV/c proton beam. The spectrometer (figure 3) starts with silicon beam planes followed closely by a silicon microstrip tracker/target with 12 silicon foil targets and 14 microstrip planes. Downstream of the tracker/target are PWC and drift chambers followed by a magnet. In the rear of the spectrometer are a set of pad and drift chambers, followed by an electromagnetic calorimeter and finally a muon detector consisting of resistive plate counters (RPC). The triggers for the E771 experiment are more complicated than usual with a dimuon trigger requiring 3 RPC pads to fire for each muon and a single muon trigger using the RPC's as well as the pad/drift chambers to trigger on high P_t muons.

Because of the late delivery of electronics for the E771 silicon microstrip detector, the E771 collaboration only began to record data in the last month of the 1991 FNAL fixed target run, nevertheless E771 recorded 1.3×10^8 dimuon triggers and 1.3×10^8 single muon triggers in that time. The two muon trigger data is currently undergoing the first stage of analysis where the J/Ψ candidates are found. This first stage process is currently 40% complete and 2-3 $\times 10^4$ J/Ψ are expected in the final dimuon sample. In addition a few hundred events are expected where both B decay to a single muon in this sample. From the dimuon data the E771 experiment expects to reconstruct about 25 B→J/Ψ + X.

In a preliminary analysis of about 5% of the Dimuon trigger sample, the E771 collaboration has at this time found 1 exclusive B decay of the type B→J/Ψ + Kπ →μμKπ. A display of the event can be seen in figure 4. Since E771 does not have particle ID the event was fit using a constrained fit and the most likely fit was B→ J/Ψ +

$K\pi$. which had a χ^2/DOF of 0.72. The track parameters of the event can be found in table 2 and the parameters of the parent B can be found in table 3. The event also fits the hypothesis of $B \rightarrow J/\Psi + \rho \rightarrow \mu\mu\pi\pi$ with a χ^2/DOF of 0.88. The event is not consistent with a decay of the type $B \rightarrow J/\Psi + K^*$, the χ^2/DOF for this topology is 19.5.

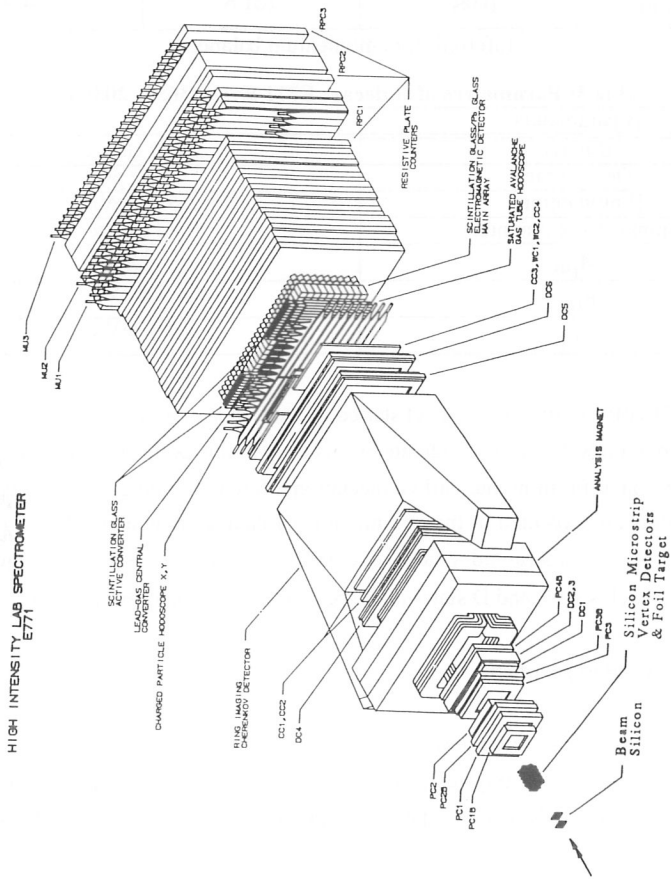

Figure 3: E771/P867 Spectrometer

Table 2: Track parameters for B→ μ1 μ2 h1 h2

Track	P (GeV/c)	θ_X (mrad)	θ_Y (mrad)
μ1 (μ^-)	74.2	-16.1	-3.3
μ2 (μ^+)	25.6	-75.4	-42.4
h1 (K^-)	15.0	11.8	26.7
h2 (π^+)	0.98*	161.8	174.9

* Inferred from momentum balance

Table 3: Parameters of B decay: E771 Event 3656- 20359

B parameters	
B mass	5.278 GeV/c
Decay time	1.099 ps
B momentum	115.6 GeV/c
B transverse momentum	2.78 GeV/c
$M_{\mu\mu}$	3.094 GeV
$P_{\mu\mu}$	99.7 GeV/c
$Pt_{\mu\mu}$	3.39 GeV/c

The E771 collaboration has not yet started the full scale processing of the one muon trigger data but a few 10's of B candidate events exist at this point from a scan of a few percent of the data. From monte-carlo expectation a few thousand partly reconstructed B→μ+X events are expected in the one muon final data sample. as well as 50 to 100 thousand partly reconstructed charm events of the type D→ μ+X. Some fully reconstructed exclusive B and D states are expected from the other B or D in the event.

4 Future FNAL B experiments

Listed in table 4 are three new FNAL fixed target experiments or proposals that will extend the reach of B physics in fixed target. In particular, proposals P865 and P867 are intended to be dedicated B physics experiments that will produce between 3×10^7 to 5×10^8 $b\bar{b}$ pair in one year of FNAL fixed target running. The P867 proposal is a dedicated B experiment that will run in the next FNAL fixed target run and is basically just the current experiment E771 in final form with the completed silicon microstrip detector and improved trigger. P865 is intended to run in later fixed target runs at very high intensity. E831 is a continuation of the very successful E687 charm photo-

production experiment and should be able to reconstruct some B decays in their next run.

Table 4: new FNAL experiments or proposals

	E831 (E687)	P865 (E789)	P867 (E771)
Experimental goals	Charm and Beauty	Beauty and Charm	Beauty and hidden Charm
Beam energy	≈200 GeV	800 GeV	800 GeV
Beam/target	γ / Be	p / Au	p/ Si,(Be)
Target (λ_I)	0.10 λ_I	0.03 λ_I	0.041 λ_I
Triggers	E_{tot}>50 GeV • n_c>4	E_t,impact parameter, secondary vertex	1μ•P_t>0.8 GeV or 1μ•(1μ•P_t>0.8 GeV), secondary vertex
Interaction rate	2×10^3 hadronic	5×10^7	5×10^6
Geometry	open	**2 arm**, 10-200 mR	open
total interactions	5×10^9	2×10^{14}	2.5×10^{13}
b pair produced	10^4-10^5	5×10^8	3×10^7
Run date	1995	1995(test) 1997	1995

5 Conclusions

Fixed target experiments clearly have an advantage in B physics from the standpoint of making B lifetime measurements. The main problem with current fixed target experiments is the low cross section that they face in presently available fixed target beam lines. This can be offset to some extent by running the experiments at very high rates, something that current fixed target experiments have proved can be done. Experience in the FNAL E771 experiment has shown that interaction rates up to 2-5 MHz can already be achieved by current open geometry experiments. The possibility of fixed target experiments at the LHC or SSC is very exciting since the beauty cross section at LHC or SSC energy will be comparable to the charm cross section at current FNAL energies and the relativistic boost at these new machines will increase the average B decay length (to 9 cm in the SSC case).

Based on the experience of E653, fixed experiments should be able to reconstruct a large fraction (~1%) of the total cross section using a high P_t trigger on a single muon with a good tracker/target and contribute high statistics B physics measurements when coupled to high rate spectrometers. Dimuon triggers will continue to be a good way to

obtain a sample of events of the type B → J/Ψ + X. Experiment P867 should record to tape ~ 5000 events with B → J/Ψ + X. and 760,000 events with B → μ + X in the next FNAL fixed target run.

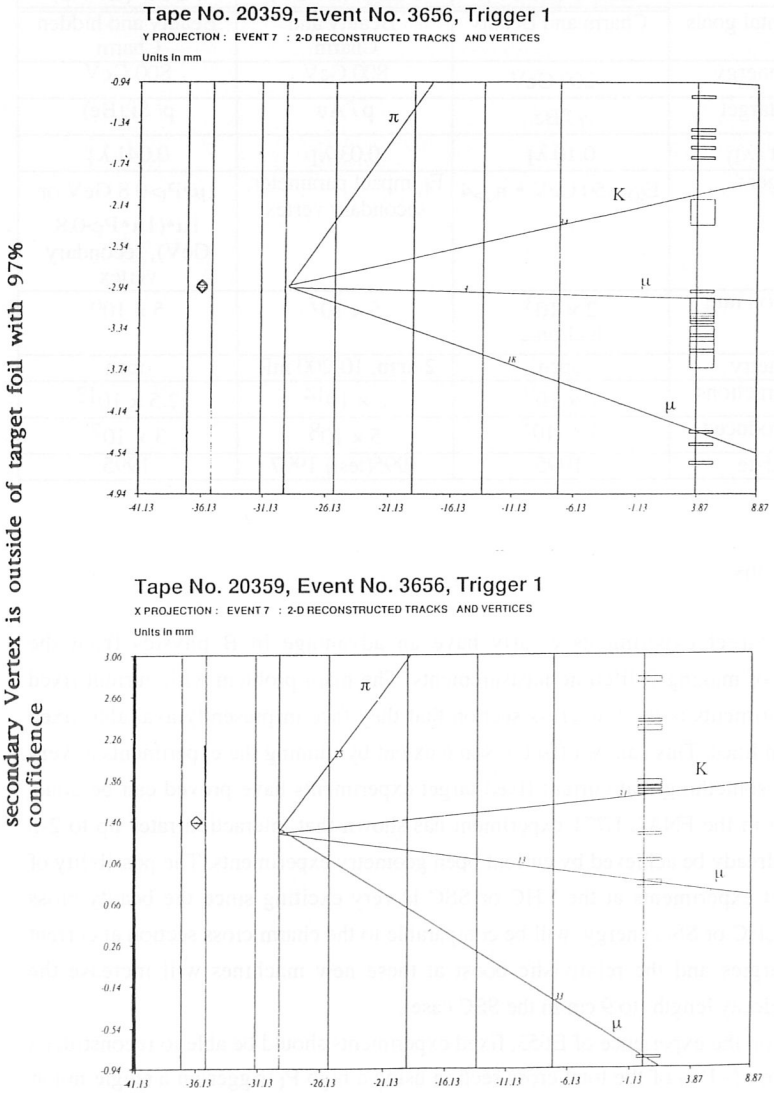

Figure 4: E771 B event: B→J/Ψ + Kπ →μμKπ

References

[1] K. Kodama *et. al.* , Phys. Lett. B303, 359-367 (1993)
[2] N. Reay, Results from E653, talk given at: Future Directions in B Physics conference (Columbus Oh, June 1991)
[3] R. Jesik *et. al.* , Heavy flavor production in π^-A collisions at 530 GeV/c, in: Proc. XXVI International Conference on High Energy Physics (Dallas Tx, 1992)
[4] R. Jesik, PHd. thesis, Unpublished (1993)
[5] T. Alexopoulos *et. al.* , P867 Proposal (May 1993)
[6] D. M. Kaplan, Private communication (May 1993)
[7] L. D. Isenhower *et. al.* , Letter of Intent for a High-Sensitivity Study of Rare Low-Multiplicity Beauty Decays (FNAL P865, Sep 1992)
[8] P.L. Frabetti *et. al.* , Nucl. Instrum. Methods A320, 519-547 (1992)
[9] R. Gardner, J. Butler, Private communications (May 1993)
[10] S. Banerjee, J. Appel, Private communications (May 1993)
[11] E. Berger, Heavy flavor production, QCD Hard Hadronic Processes, B. Cox Ed. 501-536 (1987)
[12] K. Kodama *et. al.* , Phys. Lett. B263, 579-583 (1991)

Frascati Physics Series, Vol. 1 (1993)
HEAVY QUARKS AT FIXED TARGET
Frascati, May 31st – June 2nd 1993
(pp. 111–116)

E789 AND P865: HIGH–RATE FIXED–TARGET STUDIES OF CHARM AND BEAUTY

D.M. Kaplan
Northern Illinois University, DeKalb IL 60115, (USA)

for the E789 and P865 Collaborations

Abstract

Experiment 789 at Fermilab used the high-rate E605/E772 spectrometer to study low-multiplicity charm and beauty decays. Preliminary results on charm and beauty production are presented based on analysis of $\approx 100\%$ of the charm data and $\approx 50\%$ of the beauty data. A new experiment is proposed to improve charm and beauty sensitivity by several orders of magnitude.

1. Description of E789

Experiment 789 studied charm and beauty production in 800-GeV pN collisions using the high-rate E605/E772 spectrometer (Figure 1) in Fermilab's Meson-East laboratory, upgraded with a 16-plane silicon-microstrip array and a vertex trigger processor [1]. Beam of intensity $\approx (1-6)\times 10^{10}$ protons per 20s spill was incident on thin wire targets 0.1 – 0.2 mm high and 0.8 – 3 mm thick. For the charm data the SM12 analyzing magnet was operated at 900 or 1000 amperes, and Au and Be targets were used to study the A-dependence of D production. For the beauty data a 3-mm-thick Au target was used and the SM12 current was 1500 amperes, optimizing acceptance for the J/ψ while simultaneously accepting direct two-prong B^0 decays. (Insufficient running time was available for a dedicated $B^0 \to$ dihadron run.) In the 1991 run, 4×10^8 (9×10^8) events were recorded on 240 (770) 8-mm tapes during the charm (beauty) running periods. Typical interaction rates were ≈ 2 MHz in the charm mode and ≈ 50 MHz in the beauty mode.

The silicon detectors were arrayed from $\approx 40-90$ cm downstream of the target in two arms covering the angular ranges $\pm(20-60)$ mr above and below the beam axis. The detectors, type "B" from Micron Semiconductor, were of $5\times 5\,\mathrm{cm}^2$ area, 300 μm thickness, and 50 μm pitch. In each arm, planes measuring the bend (y-z) view alternated with planes at $\pm 5°$ stereo angles. Signals from 8,544 strips were individually read out via Fermilab 128-channel amplifier cards [2] and LBL discriminators [3] synchronized to the accelerator RF. The discriminated signals were transmitted through ≈ 400 ns of multiconductor cable to coincidence registers.

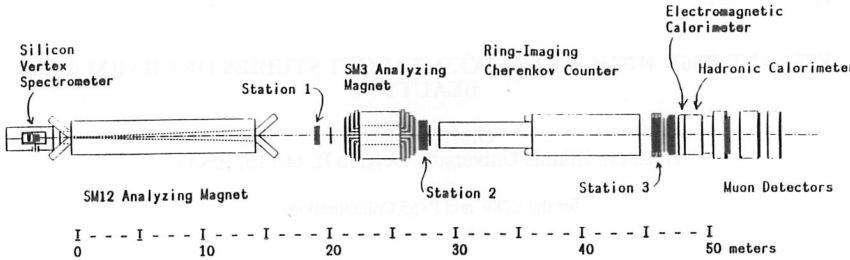

Figure 1: E789 apparatus (plan view).

The vertex processor [1], which found tracks in the bend-view drift chambers and silicon detectors and selected events with candidate decay vertices downstream of the target, was used in the charm running and provided a rejection factor of ≈ 10 against non-charm events with charm efficiency of $\approx (50-60)\%$ (caused primarily by silicon-plane inefficiencies) for decays outside the target. The thin target localized the primary interaction vertex, simplifying the design of the processor, which needed only to determine the position of the decay vertex.

2. Preliminary Results from E789

Figure 2 shows dihadron invariant mass spectra from the charm data sample for various lifetime cuts. Cherenkov π/K particle identification has not been used in this analysis, as the RICH was not optimized for the low momenta characteristic of charm decays. Rather, each plot contains two entries per event, one for the π^+K^- and the other for the π^-K^+ particle assignments. The correct particle assignments give a sharp peak ($\sigma \approx 6$ MeV), corresponding to either the D^0 or $\overline{D^0}$. The wrong particle assignments give a much broader peak ($\sigma \approx 50$ MeV). A limit on possible $D - \overline{D}$ production-rate asymmetry can be derived from the numbers of D^0 and $\overline{D^0}$ observed. At the 10% level, no significant asymmetry is observed (or expected) at the $x_F \approx 0.05$ characterizing these data. Our preliminary D cross section is consistent with previous measurements reported by E653 [4] and E743 [5]. The systematics of the A-dependence and normalization are still under study.

Figure 3a shows the invariant mass spectrum from a preliminary analysis of $\approx 50\%$ of the beauty dimuon data sample. Figure 3b shows the spectrum of events in which both tracks have impact parameters at the target center greater than $150\,\mu$m and the pair vertex satisfies $0.7 < z_{\rm vertex} < 5\,$cm, indicating a decay downstream of the target. In the J/ψ mass region, 22 events satisfy these requirements. To

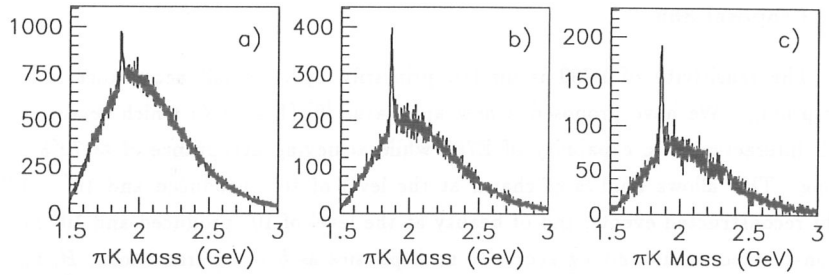

Figure 2: Dihadron invariant mass spectra from the charm data sample for three lifetime cuts: a) $\tau/\sigma_\tau > 3.9$, b) $\tau/\sigma_\tau > 6$, c) $\tau/\sigma_\tau > 7.9$.

estimate background due to tails of the target distribution (arising from possible vertex tracking errors or large Coulomb scatters in the silicon planes), we also study events with reconstructed vertices upstream of the target (Figure 3c). No upstream events are observed near the J/ψ region, supporting the likely beauty origin of the downstream J/ψ events. There is also a significant excess of continuum events in the downstream sample, attributed to semileptonic decays of $b\bar{b}$ pairs.

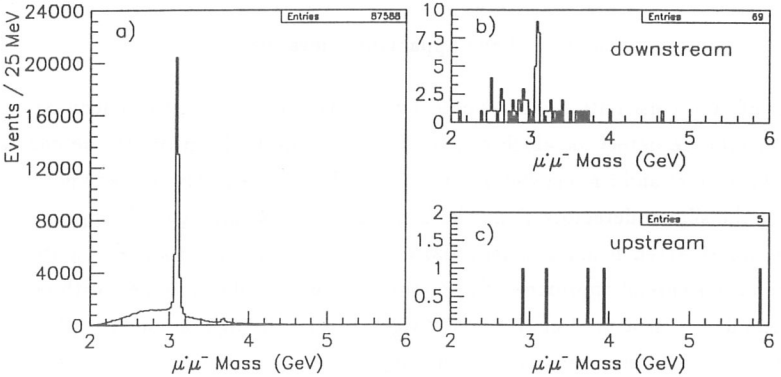

Figure 3: Dimuon invariant mass spectra from the beauty data sample: a) all events, b) $0.7 < z_{\rm vertex} < 5\,{\rm cm}$, c) $-5 < z_{\rm vertex} < -0.7\,{\rm cm}$.

3. Proposal 865

The sensitivity of E789 is limited primarily by its small acceptance ($\lesssim$10% per prong). We have proposed a new apparatus [6] (Figure 4) which retains the high interaction-rate capability of E789 while achieving acceptance of $\approx$ 70% per prong. This allows studies of charm at the level of 10^{11} produced and $10^7 - 10^8$ fully reconstructed events, and of beauty at the level of 10^8 produced and 10^4 fully reconstructed events, giving access to such physics as $b \to s\gamma$ transitions, B_s mixing, beauty semileptonic form factors, doubly-Cabibbo-suppressed charm decays, semileptonic D_s and charmed-baryon decays, and D^0 mixing and CP violation.

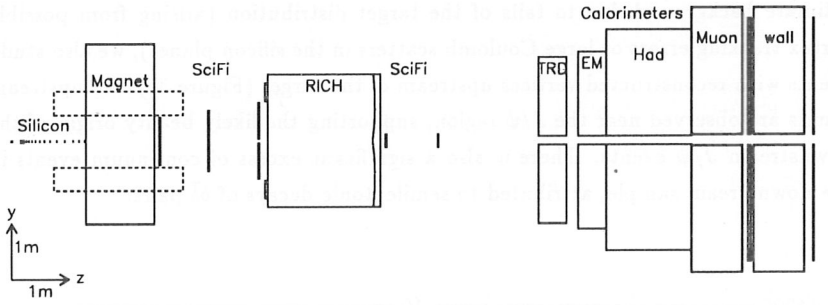

Figure 4: P865 apparatus (elevation).

A significant sensitivity limit is posed by radiation damage in the silicon detectors. To configure detectors which can survive at the desired sensitivity, we choose suitable maximum and (in one view) minimum angles for the instrumented aperture, arranging the silicon detectors along the beam axis with a small gap through which pass the uninteracted beam and secondaries below the minimum angle (Figure 5). Thus the rate is spread approximately equally over several silicon planes, with large-angle secondaries measured close to the target and small-angle secondaries farther downstream. Along the beam axis the spacing of detectors increases approximately geometrically, making the lever arm for vertex reconstruction independent of production angle. The instrumented angular range is $|\theta_x| \leq 200\,\mathrm{mr}$, $8 \leq \theta_y \leq 150\,\mathrm{mr}$, corresponding to the rapidity range $|y| \lesssim 1.5$. To maximize the rate capability of the spectrometer, the tracking is performed entirely with silicon and scintillating-fiber planes.

The scintillating fibers are read out using the solid-state "visible-light photon counters" (VLPCs) under development by a collaboration among Fermilab, UCLA,

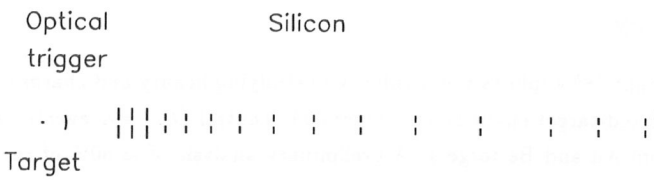

Figure 5: Detail of P865 vertex region.

and Rockwell International Science Center [7]. VLPCs are also key to the proposed Cherenkov-based optical impact-parameter trigger [8] and fast ring-imaging Cherenkov counter [9]. VLPCs are highly suitable for these applications due to their high quantum efficiency, low noise, and high speed. Quantum efficiency as high as 85% for green light has been achieved [10], and 30-MHz rate capability has been demonstrated, with single-electron noise rates of several kHz [11].

In addition to the Level-1 optical trigger, other triggering strategies appear promising. These include calorimetric E_t and high-p_t-lepton requirements and a trigger processor to reconstruct vertices and invariant masses. At each trigger level, just enough rejection should be provided to meet the input bandwidth of the succeeding level, so as to trigger on charm and beauty as efficiently as possible without restricting attention only to modes with final-state leptons. High-bandwidth data-recording technology and inexpensive workstations now or soon-to-be available should make feasible a recorded sample of $\sim 10^{11}$ events, key to the desired charm sensitivity.

P865 seeks to study the physics described above within the next few years, then upgrade the apparatus for a sensitive study of B CP violation by decade's end. This might be accomplished by increasing the interaction rate a factor ≈ 10, employing (for example) radiation-hardened silicon pixel detectors to cope with the increased event complexity and radiation dose. Alternatively, the beauty production cross section might be increased by moving to a higher-$\sqrt{s}$ interaction region. A promising idea under study [12] is to arrange collisions between a high-energy proton beam in the Tevatron, SPS, or HERA proton ring and a lower-energy beam, for example by storing protons in the HERA electron ring or constructing a small, inexpensive storage ring adjacent to the Tevatron or SPS. At $\sqrt{s} \approx (150-200)$ GeV, this scheme can provide a factor ≈ 100 increase in beauty cross section while retaining sufficient Lorentz boost to ease triggering, particle identification, and coverage of a large acceptance.

4. Summary

Experiment 789 explores the feasibility of studying beauty and charm physics in a high-rate fixed-target environment. Over 3000 neutral $D \to \pi K$ events have been observed from Au and Be targets. A preliminary analysis of $\approx 50\%$ of the dimuon beauty data yields 22 J/ψ events with decay vertices more than 7 mm downstream of the target; these are candidate $b \to J/\psi + X$ decays. Analysis is underway to determine $\sigma(b\bar{b})$ at 800 GeV. Analysis of the dihadron beauty data and $J/\psi \to e^+e^-$ data is also in progress. A new experiment, P865, has been proposed as the next step in charm and beauty sensitivity, with the ultimate goal of studying *CP* violation in beauty decays.

References

[1] C. Lee *et al.*, IEEE Trans. Nucl. Sci. **38** (1989) 461.

[2] D. Christian *et al.*, IEEE Trans. Nucl. Sci. **36** (1989) 507.

[3] B. T. Turko *et al.*, IEEE Trans. Nucl. Sci. **39** (1992) 758 .

[4] K. Kodama *et al.*, Phys. Lett. B **263** (1991) 573 .

[5] R. Ammar *et al.*, Phys. Rev. Lett. **61** (1988) 2185 .

[6] L. D. Isenhower *et al.*, "P865: Revised Letter of Intent for a High-Sensitivity Study of Charm and Beauty Decays," D. M. Kaplan, spokesperson, April 2, 1993.

[7] M. D. Petroff and M. Atac, IEEE Trans. Nucl. Sci. **36** (1989) 163;
M. Atac *et al.*, Nucl. Instr. & Meth. **A314** (1992) 56;
M. Atac *et al.*, Nucl. Instr. & Meth. **A320** (1992) 155.

[8] G. Charpak, L. M. Lederman, and Y. Giomataris, Nucl. Instr. & Meth. **A306** (1991) 439 ;
D. M. Kaplan *et al.*, Nucl. Instr. & Meth. **A330** (1993) 33;
G. Charpak *et al.*, "Experimental Study of an Impact-Parameter Optical Discriminator", CERN-PPE/93-14, to appear in Nucl. Instr. & Meth. (1993).

[9] D. M. Kaplan *et al.*, "A Fast Ring-Imaging Cherenkov Counter for a Fixed-Target Heavy-Quark Experiment," FERMILAB-Conf-93/148, to appear in *Proceedings of the First Workshop on RICH Detectors,* Bari, Italy, June 1993.

[10] M. G. Stapelbroek, M. D. Petroff, and R. Bharat, "Visible Light Photon Counters for Astronomy," to appear in *Proceedings of an ESA Symposium on Photon Detectors for Space Instrumentation,* ESA/ESTEC, Noordwijk, The Netherlands, 10–12 November 1992.

[11] M. D. Petroff and W. G. Stapelbroek, IEEE Trans. Nucl. Sci. **NS-36** (1989) 158.

[12] Y. Giomataris, "Perspectives on an Asymmetric Proton Collider with Small Crossing Angle for B Physics," this Workshop.

Frascati Physics Series, Vol. 1 (1993)
HEAVY QUARKS AT FIXED TARGET
Frascati, May 31st – June 2nd 1993
(pp. 117–130)

BEAUTY HADROPRODUCTION AT CERN IN FIXED TARGET EXPERIMENTS

G. Martellotti and M. Verzocchi
INFN, Sezione di Roma
Piazzale Aldo Moro, 2, I-00185 Roma, (ITALIA)

Abstract

This paper is organized into two parts: in the first one, we briefly review the experimental approaches proposed at CERN, aiming to the detection of beauty hadroproduction, analyze the different techniques adopted and describe in some detail the experiments that have given positive results, i.e. WA75, NA10, WA78. In the second part we discuss the WA92 experiment, currently running and making use of the Omega spectrometer: the experimental method used, the 1992 data taking, some preliminary results and future perspectives.

1. – Beauty hadroproduction experiments at Cern

1.1 Experimental approaches and techniques

Experimentation on beauty hadroproduction at SPS has been strongly affected by the small $\sigma_{B\bar{B}}$ at the available energies ($\leq$ 350 GeV/c for a π^- beam).

The first experimental attempts started at the end of the '70s, giving (negative) results in the early '80s. At that time, the predictions for cross-section and lifetimes were very uncertain and far from the presently known values (e.g.: $\sigma_{B\bar{B}} \approx 500$ nb/N[1], $\tau = 10^{-14}$ s $\div$ 10^{-13} s [2]). With $\tau \approx 10^{-14}$ s, only emulsions would have been suited to visualize the decay.

Among the techniques used we want to quote for example, experiment NA19, having an emulsion target coupled with a muon spectrometer and trigger, and a sensitivity of about 0.02 evs /nb.[3]

Various other approaches were proposed and some were ruled out when it appeared that τ was of the order of 10^{-12} s, and σ (at $\sqrt{s} \sim 25$ GeV) a few nb/N, giving a signal to background ratio $< 10^{-6}$ (experimental upper limits (NA3, 1983)[4] and QCD calculations [5]).

Neglecting, as belonging to "prehistory", early discussions on the possibility of using the EHS (with a small, high resolution, rapid cycling bubble chamber as target and vertex detector), or the attempt done with the WA11 experiment, in which one searched for a peak in the (K, ψ) final state invariant mass, we shall try to classify the experiments proposed at CERN according to the different technique used:

A) – Experiments using a dump followed by a muon spectrometer used also for triggering:
   1) NA19 and WA75, with active emulsion target, followed by a vertex detector, a dump and muon detection;
   2) NA3, and NA10, with passive heavy target plus dump and high p_T muon trigger;
   3) WA78, using a calorimeter dump for missing energy trigger plus a spectrometer for muon detection and triggering;

B) – Experiments using a sensitive decay region and the Omega spectrometer for the full event reconstruction:
   1) WA71, proposing an emulsion target and a trigger on multiplicity jump in microstrip silicon detector;
   2) WA84, developing a new microvertex detector using scintillating fibres to visualize the decay;
   3) WA92, currently running, using a silicon microstrip decay detector and a secondary vertex trigger.

1.2 Experiments reporting positive results

1.2.1 WA75.

WA75[6] used the NA19 setup with the addition of a silicon microvertex detector and a π^- beam of 350 GeV/c momentum. Fig. 1 shows the experimental layout.

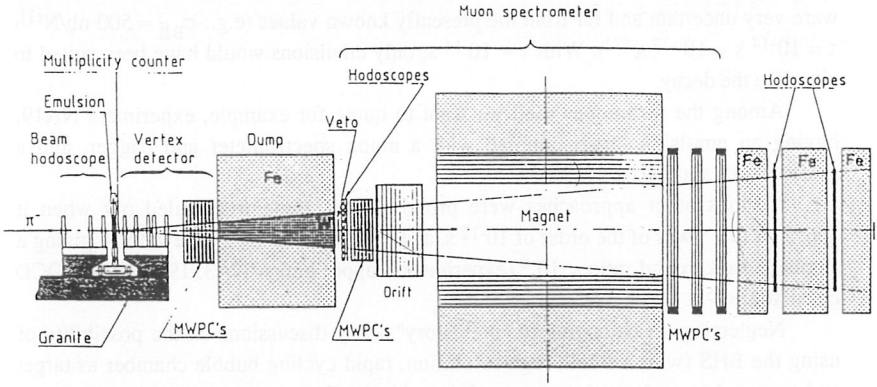

Fig. 1 – Layout of the WA75 experiment.

The scheme shows the beam hodoscope, the active emulsion target, the vertex detector (silicon microstrips and MWPC), the iron-tungsten dump and the muon

spectrometer. 3 x 10^9 interactions were observed and about 10^4 events with the p_T of the muon larger than 1GeV/c were selected.

The sensitivity was of the order of 1 evt/nb. The vertex position in the emulsion was predicted with an error of about 20 μm in the transverse direction and of 500 μm along the beam.

One event with the expected characteristics for beauty production was found, and it is shown in sehematic form in Fig. 2.

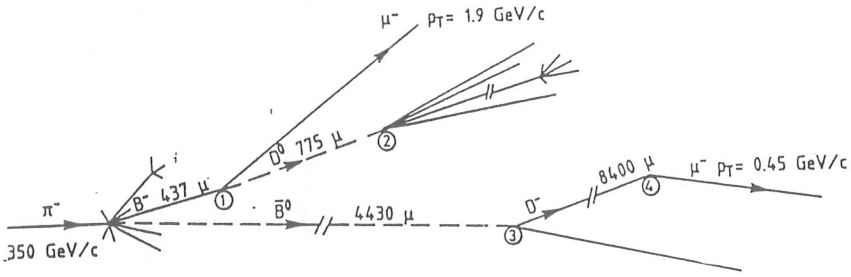

Fig. 2 – Sketch of the B^- - B^0 event found by WA75.

1.2.2 WA78

The WA78[7] experiment, whose apparatus is shown in Fig. 3, used a 320 GeV/c π^- beam, with intensity ≈ 6 x 10^6 particles per burst. A uranium/scintillator dump calorimeter, with energy resolution $\frac{\sigma_E}{E} \approx 60\% / \sqrt{E}$, designed to operate at rates ≈ 3 x 10^6 Hz was followed by a magnetic spectrometer. The trigger selected events with two or more muons in the spectrometer with a cut in the calorimeter energy ($E_{cal} \leq 280$ GeV) corresponding to the requirement of a large (> 40 GeV) leptonic energy: $E_{lept} = E_{beam} - E_{cal} = E_\mu + E_{missing}$.

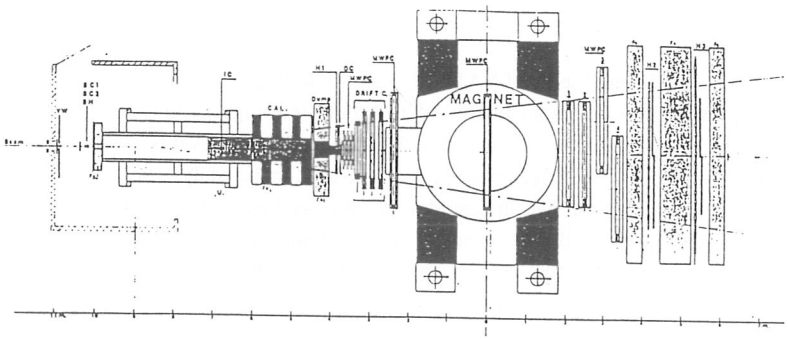

Fig. 3 - Layout of the WA78 experiment.

The calorimeter was designed so that its mean density could be changed, in order to measure the non-prompt muon background. Contamination due to double interactions or to muon halo in time were cut out by the calorimetric measurement, since the total energy measured is larger than the incoming beam energy.

In Fig. 4 the $p_{T_{total}}$ distribution for the sample of trimuon events shows increasing evidence for the signal with increasing cut on the missing energy.

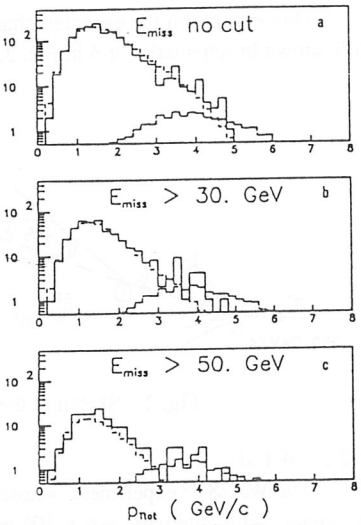

Fig. 4 – $p_{T_{total}}$ distributions for the accepted tri-muon events or increasing cuts on $E_{missing}$ (WA78).

The final analysis, based on the full sample of three muon and two like-sign muon events gives a cross-section of $\sigma = 3.5 \pm 0.4 \pm 1.1$ nb/N, assuming a mixing parameter χ_B=0.12 and a production cross-section obtained from QCD leading order calculation[9]:

$$\frac{d^2\sigma}{dx_F\, dp_T} \propto e^{-(x_F - 0.09)^2/0.3}\, e^{-p_T^2/6.9}.$$

1.2.3 NA10

The experimental setup of NA10 [8], is shown in Fig. 5.

A 286 GeV/c π^- beam interacted in a tungsten target, followed by a hadron absorber and by the muon spectrometer. The trigger selected events with at least two high-p_T muons. Only the three muon events were used in the analysis.

The production mechanism used for the cross-section evaluation was a correlated model assuming the B $\bar{B}$ pair to be the decay product of an intermediate state Υ'''', centrally produced. The cross-section dependence on Feynman x and p_T is given by:

$$\frac{d^2\sigma}{dx_F\, dp_T} \propto e^{-(1-|x_F|)^3}\, e^{-2p_T}.$$

Such peculiar production mechanism is significantly different from the one predicted by QCD calculations. The resulting cross-section is $\sigma = 14^{+6}_{-7}$ nb/N.

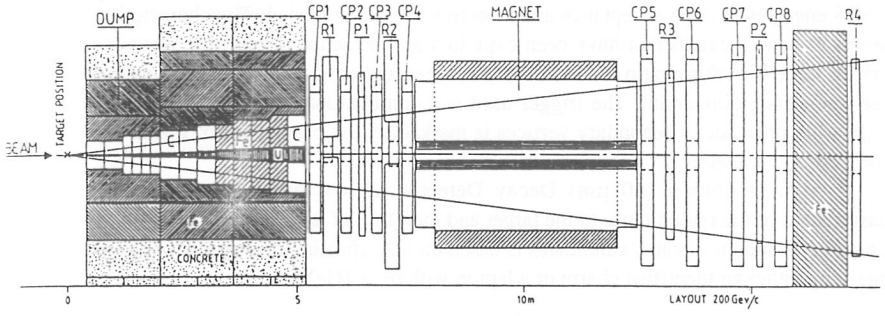

Fig. 5 – The NA10 spectrometer.

1.3.4. Discussion of results

Fig. 6 shows a comparison of theoretical predictions of leading order [9] and next to leading order [10] cross-sections with experimental results from NA10 (using the previously described model) and WA78 (using model of Ref. [9]). The apparent discrepancy between the two experiments can be explained as largely due to the different production mechanism assumed. We also show (with an asterisk) what would have been the WA78 result if the same model as NA10 had been used. In conclusion, the results of the two experiments are compatible and there is a good agreement between the WA78 result and QCD predictions.

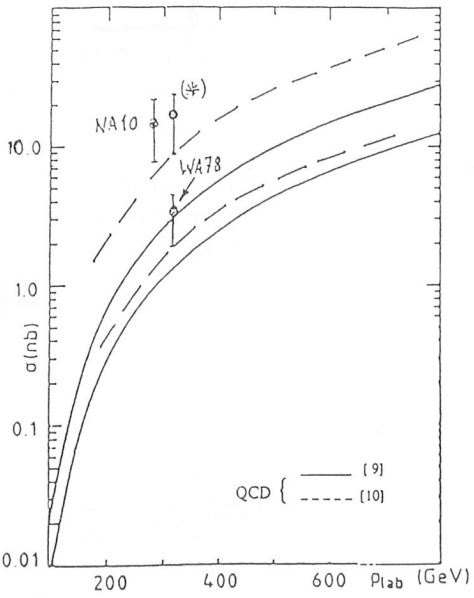

Fig. 6 – Comparison between WA78 and NA10 cross-section measurements and QCD predictions.

2.- The WA92 experiment

WA92[11] aims at the direct observation of beauty events in the reaction:

$$\pi^- N \rightarrow B\bar{B} X \qquad \text{at } 350 \text{ GeV/c}.$$

Due to the small value of the cross-section and of the signal to background ratio at the SPS energies, a large acceptance and selective trigger is needed. The characteristic features of beauty events that have been exploited are: presence of multiple secondary vertices, large branching ratio for semileptonic decay and emission of secondaries with large transverse momentum. The trigger used is a combination of these three criteria; the possible presence of secondary vertices is marked by the occurrence of tracks with large impact parameter.

A high resolution (10 μm) Decay Detector allows direct observation and measurement of the region close to the target and therefore of the complex beauty decay topologies. Search for beauty candidates is based on identification of cascade topologies containing either an identified charm or a lepton with $p_T > 1$GeV/c.

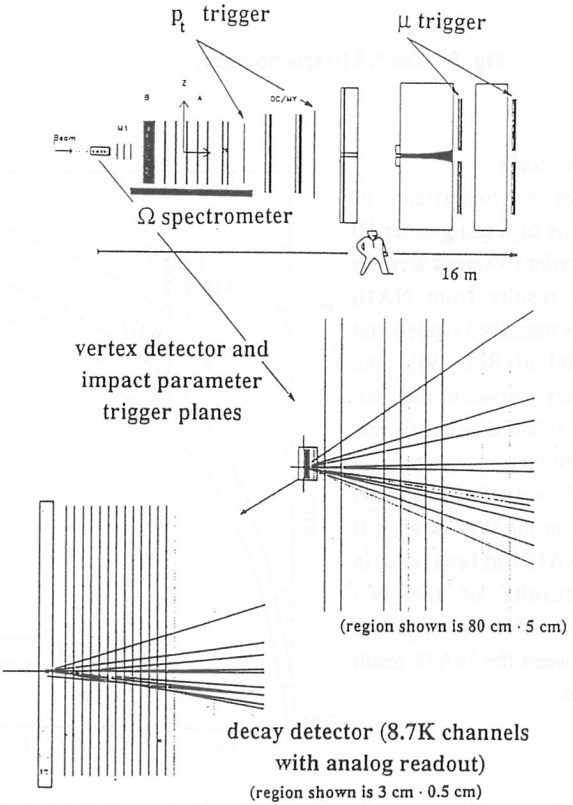

Fig. 7 – Layout of WA92 with details of Vertex and Decay Detectors.

The general layout is shown in Fig. 7. The target is 2 mm of copper or tungsten, and it is located outside the magnetic field. Following the target we find:

- the *Decay Detector (DD)*: 17 planes of silicon microstrips, with 10 μm pitch and 8.7K channels [12]. Its purpose is the visualization and measurement of the secondary vertices with high resolution. The DD is equipped with analogue readout, thus allowing offline cuts on the pulse height;
- the *Vertex Detector (VD)* : 17 planes of silicon microstrips, with 25 μm pitch and digital readout. Due to the larger lever arm, the VD is suited for the detection of impact parameter tracks; the i.p. trigger is realized by a fast parallel processor, using 6 (x, z) planes of the VD[13].
- the *Ω spectrometer,* for particles momentum measurement, with a 1.8 T bipolar magnetic field;
- the "*butterfly hodoscope*", made of two planes of scintillators shaped in such a way that their coincidence defines high p_T tracks (used for the high p_T trigger);
- the lead glass *electromagnetic calorimeter* (OLGA) for electron and π^0 identification;
- the large area *muon hodoscope,* placed behind two iron absorbers, and made of RPC planes of 3 cm pitch, equipped with digital readout; the muon trigger is based on the identification of a penetrating muon coming from the interaction region and it is realized by a dedicated hardware processor [14].

3.1 The impact parameter trigger processor - BCP

The Beauty Contiguity Processor [13] is designed to allow, in a time of 40 to 60 μs, the detection of impact parameter tracks. The number of tracks whose impact parameter is within certain intervals (0-100 μm, 100-200 μm etc...) is given as output.

Fig. 8 shows schematically the algorithm used by the BCP. We can summarize it in the following steps:

- using two of the beam chambers planes a beam line is constructed and its z–coordinate in the center of the target is calculated (Fig. 8a).
- this approximate vertex position is used to perform a transformation on all hits belonging to the 6 (x, z) planes of the VD; after the transformation, tracks coming from the primary vertex appear as straight lines parallel to the x–axis; impact parameter tracks, instead, become hyperbolas (see Fig. 8b);
- applying local operators to all hits in parallel, a connected structure is built for each primary track ; hits belonging to a connected structure are then erased, leaving only the hits of the "secondary tracks";
- with an appropriate number of local operations (depending on the i.p. class) the hyperbolas can be transformed into straight lines. When a connected structure is found, the i. p. of the track is recorded and the corresponding hits are removed.

A programmable trigger logic is finally applied so that event selection is subject to the presence of a minimum number of i.p. tracks together with a minimum number of

tracks coming from the primary vertex; the logic used in the 1992 run required the presence of at least three primary (i.p. < 100 μm), and at least two secondary tracks. The background rejection factor was around 13.

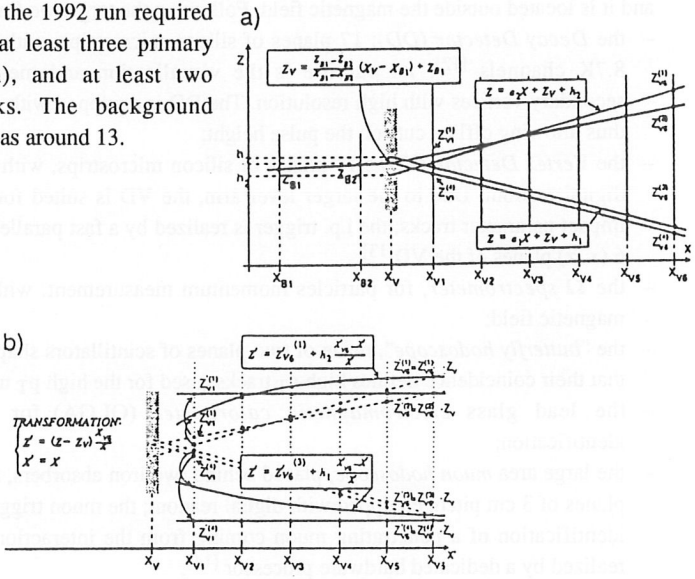

Fig. 8 - Scheme of the coordinate transformation performed by the BCP when searching for primary (a) and secondary (b) tracks.

3.2 Data sample

The 1992 data taking period was about 100 days, including the experiment installation and set-up. 50% of the data were taken with a 2 mm copper target, 50% with a tungsten target. The trigger was an OR of three conditions using high p_T, impact parameter (BCP) and muon trigger. The relative rates measured are reported:

$$\text{INT}^* \begin{cases} n\,H_{pT}{}^*\text{BCP} & (\sim 60\%)\ n = 1 \text{ for Cu } n = 2 \text{ for W} \\ n\,H_{pT}{}^*\,\mu & (\sim 30\%) \\ \mu^*\text{BCP} & (\sim 10\%) \end{cases}$$

The beauty acceptance of this trigger is approximately 35%.

8×10^7 events have been collected on tape corresponding to a sensitivity of about 160 ev/nb. Limitations of the 1992 run were mainly of two kinds: not full use of beam intensity and high value (around 50%) of deadtime. Both aspects have been investigated and substantial improvements are foreseen for the 1993 run; we expect to reach a total beauty sensitivity > 400 ev/nb.

3.3 Preliminary results

In the last 3/4 of the 1992 data taking, a special trigger stream was taken in which an identified muon, two impact parameter tracks and one or two high p_T tracks (> 600 MeV/c) were required. This enriched sample contains 1.7 x 10^6 events, and an estimated 11% of the full beauty signal on tape.

After a first stage of filter, this sample has been fully reconstructed in the spectrometer, with the additional request of at least one muon with p_T >1GeV/c (w.r.t. the beam axis) linked to a reconstructed secondary vertex or not pointing to the primary vertex within more than 100 μm.

About 1000 events survived this selection criteria. On these, a graphic interactive analysis has been performed, looking at DD and VD data, including DD pulse height information. A large fraction of the events that had been selected as containing secondary vertices was rejected as due to downstream interactions in the first DD planes (Fig 9), or to errors in the vertex finding pattern recognition program.

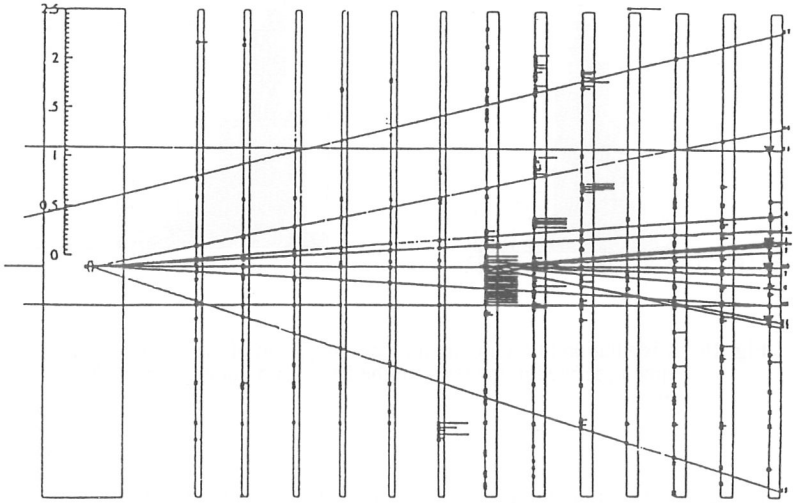

Fig. 9 – Display of an event in the Decay Detector: the secondary interaction in the 7th silicon plane is marked by the large energy deposited in the detector.

The final sample contained 72 two-prong decays (V2), 17 three-prong decays (C3), 1 four-prong decay (V4), and 10 events with chain decay topology.

The V2, C3 and V4 are all compatible with a charm semi-leptonic decay hypothesis. Moreover in ten of these events a second charm candidate is also visible.

In Fig. 10, we compare the minimum mass of the V2 system, M_{min}, and the quantity $t = LM_{D^0}/P_{vis}$ (where L is the decay length) with the MonteCarlo expectations.

The minimum mass is defined as :

$$M_{min} = \sqrt{M^2_{vis} + P^2_{Tmiss}} + P_{Tmiss}$$

where M_{vis} is the invariant mass of the visible system evaluated for the μK hypothesis, and P_{Tmiss} is the missing transverse momentum, computed with respect to the line of flight. The quantity t is similar to the proper time τ, but is calculated using the visible momentum of the system P_{vis} instead of its total momentum.

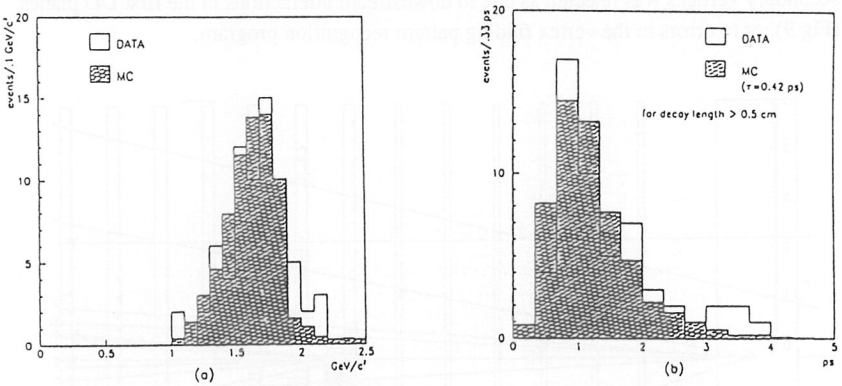

Fig. 10 – Distribution of the minimum mass M_{min} and of the pseudo-proper time t (defined in the text) for the $D^0 \rightarrow \mu\nu X$ sample and for M.C. events.

In the 10 events showing a decay chain topology the first decay vertex is incompatible with a charm interpretation (charged decay in one prong with $P_T > 1.0$ GeV/c or charged/neutral multiprong with $M_{min} > 2.0$ GeV/c^2) while the second decay is compatible with a charm interpretation. In two events a second decay chain is also observed. We conclude that these events are possible candidates for beauty decays.

One example of beauty candidate with good signature is shown in Fig. 11.

Applying the trigger and the same analysis to MonteCarlo events, we calculated an acceptance around 10^{-2} for beauty and 10^{-4}, 3 $\times 10^{-4}$ respectively for the charm meson decays $D^0 \rightarrow \mu\nu X$ and $D^{\pm} \rightarrow K^* \mu\nu$.

The expected number of charm events is in good agreement with the number of V2 and C3 found , while the expected number of beauty events is around 3 ev/nb.

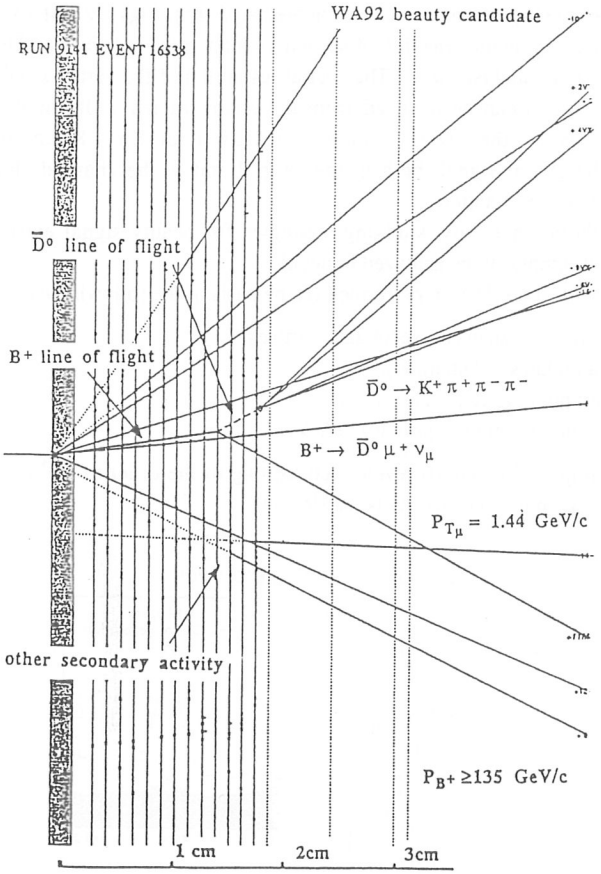

Fig. 11 -Display of one of the WA92 beauty candidates containing the decay $B^+ \rightarrow \bar{D}^0\mu\nu$ with $\bar{D}^0 \rightarrow K^+\pi^+\pi^-\pi^-$. The beauty decay vertex is marked by the presence of a high p_T (1.44 GeV/c) muon.

3.5 Analysis strategy for the full sample

Analysis of the full sample is in progress. All the 80 million events collected have been processed through a "fast filter", with the purpose of removing obvious backgrounds like double beam events (with the wrong beam selected and therefore bad prediction of the primary vertex), downstream interactions (giving rise to many impact parameter tracks) etc., situations that can be recognized without full event reconstruction. The filter has a 90% beauty acceptance and it reduces the sample to 26 million events, currently being processed in the complete reconstruction program.

The experiment performance can be appreciated from Figs. 12 and 13 . Fig. 12 shows the effect of automatic rejection of secondary interactions vertices on DD planes based on pulse height analysis only . The spatial resolution of the vertex x- coordinate (beam axis direction) can be deduced from the reconstructed width of the silicon planes. Fig. 13 shows the invariant mass distribution for $K\pi - K\pi\pi\pi$, and $K\pi\pi$ hypotheses . The charm signal, both in the neutral and in the charged channel, is consistent with M.C. expectation.

The Collaboration is now studying strategies for beauty signal extraction on strongly enriched samples to be analyzed in detail.

We estimate that a selection performed on the basis of the following elements:

– presence of more than two secondary vertices;
– charm candidates (all charged);
– K^o/Λ^o not pointing to primary vertex;
– high p_T μ not pointing to primary vertex

can lead to a sample of about 10^4 events (containing of the order of 10^2 beauty), on which interactive graphic analysis can be carried out.

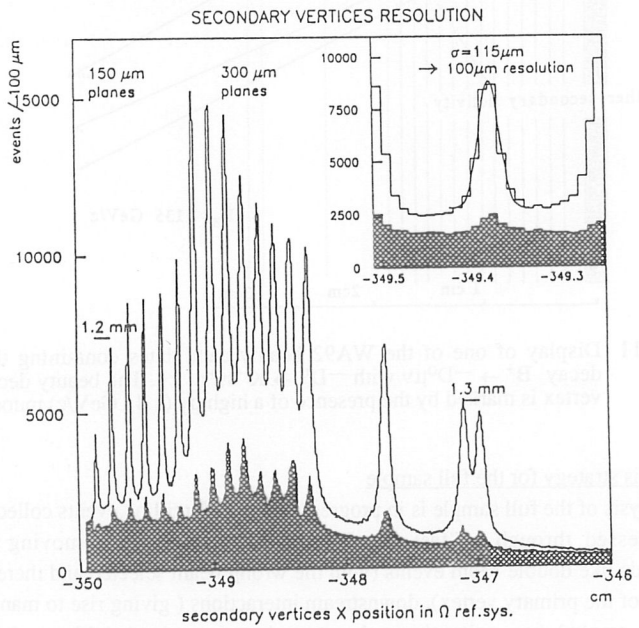

Fig. 12 – Secondary vertex x-distribution before and after (dashed histogram) the cut on the pulse height.

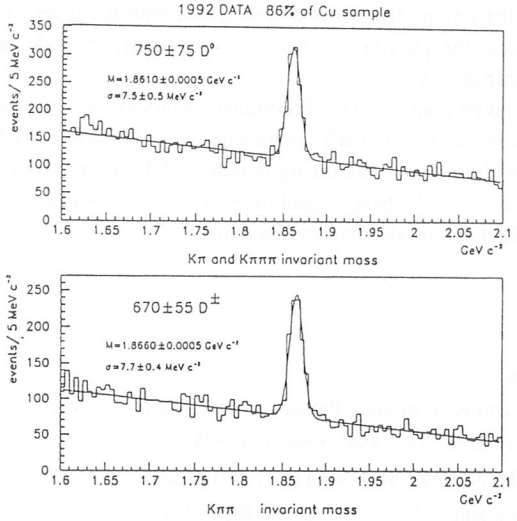

Fig. 13 – Invariant mass distributions for the D^0 decays into $K\pi - K\pi\pi\pi$, (a) and $D^{\pm}$ decays into $K\pi\pi$ (b).

4.- Conclusions

Experimentation at CERN fixed target, aiming at the detection of beauty hadroproduction, has been strongly limited by the small value of beauty cross-section. Nevertheless many experiments have been performed and different techniques studied and used.

The first beauty event has been observed in 1985 in the emulsion experiment WA75. Experiment WA78 has given the first measurement of the $B\bar{B}$ hadroproduction cross-section at 320 GeV/c: $\sigma = 3.5\pm0.4\pm1.1$ nb/N, in good agreement with QCD calculations.

In more recent years, the most interesting results on beauty have come from colliders and in particular from e^+e^- experiments, performing beautiful measurements of τ_{B^+}/τ_{B^0}, but still with large uncertainty (mainly systematic, due to assumptions on branching ratios). We notice that these results are not in good agreement with the recent one from an emulsion experiment at FNAL (E653)[15]. The result of CERN experiment WA92, using a technique different both from e^+e^- and from E653 may help to clarify this discrepancy.

WA92 has the unique feature of having a hadronic B trigger in parallel with a leptonic trigger and the possibility of visualizing beauty cascade decay in a high resolution microstrip detector.

WA92 has taken data in 1992. Preliminary analysis on a sub-sample (high p_T muon events) has shown the first $B\bar{B}$ events with decay chain directly observed in the decay detector. With the next data taking (summer ' 93), a sensitivity of ~ 400 ev/nb should be reached and > 10^2 beauty candidates should be identified, allowing a better measurement of the hadroproduction cross-section.

5. – References

(1) H. Fritzsch and K.H. Streng . Physics Letters 78B (1978) 447.

(2) M.K.Gaillard et al., Rev. Mod. Phys 47 (1975) 277.
J. Ellis et al., Nuclear Physics B131 (1977) 285.
M.K.Gaillard and L. Maiani . LAPP TH09 (1979).

(3) NA19 Collaboration. Physics Letters 122B (1983).

(4) NA3 Collaboration. Physics Letters 124B (1983).

(5) G.Altarelli, et al. Nuclear Physics B308 (1988) 724.

(6) WA75 Collaboration. Physics Letters 158B (1985) 186.

(7) WA78 Collaboration. Physics Letters B, Vol. 202 (1988) 453.

(8) NA10 Collaboration. NIM 223 (1984) 26.

(9) E.L. Berger. Physical Review D37 (1988) 1810.

(10) P. Nason et al. Nuclear Physics B327 (1989) 49.

(11) L. Rossi et al. (BEATRICE Coll.) SPSC, Cern–SPSC 90/10 (1990).

(12) M. Adinolfi et al. NIM, A329 (1993) 117.

(13) A. Beer et al.. Cern ECP 93-3 (1993). Submitted to NIM.

(14) C. Bacci et al. NIM A324 (1993) 83.

(15) E653 Coll. DPNU-92-37 (1992). Submitted to Progress. on Theor. Phys.
K. Kodama et al., Phys. Letters B303 (1993) 359.

SESSION IV

- N. Paver
  Theoretical Status of Charm and Beauty Semileptonic Decays
- E. Meroni
  Experimental Status of Charm Semileptonic Decays

Frascati Physics Series, Vol. 1 (1993)
HEAVY QUARKS AT FIXED TARGET
Frascati, May 31st – June 2nd 1993
(pp. 133–150)

THEORETICAL STATUS OF CHARM AND BEAUTY SEMILEPTONIC DECAYS

N. Paver
Università di Trieste, Dipartimento di Fisica Teorica, Sezione INFN,
Strada Costiera, 11 Miramare, I-34014 Trieste, (ITALIA)

Abstract

We review recent theoretical estimates of purely leptonic and semileptonic B and D transitions. Particular emphasis is given to developments obtained in the framework of the expansion in the heavy-quark mass.

1 Introduction

Semileptonic and purely leptonic heavy meson transitions are theoretically well understood at the constituent level, respectively in terms of heavy quark semileptonic decay and of quark-antiquark annihilation into lepton-neutrino pairs. Basically, these elementary processes are governed by the simple, lowest order weak effective Hamiltonian, involving the product of the quark and lepton $V-A$ charged currents:

$$H_{eff} = \frac{G_F}{\sqrt{2}} V_{Qq}\, \bar{Q}\gamma_\mu (1-\gamma_5)\, q\, \bar{l}\gamma_\mu (1-\gamma_5)\, \nu_l, \tag{1}$$

where $Q = c, b$ and $q = d, u, s$ denote the heavy and the light quarks respectively, and V_{Qq} are CKM matrix elements. At higher orders in the electroweak interactions, also flavor changing neutral current decays into lepton-antilepton pairs can occur, such as *e.g.* $b \to s l^+ l^-$, and the corresponding effective transition Hamiltonian inducing $B \to K(K^*) l\bar{l}$ has a structure similar to (1), in terms of V and A quark neutral currents, lepton neutral currents, CKM matrix elements and perturbative QCD coefficients. However, although final leptons are produced also in these processes, the basic mechanism is quite different as it involves loops with W and quarks (also the *top*), and consequently flavor changing neutral current decays are considered as nonleptonic rather than semileptonic.

To obtain transition amplitudes for the relevant mesons, and test the electroweak physics by comparison with the data and/or make predictions for the different processes, one has to estimate matrix elements of (1) between strongly interacting hadronic states, and thus to account for the effects of long-distance nonperturbative physics governing quark confinement. These effects are embodied in form factors and in leptonic constants. To predict them, it is necessary to adopt a hadronization scheme, which unavoidably affects theoretical predictions by some amount of model dependence, and consequently contributes an uncertainty in extracting electroweak

physics and/or Standard Model parameters from the data. This is particularly annoying in the case of semileptonic decays, which represent a direct source of information on CKM matrix elements through (1). In this regard, intensive efforts have been made recently, with the aim of formulating nonperturbative schemes which, although maybe less detailed, rely in large part on general properties and first principles of QCD, and thus minimize the role of model dependence. This should lead to more reliable analyses of the data. In Section 2 we will review the calculations of the leptonic constants, and sketch the various nonperturbative approaches on this particular example. Sections 3 and 4 will be devoted to charged current B and D semileptonic decays. Finally, Section 5 contains the conclusions.

2 Leptonic decay constants

For the purely leptonic decays $D \to \mu\nu$, $B \to \mu\nu$, *etc.*, the relevant hadronic matrix elements are defined as:

$$\langle 0|\bar{Q}\gamma_\mu\gamma_5 q|P(p)\rangle = i f_P \, p_\mu, \tag{2}$$

where $P = D, B$ denotes the heavy meson states. Thus, f_D and f_B are the analogues of f_π, which in the normalization of Eq.(2) is $f_\pi = 132\, MeV$. The leptonic transition rate is given in terms of f_P by

$$\Gamma(P \to l\nu_l) = \frac{G_F^2}{8\pi} |V_{Qq}|^2 f_P^2 M_P m_l \left(1 - \frac{m_l^2}{M_P^2}\right)^2. \tag{3}$$

While no experimental information on f_B is available, the present indications on f_D are $f_D < 310\, MeV$ [1]; $f_{D_s} = (232 \pm 45 \pm 20 \pm 48)\, MeV$ [2], and $f_{D_s} = (344 \pm 37 \pm 52 \pm 42)\, MeV$ [3]. To give a feeling on the sensitivity required to measure f_B, for $|V_{ub}/V_{cb}| = 0.1$ with $|V_{cb}| = 0.045$ and $f_B = 1.5 f_\pi$ one finds from (3): $BR(B \to \mu\nu) = 5.1 \times 10^{-7}$ and $BR(B \to \tau\nu) = 1.1 \times 10^{-4}$.

By definition, f_P's are nonperturbative parameters measuring the probability of $\bar{Q}q$ annihilation, and in the constituent quark model picture of hadrons they would be related to the bound state wavefunction at the origin. In this sense,they can indirectly enter also the determinations of form factors for B and D semileptonic decays. In addition to their intrinsic interest, they appear as key ingredients in numerous theoretical predictions for heavy flavor electroweak transitions. For example, $B^0 - \bar{B}^0$ mixing is proportional to f_B^2 [4], and consequently the value of f_B is crucial for the analysis of the CKM matrix and CP violation in the beauty sector [5]. Another case where they are needed is represented by the description of nonleptonic heavy meson decays in the factorization approximation [6]. Furthermore, of fundamental importance for the understanding of QCD is the asymptotic scaling law for large (infinite) heavy quark mass m_Q [7]:

$$f_P = \frac{\hat{f}}{\sqrt{m_P}} \alpha_s(m_Q)^{6/(33-2N_f)}, \tag{4}$$

with $\hat{f}$ a mass-independent constant. While natural in the constituent quark model, in fact Eq.(4) is a general consequence of the spin and flavor symmetry properties of QCD for heavy quarks. It has inspired the so called heavy quark effective theory, where heavy meson transition amplitudes are expanded to a good approximation in $1/m_Q$, and a great simplification of the description is achieved [8]. In particular, it gives the nice perspective of predicting B decays from measured D decays *via* scaling relations like Eq.(4). For all these reasons, considerable attention has been given recently to heavy meson decay constants, using independent theoretical nonperturbative schemes.

We just outline the basic points of the various approaches. In the constituent quark model the $(\bar{Q}q)$ wavefunction is obtained by solving a (relativistic) bound state equation with a confining potential inspired by QCD [9]. Pseudoscalar meson leptonic constants are then expressed in terms of such a wavefunction (actually, of the Fourier transform) in this form:

$$f_P = \sqrt{\frac{12}{m_P}} \int \frac{d^3k}{(2\pi)^3} \sqrt{\frac{(E_Q + m_Q)(E_q + m_q)}{4E_Q E_q}} \left(1 - \frac{k^2}{(E_Q + m_Q)(E_q + m_q)}\right) \Phi_P(k), \tag{5}$$

where k is the relative momentum. Eq.(5) clearly shows the connection with the wavefunction at the origin for $\langle k \rangle / m_Q$, $\langle k \rangle / m_q \ll 1$ (non-relativistic limit), and the scaling behavior (4) follows, provided the wavefunction at the origin is smooth in the quark mass. Quark model results, strictly relying on the notion of wavefunction, can be sensitive to the chosen form of the binding potential potential which, although inspired by QCD, cannot be derived directly from the basic QCD Lagrangian, and to the method of numerically solving the wave equation.

In the QCD sum rule method [10], which is fully relativistic and field-theoretic, the notion of wavefunction is avoided by defining meson "interpolating" fields as local products of quark fields. For example, the B, D (and B^*, D^*) will be described by:

$$J_5(x) =: \bar{Q}(x)\gamma_5 q(x) : ; \qquad V_\mu(x) =: \bar{Q}(x)\gamma_\mu q(x) : , \tag{6}$$

and one studies the propagation of these composite fields starting from short distances, where asymptotic freedom allows a perturbative calculation in terms of α_S and quark masses, and gradually going to larger distances relevant to hadrons, where the effects of non perturbative physics (breaking asymptotic freedom) start showing up in terms of vacuum averages of quark and gluon fields. This extrapolation from short distance to "moderately" large distances is done in practice by using the operator product expansion. The simplest object to study, which is also the relevant one for f_P, is the two-point correlator:

$$\Psi_5(q^2) = i \int d^4x \exp(iqx) \langle 0 | T \left(J_5(x) J_5(0)^\dagger \right) | 0 \rangle. \tag{7}$$

In QCD, the l.h.s. of (7) can be computed in terms of a perturbative term, plus a set of non-perturbative vacuum condensates, ordered according to their dimensionality. These condensates are fundamental parameters characterizing QCD confinement,

and are "universal", so that once fitted from a channel where the physics is known, their values can be used to make predictions for other channels. Applying the "duality" idea, the connection of (7) to hadrons is realized through the dispersion relation ($Q^2 = -q^2$):

$$\Psi_5(Q^2) = \frac{1}{\pi}\int ds \frac{\rho(s)}{s+Q^2} + \text{subtractions}. \tag{8}$$

It is desirable to improve the convergence of the spectral representation (8) so as to emphasize the hadronic ground state we are interested in, and also to have a well-convergent QCD representation, truncated to the lowest dimensional condensates (which are the best known). This is achieved by suitably modifying the kernel of the dispersion representation (8). The procedure is not unique, and to each choice of the new kernel corresponds a version of QCD sum rule, with its own advantages and disadvantages. For example, the "Laplace" QCD sum rule relevant to f_P, in the approximation $m_q = 0$, reads [11]:

$$f_P^2 \frac{m_P^4}{m_Q^2} \exp\left[-(m_P^2 - m_Q^2)T^2\right] = \frac{1}{\pi}\int_{m_Q^2}^{s_0} ds \exp\left[-(s-m_Q^2)T^2\right] \rho_{pert}(s) + NP. \tag{9}$$

Here, $\rho_{pert}(s)$ is the perturbative QCD spectral function, depending on α_s and m_Q, which is usually supposed to dominate the contribution of "continuum" states to the r.h.s. of (8) starting from some threshold s_0. In (9), T can be interpreted as a sort of "imaginary" time by analogy with the euclidean Green's function, and NP represents the sum over non-perturbative corrections:

$$NP = C_4\langle O_4\rangle - \frac{1}{4}m_Q^2 T\left(1 - m_Q^2 T\right) C_5\langle O_5\rangle + \cdots. \tag{10}$$

In (10) $\langle O_{4,5}\rangle$ are the (dominant)quark and gluon vacuum condensates with QCD coefficients $C_{4,5}$, and the ellipsis represent the contributions from higher dimensional operators, which are less-well known but power suppressed. As these relations show, QCD sum rules directly interface properties of hadronic states to fundamental parameters of the QCD Lagrangian, and in this sense they are are a "first principles" method, reducing the model-dependence (and the number of parameters) to a minimum. In practice, however, one must apply to Eq.(9) an "optimization" procedure minimizing the dependence of the predicted f_P and m_P from the *a priori* unknown parameters s_0 and T, which unavoidably introduces some systematic theoretical uncertainty, in addition to the errors from the input values of quark masses and vacuum condensates. Several analyses of f_P, also using alternative versions of QCD sum rules, have been performed until recently, attempting to reach improved accuracy and reliability of the predictions [12].

The large m_Q limit can be easily performed in (9), and in this limit one can reproduce (4), plus order $1/m_Q$ corrections [13, 14]. The fact that these corrections are also calculable, so that one can test the extrapolation from charm to beauty, is a welcomed feature of the framework. Actually, in the large mass limit there is a difficulty with the $O(\alpha_s)$ correction in ρ_{pert}, due to the appearance of large

$\ln m_Q$ terms. Thus, strictly speaking the limit $m_Q \to \infty$ is well-defined in (9) only after resummation of these large log terms to all orders in perturbation theory. In addition, since ρ_{pert} is known only to $O(\alpha_s)$ (*i.e.* to two loops), there is an ambiguity on the choice of the argument of α_s ($1\,GeV$ or $m_b \simeq 4.6-5\,GeV$?), which can make an appreciable numerical difference. These problems are best solved by formulating QCD sum rules in the framework of the heavy quark effective theory (HQET) [14, 15].

In this framework, the QCD heavy quark Lagrangian can be expanded as:

$$\mathcal{L} = \sum_v \left[\bar{b}_v \left(iv_\mu D_\mu\right) b_v + \bar{c}_v \left(iv_\mu D_\mu\right) c_v\right] + \mathcal{O}(1/m_Q) + \mathcal{O}(1/m_Q^2) + \cdots \qquad (11)$$

In this effective Lagrangian the quark fields are eigenstates of the velocity, $\gamma \cdot v Q_v = Q_v$ where $v_\mu = p_\mu/m_Q$; the $\mathcal{O}(1/m_Q)$ corrections are expressed in terms of higher dimensional quark operators whose explicit form we omit here. One can notice that the leading term in (11) has a $SU(2)$ heavy flavor symmetry (under $c \leftrightarrow b$), which in fact leads to relations between charm and beauty such as the one in (4), and a $SU(2)$ spin symmetry following from the absence of γ matrices, which implies *e.g.* $M_{D^*} = M_D$, $M_{B^*} = M_B$, and relations between form factors. Also, in this effective theory Feynman rules become particularly simple [8].

According to the HQET, the interpolating meson field J_5 in the two-point correlator (7) must be replaced by $\tilde{J}_5 = \bar{q}\gamma_5 Q_v$, and the corresponding Eq.(9) can be turned into a sum rule for the scale invariant parameter $\hat{f}$ of Eq.(4). In particular, with the aid of the renormalization group, the large $\ln m_Q$ can be resummed. Furthermore, this procedure indicates that the scale of strong interactions $\sim 1\,GeV$ is the appropriate argument of α_s in (9) [14, 15]. Unfortunately, this implies a large α_s correction in the numerical result for f_P, casting doubts on the validity of the perturbative expansion in this case [16].

Lattice QCD is also a "first principles" framework, and is believed to have the potential of giving the ultimate numerical answer on hadronic weak matrix elements, once some practical limitations are overcome [17]. Basically, like for QCD sum rules, one studies the propagation of the meson "interpolating" operator (here, for convenience the operator $A_5 = Q^\dagger \gamma_5 q$) at "euclidean" time $t = iT$, by approximating the space-time by a discrete set of lattice points, and computing the propagator by numerical simulations. The two-point correlator function (analogous to (7)), is defined as:

$$\mathcal{G}(T,0) = \sum_{\mathbf{x}} \langle A_5(T,\mathbf{x}) A_5^\dagger(0,\mathbf{0})\rangle = Tr\langle \gamma_0\gamma_5 S_Q(0,x)\gamma_0\gamma_5 S_q(x,0) P(0,x)\rangle, \qquad (12)$$

where S_Q and S_q are quark propagators, $P(x,0)$ is a path-ordered exponential ensuring gauge invariance, and $\langle\cdots\rangle$ means average over the gluon field configurations. In the large T limit, (12) is dominated by the ground state, the higher states being exponentially depressed:

$$\mathcal{G}(T,0) = \sum_n |\langle 0|A_5|n\rangle|^2 \exp\left(-m_n T\right) \to \frac{1}{2} m_P^2 f_P^2 \exp\left(-m_P T\right). \qquad (13)$$

Method	f_D	f_{D_s}	f_B	f_{B_s}
Quark Model [9]	182	200	231	246
Sum Rules [19]	224 ± 26	270 ± 30	180 ± 30	216 ± 36
Sum Rules [14]	180 ± 40		200 ± 50	
Lattice [18]	210 ± 15	230 ± 50	205 ± 40	235 ± 46

Table 1: Theoretical estimates of leptonic constants.

Both m_P and f_P are fitted from this relation, once the r.h.s. of (12) is numerically computed. A condition for the applicability of this method is that the lattice spacing a and the quark wavelength $\lambda_Q = 1/m_Q$ are such that $\lambda_Q \geq a$. With present lattice spacings $a^{-1} = 2 - 3\,GeV$, this condition is satisfied by the charm quark ($m_c \simeq 1.5 GeV$), but not by the beauty quark ($m_b \simeq 4.6 - 5\,GeV$). Therefore, for the B one has to adopt the large (infinite) m_Q limit, where the heavy quark becomes a static color source and the light quark q propagates in this color field. In this $1/m_Q$ expansion (12) becomes:

$$\mathcal{G}(T,0) = \frac{1}{2} m_P^2 f_P^2 \exp(-m_P T) = Tr(\frac{1+\gamma_0}{2} S_q(0,x) P(0,x)) \exp(-m_Q T), \qquad (14)$$

and the r.h.s. of (14) is now computed numerically. Notice that from this relation we have the indication that in the heavy quark limit the "binding energy" $\bar{\Lambda} = M_P - m_Q \rightarrow const$ independent of the flavor, and that $f_P\sqrt{m_P} \rightarrow \hat{f} = const$ modulo logs. Thus, only the scale invariant constant $\hat{f}$ can be calculated on the lattice. Then, the value of f_B is obtained using Eq.(4). Actually, to test the behaviour of f_P *vs* m_P and account for mass corrections, the expression $f_P\sqrt{m_P} = \hat{f} + A/m_P + B/m_P^2$ is used [18], and the constants A and B are fitted to the results in the charm region, dynamically calculated through Eq.(12).

To illustrate the predicted values of f_P, rather than making an exhaustive list which would appear confusing, we deliberately select in Tab. 1 just a few results obtained from the various methods introduced above. As one can see, the overall picture indicates large values of f_D and f_B (larger than f_π), and furthermore f_B is predicted comparable to (or even larger than) f_D, manifestly violating Eq.(4). This means that, at least in the case of the leptonic constants, the charm quark mass m_c is too light for Eq.(4) to apply straightforwardly, so that large $1/m_Q$ corrections are involved. In this regard, we remark that the concept of binding energy $\bar{\Lambda}$ introduced above also arises quite naturally in the QCD sum rules approach [13]-[15]. Actually, sum rules definitely indicate the ratio $2\bar{\Lambda}/m_Q$ as the expansion parameter around the heavy symmetry limit, rather than Λ_{QCD}/m_Q. Numerically, this parameter is small, of the order of 0.1 for the B, but is about $0.3 - 0.4$ for the D.

3 $B \rightarrow$ *charm* semileptonic decays

Semileptonic heavy meson decays have the important role, in the context of the Standard model, of representing a unique source of information on the CKM matrix

elements. In particular, from B semileptonic decays we should obtain the values of V_{cb} and V_{ub}. Furthermore, these processes give the opportunity to test the properties of QCD at the hadronic level, *via* the form factors of the different exclusive channels.

3.1 Inclusive semileptonic branching ratio

The inclusive semileptonic decay $B \to X_c l\nu$ (where only the lepton, but not the hadronic state X_c is observed experimentally, which theoretically amounts to a summation over all produced hadrons) is a crucial test of the spectator model. In this model, all decays (both semileptonic and nonleptonic) are assumed to occur by just the heavy quark decay, with the light quark not directly participating in the weak transition. In particular, by definition the inclusive decay rate should be "partonic", and determined by the corresponding decay rates for almost free heavy quarks. While we know that this mechanism by itself does not work for D-decays, due to the existence of more elementary quark transitions and of strong interaction nonperturbative effects, we would believe it to be well-verified in B-decays due to the much larger m_b. Basically, for free $b \to cl\nu$ decay:

$$\frac{d\Gamma_{sl}(b)}{E_l} = |V_{cb}|^2 \frac{m_b^5 G_F^2}{96\pi^3} F(\frac{m_c}{m_b}, E_l, \alpha_s) \tag{15}$$

where F accounts for phase space and QCD perturbative corrections [20]. Eq.(15) shows that in principle the CKM matrix element $|V_{cb}|$ is determined by the lepton spectrum (notice, however, the sensitivity to the specific value of m_b which is only approximately known). The total B width, summed over all quark and lepton species and neglecting $|V_{ub}|^2 \ll |V_{cb}|^2$, would be

$$\Gamma_b = |V_{cb}|^2 \frac{m_b^5 G_F^2}{96\pi^3} \eta_{QCD} \times (phase\ space\ factor). \tag{16}$$

With (15) and (16), the spectator model would predict $BR_{sl} \equiv (\Gamma_{sl}/\Gamma_b) \simeq 14\,\%$, somewhat larger than the current experimental determination $BR_{sl} = 10.5 \pm 0.2 \pm 0.4\,\%$ [21, 22]. A detailed analysis of the various contributions to $\Gamma(B)$ and the dependence on QCD parameters (such as α_s and quark masses) has concluded that the spectator model prediction can be decreased to about $BR_{sl} \simeq 12\,\%$ [23], so that some discrepancy with experiment still might persist. On the other hand, recent work in the framework of the $1/m_Q$ expansion of the leptonic width, based on the application of operator product expansion techniques, claims a nonperturbative reduction of Γ_{sl} [24]. This reduction would originate from the contribution in the expansion of the operator which causes the $B^* - B$ mass splitting, which is known and operates in the right direction to decrease BR_{sl}.

Concerning the determination of $|V_{bc}|$, in order to compare the spectator model prediction with the data, the b quark is considered as a virtual bound particle in the B meson, with mass

$$m_b^2 = m_B^2 + m_{spect}^2 - 2m_B\sqrt{m_{spect}^2 + \mathbf{p}^2}, \tag{17}$$

and the "partonic" lepton spectrum (15) is folded with a momentum distribution $\psi(p)$,

$$\frac{d\Gamma_{sl}(B)}{dE_l} = \int_0^{\bar{p}} dp\, p^2 \psi(p) \frac{d\Gamma_{sl}(b)}{dE_l} \equiv |V_{bc}|^2 \cdot \mathcal{K} \tag{18}$$

Alternatively, one can attempt to produce the inclusive semileptonic rate by summation of exclusive channels $B \to D$, $B \to D^*$, $B \to D^{**}$, *etc.*, so that the constant in (18) would be determined also by form factor estimates [25]. Thus, either way the theoretical coefficient $\mathcal{K}$ is calculated, up to some amount of model dependence which actually dominates the uncertainty in V_{bc}. The current determination is [22]:

$$|V_{bc}| = 0.043 \pm 0.008 \tag{19}$$

3.2 $B \to$ *charm* exclusive decays

Besides being interesting for the determination of V_{bc}, these transitions play a crucial role, *via* their dependence on the form factors, in testing the basic ideas underlying the nonperturbative frameworks adopted to predict them, briefly reviewed in Section 2. Furthermore, the fact that both the parent and the daughter mesons are heavy-light quark states leads to a simplified description, in terms of few "universal" form factors. This opportunity is reminiscent of the applications of "parton model" or "static quark model" ideas, but in fact it represents a very general consequence of QCD, similar to Eq.(4), and is a success of the description based on the heavy quark effective theory.

Concentrating on the "dominating" $0^- \to 0^-, 1^-$ decays $B \to D$ and $B \to D^*$, the form factors can be defined as [26]:

$$\langle M'(p')|J_\mu|M(p)\rangle = f_+(t)(p+p')_\mu + f_-(t)(p-p')_\mu, \tag{20}$$

$$\begin{aligned}\langle V(p',\eta)|J_\mu|M(p)\rangle = {} & \frac{2V(t)}{m_P+m_V}\epsilon_{\mu\nu\rho\sigma}\eta_\nu p_\rho p'_\sigma - iA_1(t)(m_P+m_V)\eta_\mu \\ & + i\frac{A_2(t)}{m_P+m_V}(\eta\cdot p)(p+p')_\mu + i\frac{A_3(t)}{m_P+m_V}(\eta\cdot p)(p-p')_\mu,\end{aligned} \tag{21}$$

where M, M' and V indicate B, D and D^* with polarization vector η. Also, $t = (p-p')^2$ is the momentum transfer, such that $m_l^2 \le t \le t_{max}$ with $t_{max} = (m_B - m_{D,D^*})^2$.

The calculation of form factors in the various theoretical approaches proceed as briefly sketched in Section 2. Of course, we must keep in mind that all approaches are characterized by advantages and shortcomings. Thus, in the constituent quark model detailed predictions are possible, as the form factors result from overlaps of meson wavefunctions, solutions of the bound state equation. However, in general one needs to boost the states from the rest frame, where wavefunctions are naturally defined, and this is a technical complication. In the QCD sum rules framework, the operator product expansion is applied to study three-point correlators, generalizing Eq.(7). For $B \to D$:

$$\Pi_\mu(p,p') = i^2 \int dx\, dy\, \exp\left(ip'\cdot x - ip\cdot y\right) \langle 0|T\left(J^\dagger_{5,M'}(x)\, J_\mu(0)\, J_{5,M}(y)\right)|0\rangle, \tag{22}$$

and similar ones for $B \to D^*$. As emphasized, this is a "first principles" approach, fully relativistic and avoiding the notion of constituent quark wavefunction. However, there is "systematic" uncertainty associated to the optimization procedure necessary to turn the QCD expansion into predictions for the form factors. In lattice QCD, the generalization of (12) is

$$G(T_x, T_y) = \sum_{\mathbf{x},\mathbf{y}} \langle 0|T\left(J^{\dagger}_{5,M'}(\mathbf{x}, T_x)\, J_{\mu}(0)\, J_{5,M}(\mathbf{y}, T_y)\right)|0\rangle. \tag{23}$$

However, as mentioned previously, the b quark is too heavy, so that the results with dynamical quarks are currently available only for D meson semileptonic transitions. Many calculations of form factors have been performed for finite m_c and m_b. In

Method	$f_+(0)$	$V(0)$	$A_1(0)$	$A_2(0)$
Quark Model [26]	0.69	0.71	0.65	0.69
Quark Model [27]	0.69	0.84	0.65	0.45
Sum Rules [28]	0.67 ± 0.19	0.86 ± 0.14	0.60 ± 0.102	0.36 ± 0.15

Table 2: Estimates of $B \to D, D^*$ form factors at $t = 0$.

most cases form factors are parametrized by polar forms, *e.g.*:

$$\frac{F(t)}{F(0)} = \left(1 - \frac{t}{M^2_{pole}}\right)^{-1}, \tag{24}$$

and the value of M_{pole} is either guessed independently or fit from the t-behavior of the results. Actually, in this regard it is interesting to notice that QCD sum rules give results consistent with the polar form (24) for f_+, V, A_2, but seem to prefer a

BR(%)	QM [26]	QM [25]	SR [28]	Exp.
$B \to Dl\nu_l$	$1.6\left(\frac{V_{bc}}{0.04}\right)^2$	$2.2\left(\frac{V_{bc}}{0.04}\right)^2$	$1.5\left(\frac{V_{bc}}{0.04}\right)^2$	1.8 ± 0.5
$B \to D^*l\nu_l$	$4.3\left(\frac{V_{bc}}{0.04}\right)^2$	$4.9\left(\frac{V_{bc}}{0.04}\right)^2$	$4.6\left(\frac{V_{bc}}{0.04}\right)^2$	4.6 ± 0.3

Table 3: Estimates of $B \to D, D^*$ branching ratios.

constant behavior of A_1 [29]. This is nicely consistent with the requirements of the heavy quark theory. To give an idea of the situation with form factor calculations, we report in Tab. 2 some selected examples from the constituent quark model (QM) and QCD sum rules (SR). In Tab. 3 we report results for the branching ratios in different schemes (experimental values are averages of CLEO and ARGUS data). We see that the dispersion in the results is not small, and that a substantially improved theoretical description is needed if we wish a precise determination of V_{bc} from exclusive decays.

With both m_b and m_c much larger than Λ_{QCD}, such an improvement is allowed by the heavy quark theory [8, 30]. Indeed, neglecting in this limit $1/m_Q$ corrections, the flavor and spin symmetry of the HQET implies that Eqs.(20) and (21) are all expressed in terms of just one "universal" nonperturbative form factor ξ, the so

called Isgur-Wise function. This form factor depends on $w = v \cdot v'$, with v and v' the initial and final meson four-velocities. Indeed, including QCD factors, one finds:

$$\langle D(v')|J_\mu|B(v)\rangle = \sqrt{m_B m_D}\,\xi(w)\,(v+v')_\mu \tag{25}$$

$$\langle D^*(v',\eta)|J_\mu|B(v)\rangle = \sqrt{m_B m_D}\,\xi(w)\left[i\epsilon_{\mu\nu\rho\sigma}\eta_\nu v_\rho v'_\sigma - (1+w)\eta_\mu + (\eta\cdot v)v'_\mu\right] \tag{26}$$

Notice that

$$w = v \cdot v' = \frac{m_B^2 + m_D^2 - t}{2m_B m_D} \tag{27}$$

According to Eqs.(25) and(26), the needed form factors reduce from six to one, the Isgur-Wise function, and in addition the symmetry requires the rigorous normalization at the zero recoil point $v = v'$, where $w = 1$:

$$\xi(1) = 1. \tag{28}$$

Thus, the theory is very predictive and model independent at the point $w = 1$, corresponding to $t = t_{max}$, which is a corner of the physical phase space. In this point, in the rest frame of the B, the produced D or D^* would be at rest. Also, the most relevant form factors in Eqs.(20) and (21) are protected at $t = t_{max}$ against corrections linear in $1/m_Q$ [31], and corrections start only at quadratic order (non-renormalization theorem). Away from the zero recoil point, the Isgur-Wise function must be estimated as a function of w by means of some nonperturbative approach. Also, for $t \neq t_{max}$ there are corrections of order $1/m_Q$, which are parametrized in terms of additional nonperturbative functions, so that the situation is really simple and model independent in the vicinity of the zero recoil point.

The estimate the Isgur-Wise form factor away from $w = 1$ is a nonperturbative problem, so that one must adopt a hadronization scheme. Several attempts have been made, using the constituent quark model (for example see [32] and [33]), and QCD sum rules [14, 29]. Preliminary results are now coming also from lattice QCD [34]. At present the most detailed analysis is from QCD sum rules formulated in the HQET, including $O(\alpha_s)$ corrections in the perturbative part of the QCD operator product expansion [35]. A typical behavior, found *e.g.* in [14], has the form

$$\xi(w) \simeq \left(\frac{2}{1+w}\right)^{\beta(w)}; \qquad \beta(w) \simeq 2 + \frac{0.6}{w}. \tag{29}$$

Concerning the subleading $1/m_Q$ structure, which involves four new universal form factors, this also has been studied with QCD sum rules [36]. All in all, the situation which emerges from these studies is that $1/m_Q$ corrections should not be offending the result of the heavy quark symmetry limit, so that the description around the zero recoil point should be theoretically under good control. In fact, the normalization $\xi(1) = 1$ appears to protect the heavy quark symmetry result even if the charm quark mass m_c is not so heavy. The opposite situation is met, as mentioned in Section 2, for the leptonic constants f_P.

Alternative determinations of $\xi(w)$ are discussed, for example, in [33, 37, 38]. Near $w = 1$, $\xi(w)$ can be parametrized as

$$\xi(w) = 1 - \rho^2\,(w-1) + O((w-1)^2) + \cdots, \tag{30}$$

and in general the slope ρ^2 must be bounded as $\rho^2 > 1/4$ [39]. A compilation of theoretical estimates of ρ^2 can be found in [34].

From the observations above it seems quite sensible to try to extract V_{bc} from the exclusive channel $B \to D^* l\nu$ (no $1/m_Q$ corrections at t_{max}). Clearly, in this region there is phase space suppression, so that the yield of events is poor and data are not very precise yet. The data on the differential width must be extrapolated from the region $t < t_{max}$, with an unavoidable extrapolation uncertainty, and compared to the theoretical expression:

$$\frac{d\Gamma}{dw} \propto |V_{bc}|^2 \, \xi(w)^2 \times (factor). \tag{31}$$

The result of such an analysis has led to the determination [40]:

$$|V_{bc}| = 0.050 \pm 0.008 \pm 0.002, \tag{32}$$

compatible with (19), and promising future significant improvements.

Concerning the building up of the total semileptonic rate by the sum over exclusive charmed channels, in [41] it was observed with regard to the large m_Q limit that, with the condition

$$(m_b + m_c)\Lambda_{QCD} \ll (m_b - m_c)^2 \ll (m_b + m_c)^2, \tag{33}$$

the sum of decays to the s-wave charm states should saturate the inclusive rate, namely $\Gamma(B \to D)_{sl} + \Gamma(B \to D^*)_{sl} = \Gamma(B)_{sl}$. This condition is certainly verified by $b \to c$ semileptonic decays. Although not strictly a consequence of HQET, this prediction looks quite natural as it results from naive parton-model ideas applied to heavy quark decays. However, it is surprisingly contradicted by experiment, which indicates $BR(B \to D + D^*)_{sl} \simeq 6\,\%$ and $BR_{sl} \simeq 10.5\,\%$, so that about one third of the events arises from decay modes different from $B \to Dl\nu$ and $B \to D^* l\nu$. Natural candidates to fill the gap are the decays $B \to D^{**} l\nu$, where D^{**} cumulatively denotes the positive-parity p-wave charmed meson states.

One expects four p-wave states, *i.e.* 0^+, 2^+ and two 1^+ states, which in principle would imply fourteen form factors. Heavy quark symmetry allows a dramatic simplification, reducing all that to just two independent universal form factors $\tau_{1/2}(w)$ and $\tau_{3/2}(w)$ [32, 42], which add to the Isgur-Wise function $\xi(w)$ for the complete description of $b \to c$ semileptonic decays. Different from $\xi(w)$, the normalizations of $\tau_{1/2}$ and $\tau_{3/2}$ at $w = 1$ are not fixed by heavy quark symmetry, and therefore are *a priori* unknown. There is the theoretical upper bound put by the optical sum rule [43]:

$$|\tau_{1/2}(1)|^2 + 2|\tau_{3/2}(1)|^2 < \frac{1}{2}\frac{m_D - m_c}{m_{D^{**}} - m_D} \simeq 0.5\,. \tag{34}$$

Attempts to estimate $\tau_{1/2}(w)$ and $\tau_{3/2}(w)$ have been presented in [32] (constituent quark model) and in [44] (QCD sum rules), and the results are in qualitative agreement. However, it appears that $O(1/m_Q)$ corrections should be by far more important in this case than for $B \to D, D^*$, because of lack of normalization of $\tau_{1/2}$ and $\tau_{3/2}$ at $w = 1$, so that there is much less protection against heavy quark

symmetry breaking effects. In addition, the expansion parameter becomes [44] $2\bar{\Lambda}^{**}/m_c$, with $\bar{\Lambda}^{**} = m_{D^{**}} - m_c$ the "binding energy", which is not small in this case. Recently, a significant D^{**} signal was found in B semileptonic decays, with $BR(B \to D^{**}l\nu) = (2.7 \pm 0.5 \pm 0.5)\,\%$, which would fill the gap[40]. It remains to be seen whether the HQET description can successfully account for this experimental result.

4 Heavy→light semileptonic decays

This category of semileptonic decays include transitions induced by $b \to ul\nu$, namely $B \to \pi(\eta)l\nu$, $B \to \rho(\omega)l\nu$, *etc.*; and all charmed semileptonic decays induced by $c \to sl\nu$ and $c \to ul\nu$, namely $D \to K(K^*)l\nu$, $D \to \pi(\rho,\omega)l\nu$, *etc.*

These processes play a paramount role in the determination of the CKM matrix elements V_{ub} and V_{cs}, V_{cd}. We expect $V_{ub} \ll Vcd < V_{cs}$, but $V_{ub} \neq 0$ is essential to have CP violation in the Standard Model. Another point of interest is represented by the form factors, bringing a great deal of information on strong interactions. Quite important is the fact that, due to the large available phase space, in addition to normalizations the t-behavior of form factors should be studied, so that detailed tests of model predictions can be made. Indeed, the model dependence of the form factors presently limits the accuracy of the determinations of V_{ub}. This demands for improved theoretical knowledge of form factors, and the consequent selection of "good" models. Also in this regard, a significant step towards model independence should be allowed by heavy quark symmetry. Actually, for heavy→light meson transitions, the simplification from the symmetry is not as spectacular as it is in the case of $b \to c$ transitions. However, model independent scaling laws connecting D decays to B decays can be derived, so that one can hope to transfer *via* these relations the precision attainable in experimental measurements of the more copious D-meson decays to reliable predictions for B form factors. Furthermore, with the mentioned scaling laws becoming exact at the point of zero recoil of light produced mesons, one can describe light degrees of freedom in that region of phase space by typical (and general) methods of low energy hadron physics, such as chiral Lagrangian dynamics. Clearly, models incorporating the union of heavy flavor symmetry and chiral symmetry account for fundamental properties of QCD, and therefore are general. Referring to [45] for a detailed presentation of experiments on D-semileptonic decays and for a comparison of form factor predictions, in what follows we briefly discuss $b \to u$ semileptonic decays and the applications of the heavy quark chiral theory.

4.1 $b \to u$ semileptonic decays and V_{ub}

As for V_{cb}, the measurement of V_{ub} can be attempted both from inclusive and from exclusive $b \to u$ semileptonic processes. Since $m_u \ll m_c$, inclusive searches look for an excess of leptons in the energy range above the endpoint of the favored $b \to c$ semileptonic decays, where these processes are kinematically forbidden and only $b \to u$ can go. This leaves a small "window" about $300\,MeV$ wide, near the endpoint of $b \to u$. From this one has to extrapolate the full lepton spectrum using

either the "parton" spectator quark model or the constituent quark model summing over exclusive decays, and extract the value of $|V_{ub}|$. This extrapolation turns out to be extremely sensitive to the model, and causes a considerable spread in the determination of V_{ub}. Consequently, although $V_{ub} \neq 0$ seems to be established, the actual value is quite uncertain. In addition, while until sometime ago the central value was about $V_{ub}/V_{cb} \simeq 0.1$, recent CLEO data [46] lead to a somewhat smaller value, about 0.06-0.07, which is bad news for searches of exclusive $b \to u$ processes. In Tab 4., adapted from [22], we collect some examples, which show the model and time dependence of $|V_{ub}|$. Clearly, this calls for theoretical progress in the calculation

Model	ARGUS 90	CLEO 90	CLEO 92
Ref.[25]	0.20 ± 0.02	0.15 ± 0.02	0.095 ± 0.027
Ref.[26]	0.13 ± 0.02	0.11 ± 0.02	0.065 ± 0.019
Ref.[20]	0.11 ± 0.01	0.09 ± 0.01	0.062 ± 0.018

Table 4: $|V_{ub}|/|V_{cb}|$ from inclusive $b \to u l \nu$

of the inclusive semileptonic lepton spectrum. The problem is complicated by the fact that the relevant energy range to suppress the $b \to c$ background is close to the endpoint for $b \to u$, where singular behavior can affect the theoretical differential lepton spectrum. For a QCD calculation from "first principles", the method of [24] has been generalized to this problem (both for $b \to c l \nu$ and $b \to u l \nu$), indicating the possibility of a general nonperturbative approach based on the operator product expansion [47], and improving the spectator "parton" model. The basic tensor, to be contracted by a lepton tensor to give the lepton spectrum, is

$$W_{\mu\nu} = i \int d^4x \exp(iq \cdot x) \langle B|T\left(J_\mu(x) J_\nu(0)^\dagger\right)|B\rangle, \tag{35}$$

where J_μ is the $b \to u$ (or $b \to c$) quark weak current. By the operator product expansion, Eq.(35) can be given an expression containing matrix elements between B-meson states of local operators with well-defined physical meaning.

Alternatively, the full method of QCD sum rules can be adopted [48], introducing the B-meson interpolating operator J_5 of Eq.(6), and this leads to the consideration of the four-point correlation function, generalization of (7) and (22):

$$T_{\mu\nu}(p, p', q) = i^3 \int d^4y d^4x d^4z \exp i(p' \cdot y + q \cdot x - p \cdot z) \langle 0|T\left(J_5(y) J_\mu(x) J_\nu(0)^\dagger J_5(z)^\dagger\right)|0\rangle. \tag{36}$$

Following the rules of the game, the tensor $W_{\mu\nu}$ is obtained by interfacing a double dispersion relation representation for the l.h.s of (36) with a QCD expansion of the operator product on the r.h.s., and performing the "optimization" procedure characteristic of the sum rule method. In so doing, the lepton spectrum can be expressed in terms of a perturbative QCD contribution, plus a series of familiar vacuum condensates. Time will tell whether these "first principles" attempts will lead to reliable determinations of the inclusive semileptonic $b \to u$ spectrum.

4.2 Exclusive $b \to u$ decays and heavy-quark chiral theory

In principle, V_{ub} determinations can result from $B \to \pi l\nu$, $B \to \rho(\omega) l\nu$, *etc.* Since no signal has been clearly established for any of these exclusive channels, only upper limits on V_{ub} have been obtained from these searches (for a review see [22]). As in the previous case, limits are strongly dependent on form factor models. Some examples which show the model dependence are reported in Tab. 5, and a detailed review is presented in [49]. The HQET seems to offer a good strategy to reduce the

	$f_+(0)$	$\Gamma(B \to \pi)$	$V(0)$	$A_1(0)$	$A_2(0)$	$\Gamma(B \to \rho)$
QM [26]	0.33	0.74	0.33	0.28	0.28	2.6
QM [25]	0.09	0.21	0.27	0.05	0.2	1.63
SR [49]	0.26 ± 0.02	0.51 ± 0.11	0.6 ± 0.2	0.5 ± 0.1	0.4 ± 0.2	1.2 ± 0.4
HQ [57]	0.53	1.9	0.62	0.21	0.20	2.1

Table 5: $B \to \pi$ and $B \to \rho$ form factors at $t = 0$, and decay rates in units $|V_{ub}|^2\, 10^{13}\, s^{-1}$.

theoretical uncertainty affecting $b \to u$ exclusive decays. Indeed, in the heavy→light case considered here, heavy flavor symmetry can only relate form factors of B and D decays, assuming both m_b and m_c to be heavy [50]. For example:

$$(f_+ + f_-)_{B\to\pi} = \left(\frac{m_c}{m_b}\right)\left(\frac{\alpha_s(m_b)}{\alpha_s(m_c)}\right)^{-6/25} (f_+ + f_-)_{D\to\pi}$$

$$(f_+ - f_-)_{B\to\pi} = \left(\frac{m_b}{m_c}\right)\left(\frac{\alpha_s(m_b)}{\alpha_s(m_c)}\right)^{-6/25} (f_+ - f_-)_{D\to\pi}\,, \qquad (37)$$

and more relations are found for $B \to \rho$ and $D \to \rho$. Reflecting the fact that the heavy flavor symmetry connects heavy quarks with different mass but same velocity, in these relations the arguments of the form factors correspond to equal energy of the final light meson. Thus, for equal E_π, the argument t_B on the l.h.s. of (37) is not the same as t_D on the r.h.s. Notice also that f_+ and f_- are connected in (37), so that both form factors are equally important in this framework, and should be measured in D-decay in order to extrapolate and predict the corresponding B-decay. Moreover, strictly speaking Eq.(37) (and similar ones) hold near the zero pion recoil point, where the pion kinetic energy is small, *i.e.* $t \simeq t_{max}$. The problem then is to extrapolate these relation for any values of $t \neq t_{max}$, eventually down to $t = 0$.

An interesting recent development is the formulation of an effective chiral Lagrangian, describing the interactions of heavy mesons with low energy pions [51], which incorporates both the heavy quark symmetry and the light quark $SU(3)$ and chiral $SU(3)$ symmetries. The complex of these symmetries, which are fundamental features of QCD, uniquely determines the form of the Lagrangian, which therefore represents a model-independent expansion in $1/m_Q$ as well as in $m_{\pi,K,\eta}$ and $E_{\pi,K,\eta}$ (chiral perturbation theory [52]). In this effective Lagrangian, the heavy mesons B, B^*, D, D^* with velocity v are described by the elementary field multiplet

($a = u, d, s$ is the light flavor):

$$H_a = \frac{1+\gamma\cdot v}{2}\left[\gamma_\mu P^*_{a,\mu} - \gamma_5 P_a\right], \tag{38}$$

and the $SU(3)$ octet mesons π, K, η are gathered in the matrix (λ's are $SU(3)$ matrices):

$$\Sigma = \exp\frac{\sqrt{2}i}{f_\pi}\sum_{b=1,..,8}\Pi_a\lambda_b. \tag{39}$$

Thus for example, in this notation the left-handed weak charged currents are simply expressed as

$$L_{a,\mu} = \bar{q}_a\gamma_\mu(1-\gamma_5)Q \equiv \frac{i\alpha}{2}Tr\left[\gamma_\mu(1-\gamma_5)H_b\xi^\dagger_{ba}\right] + \cdots, \tag{40}$$

where $\alpha = f_P/\sqrt{m_P}$ and the ellipsis denote subleading terms. The matrix ξ is such that $\xi^2 = \Sigma$ in (39). The strong interaction Lagrangian is

$$\mathcal{L}_{VPP} = \frac{ig}{2}Tr\left[H_a\gamma_\mu\gamma_5\left(\xi^\dagger\partial_\mu\xi - \xi\partial_\mu\xi^\dagger\right)_{ba}\bar{H}_b\right] + \cdots, \tag{41}$$

where g is connected to the $B^*B\pi$ (or $D^*D\pi$) coupling. The advantage of this Lagrangian description, using elementary meson fields, is that Feynman diagrams (tree plus loops) can be used to compute the different processes, including decays into multimeson final states [53], in terms of two universal constants, namely α and g.

To give some examples, the $SU(3)$ breaking effects in the leptonic constants are expressed as [55]:

$$\frac{f_{D_s}}{f_D} = 1 + \frac{5}{6}\left(1+3g^2\right)\frac{m_K^2}{16\pi f_\pi^2}\ln\left(\frac{m_K^2}{\mu^2}\right), \tag{42}$$

with μ a typical strong interaction scale ($\mu \sim 1\,GeV$), and similar corrections can be calculated for $B \to D(D^*)l\nu$ [56]. For $D \to \pi l\nu$ with small E_π, *i.e.* not far from t_{max}:

$$f_+ \simeq \frac{f_B}{2f_\pi}\left[1 + g\frac{m_D - E_\pi}{m_{D^*} - m_D + E_\pi}\right]. \tag{43}$$

The extrapolation of this prediction and similar ones for $D \to \rho$, from t_{max} to $t = 0$ and from charm to beauty semileptonic decays, has been discussed in [57], and we quote the results in Tab. 5.

5 Conclusions

In conclusion, it appears that the HQET could definitely represent a decisive step forward, on the way to model independence in the description of heavy meson semileptonic decays. It should be possible to obtain, in this scheme, reliable expansions of the relevant transition amplitudes in terms of few "universal" physical quantities.

Of great theoretical interest is the effective Lagrangian realization of the theory, which allows calculations of heavy→light transitions by means of familiar Feynman diagram techniques, and gives the possibility of including also higher excitations of the ground state mesons in the scheme.

The still open problems, concerning systematic applications, are the extrapolation of form factors away from the zero recoil region, and the estimate of the next-to-leading corrections in $1/m_Q$ in various cases. This challenging programme is presently vigorously pursued.

References

[1] Particle Data Book, Review of Particle Properties, Phys. Rev. D45 (1992) S1. J.Adler *et al.*, Phys. Rev. Lett. 60, 1375 (1988).

[2] S. Aoki *et al.* (WA75 Collaboration), Prog. Theor. Phys. 89, 131 (1993).

[3] Y. Kubota *et al.* (CLEO Collaboration), paper submitted to the EPS-HEP Conference (Marseille, 1993).

[4] See *e.g.* G. Altarelli, in *Proceedings of the 1987 Cargèse Summer School*, Eds. M. Lévy *et al.*, Plenum Press, New York (1988), p.261.

[5] M. Lusignoli, L. Maiani, G. Martinelli and L. Reina, Nucl. Phys. B369, 139 (1992).

[6] M. Bauer, B. Stech and M. Wirbel, Zeit. Phys. C 34,103 (1987); J. L. Rosner, Phys. Rev. D42, 3732 (1990).

[7] M. B. Voloshin and M. A. Shifman, Sov. J. Nucl. Phys. 45, 292 (1987); H. D. Politzer and M.B. Wise, Phys. Lett. B206, 681 (1988), B208, 504 (1988); N. Isgur and M. B. Wise, Phys. Lett. B232,113 (1989).

[8] For a review see *e.g.* H. Georgi, in Proc. of the Theoretical Advanced Study Institute, eds. R. K. Ellis *et al.* (World Scientific, 1992) p. 589; B. Grinstein, Ann. Rev. Nucl. Part. Sci. 42, 101 (1992).

[9] P. Colangelo, G. Nardulli and M. Pietroni, Phys. Rev. D43, 3002 (1991); P. J. O'Donnell, Phys. Lett. B261, 295 (1991); and references there.

[10] M. A. Shifman, A. I. Vainshtein and V. I. Zakharov, Nucl. Phys. B147, 385, 448 (1979); L. J. Reinders, H. R. Rubinstein and S. Yazaki, Phys. Rep. C 127, 1 (1985).

[11] T. M. Aliev and V. L. Eletsky, Sov. J. Nucl. Phys, 38, 936 (1983).

[12] C.A. Dominguez and N. Paver, Phys. Lett. B197, 423 (1987), B199, 596 (1987) (E); S. Narison, Phys. Lett. B198, 104 (1987); L. J. Reinders, Phys. Rev. D38, 423 (1988); K. Schilcher and Y. L. Wu, Zeit. Phys. C 54, 163 (1992).

[13] C. A. Dominguez and N. Paver, Phys. Lett. B269, 169 (1991); E. Shuryak, Nucl. Phys. B198, 83 (1982); V. Eletsky and E. Shuryak, Phys. Lett. B276, 191 (1992).

[14] M. Neubert, Phys. Rev. D245, 2451 (1992).

[15] E. Bagan, P. Ball, V. M. Braun and H. G. Dosch, Phys. Lett. B278, 457 (1992).

[16] D. J. Broadhurst and A. G. Grozin, Phys. Lett. B274, 421 (1992).

[17] For an updated review see *e.g.* Proc. of the Conference Lattice '92, Nucl. Phys. B (Proc. Suppl.) 30 (1993).

[18] A. Abada *et al.*, Nucl. Phys. B376, 172 (1992); C. R. Allton *et al.*, Univ. of Rome Report 93/928 (1993).

[19] C. A. Dominguez and N. Paver, Ref.[12] and work in progress.

[20] G. Altarelli, N. Cabibbo, G. Corbo, L. Maiani and G. Martinelli, Nucl. Phys. B208, 365 (1982).

[21] S. Henderson *et al.*, CLEO Collaboration, Phys. Rev. D45, 2212 (1992).

[22] For a review and references see P. S. Drell and J. R. Patterson, in Proc. of the XXVI Conference on High Energy Physics, Dallas (USA), 1992.

[23] G. Altarelli and S. Petrarca, Phys. Lett. B261, 303 (1991).

[24] I. I. Bigi, N. G. Uraltsev and A. Vainshtein, Phys. Lett. B293, 430 (1992).

[25] N. Isgur, D. Scora, B. Grinstein and M. B. Wise, Phys. Rev. D39, 799 (1989).

[26] M. Wirbel, B. Stech and M. Bauer, Zeit. Phys. C 29, 637 (1985).

[27] P. Colangelo, G. Nardulli and L. Tedesco, Phys. Lett. B272, 344 (1991).

[28] P. Colangelo, G. Nardulli, A. A. Ovchinnikov and N. Paver, Phys. Lett. B269, 201 (1991).

[29] P. Ball, Phys. Lett. B278, 457 (1992).

[30] N. Isgur and M. B. Wise, Phys. Lett. B237, 527 (1990).

[31] M. E. Luke, Phys. Lett. B252, 447 (1990); C. Glenn Boyd and D. E. Brahm, Phys. Lett. B257, 393 (1991).

[32] N. Isgur and M. B. Wise, Phys. Rev. D43, 819 (1991).

[33] M. Neubert and V. Rieckert, Nucl. Phys. B382, 97 (1992).

[34] C. Bernard, Y. Shen and A. Soni, Report BNL-49237 (1993); S. P. Booth *et. al.*, UKQCD Collaboration, Univ. of Southampton Report SHEP-92-93-17 (1993).

[35] E. Bagan, P. Ball and P. Gosdzinsky, Phys. Lett. B301, 249 (1993); M. Neubert, Phys. Rev. D47, 4063 (1993).

[36] Z. Ligeti, M. Neubert and Y. Nir, Phys. Rev. D47, 5060 (1993).

[37] J. Rosner, Ref.[6].

[38] B. Blok and M. Shifman, Phys. Rev. D47, 2949 (1993).

[39] J. D. Bjorken, SLAC Report SLAC-PUB-5278 (1990).

[40] H. Albrecht, ARGUS Collaboration, Zeit. Phys. C 57, 533 (1993).

[41] M. Voloshin and M. Shifman, Sov. J. Nucl. Phys. 47, 511 (1988).

[42] S. Balk, J. G. Körner, G. Thomson and F. Hussain, ICTP Report IC/92/397.

[43] M. Voloshin, Phys. Rev. D46, 3062 (1992).

[44] P. Colangelo, G. Nardulli and N. Paver, Phys. Lett. B293, 207 (1992).

[45] E. Meroni, this volume.

[46] F. Muhein, CLEO Collaboration, in Proc. of the 7th Meeting of the Division of Particles and Fields, Chicago (1992), World Scientific.

[47] I. I. Bigi, M. Shifman, N. G. Uraltsev and A. Vainshtein, Univ. of Notre Dame Report UND-HEP-93-BIG01.

[48] P. Ball, V. M. Braun and H. G. Dosch, Phys. Rev. D48, 2110 (1993).

[49] P. Ball, Univ. of Munich Report TUM-T31-39/93.

[50] N. Isgur and M. B. Wise, Phys. Rev. D42, 2388 (1990).

[51] M. B. Wise, Phys. Rev. D45, R2188 (1992); T. M. Yan *et. al.*, Phys. Rev. D46, 1148 (1992); G.Burdman et J. F. Donoghue, Phys. Lett. B280, 287 (1992); P. Cho, Phys. Lett. B285, 145 (1992).

[52] J. Gasser and H. Leutwyler, Nucl. Phys. B250, 465 (1985).

[53] See *e.g.* C. L. Y. Lee, Phys. Rev. D48, 2121 (1993); C. L. Y. Lee, M. Lu and M. B. Wise, Phys. Rev. D46, 5040 (1992).

[54] R. Casalbuoni, *et al.*, Phys. Lett. B292, 371 (1992); J. Schechter and A. Subbaram, Phys. Rev. D48, 332 (1993).

[55] B. Grinstein *et al.*, Nucl. Phys. B380, 369 (1992).

[56] L. Randall and M. B. Wise, Phys. Lett. B303, 135 (1993).

[57] R. Casalbuoni *et al.*, Phys. Lett. B299, 139 (1993).

Frascati Physics Series, Vol. 1 (1993)
HEAVY QUARKS AT FIXED TARGET
Frascati, May 31st – June 2nd 1993
(pp. 151–164)

EXPERIMENTAL STATUS OF CHARM SEMILEPTONIC DECAYS

E. Meroni
Università di Milano, Dipartimento di Fisica and Sezione INFN
Via Celoria, 16, I-20133 Milano, (ITALIA)

Abstract

The experimental results of D^0, D^+ and D_s^+ semileptonic decays are summarized and compared with theoretical predictions. Emphasis is given to fixed target experiment results. The most recent measurements are from the photoproduction experiment E687.

1.-Introduction

The semileptonic decays are among the best understood charm decays, since they can proceed only via the spectator diagram. The hadronic dynamics can be described in terms of form factors, which can be predicted theoretically and checked with the data.

The decay of the D meson into a pseudoscalar, as in $D \to \overline{K}\, \ell^+ \nu$, is the simplest semileptonic charm decay. The relevant matrix element is given by:

$$M = \frac{G_F}{\sqrt{2}} V_{cs} \left[(p_D+p_K)_a \, f_+(q^2) + (p_D-p_K)_a \, f_-(q^2) \right] \bar{u}_\nu \gamma^a(1+\gamma_5) u_e$$

where p_D and p_K are the four-momenta of the D and K, G_F is the Fermi constant, V_{cs} is the CKM matrix element, q^2 is the four-momentum transfer from D to K (or $M^2_{e\nu}$) and $f_\pm(q^2)$ are the form factors.

The decay rate with respect to q^2 can be written in the form[1]:

$$\frac{d\Gamma}{dq^2} = \frac{G_F^2 |V_{cs}|^2 K^3}{24\pi^3} \left| f_+(q^2) \right|^2$$

with $K = \frac{M_D}{2} \left[\left(1 - \frac{m_K^2+q^2}{M_D^2} \right)^2 - 4\frac{m_K^2 q^2}{M_D^4} \right]^{1/2}$.

In the case of muons and electrons in the final state, the contribution of the terms involving the form factor $f_-(q^2)$ is negligible since they are multiplied by m_ℓ^2.

A common theoretical assumption for the q^2 dependence of the form factor is a single pole form:

$$f_+(q^2) = \frac{f_+(0)}{1-\frac{q^2}{M_p^2}},$$

where M_p is the pole mass of the nearest exchanged particle in the t channel. For this channel it is the vector meson D_s^*.

For the decay $D \to \overline{K}\, \ell^+ \nu$ the dependence on q^2 of the form factor has been determined experimentally, as well as the branching ratio. Assuming $|V_{cs}| = |V_{ud}|$, which follows from the unitarity of the CKM matrix, a value for $f_+(q^2)$ at $q^2=0$ can be computed and compared with theoretical predictions.

Decays of the D meson to vector particles ($D \to \overline{K}^* \ell^+ \nu$) introduce Lorentz invariant products of momenta and spins. The decay rate can be written in terms of the three helicity amplitudes H_0, H_+ and H_- of the vector meson:

$$\frac{d\Gamma}{dq^2} = \frac{G_F^2 |V_{cs}|^2 K\, q^2}{96\pi^3 M_D^2}\left(|\overline{H}_+|^2 + |\overline{H}_-|^2 + |\overline{H}_0|^2\right)$$

The helicity amplitudes $\overline{H}_\pm$ correspond to the contribution of the transverse polarizations of the vector meson and are related to the axial form factor $A_1(q^2)$ and to the vector one $V(q^2)$ by[2]:

$$\overline{H}_\pm(q^2) = (M_D + M_{K^*})\, A_1(q^2) \pm \frac{2M_D K}{M_D + M_{K^*}}\, V(q^2).$$

$\overline{H}_0$ comes from the contribution of the longitudinally polarized K^* and is a linear combination of the axial form factors $A_1(q^2)$ and $A_2(q^2)$:

$$\overline{H}_0(q^2) = \frac{1}{2M_{K^*}\sqrt{q^2}} \times \left[(M_D^2 - M_{K^*}^2 - q^2)\,(M_D + M_{K^*})\, A_1(q^2) - \frac{4M_D^2 K^2}{M_D + M_{K^*}}\, A_2(q^2)\right].$$

To study this decay we should have the q^2 dependence of all three form factors separately and find the magnitudes of the form factors at a fixed point.

At present, experiments have assumed a single pole form for the q^2 dependence of the form factors and since $A_1(q^2)$ is common to all three helicity amplitudes and can be factorized, they have measured the ratios of the form factors $R_2=A_2(q^2)/A_1(q^2)$ and $R_V=V(q^2)/A_1(q^2)$ evaluated at $q^2=0$.

2.-Fixed target experiments

E691, E653, WA82 and E687 are the fixed target experiments which provided recent results on semileptonic decays. Because the ν momentum cannot be directly measured, they need precise positions of the primary and secondary vertices to measure the D momentum. Therefore these experiments have to rely on a good vertex detector to enhance the signal over background. To reconstruct the secondary vertex they take advantage of the long decay path of the D meson. To reduce the fake vertices, the lepton and the kaon are required to verticize with a given confidence level and the secondary vertex is required to be isolated from other tracks to remove higher multiplicity decay channels. The cut on error normalized decay length, ℓ/σ_ℓ, is important to reduce the non charm background events.

3.-The decay $D\rightarrow \overline{K}\,\ell^+\nu$

This decay is often studied by tagging the D^0 through the decay chain $D^{*+}\rightarrow D^0\,\pi^+$; the signature of this decay is the presence of a peak in the D^* region. The photoproduction experiment E691[3] followed this method; fig.1a shows the invariant mass spectrum of the $(K^-e^+\nu)\pi^+$ system obtained by imposing $M_{Ke\nu} = M_{D^0}$. The longitudinal component of the neutrino momentum is calculated in a reference frame where the Ke longitudinal momentum along the D^0 direction is zero. In the boosted frame they require that $E_\nu>0$. There is a quadratic ambiguity and two solutions are possible: if both the solutions are acceptable, the one producing the lower D^{*+} mass is selected.

The random background shape is given by wrong sign combinations (fig. 1b); fig 1c shows the background subtracted effective mass distribution for $(K^-e^+\nu)\pi^+$ events.

Feedthroughs from the non-leptonic charm decay modes are negligible because of the good rejection of pions in the electron sample ($e/\pi \approx 7 \cdot 10^{-3}$). Moreover the D^* tag requirement suppresses any contribution from semileptonic decays of D^+ and D_s^+ mesons. The only large feedthrough comes from $D^0 \to K^- \pi^0 e^+ \nu$. To determine this contribution (estimated to be 7% of the total rate) they assume $\Gamma(D^0 \to K^{*-} e^+ \nu) = \Gamma(D^+ \to \overline{K}^{*0} e^+ \nu)$ which follows from isospin invariance. E691 calculated the BR relative to the decay channel $D^0 \to K^- \pi^+$. The result is shown in table 1 with other experimental results.

The photoproduction experiment E687[4] followed the same procedure. The contribution to the D^* peak from the decay $D^0 \to K^{*-} \mu^+ \nu \to K^- \pi^0 \mu^+ \nu$ is estimated to be 14%, and from hadronic decays $D^0 \to K^- \pi^+ \pi^0$ and $D^0 \to K^- \pi^+ \pi^0 \pi^0$ where the π is misidentified as a μ (1.7%) and the π^0 is undetected, to be 12%. Table 1 reports the E687 result for an analysis based on the data from the 1987-88 run, which consists of approximately 60 million multihadronic triggers, and from a preliminary result based on the data accumulated in the 1990 run (~200 million multihadronic triggers).

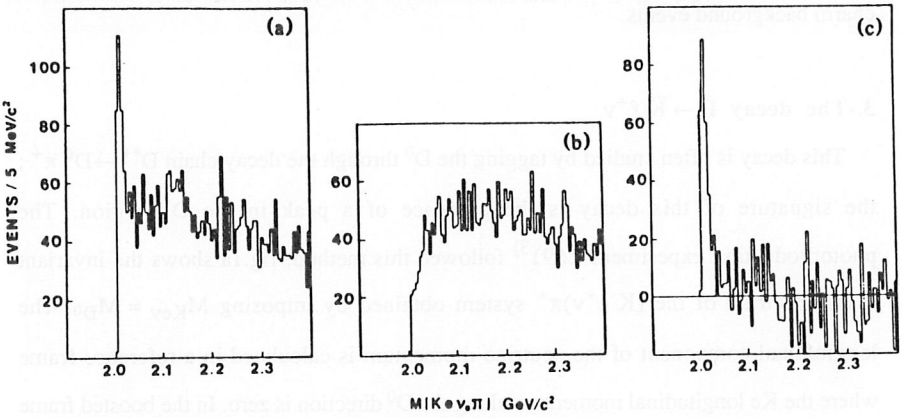

Fig. 1: E691- Effective mass distribution (a) for right sign $K^- e^+ \nu \pi^+$, (b) for wrong sign $K^+ e^+ \nu \pi^+$, $K^- e^- \nu \pi^+$ and $K^+ e^- \nu \pi^+$ combinations, (c) Background subtracted events

Experiment E653[5] used the minimum parent mass distribution (fig. 2), defined as $M_{min} = \sqrt{M_{vis}^2 + p_\perp^2} + \sqrt{M_{neu}^2 + p_\perp^2}$, to select the fraction f of $D^0 \to K^- \mu^+ \nu$ decay .

The fraction f is determined from a maximun likelihood fit to the experimental M_{min} distribution, $\ln L = \sum_{events} \ln \{0.97[f\,(I_{K\mu\nu}+0.11 I_{\pi\mu\nu})+(1-1.11f)I_{\mu\nu X}]+0.03 I_{had}\}$, where the $I_i(M_{min})$ are MC distributions for $D \to K\mu\nu$ and $\pi\mu\nu$, as well as for $K\mu\nu X^0$ and for the 3% feedthrough of hadronic decays. The branching ratio (table 1) have been calculated from the f value and from the world-average value for semileptonic branching ratio $B(D^0 \to \mu^+ X)=0.96\ B(D^0 \to e^+ X)$.

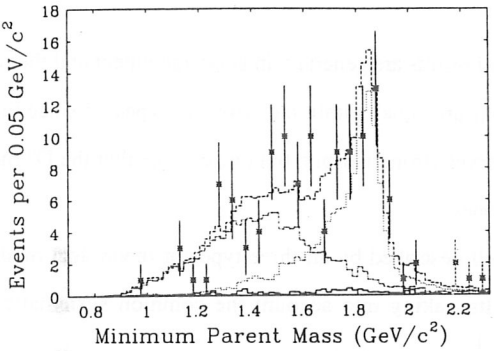

Fig. 2: Comparison of M_{min} distribution for $D^0 \to K^-\mu^+\nu$ combinations with fitted MC distributions: total (dashed), $K\mu\nu$ plus $\pi\mu\nu$ (dotted), $K\mu\nu X^0$ (dot–dashed) and hadronic decay feedthrough (solid).

Table 1a: $D \to \overline{K}\,\ell^+\nu$: experimental results

EXPERIMENTS	$\frac{D \to \overline{K}\ell^+\nu}{D \to K^-\pi^+}$	BF($D \to \overline{K}\,\ell^+\nu$) (%)
	$D^+ \to \overline{K}^0\,\ell^+\nu$	
MARKIII (e)[7]		$6.5^{+1.6}_{-1.1}\pm0.7$
E691 (e)[3]		6.1±0.9±1.6
Average		6.3±1.2
	$D^0 \to K^-\,\ell^+\nu$	
MARKIII (e)[7]		3.4±0.5±0.4
CLEO (e)[8]	.90±.06±.06	3.8±0.3±0.6
CLEO (μ)[8]	.79±.08±.09	3.3±0.3±0.6
E691 (e)[3]	.91±.07±.11	3.8±0.5±0.6
E653 (μ)[5]		2.4±0.4±0.5
E687(87-88) (μ)[4]	.82±.13±.13	3.4±0.5±0.7
E687(90) (μ)[4]	.87±.08±.06	3.7±0.3±0.6
Average	0.87±0.05	3.2±0.4
$\Gamma(D^+ \to \overline{K}^0\,\ell^+\nu) = 5.9\pm1.1\ \ 10^{10}s^{-1}$		
$\Gamma(D^0 \to K^-\,\ell^+\nu) = 7.7\pm0.8\ \ 10^{10}s^{-1}$		
$\Gamma(D \to \overline{K}\,\ell^+\nu) = 7.1\pm0.6\ \ 10^{10}s^{-1}$		

Table 1b: Theoretical predictions

THEORY	Rate $10^{10}s^{-1}$
QUARK MODEL	
GS[1]	7.1
WSB[2]	8.26
ISGW[9]	8.5
KS[10]	10.2(e) - 9.9(μ)
LATTICE GAUGE CALCUL.	
CMHS[11]	9.5±4.
LMMS[12]	5.8±1.5
BKS[13]	12.±2.±5.
QCD SUM RULES	
BBD[14]	6.4±1.4
DP[15]	8.2±1.1
AEK[16]	5.1±1.7
AOS[17]	9.1±4.5

Table 1 shows measurements and predictions for the BR of the decay channel $D \rightarrow \overline{K}\, \ell^+ \nu$ both for neutral and charged D mesons. All the results, except for MARKIII and E653, are normalized to the MARKIII branching ratios $B(D^0 \rightarrow K^- \pi^+)= 4.2 \pm 0.4 \pm 0.4\%$ and $B(D^+ \rightarrow K^- \pi^+ \pi^+)=9.1 \pm 1.3 \pm 0.4\%$. To compute the partial decay widths, the lifetime values from PDG[6] are used and, mainly due to the reduced phase space, the muon BF have been multiplied by 1.017 before averaging with the electron ones.

The experimental results are generally in good agreement and the semileptonic widths of the two D mesons are equal within the errors as expected since the Cabibbo favored weak current conserves strong isospin, but one can see that the D^0 measured widths are larger than the D^+ ones.

The data are well described by all three types of theoretical models. Averaging the experimental results, taking into account the common systematic errors, we obtain $\Gamma_K = 7.1 \pm 0.6\ 10^{10} s^{-1}$.

Several groups have shown that the q^2 dependence of the data is consistent with the single pole shape of the form factor. As an example,the data for E691 are shown in fig.3.

Values of the pole mass, found by different experiments, are given in table 2. The average value is consistent with the known D_s^+ mass of 2.1 GeV/c^2. Integrating the rate over q^2, using a monopole dependence for the form factor with a pole mass of 2.1 GeV/c^2, we obtain this relationship:

$$\Gamma_K = 1.51\ 10^{11}\ |f_+(0)|^2\ |V_{cs}|^2\ s^{-1}$$

Using the average value for Γ_K and assuming $|V_{cs}|=|V_{ud}|=0.9744$, an experimental value for $f_+(0)$ can be obtained. It is shown in table 3a both for charged and neutral D decays. The theoretical predictions for all three types of models agree with the data (table 3b).

We can conclude that the $D \rightarrow \overline{K}\, \ell^+ \nu$ decay is quite well understood. Several different theoretical approaches and different experimental techniques are in agreement.

Table 2: pole mass for $D \to \overline{K}\, \ell^+\nu$

Experiment	m_{pole} (GeV/c^2)
MARKIII(e)[7]	$1.8^{+0.5\ +0.3}_{-0.2\ -0.2}$
CLEO(e)[8]	$2.0^{+0.4\ +0.3}_{-0.2\ -0.2}$
E691(e)[3]	$2.1^{+0.4}_{-0.2}\pm 0.2$
E687(90)(μ)[4]	$2.1^{+0.7\ +0.7}_{-0.3\ -0.3}$
Average	2.0±0.2

Table 3b: $f_+(0)$

THEORETICAL PREDICTIONS	
QUARK MODEL	
GS[1]	0.69
WSB[2]	0.76
ISGW[9]	0.76
KS[10]	0.76
LATTICE GAUGE CALCULATIONS	
CMHS[11]	0.74±0.17
LMMS[12]	0.63±0.08
BKS[13]	0.9±0.08±0.21
QCD SUM RULES	
BBD[14]	0.6±0.15
DP[15]	0.75±0.05
AEK[16]	0.6±0.15
AOS[17]	0.8±0.2

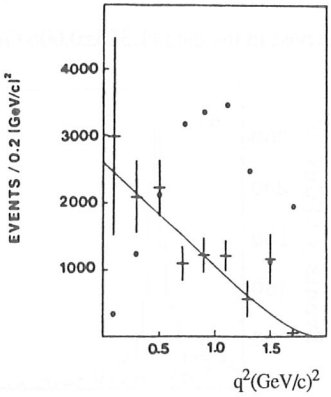

Fig. 3: E691–dN/dq^2 distribution; the dots indicate the reconstruction efficiency.

Table 3a: $f_+(0)$ for $D \to \overline{K}\, \ell^+\nu$

EXPERIMENTAL RESULTS	
	$f_+(0)$
D^0	0.73±0.04
D^+	0.64±0.06
Average D	0.70±0.03

4.-The decay $D \to \overline{K}^*\, \ell^+\nu$

To study this decay, three particle $K\pi\,\ell$ combinations are selected with the requirement that the kaon and the lepton have opposite sign. All the experimental evidences confirm that the decay is dominated by K^* resonance as shown in fig.4 where the $K\pi$ invariant mass is plotted for E687[4] data.

The charm decay backgrounds for $D^+ \to \overline{K}^{*0}\mu^+\nu$ channel are: $D^+ \to (K^-\pi^+)_{n.r.}\mu^+\nu$, $D^{*+} \to (K^-\mu^+\nu)\pi^+$, $D^+ \to (K^-\pi^+)\pi^0\mu^+\nu$ and $D^+ \to (K^-\pi^0)\pi^+\mu^+\nu$. To set a quantitative limit on contamination, E687 fits the two dimensional distribution of the $K^-\pi^+$ and $K^-\pi^+\mu^+$ mass. The fit function is a combination of the MC distributions of the signal and of the charm background decays. The fit gives:

$$\frac{\Gamma(D^+ \to (K^-\pi^+)_{nr}\mu^+\nu)}{\Gamma(D^+ \to (K^-\pi^+)\mu^+\nu)} = 0.083\pm0.029 \quad \text{and} \quad \frac{\Gamma(D^+ \to (K^-\pi^+)\pi^0\mu^+\nu)}{\Gamma(D^+ \to (K^-\pi^+)\mu^+\nu)} < 0.042 \text{ at } 90\% \text{ of}$$

C.L. The small contribution found for the decay channel with an additional neutral track

($D^+ \to \overline{K}^{*0}\pi^0\mu^+\nu$) is confirmed by comparing the average $K^-\pi^+\mu^+$ invariant mass observed in the data (1.373±0.006 GeV/c^2) with the MC prediction (1.379 GeV/c^2).

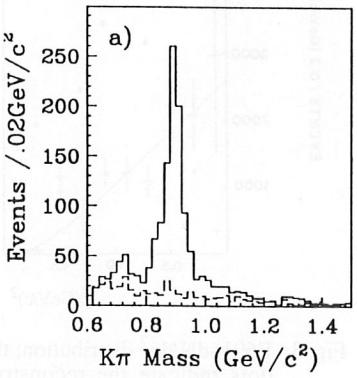

Fig.4: E687- Kπ invariant mass for $\overline{K}^*\mu\nu$ events.

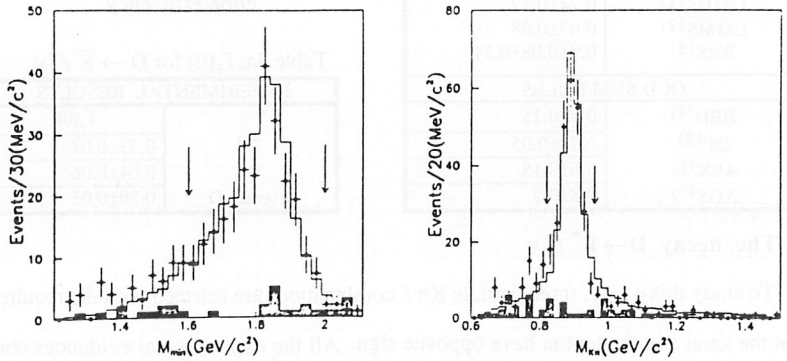

Fig 5: E653- $D \to \overline{K}^*\mu\nu$ decay: (a) M_{min} distribution, (b) Kπ invariant mass.

Experiment E653[5] measured the ratios $\frac{\Gamma(D^+ \to \overline{K}^{*0}\mu^+\nu)}{\Gamma(D^+ \to K^-\pi^+\pi^+)}$ and $\frac{\Gamma(D^+ \to \overline{K}^{*0}\mu^+\nu)}{\Gamma(D^0 \to K^-\mu^+\nu)}$. They uses the minimum parent mass to reduce potential contamination from decay channels with unobserved neutral hadrons such as $D^+ \to \overline{K}^{*0}\pi^0\mu^+\nu$. Additional neutral decay products cause the peak to broaden out and to shift to lower mass (Fig. 5a). To suppress this contamination they impose the cut $1.6 < M_{min} < 2.0$ GeV/c^2. Fig.5b shows the Kπ invariant mass for the events surviving the M_{min} cut.

Table 4 shows the measured decay widths for both charged and neutral charm D mesons to K*. The semileptonic widths for the two D's are expected to be equal, and they are within the errors. We can average the results to obtain $\Gamma_{K^*}=4.5\pm0.5\ 10^{10}\ s^{-1}$. Although the measurements are generally in good agreement with one another and with the lattice and the QCD sum rules predictions, they are a factor of two smaller than the quark model predictions. The same discrepancy appears in the measurement of the ratio $\frac{\Gamma(D \to \overline{K}^* \ell^+ \nu)}{\Gamma(D \to \overline{K} \ell^+ \pi^+)}$, as shown in table 4; the experimental width $\Gamma(D \to \overline{K}^* \ell^+ \nu)$ is half of the width $\Gamma(D \to \overline{K} \ell^+ \nu)$. MARKIII value refers to the $K\ell 4/K\ell 3$ ratio: they do not have sufficient sensitivity to quote a BF ratio for the $D \to \overline{K}^* \ell^+ \nu$[4]. QCD sum rules predictions on the ratio of the two widths tend to agree better with the experimental measurements.

Table 4: $BR(D \to \overline{K}^* \ell^+ \nu)$

Experiment	$BR(D \to \overline{K}^* \ell^+ \nu)$ (%)	$\frac{\Gamma(D \to \overline{K}^* \ell^+ \nu)}{\Gamma(D \to \overline{K} \ell^+ \nu)}$
	$D^+ \to \overline{K}^{*0} \ell^+ \nu$	
MARKIII(e)[7]	$5.3^{+1.9}_{-1.1}\pm0.6$	$1.0^{+0.3}_{-0.2}$
ARGUS(e)[19]	4.2±0.6±1.0	
E691[3]	4.4±0.4±0.8	0.55±0.14
WA82(e)[20]	5.6±1.6±0.9	
E653(μ)[5]	4.18±.66±.96	0.43±0.09±.09
E653/(kμν)	3.25±0.71±.75	
E687(μ)[4]	5.1±0.4±0.9	0.59±0.10±.13
Average	4.7±0.6	
	$D^0 \to K^{*-} \ell^+ \nu$	
MARKIII(e)	$4.4^{+1.9}_{-1.0}\pm0.6$	
CLEO(e)[8]	1.9±0.6±0.5	0.51±0.18±.06
ARGUS(e)	1.8±0.3±0.5	
Average	2.1±0.5	0.55±0.07
$\Gamma(D^+ \to \overline{K}^{*0} \ell^+ \nu)$	$= 4.4\pm0.6\ 10^{10} s^{-1}$	
$\Gamma(D^0 \to K^{*-} \ell^+ \nu)$	$= 4.9\pm1.1\ 10^{10} s^{-1}$	
$\Gamma(D \to \overline{K} \ell^+ \nu)$	$= 4.5\pm0.5\ 10^{10} s^{-1}$	

THEORY	$\Gamma(D \to \overline{K}^* \ell^+ \nu)$ $10^{10} s^{-1}$	$\frac{\Gamma(D \to \overline{K}^* \ell^+ \nu)}{\Gamma(D \to \overline{K} \ell^+ \nu)}$
QUARK MODEL		
GS[1]	9.8	1.4
WSB[2]	9.53	1.15
ISGW[9]	9.4	1.1
KS[10]	9.8(e) - 9.3(μ)	0.95
LATTICE GAUGE CALCULATIONS		
LMMS[12]	5.0±0.9	0.86±0.27
QCD SUM RULES		
BBD[14]	3.8±1.5	0.5±0.15
AOS[17]	7.9±3.9	

The analysis for the determination of the form factors in the decay $D \to \overline{K}^* \ell^+ \nu$ is complex. The quantities to be experimentally determined are the ratios of the form factors

$R_2 = A_2(0)/A_1(0)$ and $R_V = V(0)/A_1(0)$ and the ratio of longitudinal and transverse widths.

The form factors are assumed to follow a monopole behavior and the pole mass is fixed at 2.5 GeV/c^2 for $A_{1,2}(q^2)$ and 2.1 GeV/c^2 for $V(q^2)$. In order to measure R_2 and R_V the experiments follow this sequence: generate MC events for a given value of R_2 and R_V, compare the MC results with the data to construct a Likelihood function L, and repeat until the maximum of the L function is found. The fit is performed to the data distributions of $\cos\theta_V$, the angle between the π and the D direction in the $\overline{K}^*$ rest frame, $\cos\theta_\ell$, the angle between the ν and the D direction in the $\ell\nu$ rest frame, χ, the angle between the planes of the $\ell\nu$ and the $K\pi$ system and q^2 [3]:

$$\frac{d\Gamma}{dq^2 d\cos\theta_V d\cos\theta_\ell d\chi} = \frac{3G_F^2 |V_{cs}|^2 K q^2}{2048\pi^4 M_D^2} \times \left[(|H_+|^2 + |H_-|^2)(1+\cos^2\theta_V)\sin^2\theta_\ell \right.$$

$$+4|H_0|^2 \sin^2\theta_V \cos^2\theta_\ell + 2\eta (|H_+|^2 + |H_-|^2) \cos\theta_V \sin^2\theta_\ell$$

$$-2\mathrm{Re}(|H_+ H_-^*) \sin^2\theta_V \sin^2\theta_\ell \cos 2\chi - \mathrm{Re}((H_+ + H_-) H_0^*) \sin 2\theta_V \sin 2\theta_\ell \cos\chi$$

$$\left. -\mathrm{Re}((H_+ - H_-) H_0^*) \sin\theta_V \sin 2\theta_\ell \cos\chi \right]$$

Table 5: BR($D \rightarrow \overline{K}^* \ell^+ \nu$) Form Factors

EXPERIMENT	Γ_L/Γ_T	$R_2=A_2(0)/A_1(0)$	$R_V=V(0)/A_1(0)$
MARKIII[7]	$0.5\ ^{+1.0}_{-0.1}\ ^{+0.1}_{-0.2}$		
E691[3]	$1.8\ ^{+0.6}_{-0.4} \pm 0.3$	$0.0 \pm 0.5 \pm 0.2$	$2.0 \pm 0.6 \pm 0.3$
E653[5]	$1.18 \pm 0.18 \pm 0.08$	$0.82\ ^{+0.22}_{-0.23} \pm 0.11$	$2.0\ ^{+0.34}_{-0.32} \pm 0.16$
WA82[20]	$0.6 \pm 0.3\ ^{+0.3}_{-0.1}$		
E687[4]	$1.20 \pm 0.13 \pm 0.13$	$0.78 \pm 0.18 \pm 0.10$	$1.74 \pm 0.27 \pm 0.28$
Average	1.12 ± 0.12	0.73 ± 0.15	1.85 ± 0.25
THEORY			
QUARK MODEL			
GS[1]	1.2	0.8	1.9
WSB[2]	0.9	1.3	1.4
ISGW[9]	1.1 ± 0.2	1.0 ± 0.3	1.4 ± 0.4
KS[10]	1.1	1.0	1.0
LATTICE GAUGE CALCULATIONS			
LMMS[12]	1.51 ± 0.27	0.36 ± 0.4	1.6 ± 0.2
BKS[13]		0.7 ± 0.3	2.0 ± 0.4
QCD SUM RULES			
BBD[14]	0.86 ± 0.06	1.2 ± 0.2	2.2 ± 0.9
AOS[17]		0.89 ± 0.39	1.89 ± 0.79

Fig. 6 shows the fit projections from experiment E653.

Experiment E687 used a binned *L* function technique. They bin the sample into three bins in $\cos\theta_v$, 3 bins in $\cos\theta_\mu$, and two in q^2/q^2_{max}, integrating over the angle χ. Due to finite muon mass, the matrix element in the fit includes an overall factor of $\left(1-\frac{M_\mu^2}{t}\right)$. To verify their assumption, that the F.F. R_3 is zero, a fit with $R_3=0$ and $R_3=3$ is performed and the results are found to vary by less than 7% of the statistical error.

E687 results confirm the large polarization value from E691 and E653 (table 5). These three experiments are in agreement in the determination of the ratio R_v, but E691 disagrees in R_2. The theoretical predictions are in good agreement for R_v and prefer E653 and E687 for R_2.

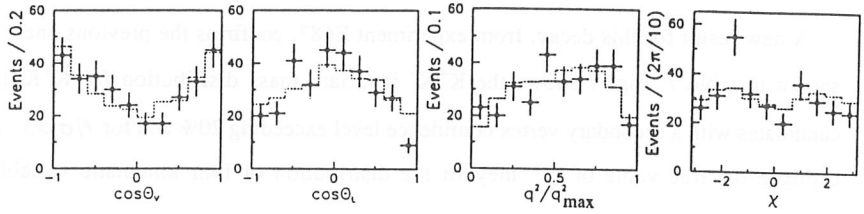

Fig.6: E653- $D\rightarrow \overline{K}^*\mu\nu$ decay: $\cos\theta_v$,$\cos\theta_\ell$,q^2/q^2_{max} and χ distributions.The dashed histrograms are the projections of the fit results.

5.-Sum of semileptonic decay widths

The exclusive semileptonic decay rates are unable to account for all the inclusive decay rate (table 6a). Possible explanation for this shortfall are the non-resonant decays and the contribution of higher K^* resonances, but their contribution is only a small fraction of the total semileptonic rate, as shown in table 6b.

The rate of the Cabibbo suppressed channel $D^0\rightarrow\rho^-\ell^+\nu$ is predicted to be $\equiv\Gamma(D^0\rightarrow\pi^-\ell^+\nu)$ so it could account for 5%. The sum of the rates for D^+ into $(\eta,\eta',\rho,\omega)\ell^+\nu$ is predicted to be ~3 times the $\Gamma(D^+\rightarrow\pi^-\ell^+\nu)$ so it could account for 10%. Hence, at least 15% of the inclusive semileptonic width is missing. The statistical significance of the

shortfall is larger if the PDG branching ratios $B(D^0 \to K^-\pi^+)$ and $B(D^+ \to K^-\pi^+\pi^+)$ are used.

Table 6a: Inclusive and exclusive decay widths

	D^0	D^+
	Rate 10^{10} s^{-1}	Rate 10^{10} s^{-1}
$\Gamma(D \to \overline{K}\, \ell^+\nu)$	7.7±0.8	5.9±1.1
$\Gamma(D \to \overline{K}^*\, \ell^+\nu)$	4.9±1.1	4.4±0.6
$\Gamma(D \to (\overline{K}+\overline{K}^*)\ell^+\nu)$	12.6±1.4	10.3±1.3
$\Gamma(D \to \pi\ \ell^+\nu)$ [5]	0.9±0.4	0.5±0.3
$\Gamma(D \to (\overline{K}+\overline{K}^*+\pi)\ell^+\nu)$	13.5±1.5	10.8±1.3
$\Gamma(D \to e^+ + \text{anything})$ [5]	18.3±2.9	16.1±2.7
Missing decays	4.8±3.3	5.3±3.0

Table 6b:

Experim.		Rate 10^{10} s^{-1}
E691	$D \to (\overline{K}\pi)_{nr}\ell^+\nu$	0.4±0.4
E687		0.3±0.1
E691	$D \to \overline{K}^*\pi\ell^+\nu$	< 1.1
E691	$D \to (K\pi)_{nr}\pi\ell\nu$	< 0.8

6.-The decay $D_s^+ \to \phi\mu^+\nu$

A new result for this decay, from experiment E687, confirms the previous ones, as shown in table 7. Fig. 7 shows the K^+K^- invariant mass distribution for $K^+K^-\mu^+$ candidates with a secondary vertex confidence level exceeding 20% and for $\ell/\sigma_\ell > 3$. To estimate the true value of D_s^+ they fit the distribution of four kinematic variables measured for the $\phi\mu^+\nu$ candidates to a linear combination of the distributions predicted for the signal and for six non-negligible background sources. Three of these possible contaminations are $D_s^+ \to \phi\pi^+\pi^0$, $\phi\pi^+\pi^+\pi^-$, and $D^+ \to \phi\pi^+\pi^0$. They can be estimated from their known BR, from the probability that a pion is misidentified as a muon (1.±0.1%) and from the relative production rate $D_s/D^+ = 0.6\pm0.2$. The other sources of background are : $D_s^+ \to \phi\pi^0\mu^+\nu$, $D^+ \to \phi\mu^+\nu$, and $D^+ \to \phi\overline{K}^0\mu^+\nu$. The four variables include the $\phi\mu$ invariant mass, to differentiate the signal from the decay channels with undetected neutral products, the reconstructed proper time, to provide discrimination against D^+, $\cos\theta_\nu$ (θ_ν is the angle between the K and the D_s in the ϕ rest frame), and $\cos\theta_\mu$ (θ_μ is the angle between the ν and the D_s in the $\mu\nu$ rest frame). The fit attributes the bulk (79±9%) of the ϕ yield to the $D_s^+ \to \phi\mu^+\nu$. The BR is determined relative to $D_s^+ \to \phi\pi^+$, selected with the same criteria. The result is reported in table 7.

Table 7:

Experiment	$\Gamma(D_s^+ \to \phi\mu^+\nu)/\Gamma(D_s^+ \to \phi\pi^+)$
E687	$0.58 \pm 0.17 \pm 0.07$
E691	<0.45
CLEO	$0.49 \pm 0.10 \,^{+0.10}_{-0.14}$
ARGUS	$0.57 \pm 0.15 \pm 0.15$
Average	0.54 ± 0.10

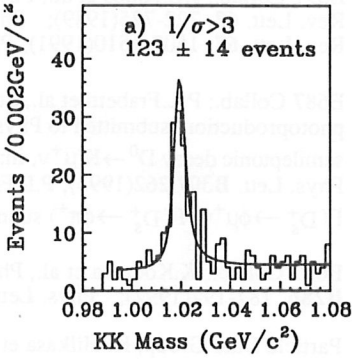

Fig. 7: E687- KK invariant mass

From the ratio $\Gamma(D_s^+ \to \phi\mu^+\nu)/\Gamma(D_s^+ \to \phi\pi^+)$, we can estimate the absolute branching ratio $D_s^+ \to \phi\pi^+$. The width for the decay $D_s \to \phi\ell^+\nu$ is F times the width of the decay $D^+ \to \overline{K}^{*0}\ell^+\nu$. The factor F is given by theoretical models and accounts for the difference in mass and wave functions between hadrons in both the initial and final states. It ranges from 0.78 to 1.02. If we use F =0.9±0.12, the lifetimes from PDG, and the average of $\Gamma(D_s^+ \to \phi\mu^+\nu)/\Gamma(D_s^+ \to \phi\pi^+)$, we obtain $\Gamma(D_s^+ \to \phi\pi^+)$= 0.033±0.008.

7.-Summary

The decay channel $D \to \overline{K}\,\ell^+\nu$ has been studied from several experiments and the measurements of decay rate and form factors agree with one another and with the theoretical predictions. The measurements of the decay rate and form factors for the decay channel $D^+ \to \overline{K}^*\mu^+\nu$ agree with one another but not with the predictions of the quark models. E687 and E653 are measuring the form factors for $D_s^+ \to \phi\mu^+\nu$ decay.

7.-References

(1) F.J.Gilman, R,L.Singleton,Jr, Phys. Rev. **D41**, 142-150(1990)

(2) M.Wirbel, B.Stech, M.Bauer, Z.Phys. **C29**, 637-642(1985)
M.Bauer, M.Wirbel, Z.Phys. **C42**, 671-678(1989)

(3) E691 Collab.: J.C.Anjos et al., Phys. Rev. Lett. **62**, 1587-1590(1989); Phys. Rev. Lett. **62**, 722-725(1989); Phys. Rev. Lett. **65**, 2630-2633(1990); Phys. Rev. Lett. **67**, 1507-1510(1991); Phys. Rev. Lett. **64**, 2885-2888(1990)

(4) E687 Collab.: P.L.Frabetti et al., Study of $D^0 \to K^- \mu^+ \nu$, in high energy photoproduction, submitted to Phys.Lett.B; W.E.Johns, Recent results on semileptonic decay $D^0 \to K^- \mu^+ \nu$, in: Proc. of D.P.F.(1992); P.L.Frabetti et al., Phys. Lett. **B307**,262(1993); P.L.Frabetti et al., A measurement of $\Gamma(D_s^+ \to \phi \mu^+ \nu)/\Gamma(D_s^+ \to \phi \pi^+)$ submitted to Phys.Lett.B.

(5) E653 Collab.: K.Kodama et al., Phys. Rev. Lett. **66**, 1819(1991); Phys. Lett. **B286**, 187-194(1992); Phys. Lett. **B274**, 246-252(1992)

(6) Particle Data Group, K. Hilkasa et al., Phys. Rev. **D45**, S1(1992)

(7) MARKIII Collab.: Z.Bai et a., Phys. Rev. Lett. **66**, 1011-1014(1991)

(8) CLEO Collab.: G.Crawford et al., Phys. Rev. **D44**,3394-3401(1991); J.A.Alexander et al., Phys. Rev. Lett. 65, 1531-1534(1990).

(9) N.Isur, D.Scora,B.Grinstein, M.B.Wise, Phys. Rev. **D39**, 799-818(1989) isgw D.Scora,N.Isur, Phys. Rev. **D40**, 1491-1496(1989)

(10) J.G.Körner, G.A.Shuler, Z.Phys. C46, 93-109(1990).

(11) M.Crisafulli, G.Martinelli, V.J.Hill, C.T.Sachrajda Phys. Lett.**B223**,90-96(1989).

(12) V.Lubicz, G.Martinelli, C.T.Sachrajda, Nucl. Phys. **B356**, 031-317(1991); V.Lubicz, G.Martinelli, M.S.McCarthy, C.T.Sachrajda, Phys. Lett. **B254**, 415-420(1992)

(13) C.W.Bernard, A.X.El-Khadra, A.Soni, Phys. Rev. **D45**, 869-874(1992); Phys. Rev. D43, 2140-2156(1991).

(14) P.Ball, V.M.Braun, H.G.Dosch, M.Neubert, Phys. Lett. **B259**, 481-483(1991) P.Ball, V.M.Braun, H.G.Dosch, Phys. Rev. **D44**, 3567-3581(1991)

(15) C.A. Dominguez, N.Paver, Phys. Lett. **B207**, 499-503(1988)

(16) T.M.Aliev, V.L.Eletskii, Ya.I.Kogan, Sov.J. Nucl. Phys.**40**, 527-531(1984)

(17) T.M.Aliev, A.A.Ovchinnikov, V.A.Stobodenyuk IC-89-382 (1989)

(18) MARKIII Collab.: J.Izen private communication.

(19) ARGUS Collab.: H.Albrecht et al., Phys. Lett. **B255**, 634-638(1991); H.Albrecht et al.,Study of the semileptonic decay $D^0 \to K^{*-} e^+ \nu$ to be published.

(20) WA82 Collab.: M. Adamovich et al., Phys. Lett. **B268**, 142-144(1991)

SESSION V

- M. Dameri
  A Review on the Experimental Status of Charm Hadroproduction
- S. Brons
  First Results on Charm Production by the CERN Hyperon Beam Experiment WA89
- J. Wiss
  High Energy Charm Photoproduction
- D. Barberis
  Charmed Meson Decays: an Overview of Recent Results
- A. Zallo
  Recent Results on Charm Decays with π^0's or η's
- S. P. Ratti
  Charm Baryon Decays in Fixed Target Experiments
- L. M. Cremaldi
  Status of Heavy Quark Lifetime Measurements

Frascati Physics Series, Vol. 1 (1993)
HEAVY QUARKS AT FIXED TARGET
Frascati, May 31st – June 2nd 1993
(pp. 167–180)

A REVIEW ON THE EXPERIMENTAL STATUS OF CHARM HADROPRODUCTION

M. Dameri
Università di Genova, Dipartimento di Fisica
Via Dodecaneso, 33, I-16136 Genova, (ITALIA)

1 Introduction

The existence of the charm quark, assumed as a postulate in 1970 by Glashow, Iliopoulos & Maiani to explain the absence of strangeness-changing neutral currents[1], had the first experimental confirmation in 1974 with the discovery of the J/Ψ, a particle composed of a charm quark and charm antiquark. This evidence came from e^+e^- annihilations [2] and from hadroproduction[3]. In spite of this very first observation, for a long period charm hadroproduction picture was marked by low statistics, indirect and biased data. It is only from 1986 that experiments in FNAL and CERN, all of them at fixed target, have collected cleaner and less biased data. Distinguishing features of these experiments, so called II generations experiments, are high precision measurements of trajectories of charged particles, a detailed reconstruction of the decay vertices and a high statistical precision. During the same period of time there has also been progress in theoretical calculations of the quantum chromodynamic (QCD). The agreement between the charm hadroproduction QCD predictions, including next-to-leading order (NLO) contribution, and the data had increased the confidence in the interpretation of charm results in terms of this theory.

1.1 A brief Account on the Physics of Charm Hadroproduction

In the QCD framework the elements entering in the calculation of the hadroproduction process are: the hard scattering between quarks and gluons of the incident hadrons, the distribution of quarks and gluons inside the hadrons and the hadronization of the produced quarks. The inclusive production cross section for a hadron H containing a heavy quark Q in a hadronic collision $h + A \Rightarrow H + X$ has the general form :

$$\sigma(hA \to HX) = \sum_{a,b} G_{a/h} G_{b/A} \hat{\sigma}(ab \to Q + X) D_{H/Q}$$

where:

G's are the structure functions of the colliding hadrons, they are independent of the underlying hard process. Nucleon quark structure functions are derived from data on deep inelastic lepton scattering, gluon structure functions are

badly determined, even unknown for mesons;

$\hat{\sigma}$ is the hard subprocess cross section which is function of the momenta of incident partons, the renormalization scale μ, the total CMS energy; $\hat{\sigma}$ is usually calculated in a perturbative series in the strong interaction coupling constant $\alpha_s(\mu^2)$;

D's are the heavy quark fragmentation functions;

a, b are the relevant partons of the colliding hadrons.

Recent works of Nason, Dawson & Ellis (NDE)[4, 5] and Mangano, Nason & Ridolfi (MNR)[6] provide a fully parton cross section calculations to order $O(\alpha_s^3)$ including processes like $gg \to Q\bar{Q}g$ and $gq \to Q\bar{Q}q$. MNR predictions are specific for fixed target experiments at the present available energies. The QCD even if significant uncertainties remain (the precise values of the effective mass of the charm quark and the renormalization scale, the effects associated with the spectator partons are neglected, etc), furnishes a powerful tool in understanding the charm hadroproduction.
The fragmentation functions are usually evaluated from Monte Carlo calculations based on three different models: string fragmentation, cluster fragmentation and independent fragmentation. The well known programs ISAJET[8], PYTHIA[9] EUROJET[10] and, specific for fixed target, FRITIOF[11, 12] are used to modeling the final state kinematical distributions. An exhaustive review on these models has been published by Sjöstrand[7].

1.2 Overview on Experiments

Recent results on charm hadroproduction have been published or submitted to publication by:

E653 : Pair Production;
E769 : A-dependence, Leading Effect, Differential Cross Sections ;
E789 : A-dependence, Total Cross Section (preliminary);
NA32 : Pair Production;
WA82 : A-dependence, Leading Effect, Differential Cross Sections ;
WA89 : A-dependence, Differential Cross Sections (preliminary);
E791 : Mass Spectra (preliminary).

All these experiments are equipped with silicon microvertex detectors (SMDs) which supply spatial resolution of some μm transverse to the beam and some hundred μm along the beam. Such a resolution allows to see the charm decay with efficiencies that can be as large as 50% depending on charm particle lifetime. Charm samples are clean with signal-to-background ratios ranging from 1 to 15. The present statistics of charm events has a sufficient size so as to allow meaningful comparisons with QCD predictions. Details of these experiments are found in many review works [13, 14] and

references quoted therein. Here only the peculiar features are recalled: the target is thin, solid and in some cases segmented, E653 uses nuclear emulsion; the trigger selection criteria are open, based on particle identification, transverse energy, impact parameter; the acceptance is usually the full forward hemisphere, for E653 the full Feynman-x (x_F) range, E789 sees only two-body decays around $x_F = 0$.

2 Total Charm Cross Section

The total inclusive cross section measurements reported in the Table 1 are scaled assuming a linear dependence of cross section as a function of the mass number of the target and using decay branching ratios measured by different experiments. The data which show increasing values with the beam energy and relative errors of the order of 10% dominated by systematics, agree with NLO QCD predictions [6] as shown in fig.1a. A

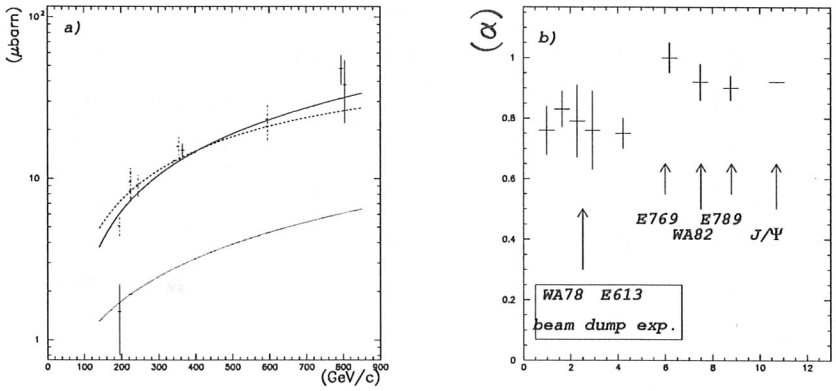

Figure 1: a) Variation of σ_c with incident beam energy, the curves shown are NLO QCD parton model predictions from MNR with m_c=1.5 GeV and Λ_5 = 200 MeV. Full bars and curve refer to protons, dashed bars and curve to pions. About the dotted curve see the text. b) Summary of α measurements for open and hidden charm; the x-axis has no meaning .

charm quark effective mass m_c of about 1.5 GeV is favoured by a simple fit. This almost impressive agreement between QCD predictions and data is not observed deriving the theory parameters from a fit on the differential distributions. An analysis [28] based on E653 and NA32 pion data demonstrates that as the x_F and p_T^2 distributions predicted by MNR for the charm quark stiffen with the c mass, fitting this mass on the differential cross section distributions, the predicted total cross sections decrease as shown by the dotted curve in fig.1a. Therefore NLO QCD is unable to fit both the differential distributions and the total cross sections by changing only m_c. The answer of the authors of [6] is " *we ... conclude that, when theoretical uncertainties are correctly taken into*

account, the data are still consistent with the theoretical predictions even for $m_c = 1.5$ *GeV*". A source of this discrepancy can be hadronization effects, not taken into account in the above analysis, which, as seen in section 4, modify the x_F distributions.

The new data are in fair agreement with the previous data vintage confirming that the pion production cross section has a size similar or larger than that for protons at the same incident energy suggesting a harder gluon distribution in the mesons and a dominant process at these energies $gg \to c\bar{c}$.

Table 1: Total open charm cross section data

Expt	*Target*	*Beam*	E(GeV)	$\sigma_{x_F>0}(\mu\text{barn})$	Ref.
NA32	Si	π^-	200	$5.1^{+0.6}_{-0.5} \pm 0.3$	[15]
NA32	Cu	π^-	230	$9.5 \pm 0.4 \pm 1.9$	
E769	Be Al Cu W	π^-	250	$9.1 \pm 2.1 \pm 1.2$	[16]
NA27	H	π^-	360	15.8 ± 2.7	[21]
E653	Emuls.	π^-	600	$23.33 \pm 0.84 \pm 6.08$	[28]
NA32	Si	p	200	$1.5 \pm 0.7 \pm 0.1$	[15]
NA27	H	p	400	15.1 ± 1.7	[21]
E743	H	p	800	$48^{+10.}_{-8.}$	[22]
E789	Be Au	p	800	$32. \pm 7.$ (only D^0)	[20]
E653	Emuls.	p	800	$38. \pm 9. \pm 14.$	[28]

3 Nuclear Target Dependence

The full exploitation of SMDs requires the use of thin solid targets. This necessary implies the matter of the dependence of results on the target material. The importance of this subject is twofold :

-to compare results among experiments with different target materials;

-to establish if perturbative QCD calculations are applicable in the case of charm.

The total production cross section is usually parameterized as $\sigma(A) = \sigma_0 A^\alpha$, where A is the target mass number and σ_0 is the single nucleon cross section. For pointlike processes α should be close to 1, as predicted by QCD in the perturbative approximation (the charm cross section is calculated as incoherent sum of elementary process on partons and hence proportional to the number of quarks); for nuclear scale processes

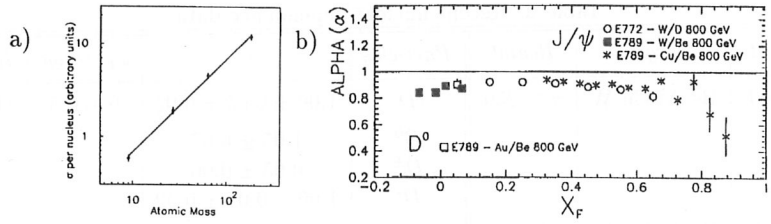

Figure 2: a)Nuclear target dependence of the D meson cross section as a function of the atomic mass.The line is a fit by the form A^{α} with $\alpha = 1.00 \pm 0.05$. b) $J/\Psi A$-dependence as a function of x_F. The preliminary value of α obtained by E789 is indicated by a $\Box$.

α should be close to 2/3, that is $\sigma(A)$ should scale with the projected surface area. Early indirect measurements by WA78[25, 26] and E613[27] suggested $\sigma(A) \propto A^{3/4}$. This strengthen the belief that perturbative QCD calculations where not applicable in the charm physics. Recently A-dependence results from direct measurements (charm particles produced in different target materials at the same time) have been published by E769[17] and WA82[30]. Both experiments use pions as incident beam and targets composed by different materials, segmented along the beam in E769, transverse to the beam in WA82. These α measurements, which systematic errors are negligible with respect to the statistical ones, are presented in Table 2 together with the very preliminary results from E789[20] and WA89[31] which use as incident beam respectively protons and Σ^-. The recent α values for production of D mesons (neutral or charged) are compatible with 1 and are inconsistent with the earlier indirect measurement as shown in fig.1b and in fig.2a. Decrease of α with x_F has been recently observed in J/Ψ production by protons[32] as plotted in fig.2b and some indications suggested that α may decrease with x_F in open charm production by pions[33]. However as shown in fig.3, E769 and WA82 data do not indicate any dependence of α on x_F and p_T.

Within the present statistical accuracy the α parameter for open charm production is compatible with that predicted by perturbative QCD and agrees with the values obtained for hidden charm production by protons and by pions.

4 Longitudinal Momentum Distributions

The common parameterization of cross section as a function of the scaled longitudinal momentum x_F is $d\sigma/dx_F = k(1 - x_F)^n$. The measurements of n reported in the Table 3 seem to indicate a weak dependence on the beam energy in agreement with NLO QCD calculations which predicts somewhat softer longitudinal momentum distributions increasing the beam energy.

Fit to the form $d\sigma/dx_F = k(1 - x_F)^n$ are in good agreement with data for x_F ranging from 0.1 to 0.7; outside this region E769 [18] and WA82[19] data show an anomalous

Table 2: Recent nuclear dependence data

Expt	*Target*	*Beam*[1]	*Particles*	α	x_F *range*	*Ref.*
E769	Be Al Cu W	π^- 250	D	$1.00 \pm 0.05 \pm 0.02$	$0 \div 0.5$	[16]
			D^0	1.05 ± 0.07		
			$D^\pm$	0.95 ± 0.06		
			D^*	$1.00 \pm 0.07 \pm 0.02$		
E769	Be Al Cu W	π^+ 250	D	1.03 ± 0.15	$0 \div 0.5$	[16]
WA82	Si Cu W	π^- 340	D	0.92 ± 0.06	$0 \div 0.85$	[30]
			D^0	0.98 ± 0.08		
			$D^\pm$	0.84 ± 0.08		
E789	Be Au	p 800	D	0.90 ± 0.04		[20]
WA89	C Cu	Σ^- 330	$D^\pm$	1.2 ± 0.2	> 0.2	[31]

Note 1 :Beam Particle and Energy(GeV)

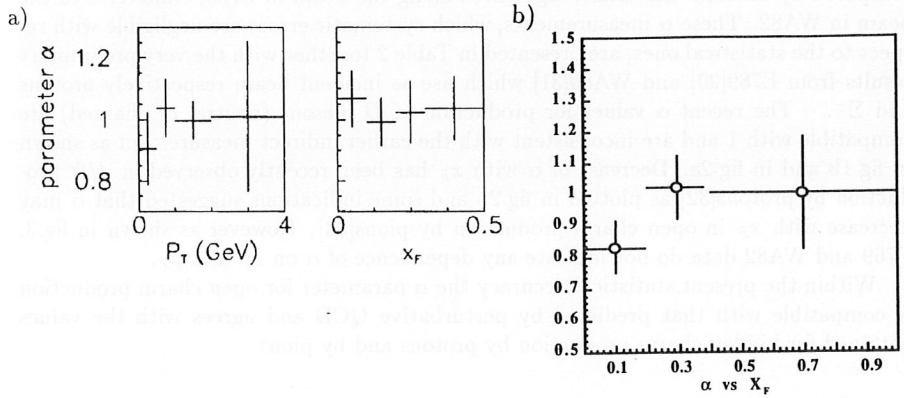

Figure 3: The parameter α for charm production measured a) by E769 as a function of p_T and x_F and b) by WA82 as a function of x_F

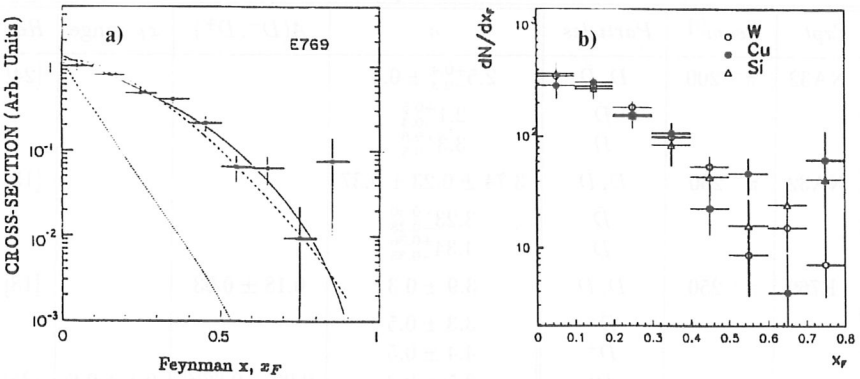

Figure 4: a)E769 $D^{\pm}x_F$ distribution. The solid curve is the best fit of the form $(1-x_F)^n$. The dashed curve is the c quark production from NDE. The dotted curve is this distribution convoluted with charm fragmentation functions derived from e^+e^- annihilations. b) WA82 $D^{\pm}x_F$ distributions produced in π^- interaction on Si,Cu and W.

excess at high x_F and a small deficiency at low x_F where nuclear effects become important. As plotted in fig.4a and fig.5 NLO QCD theoretical predictions[4] for c quark production with a c mass = 1.5 GeV match almost well the data in the x_F range 0 to 0.7. If the charm production is a short distance process, then the x_F and p_T distributions should be independent of the atomic mass of the target material. In comparison results from W,Cu and Si (see the fig.4b), WA82 concludes that there is no evidence of x_F dependence on the atomic mass of the target[34]. A similar result is reported by E769 for interactions on Be,Al,Cu and W.

4.1 Leading Effect

From QCD predictions in the perturbative approximation one would expect the x_F distributions for all charmed hadrons to be very similar following those of the produced charm quarks. Early results from NA27 indicated enhancement of leading charmed mesons (mesons containing a beam valence quark) at high x_F in π^--p reactions. Results of NA32 suggested a difference in the x_F distribution between leading and non-leading mesons in π^--Cu reactions. Both charged and neutral mesons have been used in those analysis. From the values of the parameter n quoted in Table 3 we observe that all the experiments show the non-leading x_F shape softer than the leading one.
In π^- interactions only charged D have the leading/nonleading property whether the charged D is directly produced or results from a D^* decay, while this is not true for the D^0. Charmed vector mesons have a unambiguous leading/nonleading character too. E769 and WA82 studies based on charged D and D^* have observed a different

Table 3: x_F dependence

Expt	*Beam*[1]	*Particles*	n	$A(D^-, D^+)$	x_F range	*Ref.*
NA32	π^- 200	$D, \bar{D}$	$2.5^{+0.4}_{-0.3} \pm 0.3$			[24]
		$\bar{D}$	$2.1^{+0.5}_{-0.4}$			
		D	$3.3^{+0.6}_{-0.5}$			
NA32	π^- 230	$D, \bar{D}$	$3.74 \pm 0.23 \pm 0.37$			[15]
		$\bar{D}$	$3.23^{+0.30}_{-0.28}$			
		D	$4.34^{+0.36}_{-0.35}$			
E769	π^- 250	$D, \bar{D}$	3.9 ± 0.3	0.18 ± 0.03		[18]
		D^-	3.3 ± 0.5			
		D^+	4.4 ± 0.5			
		D^*	3.5 ± 0.3	0.09 ± 0.06[2]	$0.1 \div 0.6$	[35]
		D^{*-}	2.9 ± 0.4			
		D^{*+}	4.1 ± 0.5			
		D^0[3]	3.0 ± 0.4		$0.1 \div 0.6$	
		$\bar{D}^0$[3]	5.2 ± 0.7		$0.1 \div 0.6$	
WA82	π^- 340	$D, \bar{D}$	3.1 ± 0.3	0.15 ± 0.06		[19]
		D^-	2.8			
		D^+	3.9			
		D^*		0.29 ± 0.12[2]		[19]
NA27	π^- 360	$D, \bar{D}$	3.8 ± 0.6			[23]
		$\bar{D}$	$1.8^{+1.6}_{-0.5}$			
		D	$7.9^{+1.6}_{-0.99}$			
E653	π^- 600	$D, \bar{D}$	$4.25 \pm 0.24 \pm 0.23$			[28]

Note 1:Beam particle and Energy(GeV) Note 2 : $A(D^{*-}, D^{*+})$ Note 3 : D^0 daughter of D^*

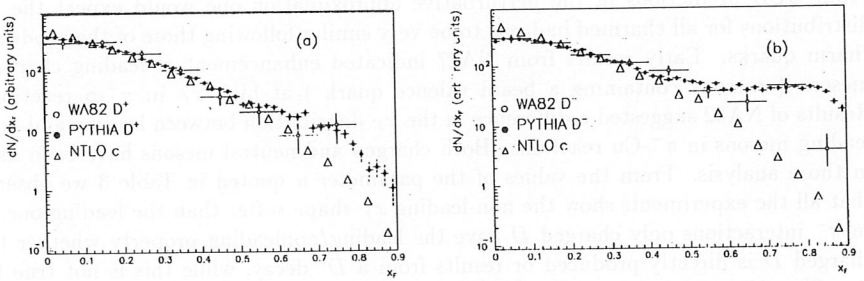

Figure 5: WA82 x_F measured $d\sigma/dx_F$ from π^- interactions and comparisons with the NLO QCD prediction for quarks and the PYTHIA predictions for charm meson. The PYTHIA ingredients are : $m_c = 1.5 GeV/c^2$, $\Lambda_{QCD} = 200$ MeV, EHLQ nucleon structure functions, OWENS pion structure functions , Lund fragmentation function

shape in x_F distributions for negative and positive mesons. The fitted parameters n are reported in the Table 3. As further test E769 and WA82 analyze the asymmetry $A(K,L) = A(\sharp K - \sharp L)/A(\sharp K + \sharp L)$ where $\sharp K$ is the number of meson K divided by acceptance for $x_F > 0$. A 3σ asymmetry is observed in charged D channel but no effect in the neutral one as plotted in fig.6b. As a cross-check E769 and WA82 using charmed vector mesons find an excess of negative over positive particles but with less significance with respect the pseudoscalar case. A similar behaviour is also shown in E769 data by the daughter D^0 mesons from the charged D^* decays.
As the leading effect should be stronger at large x_F, WA82 studied the differences between $\sigma(D^+)$ and $\sigma(D^-)$ as a function of the longitudinal momentum. The asymmetry $A(D^-, D^+)$ plotted in fig.6a exhibits that the excess of D^- over D^+ increases with x_F. A combined χ^2-run test indicates that the probability that the D^- and D^+ normalized distributions be two random samplings of the same limit distributions is less than 1%. Moreover the WA82 analysis proves that the leading effect is qualitatively reproduced by the PYTHIA event generator as hadronization effect in the Lund string fragmentation model: a $\bar{d}$ quark necessary to form D^+ must be produced by string fragmentation, a d quark necessary to form D^- is often present in the forward hemisphere as a spectator quark from the beam π^-. There are therefore additional ways for producing a D^-. In the fig.4 the WA82 D^- and D^+ distributions are compared with the PYTHIA predictions and the $c\bar{c}$ distributions from NLO QCD calculations. For positive mesons PYTHIA and NLO c quark x_F are very similar and both agree with data. For negative meson data agree better with PYTHIA.
WA82 and E769 data confirm the leading particle effect in pion interactions but not as large as observed by NA27: the comparison with theory shows that non-perturbative effects should probably explain the relative abundance and the longitudinal distributions of the different charmed mesons. Moreover the reproduction of the x_F distribution by PYTHIA damp the motivations to look for unconventional mechanisms of charm production as the intrinsic charm model.

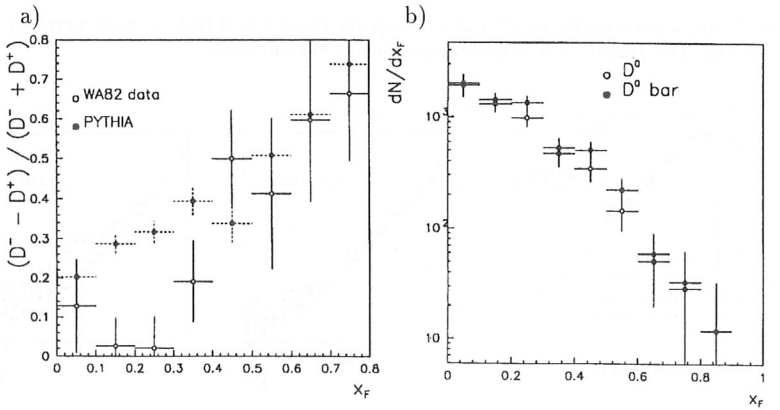

Figure 6: a) WA82 asymmetry in D^+D^- x_F distributions from negative pion production and comparison with the PYTHIA event generator predictions. b) WA82 D^0 and $\bar{D}^0$ x_F distributions.

5 Transverse Momentum Distributions

The common parameterization of the inclusive charm cross section as a function of the transverse momentum p_T is the Gaussian $d\sigma/dp_T = e^{(-bp_T^2)}$ which models in a satisfactory manner data for $p_T^2 < 4.$. At higher values of p_T E769 and WA82 results show a significant deviation from the above form. This effect was not seen in experiments with smaller statistics. A small contribution to this effect could come from the beauty quark production: however the beauty cross section at these energies is not enough large to fully demonstrate the effect. For $p_T > 0.8$ GeV $d\sigma/dp_T$ is well fit by the form $d\sigma/dp_T = e^{(-bp_T)}$ as plotted in fig.7. The average p_T is approximatively 1 GeV in agreement with LO QCD calculations which model almost well the differential distributions as shown by E769 data in fig.8. Likewise a comparison with PYTHIA predictions plotted in fig8b and 8c points out a good agreement with data for $m_c = 1.5$ GeV. As a confirmation of the short range of the charm hadroproduction E769 and Wa82 p_T distributions do not indicate any dependence on the atomic mass of the target material.

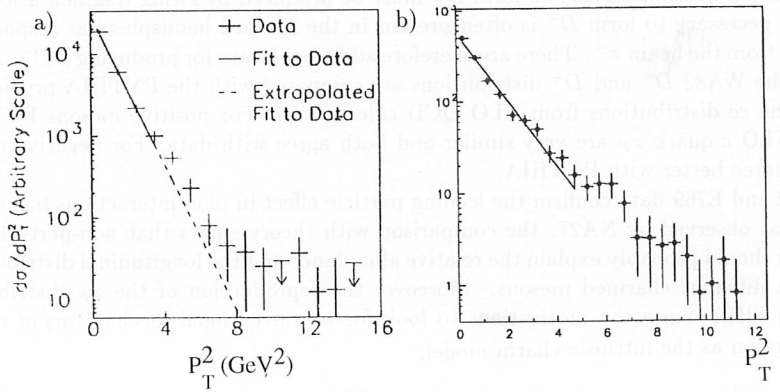

Figure 7: Measured $d\sigma/dP_T^2$ vs P_T^2 and a fit over the range 0 to 4 GeV^2 (solid curve) for a) E769 and b) WA82. The dashed curve is the extrapolation to the full range.

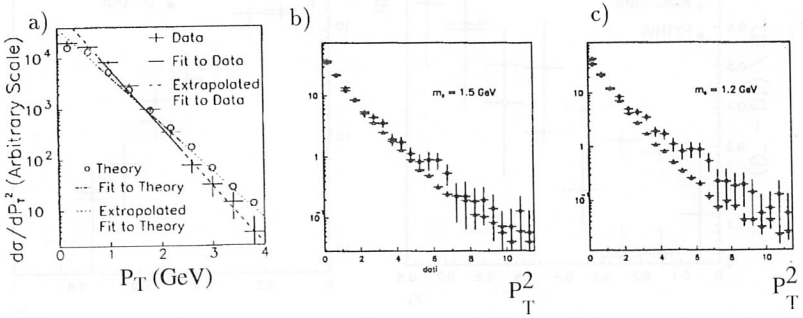

Figure 8: $d\sigma/dP_T^2$ measured a) by E769 as a function of P_T and comparison with LO QCD prediction for quarks, and b) and c) by WA82 as a function of P_T^2 with the PYTHIA predictions indicated by $\triangle$ for $m_c = 1.5$ GeV in b) and $m_c = 1.2$ GeV in c).

6 Charmed Pair Correlations

A recent work of NA32[36] analyzes a sample of 557 charm events with both decay vertices being observed in comparison with the latest NLO QCD calculations. They find that the correlation variables depend but little on the energy of the light quark in the charmed hadron. Hence no evidence of leading effect is observed in the pseudorapidity gap $\triangle\eta$ distributions. As shown in fig.9 the three classes of events with 0,1 and 2 leading quarks, exhibit similar shapes in $\triangle\eta$ when in presence of leading effect one would expect larger $\triangle\eta$ for the class with 1 leading quark.

The comparison between NLO QCD predictions and the data exhibits a reasonable consistence in the $\triangle\eta$ distribution, but the azimuthal-angle $\triangle\phi$ distribution is definitely much broader than the predictions. This discrepancy is not easily ascribable to experimental effects as it is well consistent with measurements from WA75[38, 39],NA27[37] and E613[40]. The authors of [6] discuss the discrepancy comparing data with analytical calculations and with Monte Carlo predictions. These last model the measured $\triangle\phi$ distributions, but with an intrinsic p_T value which is too large with respect to the values obtained in other contexts.

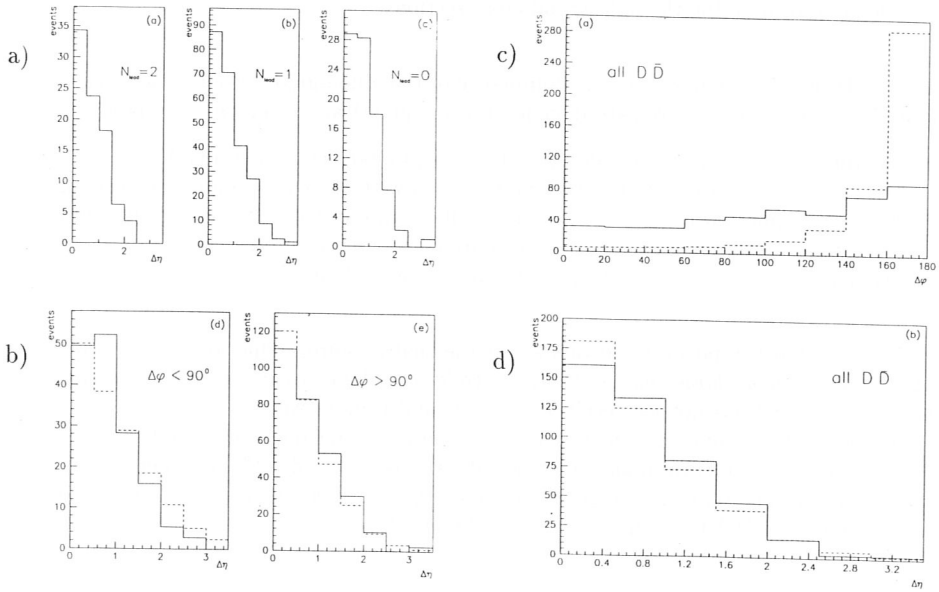

Figure 9: a) NA32 pseudorapidity gap $\triangle\eta$ distribution for $D\bar{D}$ pairs with 2, 1 and 0 leading quarks. b) NA32 $\triangle\eta$ for the azimuthal angle difference $\triangle\phi < 90^0$ and $\triangle\phi > 90^0$. The dashed curves are the normalized NLO QCD predictions. c) NA32 $\triangle\phi$ and d) NA32 $\triangle\eta$ with comparison with NLO QCD predictions.

7 Conclusion

Charm hadroproduction is enjoying a period rich of data and significant improvements in theoretical calculations. The copious results produced in these last years, mainly by fixed target experiments, are consistent with the predictions based on modern calculations of quantum chromodynamics in perturbative approximation to the next-to-leading order.

The recent results are shaping a charm hadroproduction picture marked by :

- no evidence of large effects on the target nucleus. The total cross section shows a linear dependence on the atomic mass of the target material; the differential cross sections appear independent of the target nucleus;
- open and hidden charm productions exhibit the same behaviour but more statistics is required to study the presence of possible suppression effects in open charm production;
- the leading effect is confirmed at high longitudinal momentum values but not large as in the early observation;
- classical parameterization forms of the x_F and p_T distributions are not yet adequate to describe the differential cross sections;

The QCD predictions based on the dominance of the gluon-gluon fusion process calculated in NLO approximation, are in general, even quantitative, accord with data:

- the total cross sections are well fit with a charm quark mass of 1.5 GeV;
- the differential cross sections are well described with the exception of the very forward hemisphere where non-perturbative effects are probably becoming important;
- for charmed pair theoretical predictions are reasonably consistent with data; only the azimuthal angle distributions are much broader than the predictions.

In short the most important question about the charm hadroproduction *" is the charm quark mass enough large that perturbative QCD calculations can be applied in charm hadroproduction?* has not yet received a unique and firm answer.

Higher statistics of events in the extreme kinematical regions, high longitudinal and high transverse momentum, and of charmed pairs is required to fully understand the charm hadroproduction. The huge sample of events collected by E791 and the detailed measurements of WA92 should disentangle the question.

References

[1] S.L. Glasow,J. Iliopoulos,L. Maiani, *Phys. Rev.* D2:1285(1970)

[2] J.E.Augustin et al., *Phys. Rev. Lett.* 33:233 (1975)

[3] Aubert,J.J., et al., *Phys. Rev. Lett.* 33:1404 (1974)

[4] P. Nason,S. Dawson,R.K. Ellis, *Nucl. Phys.* B303:607 (1988)

[5] P. Nason,S. Dawson,R.K. Ellis, *Nucl. Phys.* B327:49 (1989)

[6] M.L. Mangano,P. Nason,G. Ridolfi, *IFUP-TH-37/92 GEF-TH-15/1992* (1992)

[7] T. Sjöstrand, *Int. J. Mod. Phys.* A3:751(1988)

[8] F.E. Paige, S.D. Protoponescu in *Proc. 1986 Summer Study on the Physics of the Superconducting Super Collider* Snowmass CO. (1986)

[9] U.H. Bengtsson, T. Sjöstrand, *Comput. Phys.Commun.*46:43(1987)

[10] A.Ali, B. van Eijk, I. ten Have *Nucl. Phys.* B292:1(1987)

[11] B. Andersson et al., *Nucl. Phys.* B281:289

[12] B. Nilsson-Almqvist, E.Stenlund, *Comput.Phys.Commun.* 43:387(1987)

[13] J.A. Appel, *Ann.Rev.Nucl.Part.Sci.* 42:367(1992)

[14] S.P. Tavernier, *Rep.Prog.Phys.* 50:1439(1987)

[15] S. Barlag et al., *Z. Phys.* C49:555(1991)

[16] Z. Wu, PhD disseration, Yale Univ., New Haven, CT (unpublished) (1991)

[17] G.A. Alves et al., *Phys. Rev. Lett.* 70:772(1993)

[18] G.A. Alves et al., *Phys. Rev. Lett.* 69:3147(1992)

[19] M. Adamovich et al., *CERN/PPE 93-10* (1993)

[20] D.M. Jansen et al., Submitted as Fermilab Preprint.(1993)

[21] M. Aguilar-Benitez et al. *Z. Phys.* C31:511(1986)

[22] R. Ammar et al. *Phys. Rev. Lett.* 61:2185(1988)

[23] M. Aguilar-Benitez et al. *Phys. Lett.* B161:400(1985)

[24] S. Barlag et al., *Z. Phys.* C39:451(1988)

[25] H. Cobbaert et al., *Phys. Lett* B191:456(1987)

[26] H. Cobbaert et al., *Phys. Lett* B206:546(1988)

[27] M.E. Duffy et al., *Phys. Rev. Lett* 55:1816(1985)

[28] K. Kodama et al., *Phys. Lett.* B263:573(1991)

[29] K. Kodama et al., *Phys. Lett.* B284:461(1992)

[30] M. Adamovich et al., *Phys. Lett.* B284:453(1992)

[31] B. Michaels et al., *QCD and High Energy Hadronic Interactions* MORIOND (1993)

[32] D.M. Alde et al., *Phys. Rev. Lett.* 66:133(1991)

[33] MacDermott,M.,Reucroft,S., *Phys. Lett.* B184:108(1987)

[34] C. Roda, PhD disseration, Pisa Univ., Pisa, I (unpublished) (1993)

[35] G.A. Alves et al., *FERMILAB-Pub-93/081-E* (1992)

[36] S. Barlag et al., *Phys. Lett.* B302:112(1993)

[37] M. Aguilar-Benitez et al. *Z. Phys.* C40:321(1988)

[38] S. Akoi et al. *Phys. Lett.* B209:213(1988)

[39] S. Akoi et al. *Prog. Theor. Phys.* 87:1305(1992)

[40] K. Kodama al. *Phys. Lett.* B263:579(1991)

Frascati Physics Series, Vol. 1 (1993)
HEAVY QUARKS AT FIXED TARGET
Frascati, May 31st – June 2nd 1993
(pp. 181–188)

FIRST RESULTS ON CHARM PRODUCTION BY THE CERN HYPERON BEAM EXPERIMENT WA89

WA89 Collaboration
presented by S. Brons
Max–Plank– Institut für Kernphysik, Postfach 103 980,
D–6900 Heidelberg 1, (GERMANY)

ABSTRACT

First results on charm production by the Σ^- hyperon beam experiment WA89 at CERN are presented. Estimates of the x_F and nuclear A dependence of the inclusive cross section for D mesons are shown as well as preliminary results on the production of charmed baryons.

1 – Introduction

Studying charm production in a hyperon beam is a very interesting alternative to the production by "conventional" beam particles, such as protons and pions. First, it provides a tool to test the flavour dependence of the charm producing mechanism. Secondly, if there is a strong leading effect, i.e. an enhancement of the cross section at large x_F when the beam and the charm particle overlap in their flavour content, then usage of a beam which contains an s-quark should provide an advantage for the study of all charm final states containing strangeness.

This should be particularly true for the production of charmed strange baryons, where the produced daughter particles share a maximum of quarks with the incoming beam. The aims of the CERN hyperon beam experiment WA89 concerning charm production are thus to study the production of charmed strange baryons in Σ^-–nucleus interactions at 330 GeV/c, as well as to examine their lifetimes and to look for the symmetric partner states.

We present here results from the analysis of about 75 interaction triggered events of our 1991 data taking (about 70 %). In 1993 we took another 200 million events with a much improved detector setup.

2 – The experimental setup

Figure 1 shows the setup of the WA89 apparatus in the 1991 configuration. It has been constructed around the Omega facility at the CERN SPS, but in contrast to most other Omega experiments the target area is located about 14 m upstream of the spectrometer to ensure a good acceptance at high x_F for states containing a strange baryon in the decay channel.

Hyperons are produced by interactions of 450 GeV/c protons from the CERN SPS in a 40 cm long beryllium target, which is placed 10 m upstream of the experimental target. A magnetic channel selects negatively charged secondaries with a mean momentum of 340 GeV/c. The resulting beam contains π's and Σ^-'s in a ratio of about 2.5:1. The pions are suppressed online by means of a TRD. The experimental target consists of two slabs of copper and carbon of 4 % interaction length each, placed side by side.

The vertex detector downstream of the target consists of 12 planes of silicon microstrip counters. It is followed by a 10 m long decay region, that is equipped with 36 drift chambers to detect V0 and cascade decays. The spectrometer itself is equipped with 38 MWPC planes in the magnetic field region and a set of big "Lever Arm" chambers (8 drift chambers and 4 MWPC's) behind the magnet. A ring–imaging Cherenkov counter (RICH)[1] is placed downstream of the spectrometer. It accepts particles with momenta p >15 GeV/c and provides $\pi/K/p$ separation up to 100 GeV/c. Following behind the RICH counter there is an electromagnetic Lead Glass calorimeter[2], to detect photons from radiative decays and π^0's and a hadron calorimeter of the "spaghetti" type to identify neutrons and protons.

3 – Event reconstruction

The different steps of our charm analysis are as follows. All charged tracks are reconstructed in the spectrometer and may be used for V0 and cascade reconstruction. Tracks are identified, if possible, as kaons or protons using the RICH. The tracks are extended into the silicon vertex detector, where the vertex topology is reconstructed. Charm decays are isolated using cuts on the separation of the charm vertex from the main vertex (typically 6 σ) and on the impact parameter of the charm particle relative to the interaction vertex ($< 60\mu$m), as well as requirements for the unambiguous association of tracks to vertices.

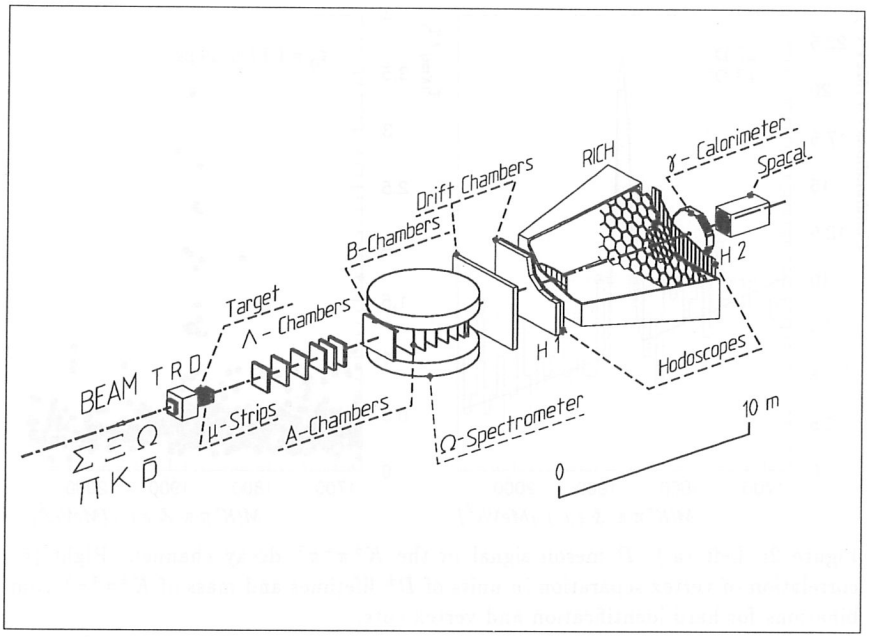

Figure 1: Setup of the WA89 experiment

4 – Results on D meson production

The study of the signal obtained for charged D meson production represents a convenient tool to check the reconstruction algorithms. Because of the relatively long lifetime and the clean vertex topology the reconstruction should not be very sensitive to the details of the vertex reconstruction. However, due to the rather steep decrease of D production with x_F in baryonic beams, we expect a signal of rather modest statistics in our acceptance.

Figure 2 a.) represents the signal for $D^- \rightarrow K^+\pi^-\pi^-$ & c.c., that we obtain using hard identification and lifetime cuts and figure 2 b.) shows the correlation of mass versus vertex separation for the same sample. For any reasonable set of analysis cuts we observe more (1.7:1) D^- than D^+, which might be explained by the fact that the D^- has the d quark in common with the Σ^- beam particle while the D^+ does not. Applying a maximum likelihood analysis to these data we obtain a value for the $D^\pm$ lifetime of 1.17 ± 0.24 ps, that is not yet corrected for vertex cuts or experimental biases (corrections are expected to be less than 30 %). The value is in agreement with the world average[3] of 1.07 ps.

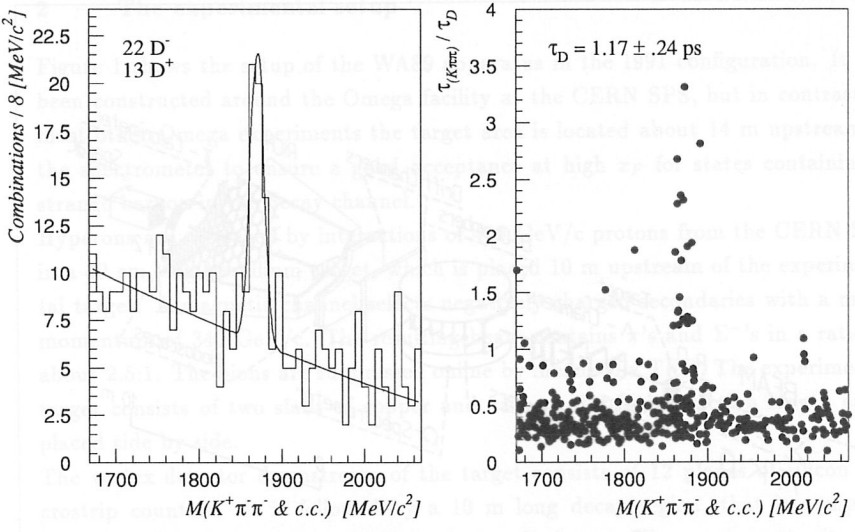

Figure 2: Left (a.) D meson signal in the $K^{\pm}\pi^{\mp}\pi^{\mp}$ decay channel. Right (b.) correlation of vertex separation in units of $D^{\pm}$ lifetimes and mass of $K^{\pm}\pi^{\mp}\pi^{\mp}$ combinations for hard identification and vertex cuts.

Comparing the yields from the carbon and the copper target we obtain the nuclear A dependence for D production in the usual $\sigma = \sigma_0 A^{\alpha}$ parameterization, resulting in $\alpha = 1.2 \pm 0.2$ (stat.) where the systematical error is smaller than the statistical one. As a cross check, we performed the same analysis for K^0 production, with subsequent $K_s^0 \rightarrow \pi^+\pi^-$ decay occurring within 1 cm of the target. The target corrections are even larger in this case due to the larger vertex error for the two-prong vertices of the K^0. For the K^0 we obtain $\alpha = 0.70 \pm 0.03(\text{stat.}) \pm 0.04(\text{syst.})$ at $< x_F >= 0.14$ which is in reasonable agreement with pion beam data[4].

Figure 3 a.) shows the acceptance of our apparatus for D mesons as a function of x_F, calculated from a Monte Carlo simulation. The steep drop-off at $x_F < 0.2$ reflects the geometrical acceptance of the Omega spectrometer for low momentum tracks produced upstream of the magnet. The area between the two curves represents a rather generous estimate of the normalization uncertainty in the simulation but does not affect the shape of the efficiency distribution. Applying this correction to the background subtracted D signal we obtain the x_F distribution shown in figure 3 b.). Fitting the usual $(1 - x_F)^n$ parameterization to this distribution we obtain a value of $n = 6.3 \pm 0.9$ (stat.), which is in good agreement with the value of 5.5 ± 0.8 derived for pN–reactions[5]. Integrating the D^- cross section in the range $x_F > 0.15$ and assuming an A dependence of α=1 we obtain a preliminary value of

about $1.6 \pm \mathcal{O}(1)\mu$barn/Nucleon, which agrees roughly with the values determined by ACCMOR[6] and LEBC-EHS[7] for πN reactions at 230 GeV/c and pp reactions at 400 GeV/c ($0.71 \pm 0.15\,\mu$barn/Nucleon GeV and $2.4 \pm 0.4\,\mu$barn/Nucleon GeV resp.).

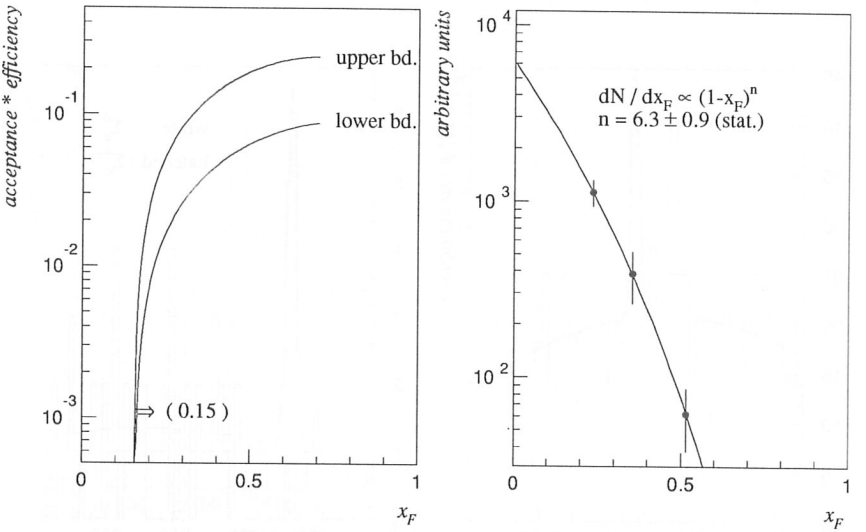

Figure 3: Left (a.) Approximate efficiency for D meson reconstruction as a function of x_F. The curves indicate the upper and lower bound bound on the efficiency given by the normalization uncertainty in the detector simulation. Right (b.) background subtracted and efficiency corrected x_F distributions of D mesons. The curve corresponds to the parameterization $dN/dx_F \sim (1 - x_F)^n$ with n=6.3 .

5 – Results on non–strange charmed baryon production

We have also looked for the non–strange charmed baryon states Λ_c, Σ_c^0 and Σ_c^{++}, using the decay $\Lambda_c \rightarrow pK^-\pi^+$. The short lifetime of the decaying baryon makes these states difficult to observe, but background can be strongly suppressed using RICH identification of the proton and kaon. Even if we do not expect to benefit for these kind of reactions from the strange content of our beam, the use of a baryonic beam should be profitable for charmed baryon production rather than in the meson case.

Figure 4 a.) shows the mass distribution we obtain for the Λ_c if we demand the proton to be identified by the RICH and impose a cut of 5 σ on the separation between Σ^- interaction vertex and $pK^-\pi^+$ vertex. All combinations in the signal

region have $x_F > 0.3$. Making a cut of ± 10 MeV on the Λ_c mass at 2285 MeV and looking for the mass difference between $\Sigma_c^0 - \Lambda_c$ and $\Sigma_c^{++} - \Lambda_c$ in the channels $\Sigma_c^0 \to \Lambda_c \pi^-$ and $\Sigma_c^{++} \to \Lambda_c \pi^+$, we obtain a small peak near the world average[3] 167 MeV mass for the Σ_c^0 case (which shares two d quarks with the incoming Σ^- beam), but nothing for the Σ_c^{++} (see figure 4 b.).

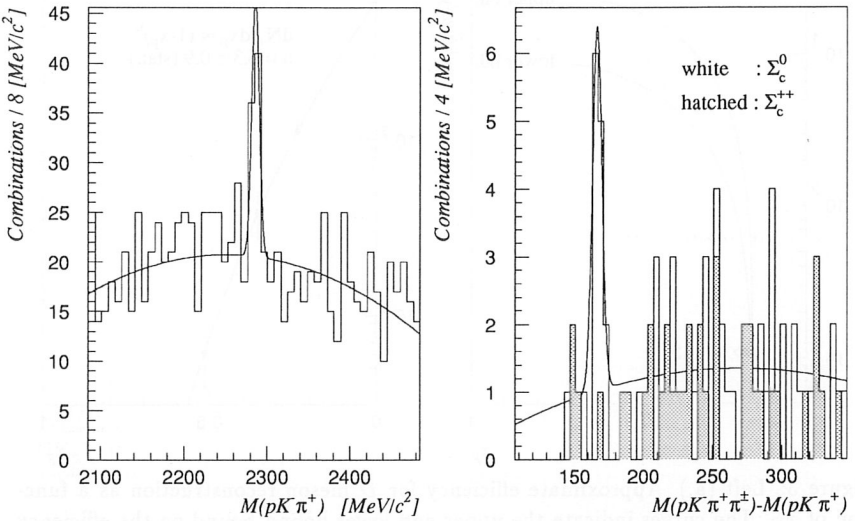

Figure 4: Left (a.) Λ_c^+ signal in the channel $pK^-\pi^+$. Right (b.) mass difference $\delta m = m(pK^-\pi^+\pi^\pm) - m(pK^-\pi^+)$ for Σ_c^0 (white) and Σ_c^{++} (hatched).

We also tried to measure the lifetime of the Λ_c. However, due to the limited resolution of our 1991 vertex detector, it is difficult to extract a precise value for this quantity from the 1991 data, given the fact that the background has an effective lifetime that is comparable in size.

6 – Status of Ξ_c search

We have looked for Ξ_c^+ decaying into $\Xi^-\pi^+\pi^+$ and $\Lambda K^-\pi^+\pi^+$. The status of these searches is shown in figures 5 a.) and b.). There is a clear peak in both channels at a mass of $2450 \pm 4(\text{stat.}) \pm 7$ (syst.) MeV, which deviates by about -15 MeV (2 σ) from the today's world average. The x_F of the combinations in the signal region ranges from 0.35–0.75 . Work is in progress to understand the reason for the mass shift and to measure the lifetime.

No final evaluation of the cross section has yet been undertaken. However one might

argue on a purely qualitative level that, since the efficiency for final states containing a V0 or a cascade is lower than for a clear 3–prong decay (as in the D and Λ_c case), the amount of Ξ_c^+ found in our experiment with respect to the yield of charmed final states without strangeness seems to confirm the observation of an enhanced charmed–strange baryon production in forward direction, as observed by WA62[8].

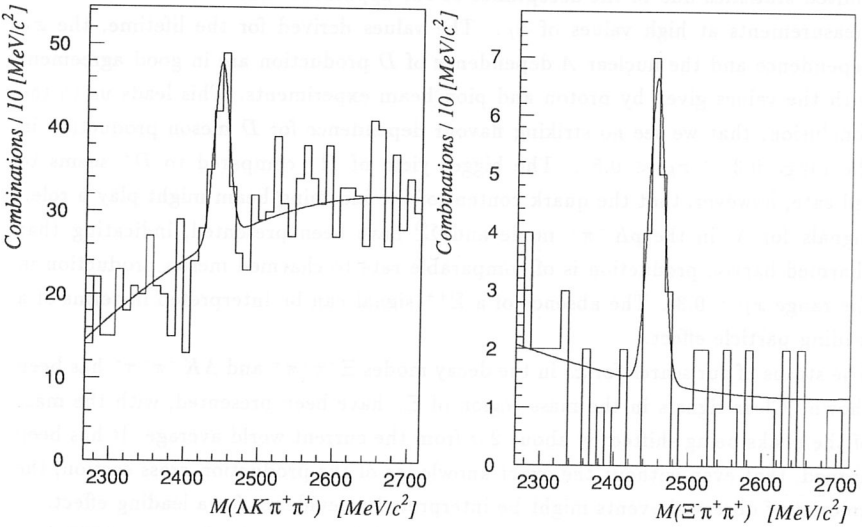

Figure 5: Ξ_c^+ search in the channels $\Lambda K^-\pi^+\pi^+$ (left) and $\Xi^-\pi^+\pi^+$ (right).

7 – Conclusions

First results from the analysis of the 1991 data sample of the WA89 hyperon beam experiment at CERN have been presented.

We have shown a clear signal for $D^{\mp}$ decaying to $K^{\pm}\pi^{\mp}\pi^{\mp}$ with, however, rather limited statistics due to the acceptance of our apparatus that has been tailored for measurements at high values of x_F. The values derived for the lifetime, the x_F dependence and the nuclear A dependence of D production are in good agreement with the values given by proton and pion beam experiments. This leads us to the conclusion, that we see no striking flavour dependence for D meson production in the range $0.3 < x_F < 0.5$. The bigger yield of D^- compared to D^+ seems to indicate, however, that the quark content of the incoming beam might play a role.

Signals for Λ_c in the $pK^-\pi^+$ mode and Σ_c^0 have been presented, indicating that charmed baryon production is of comparable rate to charmed meson production in the range $x_F > 0.3$. The absence of a Σ_c^{++} signal can be interpreted in terms of a leading particle effect.

The status of our search for Ξ_c in the decay modes $\Xi^-\pi^+\pi^+$ and $\Lambda K^-\pi^+\pi^+$ has been shown. Clear signals in the mass region of Ξ_c^+ have been presented, with the mass of the peaks being shifted by about 2 σ from the current world average. It has been argued, that even without the exact knowledge of the production cross section, the amount of observed events might be interpreted as evidence for a leading effect.

Finally, it should be noted that we expect much better results from our 1993 data taking, when we recorded about 200 million events with a much improved detector setup. Precision measurement of charmed baryon lifetimes should then be possible.

References

(1) W. Beusch et al., NIM **A323**, 373 (1992)
(2) W. Brückner et al., NIM **A313**, 345 (1992)
(3) Review of Particle Properties, Phys. Rev. **D45**, No. 11 (1992)
(4) WA82 collaboration (M. Adamowich et al.), Phys. Lett. **B284**, 453 (1992)
(5) WA82 collaboration (M. Adamowich et al.), CERN–EP 89–123
(6) ACCMOR collaboration (S. Barlag et al.), Z. Phys. **C49**, 555 (1991)
(7) LEBC–EHS collaboration (M. Aguilar–Benitez et al.), Phys. Lett. **B189**, 467 (1987)
(8) WA62 collaboration (S.F. Biagi et al.), Phys. Lett. **B122**, 455 (1983)

Frascati Physics Series, Vol. 1 (1993)
HEAVY QUARKS AT FIXED TARGET
Frascati, May 31st – June 2nd 1993
(pp. 189–205)

HIGH ENERGY CHARM PHOTOPRODUCTION

Jim Wiss
University of Illinois at Urbana Champaign, Department of Physics
1110 West Green St., Urbana IL 61801, (USA)

Abstract

I report on the investigation of the charm photoproduction mechanisms including recent data on inclusive D production and on $D\overline{D}$ charm pair correlations. I will conclude by offering a prognosis of the ability of future high energy photoproduction experiments to measure absolute charm particle branching ratios through through kinematically tagged pions from $D^{*+} \rightarrow \pi D^o$ decay.

1. Inclusive Photoproduction Studies

Much of the recent data on inclusive charm photoproduction comes from the E687, NA14/2 [2] [1] and E691 [3] [4] experiments which collectively span an appreciable photon energy range. Each experiment utilizes downstream silicon vertex detectors [1] to obtain reasonably clean, high statistics charm samples. Table 1 summarizes the average energies reported and the the approximate reconstructed sample size used for inclusive charm photoproduction studies

Table 1. Recent Fixed Target Photoproduction Experiments

Exp	$< E_\gamma >$	N_{sample}
E687	220 GeV	$\approx$ 50K
NA14/2	95 GeV	$\approx$ 1K
E691	145 GeV	$\approx$ 10K

The inclusive charm cross sections show a consistent trend with increasing photon energies and are in generally good agreement with the predictions of the

[1] In addition, NA14/2 uses an active,segmented Si target

next to leading order (NLO) photon-gluon fusion model [5]. Figure 1 compares the observed $d\sigma/dx_F$ distributions for charmed mesons obtained by the three experiments. The x_F distributions are remarkably consistent between the experiments even though they span nearly a factor of two in average beam energy.

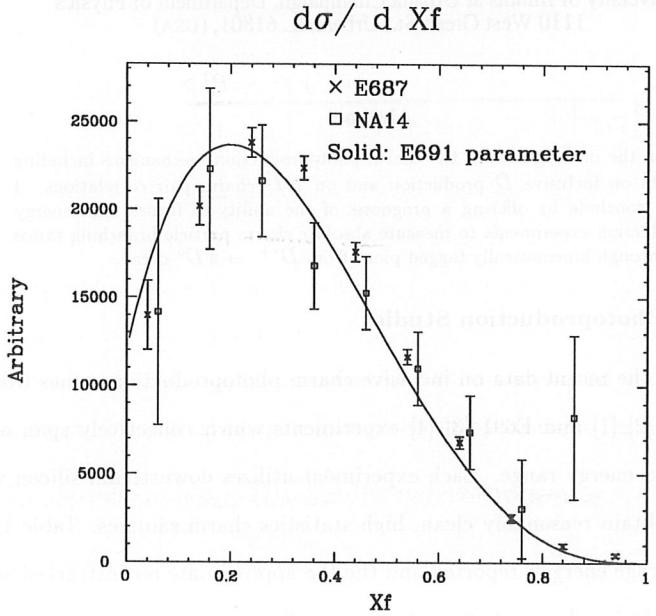

Figure 1. $d\sigma/dx_F$ distributions

We note that the most probable charmed *meson* x_F observed by all experiments is approximately 0.2 which is considerably lower than which is the average x_F of 1/2 expected for charmed *quarks* in the naive photon-gluon fusion model. Dressing/fragmentation effects appear to play important in high energy charm photoproduction.

We turn next to measurements of the P_t distribution with respect to the incident photon beam for inclusive, photoproduced charmed mesons. The E691

Collaboration [3] has fit their observed P_t dependence to the form $dN/dP_t^2 = A\ exp(aP_t^2 + bP_t^4)$. Their shape parameters and average P_t^2 values (in GeV^2) are compared to those obtained by the E687 collaboration operating at a higher average beam energy in Table 2.

Table 2. Charm P_t Dependence

	$a\ (GeV^{-2})$	$b\ (GeV^{-4})$	$< P_t^2 >$
E687	-0.85 ± 0.02	0.03 ± 0.01	1.51 ± 0.02
E691	-1.07 ± 0.05	0.04 ± 0.01	1.16 ± 0.04

One observes evidence for increasing P_t growth of charm mesons with in creasing beam energy as expected in the photon-gluon fusion model. Figure 2 compares the P_t^2 distribution of E687 and NA14/2. The NA14/2 data was scaled up to match the first E687 bin. The NA14/2 distribution taken at a lower beam energy appears to have a softer P_t distribution than the higher energy E687 data.

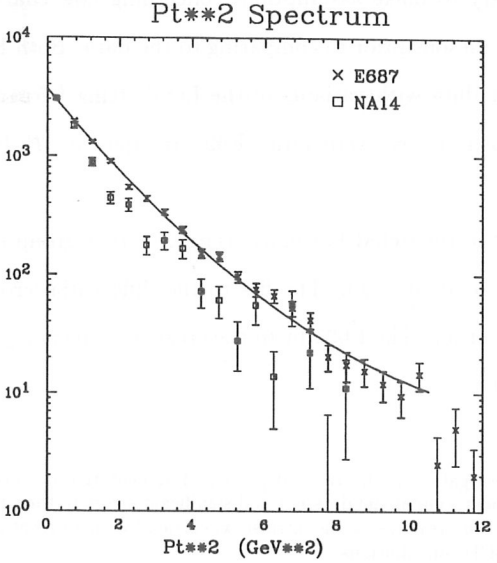

Figure 2. P_t distribution obtained by E687 compared to NA14/2.

Both the E691[4] and NA14/2[1] Collaborations have performed fits of their inclusive photoproduced D^o and D^+ spectra in order to measure parameters of the photon-gluon fusion model. To lowest order, the cross section for photoproduced charmed quarks (in the photon-gluon center of mass frame) can be written as an integral over the gluon distribution function and the partonic cross section of the form:

$$\frac{d\sigma}{d\Omega^*} = \int_{4m_c^2}^{s} \frac{d\hat{s}}{s} \; g(x = \hat{s}/s) \quad \frac{d\hat{\sigma}}{d\Omega^*}(\hat{s}, \theta^*) \tag{1}$$

where m_c is the charmed quark mass, $\hat{s}$ is the squared photon-gluon center of mass energy and $\hat{\sigma}$ is partonic cross section. The charmed quark mass m_c influences the inclusive quark cross section through both the partonic cross section and limits of integration. Information on the gluon distribution, parameterized in its simplest form as $xg(x) \propto (1-x)^{n_g}$, can also be measured over the range $x \approx 0.03 \rightarrow 0.25$ probed by charm photoproduction experiments near 100 GeV.

It is necessary to make assumptions concerning how charmed quarks fragment into charmed mesons prior to comparing to the data. Both E691 and NA14-2 have unfolded their data with variants of the Lund string [2] fragmentation model. In order to diminish the k_t systematic, E691 restricts its P_t fits to the region $P_t^2 > 2\ GeV^2$

Because of the restricted kinematic range, neither group includes a Q^2 dependence in either α_s or in $g(x)$. The fits to the differential cross section shapes are done in leading order. The E691 fit to the cross section energy dependence uses next to leading order. [3]

[2] E691 has also investigated alternative, independent fragmentation models and concludes that variations in the fragmentation model does not add significant errors to their measurements. Their dominant systematic is uncertainties in the intrinsic k_t carried by the incident gluon which partially reflects higher order QCD contributions.

[3] Since shape corrections to the next to leading order calculations are small; while the cross section itself changes by 32 % going from LO to NLO.

Table 3. Fits to PGF parameters

Exp.	m_c	$xg(x) = (1-x)^{n_g}$	In fit
E691‡	$1.74^{+.13}_{-.18}$	$n_g = 7.2 \pm 2.2$	P_t^2 x_F $\sigma(c\bar{c})$
NA14/2	$1.58 \pm .07$†	$n_g = 5$ (assumed)	P_t^2

† Statistical error only

‡ k_t^2 systematics reduced by fitting $P_t^2 > 2\ GeV^2$

2. $D\overline{D}$ Correlations

We begin by discussing photoproduced events where both the D and $\overline{D}$ are fully reconstructed into the states $K\pi$, $K2\pi$ and $K3\pi$. The NA14/2 Collaboration [2] reports on a sample of 22 fully reconstructed double charm events; the E687 Collaboration [6] reports on a sample of 325 fully reconstructed double charm events. Figure 3 shows a scatterplot of the D versus $\overline{D}$ normalized mass distribution obtained in E687. The normalized mass, which allows one to combined different decay modes and states with differing resolutions, is the difference between the reconstructed and nominal mass over the mass computed mass resolution resolution. A fit to the D projection for events in the $\overline{D}$ mass band reveals a $D\overline{D}$ sample of about 325 very clean events.

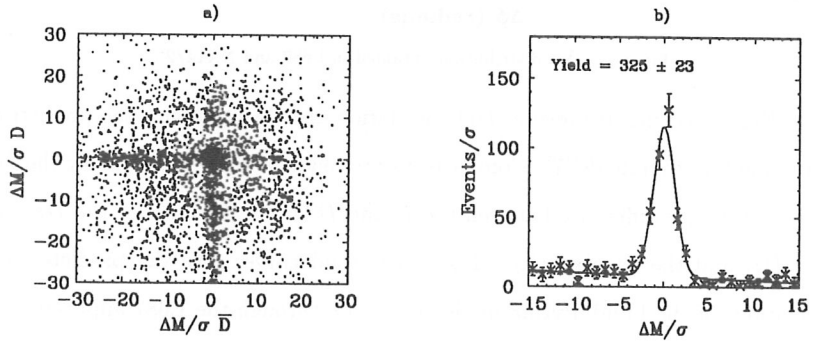

Figure 3. (a) Normalized $D\overline{D}$ scatterplot (b) $\overline{D}$ normalized mass for events in the D band

Figure 4 compares the area normalized $D\overline{D}$ acoplanarity angle distribution obtained by E687 and NA14/2. The acoplanarity ($\Delta\phi$) distribution describing the azimuthal angle between the D and $\overline{D}$ projected in a plane transverse to the photon, is easily compared between experiments because it has good resolution and fairly uniform acceptance. This distribution would spike at π radians except for the effects of intrinsic k_t, gluon radiation, and quark fragmentation. Both experiments see a considerably smeared acoplanarity distribution.

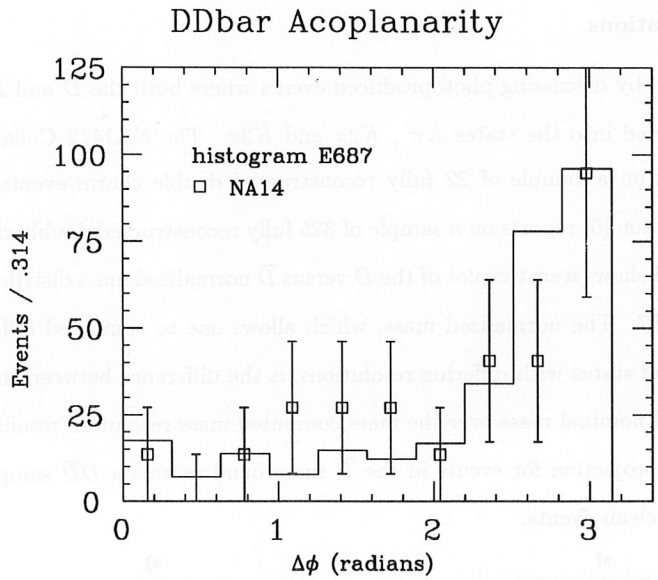

Figure 4. $\Delta\phi$ distribution obtained in E687 and NA14/2

Figure 5 compares several $D\overline{D}$ correlation distributions with the predictions of the Lund/Pythia model[7]. Comparisons are made to the P_t^2 carried by the $D\overline{D}$ pair, the rapidity difference between the D and $\overline{D}$ (ΔY), the mass of the $D\overline{D}$ pair ($M(D\overline{D})$) and the acoplanarity. The inner, solid curves give the predicted $D\overline{D}$ correlations of the Lund/Pythia model as viewed through the E687 apparatus[8] –

after correction for resolution and acceptance. The dashed, outer curves show what the predictions would be in the absence of acceptance and resolution effects and allow the reader to judge the importance of these effects. These "acceptance-less" distributions are normalized to the peak bin.

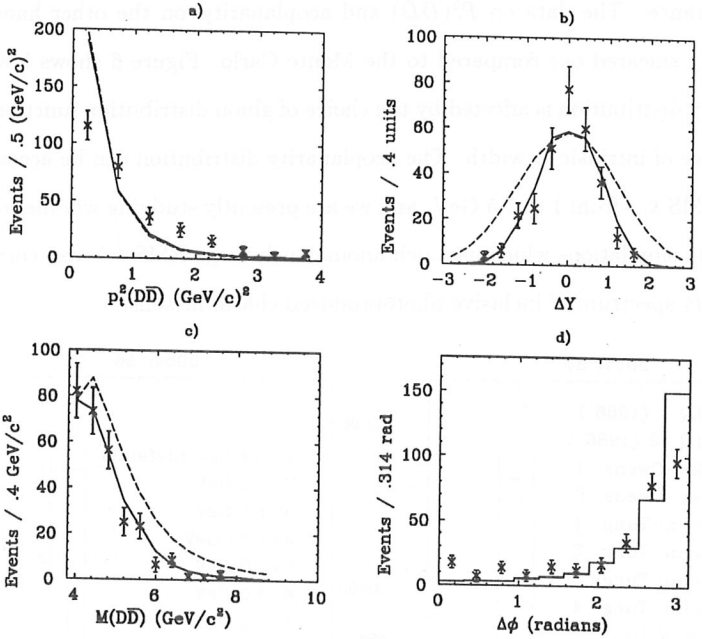

Figure 5. $D\overline{D}$ correlations.

The predictions of Figure 5 are based on the Pythia (PYTHIA56,JETSET73) version of the lowest order photon-gluon fusion mechanism which includes some higher order corrections in the form of partonic showers initiated as gluonic bremsstrahlung.

The Lund/Pythia curves are computed using the EHLQ gluon structure functions although the results are fairly insensitive to the exact choice of structure functions in the x range probed by E687. Standard Lund string fragmentation is used throughout. Perhaps the most important parameter of the model is the intrinsic

k_t of the incident gluon which is modeled in projection as a Gaussian distribution with $\sigma = 0.44$ GeV/c.

We note that the Monte Carlo distributions for rapidity difference and $D\overline{D}$ invariant mass are reasonably consistent with the data over the range where we have acceptance. The data on $P_t^2(D\overline{D})$ and acoplanarity, on the other hand are considerably smeared out compared to the Monte Carlo. Figure 6 shows how the acoplanarity distribution is affected by the choice of gluon distribution function and by the choice of intrinsic k_t width. The acoplanarity distribution can be accommodated by RMS k_t's from 1 to 1.5 GeV, and we are presently studying whether or not Monte Carlo simulations which use such anomalously large RMS k_t's can correctly model the P_t spectrum of inclusive photoproduced charm mesons.

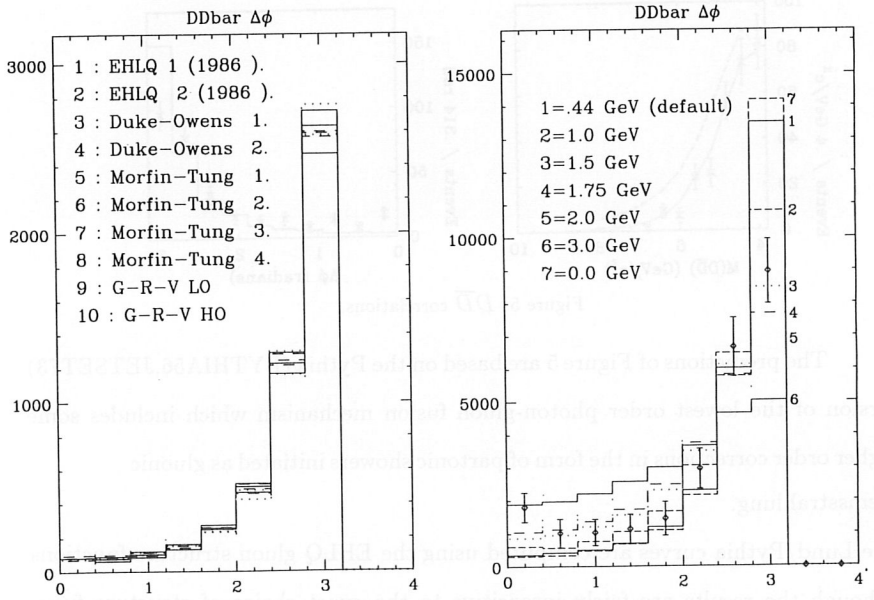

Figure 6. $\Delta\phi$ predictions (a) Various gluon PDF's (b) Various RMS k_t

Finally, Figure 7 compares the acoplanarity distribution obtained in photoproduced E687 data with that of hadroproduced charm particles from the ACCMOR collaboration [9]. Clearly the $D\overline{D}$ acoplanarity distribution for hadroproduced charm is much more smeared out than that for photoproduced charm. Perhaps this is because hadroproduced charm is dominated by gluon-gluon fusion and one suffers the intrinsic k_t of two rather one incident gluons.

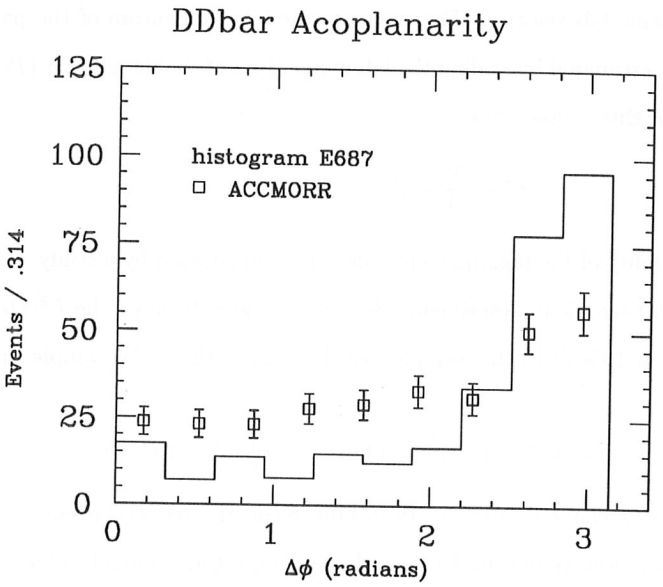

Figure 7. Comparison of Hadro- and Photo-produced $\Delta\phi$ distributions

3. $D\overline{D}$ Physics with D^* Decay Pion Tags

E687 has recently shown[6] that it is also possible to study $D\overline{D}$ correlations using kinematically tagged pions from $D^{*+} \rightarrow \tilde{\pi}^+ D^o$ decay. This allows us to greatly increase the statistical sample size and study correlations over a much larger

kinematic range because of considerably increased acceptance. The basic technique is to fully reconstruct a recoil charm particle in any of the three "golden" modes of $K\pi$, $K2\pi$, $K3\pi$. One then searches the primary vertex for $\tilde{\pi}$ candidates with the correct charge whose scaled momentum approximately balances the P_t of the fully reconstructed recoil charm particle.

The scaled momentum follows from the kinematic observation that the low energy release of the process $D^{*+} \rightarrow \tilde{\pi}^+ D^o$ implies that the D^{*+} and $\tilde{\pi}^+$ have essentially the same lab velocity. This suggests the lab momentum of the parent D^{*+} (P^*) can be estimated by scaling the lab momentum of the daughter $\tilde{\pi}$ ($P_{\tilde{\pi}}$) by the parent to daughter mass ratio:

$$\vec{P}^* \approx \frac{M_{D^*}}{M_\pi} \vec{P}_{\tilde{\pi}} \approx 13.8 \vec{P}_{\tilde{\pi}} \tag{2}$$

The feasibility of the tagging technique can be illustrated by a study of fully reconstructed $D\overline{D}$ sample in described in Section 2. Figure 8 shows the $P_t^2(D\overline{D})$ is typically less than 4 GeV^2 in this sample, which suggests the $\tilde{\pi}^+ \overline{D}_r$ sample should satisfy:

$$\Delta_t^2 \equiv \left(13.8 P_x^{(\pi)} + P_x^{(r)}\right)^2 + \left(13.8 P_y^{(\pi)} + P_y^{(r)}\right)^2 < 4 \; GeV^2 \tag{3}$$

The primary vertex charged multiplicity in fully reconstructed $D\overline{D}$ events is only 2.2 tracks [4] and is well reproduced by our Lund Monte Carlo model. Finally the momentum spectrum of primary vertex tracks is well reproduced by our Monte Carlo. A right sign - wrong sign subtraction should be highly effective in isolating the $\tilde{\pi}$ sample since the photoproduced primary vertex is very sparsely populated and subtraction systematics should be very easy to control and understand since it is well reproduced by our Lund-based Monte Carlo.

[4] We use $D\overline{D}$ events to eliminate any confusion from partially reconstructed charm particles with secondaries which are consistent with intersecting the primary vertex due to finite resolution.

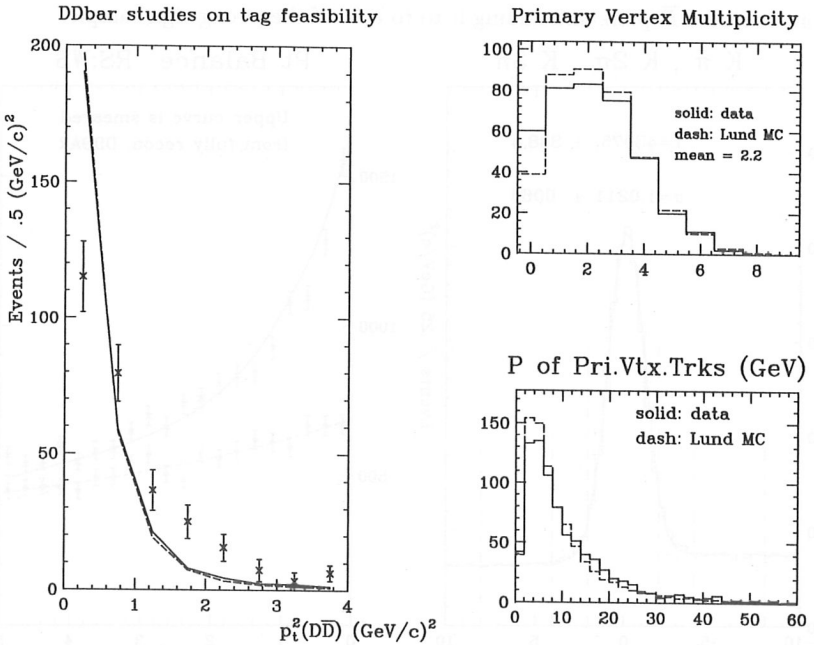

Figure 8. $P_t^2(D\overline{D})$ and primary vertex distributions from fully reconstructed $D\overline{D}$ sample

We begin with a recoil fully reconstructed D_r sample consisting of about 44,000 fully reconstructed $K\pi$, $K2\pi$, and $K3\pi$ decays whose normalized mass plot is shown in Figure 9. A mass sideband charm subtraction region is illustrated. The charm subtracted, Δ_t^2 balance distribution of Figure 9 demonstrates our ability to isolate a kinematically tagged $\tilde{\pi}^+\overline{D}_r$ sample. The upper curve shows the P_t^2 balance variable for right sign $\tilde{\pi}$ candidates; the lower curve shows the balance variable for wrong sign candidates. A clear excess of right sign events is observed in the expected region $\Delta_t^2 < 4\ GeV^2$ which is in excellent agreement with the upper solid curve which is computed by smearing [5] the P_t^2 of Figure 8 obtained for the fully

[5]Based on a Monte Carlo study, we parameterized a the smearing function as a function of Δ_t^2 which has an average rms width of approximately 0.8 GeV/c in $\Delta_{x,y}$

reconstructed $D\overline{D}$ pairs and adding it to to a fit of the wrong sign sample.

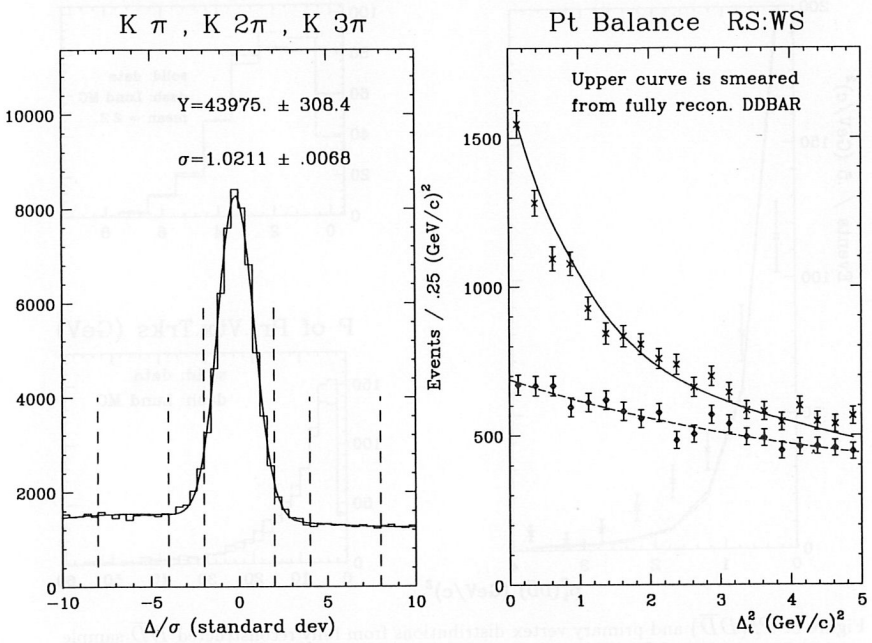

Figure 9. (a) Golden mode normalized mass sample (b) P_t balance variable

The right sign excess with $\Delta_t^2 < 4\ GeV^2$ is about 4300 events or about 1/10 the baseline golden mode sample of inclusive $K\pi$, $K2\pi$, and $K3\pi$ charm decays. The background subtracted, kinematic $D\overline{D}$ correlation distributions for this 4300 event $\tilde{\pi}^+\overline{D}_r$ sample is shown in Figure 10. In Figure 10a and 10b the inner solid curves give the predicted $D\overline{D}$ correlations predicted by the Monte Carlo – after correction for resolution and acceptance while the dashed curve gives the predictions in the absence of acceptance and resolution effects. In Figure 10c the acoplanarity for the $\tilde{\pi}^+\overline{D}_r$ sample is compared to a smeared [6] version of the acoplanarity for the fully reconstructed $D\overline{D}$ sample. The $\tilde{\pi}^+\overline{D}_r$ sample is about 10 times more copious

[6]The rms resolution smearing due to the finite energy release in the decay $D^* \rightarrow \tilde{\pi}D^0$ was determined from a Monte Carlo study to be 0.3 radians.

measurements of the absolute branching ratio for the D^o.

The basic idea here is to reconstruct a $D^{*+} \rightarrow D^o\pi^+$ final state through a specific decay mode of the D^o produced along with a fully reconstructed $\overline{D}_r$ recoil. One would then measure the absolute branching ratio for *eg* $D^o \rightarrow K^-\pi^+$ as shown below:

$$B(K\pi) = \frac{1}{\epsilon} \frac{(K\pi)\tilde{\pi}^+}{(\ )\tilde{\pi}^+} \tag{4}$$

The numerator of this ratio is portion of the fully reconstructed $D\overline{D}$ sample which includes a $D^{*+} \rightarrow (K^-\pi^+)\pi^+$ and dominates the statistical error bar. The denominator will be the far more copious $\tilde{\pi}^+\overline{D}_r$ sample. In order to boost the statistics of the numerator, many D^o decay modes can be combined since the relative branching ratio between decay modes can be very well measured from the ratio of their inclusive yields.

Let us estimate the statistical precision of absolute D^o branching ratio measurements obtainable in a future run of E831. The yield of $\tilde{\pi}$ tags will scale from 4500 events to about 45000 events in E831 and hence denominator statistics will have a negligible fractional error of about 1/2 of a percent. The roughly 400 fully reconstructed $D\overline{D}$ events obtainable in E687 will become 4000 $D\overline{D}$ events in E831, but only about 500 of these will have the useful topology of: $(K\pi)\pi$ and $(K3\pi)\pi$ against $K\pi, K2\pi, K3\pi$. This suggests a fractional statistical error of $1/\sqrt{500} = 4.5\%$ if we restrict ourselves to $(K\pi)\pi$ and $(K3\pi)\pi$ against either $K\pi$,$K2\pi$, or $K3\pi$. One can probably expand this base to include additional D^o , D^+ , and D_s^+ decay modes including those modes with a missing neutral which can be reconstructed by demanding P_t balance about the inter-vertex line and tagged through the D^* such as $D^{*+} \rightarrow (K^-\pi^+\pi^o)\pi^+$. By expanding the base of charm particles considered, we can hope to get statistical errors as low as $2.5 \rightarrow 3.5\%$ for the D^o absolute branching ratio. At present the best information on the D^o absolute branching ratio comes from

the Mark III experiment and LEP which obtain fractional errors $12 \rightarrow 15\%$ although I've recently been made aware of the possibility that the CLEO collaboration will soon release more precise branching ratios.

It is also possible to boot strap measurements of the D^o absolute branching ratio into D^+ absolute branching ratio's by comparing the yields of D^{*+} reconstructed through the two decays $D^{*+} \rightarrow (K^-\pi^+)\pi^+$ and $D^{*+} \rightarrow (K^-\pi^+\pi^+)\pi^o$. The ratio of branching ratio's $B(K^-\pi^+\pi^+)/B(K^-\pi^+)$ can be measured by equating a consistent D^{*+} yield through either channel.

$$\#\ D^{*+} = \frac{\#(K\pi)\pi^+}{\epsilon_+\ B(K\pi)\ B^*_+} = \frac{\#(K2\pi)\pi^o}{\epsilon_o\ B(K2\pi)\ B^*_o}$$

One could then extract the $B(K2\pi)$ absolute branching ratio for the D^+ from $B(K\pi)$ measured as described above and the well measured D^* branching ratios from CLEO:

Table 4. D^{*+} branching ratios from CLEO

Mode	CLEO values	
$D^{*+} \rightarrow D^o\pi^+$	$68.1\pm1.0\pm1.3\%$	B^*_+
$D^{*+} \rightarrow D^+\pi^o$	$30.8\pm0.4\pm0.8\%$	B^*_o

At present E687 observes about 75 clean, reconstructed $D^{*+} \rightarrow D^+\pi^o$ decays in its inner electromagnetic shower calorimeter. If both the inner and outer electromagnetic calorimeter are used, a sample of roughly 2000 $D^{*+} \rightarrow D^+\pi^o$ should be obtainable in E831 which should result in a systematically dominated measurement.

Finally it might even be possible to measure charm baryon absolute branching ratios. Many photoproduction groups report an excess of Λ_c^+ compared to $\overline{\Lambda_c^+}$ charmed baryons. Traditionally this excess has been attributed to the associated production process $\gamma N \rightarrow \overline{D}\Lambda_c^+ X$. If one makes this assumption, it is possible to

than the fully reconstructed sample and offers a considerably larger kinematic range over which correlation studies can be performed. The $\tilde{\pi}^+\overline{D}_r$ acoplanarity distribution appears consistent with that obtained for the fully reconstructed $D\overline{D}$ sample. The rapidity difference and inferred $M(D\overline{D})$ invariant mass are consistent with our Lund/Pythia Monte Carlo.

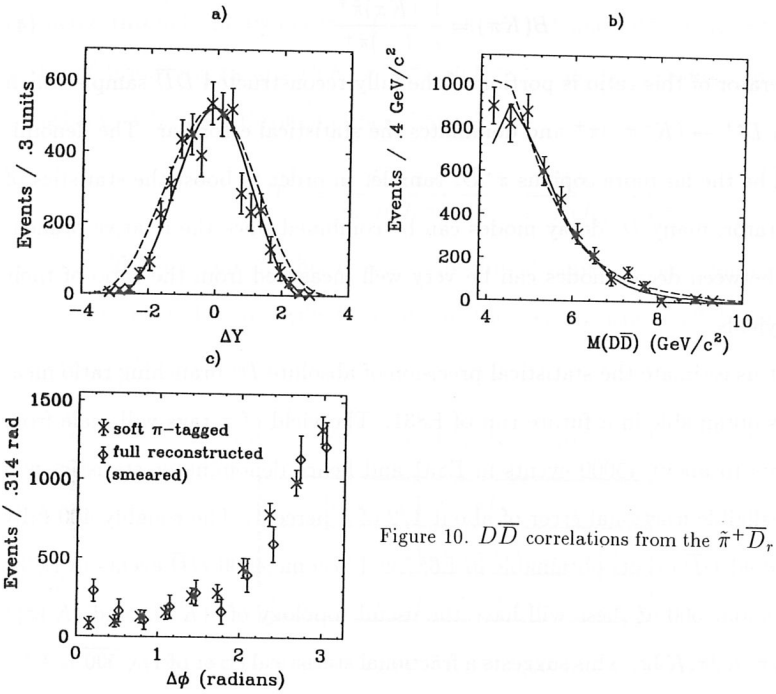

Figure 10. $D\overline{D}$ correlations from the $\tilde{\pi}^+\overline{D}_r$ sample

4. Absolute Charm Branching Ratios in Fixed Targets

The ability to reliably kinematically tag $\tilde{\pi}$'s from $D^{*+} \to \tilde{\pi}^+ D^o$ suggests a method for computing the absolute branching ratio for charm mesons. I would like to explore this possibility for a future fixed target photoproduction experiment, E831, which is anticipated to have $\times 10$ the charm sample of E687. We begin with

bootstrap to a charmed baryon absolute branching ratio by using a consistent excess expression:

$$\#\ \overline{D}\Lambda_c = \frac{\#PK\pi - \#\overline{PK\pi}}{\epsilon_\Lambda\ B(PK\pi)} = \frac{\#\overline{D} - \#D}{\epsilon_D\ B(D)}$$

The likely systematics problem is understanding the relative ϵ_Λ and ϵ_D efficiencies given that the momentum spectrum for associatedly produced charmed baryons is model dependent and the model is not well specified to my knowledge.

5. Summary

Studies of inclusive D meson photoproduction at beam energies of 100 - 300 GeV show remarkably consistent trends between three recent experiments. In particular the x_F distributions of NA14/2, E691, and E687 are very consistent and peak at a most probable $x_F \approx 0.2$. The average P_t is observed to grow with increasing beam energy. Fits of the inclusive D photoproduction sample suggest charm quark masses in the vicinity of 1.5 to 1.87 GeV and fits gluon parton distribution $xg(x) = (1-x)^{n_g}$ with n_g ranging from 5 to 10.

New data has recently become available on photoproduced $D\overline{D}$ correlations. Both E687 and NA14/2 obtain consistent $D\overline{D}$ acoplanarity distributions which are more smeared out (away from π) than expected in the default Lund/Pythia model but smeared out far less than the $\Delta\phi$ obtained in charm hadroproduction experiments. The data is in good agreement with the Lund/Pythia predictions for the $D\overline{D}$ rapidity difference and invariant mass.

A technique for kinematic tagging of $\tilde{\pi}^+\overline{D}_r$ events was demonstrated which allows one to study $D\overline{D}$ correlations with larger statistics and over a broader kinematic range than with fully reconstructed $D\overline{D}$ events. The ability of a future charm photoproduction experiment, E831, to use kinematically tagged $\tilde{\pi}^+\overline{D}_r$ events to measure charm absolute branching ratio's was discussed.

6. Acknowledgements

I would like to acknowledge the efforts of my E687 Colleagues who made much of this work possible and especially acknowledge the massive help of Drs. Rob Gardner and Ray Culbertson. This work was supported in part by the US Department of Energy,

7. References

1. M. P. Alvarez *et al.*,*Physics Letters* **B278** (1992)385.
2. M. P. Alvarez *et al.*,submitted to Zeitshrift fur Physik C, (CERN-PPE/92-28)
3. J. C. Anjos *et al. Phys. Rev. Lett.* **62** (1989) 513.
4. J. C. Anjos *et al. Phys. Rev. Lett.* **65** (1990) 2503.
5. R. K. Ellis and P. Nason, *Nucl. Phys.* **B312** (1989) 551.
6. Rob Gardner for the E687 Collaboration, The Fermilab Meeting DPF92, World Scientific (1993) 762.
7. T.Sjostrand, Computer Phys. Comm. 39 (1986) 347;
   T.Sjostrand, H.-U.Bengtsson, Computer Phys. Comm. 43 (1987) 367;
   H.-U.Bengtsson, T.Sjostrand, Computer Phys. Comm. 46 (1987) 43.
8. E687, P. L. Frabetti *et al.*, *Nucl. Instrum. Methods.* **A320** (1992) 519.
9. ACCMOR,S. Berlag *et al.*, *Phys. Lett.* **B302** (1993) 112.

Frascati Physics Series, Vol. 1 (1993)
HEAVY QUARKS AT FIXED TARGET
Frascati, May 31st – June 2nd 1993
(pp. 207–216)

CHARMED MESON DECAYS: AN OVERVIEW OF RECENT RESULTS

D. Barberis
Università di Genova, Dipartimento di Fisica and Sezione INFN
Via Dodecaneso 33, I–16136 Genova, (ITALIA)

1 Introduction

Since the discovery of the charmed particles in the mid-seventies a large number of experiments have been performed to measure their properties, particularly their life-times and decay branching ratios. Because of the large mass difference between the c quark and the light quarks, many decay channels are open for all charmed mesons and baryons, which in turn means that the study of all but a few single decay channels has been so far limited by statistics. Nevertheless the picture is now reasonably clear for what concerns most Cabibbo-favoured decays [1]; this review will therefore concentrate mainly on the singly and doubly Cabibbo-suppressed decays of charmed mesons and on the possibility of final-state interactions.

1.1 Models of Charmed Meson decays

The simple spectator model (fig.1), in which one assumes that the decay of the c quark is independent of the particle the quark belongs to, does not describe correctly the relative lifetimes and branching ratios of the charmed mesons. Refined versions of the model have been proposed by several authors to take into account additional mechanisms which could enhance or suppress some decay diagrams relative to other ones. The main uncertainty is in the way quarks recombine after the decay to form the mesons we observe in the final state. Naively the inner-W decay should be suppressed by colour

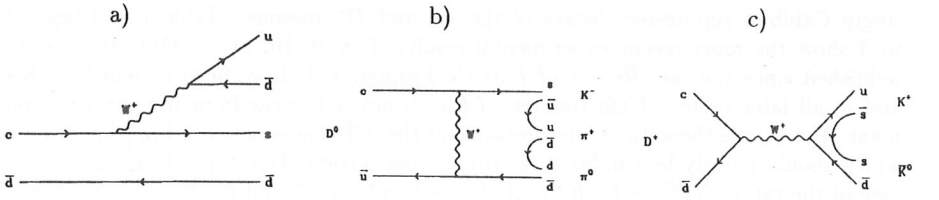

Figure 1: Feynman diagrams of some charmed meson decays: a) spectator diagram; b) W exchamge diagram; c) annihilation diagram.

matching, but if we assume that the decay occurs in a cloud of soft gluons a kind of "colour bleaching" might take place. A similar argument can be applied to the W exchange diagrams. As we will see, the indications from experiments are contradictory if interpreted in terms of simplistic models and it could well be that final state interactions play such an important role as to completely determine the branching ratios.

1.2 Overview of Experiments

Recent results on charm meson decays measured in fixed target experiments have been published or submitted for publication by the following experiments:

- E687 : photoproduction (at FNAL) [2];
- E691 : photoproduction (at FNAL) [3];
- WA82 : hadroproduction with an impact parameter trigger (at CERN) [4].

All these experiments are equipped with silicon microvertex detectors which provide a spatial resolution of some μm transverse to the line of flight. Such resolutions enable us to see the charm decay with efficiencies that can be as large as 50% depending on the charmed particle lifetime and the decay multiplicity. Charm samples for the "easiest" decays ($D^+ \to K^-\pi^+\pi^+, D^0 \to K^-\pi^+, D^0 \to K^-\pi^+\pi^+\pi^-$) are clean with signal-to-background ratios ranging from 1 to 15. The present statistics of charm events has a sufficient size to allow meaningful comparisons with models. Details of these experiments are found in several review works [5, 6] and references quoted therein. Here only the peculiar features are recalled:

- the target is thin, solid and in some cases segmented;
- the hardware and software selection criteria are open, based on particle identification, transverse energy, impact parameter;
- the acceptance covers the full forward hemisphere.

Recently the e^+e^- experiment CLEO has collected enough statistics to be competitive with fixed-target experiments also on rare decays.

2 Singly Cabibbo Suppressed Decays

A considerable amount of data has been accumulated on the branching ratios of the singly Cabibbo suppressed decays of the D^0 and D^+ mesons. Table 1 and figs. 2 to 4 show the most recent experimental results [7, 8, 9, 10, 11]. Only the results published since the last *Review of Particle Properties* [1] have been included in this and in all later tables. Unfortunately if the situation is clear from the experimental point of view, the theoretical interpretation of the differences between branching ratios which should naively be similar is far from being settled. One typical example is the case of the ratios $\Gamma(D^0 \to K^-K^+)$ / $\Gamma(D^0 \to \pi^-\pi^+) \approx 2.5$ and $\Gamma(D^0 \to K^-K^+\pi^+\pi^-)$

/ $\Gamma(D^0 \to \pi^-\pi^+\pi^+\pi^-) \approx 0.3$, where the phase-space factor would be insufficient to explain the large difference.

One possible explanation could come from the interpretation of all decays as chains of two-body decays: in this scheme the charmed meson would decay to some superposition of excited states of a pair of vector and/or pseudoscalar mesons, and the relative branching ratios would therefore be strongly affected by interference effects and final-state interactions. The detailed analysis by the CLEO collaboration of the decays $D^0 \to \pi^-\pi^+\pi^+\pi^-$ (where they observe at least 1 ρ^0 per event) and $D^0 \to K^-K^+\pi^+\pi^-$ (which is compatible with being due entirely to $D^0 \to \phi\rho^0$) supports this idea.

Table 1: Branching ratios of singly Cabibbo suppressed decays.

	WA82	*E687*	*CLEO*	*PDG 92*
$\frac{D^+\to\pi^-\pi^+\pi^+}{D^+\to K^-\pi^+\pi^+}$	$0.032 \pm 0.011 \pm 0.003$	$0.035 \pm 0.006 \pm 0.004$		0.035 ± 0.007
$\frac{D^+\to\phi\pi^+}{D^+\to K^-\pi^+\pi^+}$	$0.062 \pm 0.017 \pm 0.006$			0.075 ± 0.007
$\frac{D_s^+\to\pi^-\pi^+\pi^+}{D_s^+\to\phi\pi^+}$	$0.33 \pm 0.10 \pm 0.04$	$0.33 \pm 0.08 \pm 0.04$		0.44 ± 0.11
$\frac{D^0\to\pi^-\pi^+}{D^0\to K^-\pi^+}$	$0.048 \pm 0.013 \pm 0.008$			0.045 ± 0.005
$\frac{D^0\to K^-K^+}{D^0\to K^-\pi^+}$	$0.107 \pm 0.029 \pm 0.015$	$0.138 \pm 0.027 \pm 0.010$		0.113 ± 0.007
$\frac{D^0\to\pi^-\pi^+\pi^+\pi^+}{D^0\to K^-\pi^+\pi^+\pi^+}$	$0.115 \pm 0.023 \pm 0.016$	$0.108 \pm 0.024 \pm 0.008$	0.102 ± 0.013	0.100 ± 0.011
$\frac{D^0\to K^-K^+\pi^+\pi^+}{D^0\to K^-\pi^+\pi^+\pi^+}$			0.031 ± 0.010	0.032 ± 0.005

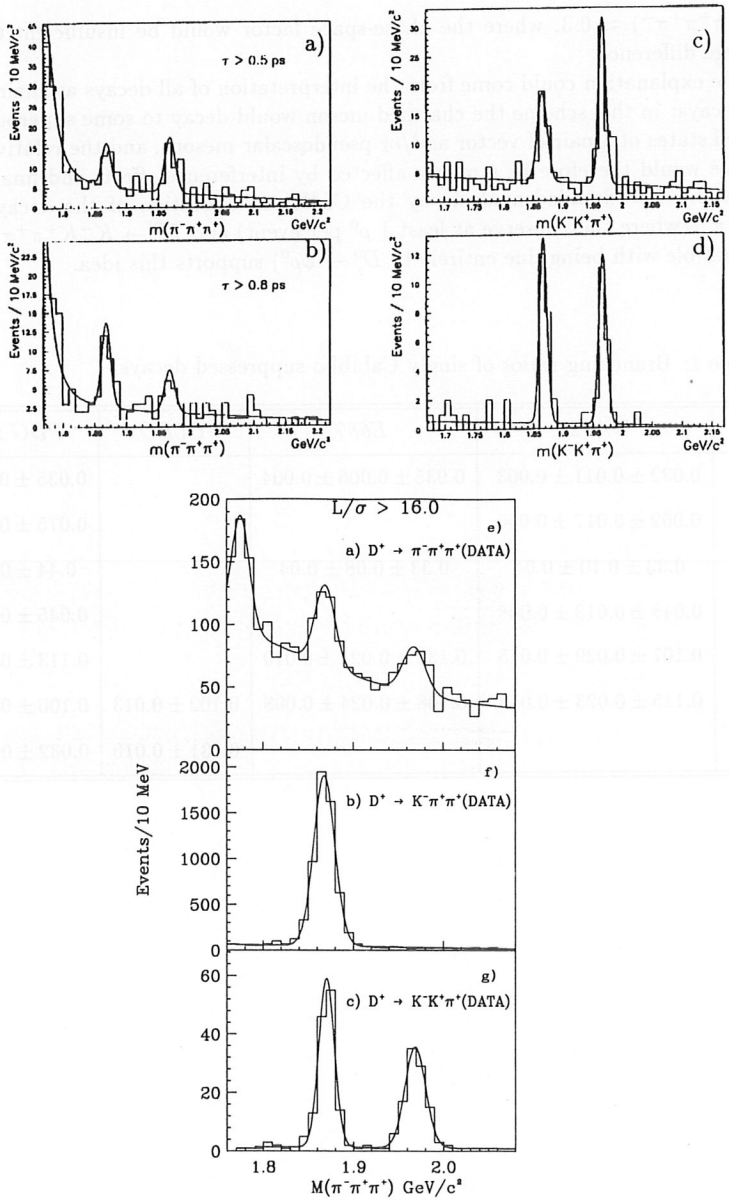

Figure 2: Mass spectra of the decays $D^+ \to \pi^-\pi^+\pi^+$ and $D^+ \to K^-K^+\pi^+$ from $WA82$ (a) to d)) and $E687$ (e) to g)).

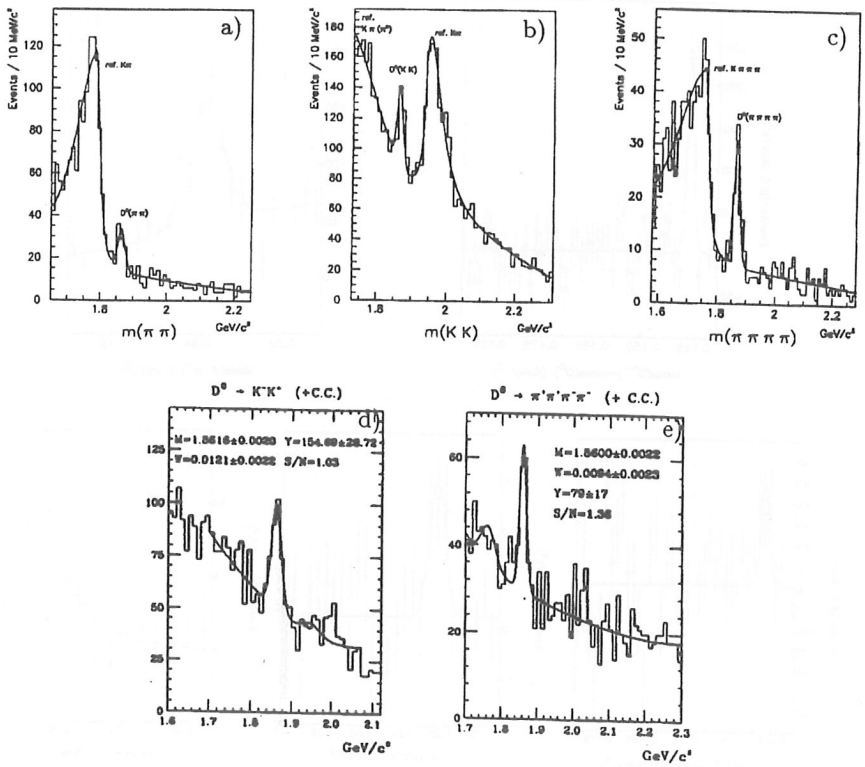

Figure 3: Mass spectra of the decays $D^0 \to \pi^-\pi^+$, $D^0 \to K^-K^+$ and $D^0 \to \pi^-\pi^+\pi^+\pi^-$ from $WA82$ (a) to c)) and $E687$ (d) and e)).

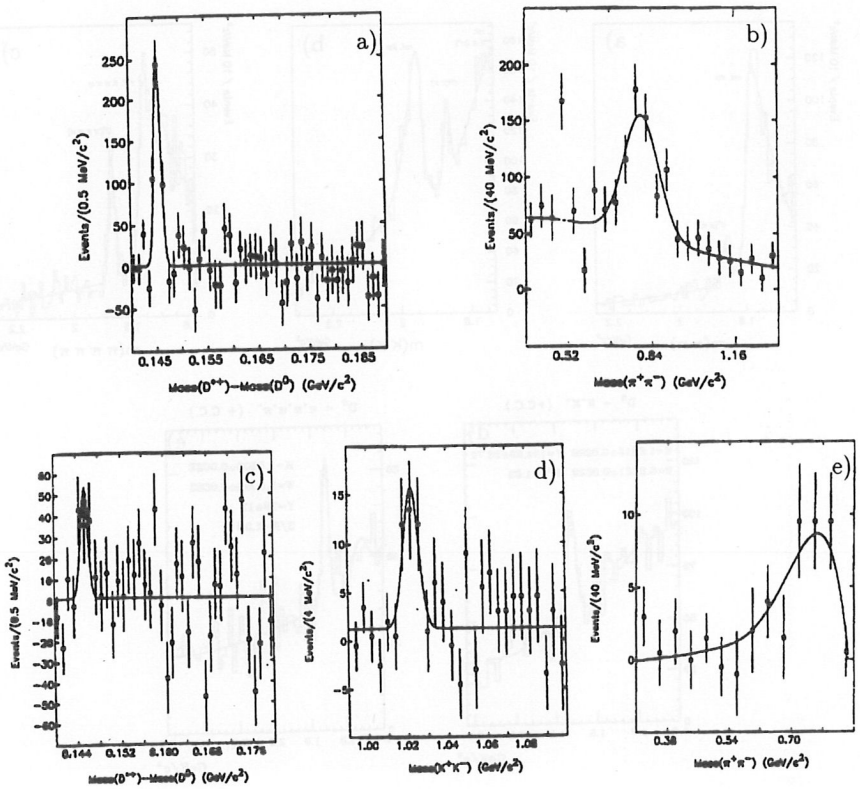

Figure 4: Mass spectra of the decays $D^0 \to \pi^-\pi^+\pi^+\pi^-$ and $D^0 \to K^-K^+\pi^+\pi^-$ from $CLEO$. a) $D^{*+} - D^0$ mass difference when $D^0 \to 4\pi$. b) $\pi^+\pi^-$ mass in the 4π system. c) $D^{*+} - D^0$ mass difference when $D^0 \to KK\pi\pi$. e) K^+K- mass in the $KK\pi\pi$ system. e) $\pi^+\pi^-$ mass in the $KK\pi\pi$ system.

3 Colour Bleaching and Final State Interactions

A recent study performed by the E691 collaboration[12] on the decays $D^0 \to \bar{K}^0\pi^0$ and $D^0 \to \bar{K}^0K^0$ shows the importance of colour bleaching and/or final state interactions. The results, in mild disagreement with earlier data, are shown in fig.5 and summarized in table 2. The decay $D^0 \to \bar{K}^0\pi^0$ can have a similar amplitude to the "favourite" decay $D^0 \to K^-\pi^+$ if some colour bleaching mechanism is effective, that is the decay occurs within a cloud of gluons which rearrange immediately the quarks into colour singlets. Another possibility is that final state interactions rearrange all valence quarks in the final state irrespective of the actual c quark decay mechanism. The direct decay $D^0 \to \bar{K}^0K^0$ is suppressed by the GIM[13] mechanism, but it can occur through an

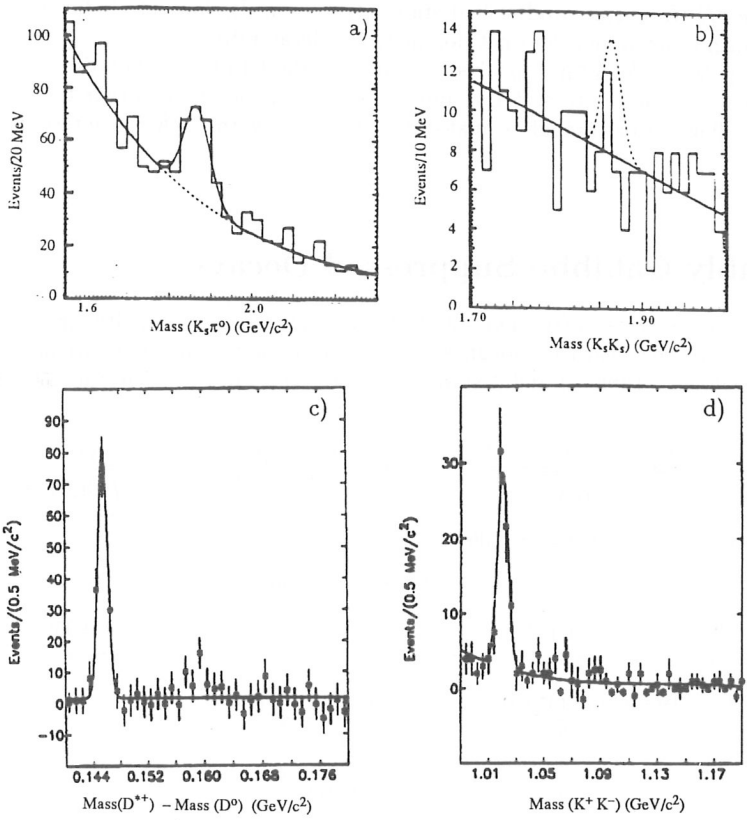

Figure 5: a) $K_s^0\pi^0$ mass spectrum from $E691$. b) $K_s^0K_s^0$ mass spectrum. c) $D^{*+} - D^0$ mass difference when $D^0 \to \bar{K}^0K^+K^-$ from $CLEO$. d) K^+K^- mass in the $\bar{K}^0K^+K^-$ system.

Table 2: Branching ratios of D^0 decays with possible final-state interactions.

	E691	*PDG 92*
$\frac{D^0 \to \bar{K}^0 \pi^0}{D^0 \to K^- \pi^+}$	$1.36 \pm 0.23 \pm 0.22$	0.57 ± 0.14
$\frac{D^0 \to \bar{K}^0 K^0}{D^0 \to K^- \pi^+}$	< 0.032	0.029 ± 0.014
$\frac{D^0 \to \bar{K}^0 \phi}{D^0 \to K^- \pi^+}$		0.24 ± 0.04
$\frac{D^0 \to \bar{K}^0 (K^+ K^-)_{non-\phi}}{D^0 \to K^- \pi^+}$		0.14 ± 0.03

intermediate "$K^- K^+$" state and a final state interaction. Its low rate indicates that this mechanism is active but does not dominate the decay rate.

The decay $D^0 \to \bar{K}^0 K^+ K^-$ has been studied by the CLEO collaboration[11] and has been shown to be due to $\approx \frac{1}{2} \bar{K}^0 \phi$ and $\approx \frac{1}{2} \bar{K}^0 a_0$; this decay can occur through a W-exchange diagram or through a final-state interaction with a "$\bar{K}^0 \eta'$" intermediate state.

4 Doubly Cabibbo Suppressed Decays

Very little evidence exists so far on doubly Cabibbo suppressed decays, although recent experiments have now reached enough sensitivity to allow the first measurements of these rare channels. Tables 3 and 4 summarize the results published in the last year

Table 3: Branching ratios of doubly Cabibbo suppressed D^+ decays.

	WA82	*E691*	*E687*	*PDG 92*
$\frac{D^+ \to K^+ K^+ K^-}{D^+ \to \phi \pi^+}$	$0.49 \pm 0.23 \pm 0.06$			
$\frac{D^+ \to K^+ \phi}{D^+ \to \phi \pi^+}$		$0.058^{0.032}_{0.026} \pm 0.007$		
$\frac{D^+ \to K^+ \pi^+ \pi^-}{D^+ \to K^- \pi^+ \pi^+}$	< 0.042		< 0.007	< 0.050

Table 4: Branching ratios of doubly Cabibbo suppressed D^0 decays.

	CLEO
$\frac{D^0 \to K^+ \pi^-}{D^0 \to K^- \pi^+}$	< 0.011
$\frac{D^0 \to K^+ \pi^- \pi^+ \pi^-}{D^0 \to K^- \pi^+ \pi^+ \pi^-}$	< 0.018

[8, 14, 11]; some new results are also reported elsewhere in these proceedings[15]. The decay $D^+ \to K^+K^+K^-$ can proceed through an annihilation diagram with the creation of an $s\bar{s}$ pair or through a simpler spectator diagram with the production of a "$K^+\eta\prime$" intermediate state and a final state interaction. An increased accuracy in this measurement would help disentangling the different contributions, but for the time being the incompatible results from WA82 and E691 (fig.6) do not help to clarify the situation.

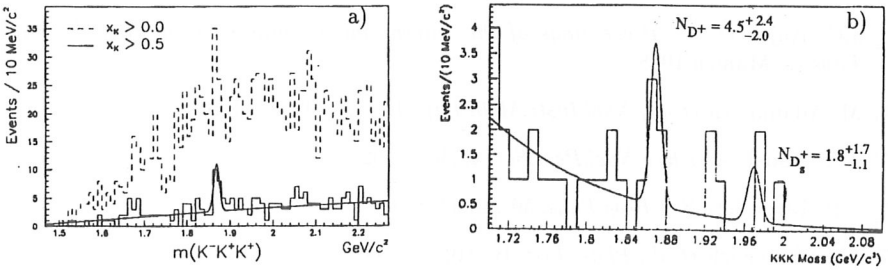

Figure 6: a) $K^+K^+K^-$ mass spectrum from $WA82$. b) $K^+\phi$ mass spectrum from $E691$.

5 Conclusion

Considerable progress has been made in the last few years on the measurement of charmed-meson decay rates. Nevertheless our theoretical understanding is still far from being complete. It is now clear that the "naive" spectator model explains only the gross features of the decay rates, but it is not clear which other mechanisms give the major contribution. Several questions are still open:

- what are the relative and absolute importance of colour bleaching and final-state interactions?
- what about the $\Delta I = \frac{1}{2}$ rule?
- what about the pseudoscalar/vector ratios?

Some decisive contribution towards answering these questions will come from the analysis of large data sets which have been recently collected by CLEO (2 million produced charm events), E687 (100k reconstructed events) and E791 (200k reconstructable events).

Acknowledgment: This paper would not have appeared without the constant support and help of Drs M.Dameri, G.Darbo, B.Osculati, O.Nalivkina and L.Rossi.

References

[1] Particle Data Group, *Review of Particle Properties, Phys.Rev.* D45(1992).

[2] P.L. Frabetti *et al.*, Fermilab-PUB-92-320-E.

[3] J.C. Anjos *et al.*, *Proceedings of the International Conference on High Energy Physics*, Munich 1988.

[4] M. Adamovich *et al.*, *Nucl.Instr.Meth.Phys.Res.* A 309,401(1991).

[5] J.A. Appel, *Ann.Rev.Nucl.Part.Sci.* 42,367(1992).

[6] S.P. Tavernier, *Rep.Prog.Phys.* 50,1439(1987).

[7] M. Adamovich *et al.*, *Phys. Lett.* B 280,163(1992).

[8] M. Adamovich *et al.*, CERN-PPE-93-27 (1993).

[9] S. Malvezzi, *Proceedings of the 1993 Rencontres de Moriond*, to be published.

[10] P.L. Frabetti *et al.*, *Phys. Lett.* B 281,167(1992).

[11] R. Ammar *et al.*, *Phys.Rev.* D44,3383(1991).

[12] J.C. Anjos *et al.*, *Phys.Rev.* D46,R1(1992).

[13] S.L. Glashow, J. Iliopoulos, L. Maiani, *Phys.Rev.* D2,1285(1970).

[14] J.C. Anjos *et al.*, *Phys.Rev.Lett.* 69,2892(1992).

[15] M. Purohit, *these proceedings.*

Frascati Physics Series, Vol. 1 (1993)
HEAVY QUARKS AT FIXED TARGET
Frascati, May 31st – June 2nd 1993
(pp. 217–228)

RECENT RESULTS ON CHARM DECAYS WITH π^0's OR η's

A. Zallo
INFN – Laboratori Nazionali di Frascati
P.O.Box 13, I–00044 – Frascati (Roma), (ITALIA)

ABSTRACT

A review of recent results from fixed target experiments on charms decays involving π^0's is presented. The aim is a comparison with similar measurements done at e^+e^- colliders.

1 Introduction

Recent results obtained by CLEO at e^+e^- colliders have increased the interest of studying charm decays with neutrals in the final state. The reconstruction of π^0's or γ's not only opens the possibility to measure new branching ratios, but gives a strong contribution to the study of radiative processes, check of the validity of conservation rules, test of many decay mechanisms etc. The measurement of these new channels has been possible because of the installation of a huge ($\simeq$ 7800 crystals), high resolution CsI electromagnetic calorimeter [1]. A similar improvement has not been done at fixed target;new experiments have collected large samples of data, but with the same quality of the previous results.

The Fermilab experiment E687 has reconstructed more than 100K charged charms[2]; E791[3] has collected 20 billions of triggers, reconstructed more than 50K charged charms and the final sample should be bigger than 200K. Both experiments should be able to produce large samples of charm decays with neutrals, but at the present are available only preliminary results by E687.

A few CLEO recent measurements will also be reviewed in order to do a comparison with fixed target.

2 Fixed target recent results

2.1 Fermilab experiment E653

The Fermilab experiment E653 has presented [4] preliminary results on the decay channel $D_s \rightarrow \eta\mu^+\nu + \eta'\mu^+\nu$. It was exploited the fact that

$$\eta \rightarrow \pi^+\pi^-\pi^0$$

$$\eta' \rightarrow \pi^+\pi^-\eta, \eta \rightarrow neutrals$$

have nearly identical $\pi^+\pi^-$ mass spectra that peak near threshold; 29 events below a $\pi^+\pi^-$ mass of 0.40 GeV/c^2 were collected.

The branching ratio obtained was

$$\frac{\Gamma(D_s^+ \rightarrow (\eta\mu^+\nu + \eta'\mu^+\nu))}{\Gamma(D_s^+ \rightarrow \phi\mu^+\nu)} = 2.4 \pm 1.2$$

to be compared with a theoretical prediction of 0.88.

In order to isolate η', 5 prongs events were selected of the type

$$D_s^+ \rightarrow \eta'\mu^+\nu, \eta' \rightarrow \pi^+\pi^-\eta, \eta \rightarrow \pi^+\pi^-\pi^0 + \pi^+\pi^-\gamma.$$

From the branching ratio obtained

$$\frac{\Gamma(D_s^+ \rightarrow \eta'\mu^+\nu)}{\Gamma(D_s^+ \rightarrow \phi\mu^+\nu)} < 2.0$$

the authors conclude that $D_s^+ \rightarrow (\eta\mu^+\nu + \eta'\mu^+\nu)$ is unlikely to be dominated by $D_s^+ \rightarrow \eta'\mu^+\nu$.

2.2 Fermilab experiment E687

E687 has been able to observe the Knπ, multi-pionics and Cabibbo suppressed decay modes using the 100K charged charms decay sample[2]. A similar program seems to be possible for the neutral decays for which more than 10K should be reconstructed.

E687 is equipped with two electromagnetic calorimeters. The inner is made of lead-scintillating fibers, for a total of 7 longitudinal independent views, covering the angular region below 30 mrad; the outer is a lead-scintillator calorimeter with a total of 9 longitudinal independent views, that covers the wide angle region up to $\simeq$ 150 mrad.

The energy resolution is worse than that obtained by CLEO (5% at 1 GeV). For example the outer electromagnetic calorimeter has a typical energy resolution

$$\frac{\sigma_E}{E} = \frac{11\%}{\sqrt{E}} \oplus 2.5\%$$

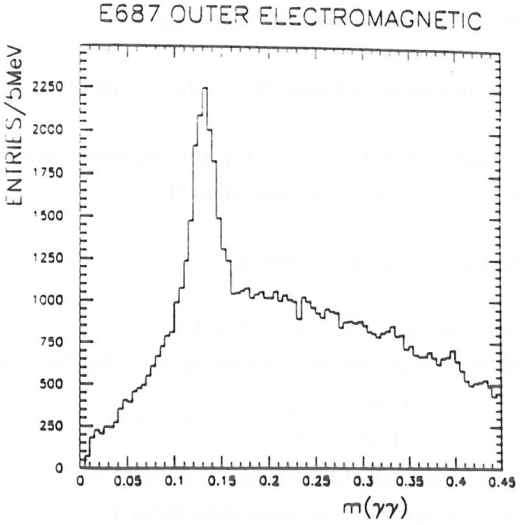

Figure 1: $M_{\gamma\gamma}$ (GeV/c^2) distribution for the E687 Outer Electromagnetic Calorimeter for $P_{\gamma\gamma} \simeq 2\ GeV/c$. The $\sigma_M(\pi^0)$ is $\simeq 10\ GeV/c^2$.

that is only 11.3% at 1 GeV. But because of a quite good angular resolution and a relatively high energy of the π^0's, the mass resolution achieved (Fig. 1) is $\sigma_{M_{\pi^0}} \simeq 10\ MeV/c^2$ to be compared to $\simeq 5\ MeV/c^2$ for CLEO [1].

In the following I will summarize preliminary results that do not refer to the full statistics and that request to run Montecarlo programs in order to get the reconstruction efficiencies and estimation of systematic errors.

2.2.1 Charm Meson decays

The following signals have been observed [5]:

$$D^0 \rightarrow K^-\pi^+\pi^0$$

$$D^0 \rightarrow K^-\pi^+\pi^-\pi^+\pi^0$$

$$D^0 \rightarrow K^-\pi^+\pi^0\pi^0$$

$$D^+ \rightarrow K^-\pi^+\pi^+\pi^0$$

The event selection criteria have been the following:

at least one π^0 reconstructed with $(90 \leq M_{\pi^0} \leq 160) MeV/c^2$

a minimum separation between primary and secondary vertices of 5 l/σ (σ is the error associated to the separation l)

at least 2 tracks in the primary vertex.

The resulting signals are shown in Fig. 2, 3 and 4.

For $D^0 \rightarrow K^-\pi^+\pi^0$ a preliminary branching ratio has been measured:

$$\frac{\Gamma(D^0 \rightarrow K\pi\pi^0)}{\Gamma(D^0 \rightarrow K\pi)} = 2.99 \pm 0.31$$

that is in good agreement with the PDG value of 3.09 ± 0.35.

E687 has also measured [6] the mass differences $D^{*0} - D^0$ through the measurement of the process $D^{*0} \rightarrow D^0\pi^0$ ($D^0 \rightarrow K\pi$). The result, shown in Fig. 5, preliminary and with the systematic error still to be studied is $M_{D^*} - M_{D^0} = 141.6 \pm 0.09\ MeV/c^2$.

2.2.2 Charm Baryon decays

A large number of charmed baryons decay with Σ or Ξ in the final state have very high branching ratios to π^0 or γ (Table 1). So new channels can be discovered if an efficient electromagnetic calorimeter is available.

E687 has presented preliminary results [7] on $\Lambda_c^+ \rightarrow pK^-\pi^+\pi^0$ through the decay chain $\Lambda_c^+ \rightarrow \Delta^+K^{*0} \rightarrow pK^-\pi^+\pi^0$. The observation of this channel is important because it goes through the W-exchange decay mechanism only. W-exchange decay diagrams can be studied only in baryon decays where they are not helicity or colour suppressed as in meson decays. The signal, shown in Fig.6, is preliminary.

E687 has measured also the branching ratio [8]

$$\frac{\Gamma(\Lambda_c^+ \rightarrow \Sigma^+\phi \rightarrow p\pi^0\phi)}{\Gamma(\Lambda_c^+ \rightarrow \Sigma^+\pi^+\pi^- \rightarrow p\pi^0\pi^+\pi^-)}$$

where the Σ^+ is detected through the decay $\Sigma^+ \rightarrow p\pi^0$. The measurement of the π^0 is not essential, because the knowledge of the Σ^+ direction and of the proton momentum gives, assuming the particle nominal masses, the Σ^+ momentum. E687 has reconstructed the π^0's requiring that the $p\pi^0$ momentum matches well the Σ^+ track direction. Fig.7 shows the $\Sigma^+ \rightarrow p\pi^0$ invariant mass distribution for two different requirements on the matching of the $p\pi^0$ vector with the Σ^+ track.

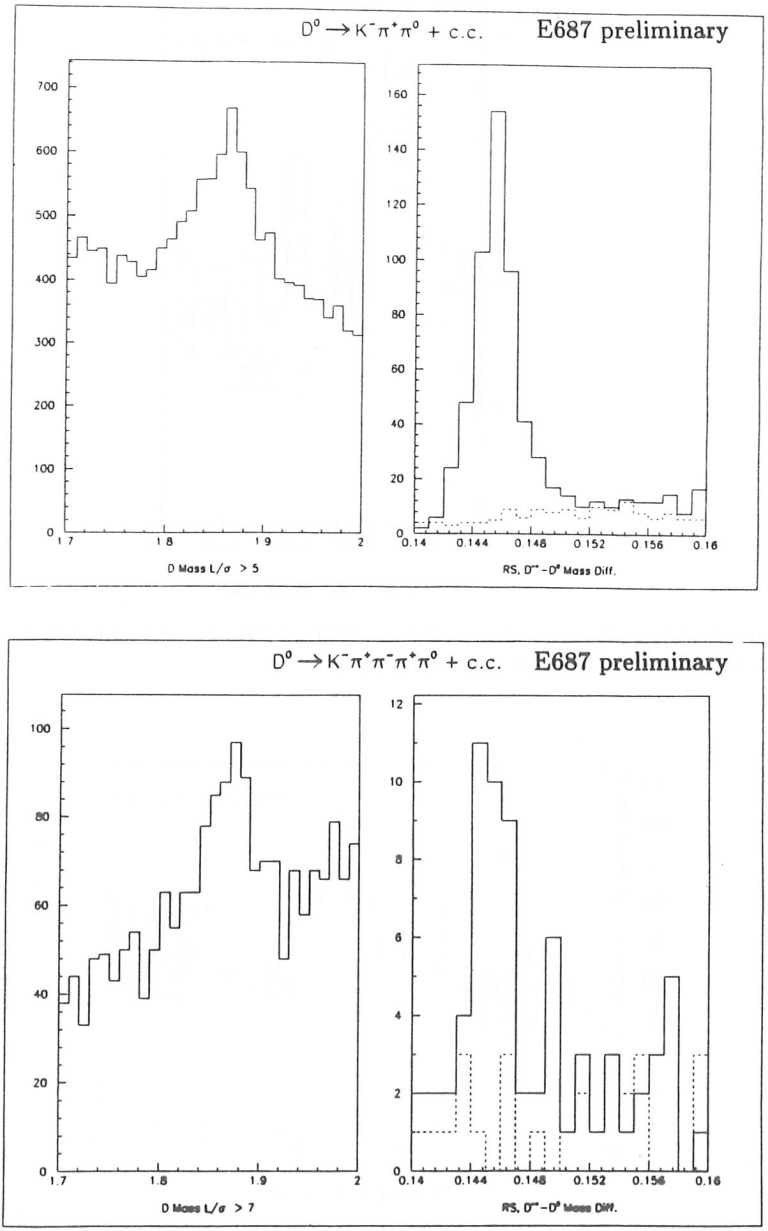

Figure 2: $D^0 \to K^-\pi^+\pi^0$ and $D^0 \to K^-\pi^+\pi^-\pi^+\pi^0$ mass distributions (GeV/c^2). On the right side are shown the right sign (full lines) and wrong sign (dot lines) $D^{*+} - D^0$ mass differences (GeV/c^2).

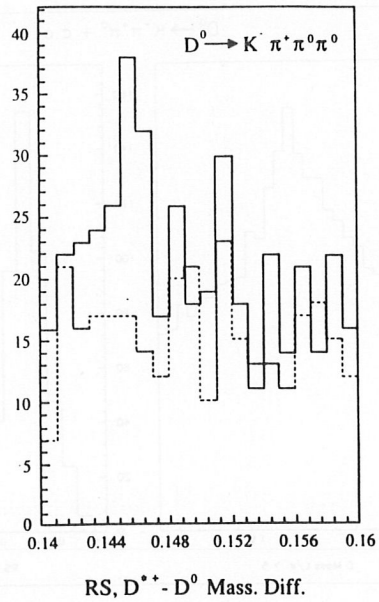

Figure 3: $D^{*+} - D^0$ right sign (full lines) and wrong sign (dot lines) mass differences (GeV/c^2) for $D^0 \to K^-\pi^+\pi^0\pi^0$.

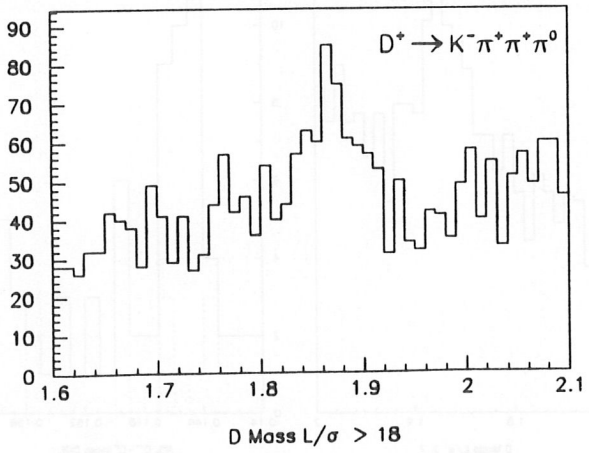

Figure 4: $D^+ \to K^-\pi^+\pi^+\pi^0$ mass distribution (GeV/c^2).

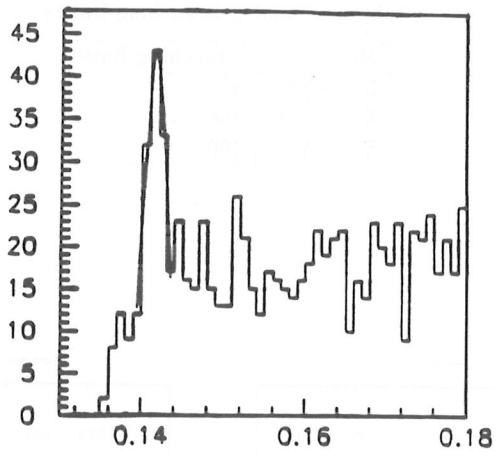

Figure 5: $D^{*0} - D^0$ mass difference (GeV/c^2).

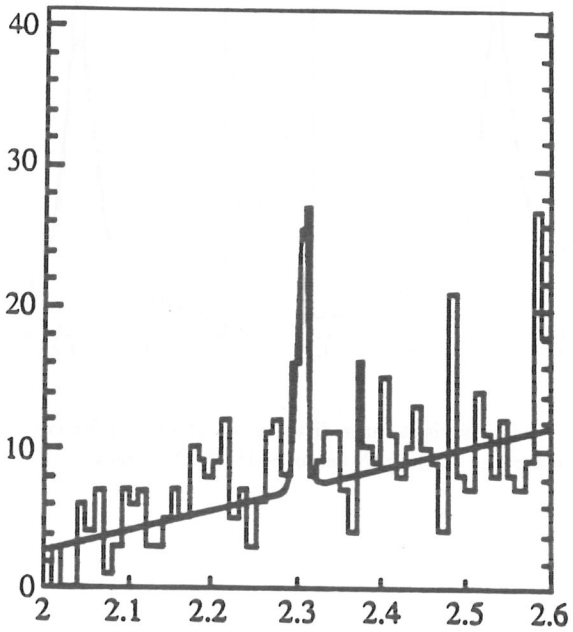

Figure 6: $\Lambda_c^+ \to pK^-\pi^+\pi^0$ mass distribution (GeV/c^2).

Table 1: Σ and Ξ Branching Ratios

Mode	Branching Ratio
$\Sigma^+ \to p\pi^0$	51.6
$\Sigma^0 \to \Lambda^0\gamma$	100
$\Xi^0 \to \Lambda^0\pi^0$	100

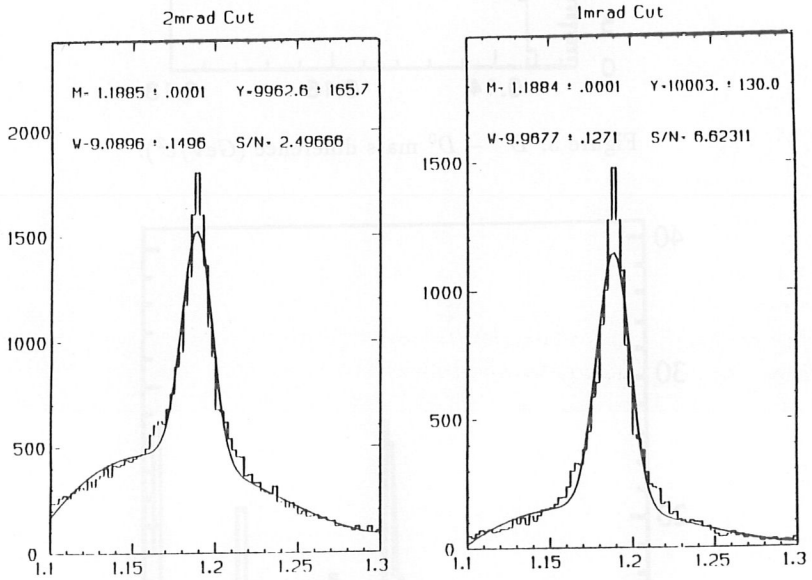

Figure 7: $\Sigma^+ \to p\pi^0$ invariant mass distribution (GeV/c^2) for two different requirements on the matching of the $p\pi^0$ vector with the Σ^+ track.

Table 2: $D \to \pi\pi$ Branching Ratios

mode	Yield	CLEO BR (%)	Theory
$D^0 \to \pi^+\pi^-$	171 ± 17	$0.126 \pm 0.011 \pm 0.011$	$0.11 - 0.29$
$D^0 \to \pi^0\pi^0$	32 ± 7	$0.082 \pm 0.015 \pm 0.012$	$0.008 - 0.17$
$D^+ \to \pi^+\pi^0$	28 ± 7	$0.23 \pm 0.005 \pm 0.05$	$0.08 - 0.21$

3 CLEO recent results

I will summarize only a few among the recent CLEO results in this field :

3.1 Test of the $\Delta I = 1/2$ Rule

It is well known that in K decays to two pion final states the A_2 ($\Delta I = 3/2$) isospin amplitude is much smaller than the A_0 ($\Delta I = 1/2$) one. Like the kaon the D meson is isospin 1/2. The A_2 ($\Delta I = 3/2$) amplitude is obtained measuring the $D^+ \to \pi^+\pi^0$ decay ($A^{+0} = \sqrt{3/2}A_2$). To obtain A_0 it is necessary to measure both $D^0 \to \pi^0\pi^0$ and $D^0 \to \pi^+\pi^-$ decays.

CLEO has measured all the three processes [9]. The yield and the branching ratios obtained are summarized in Table 2.

Once extracted from the data the branching ratios, the isospin amplitudes can be easily obtained. To reduce systematic errors the authors use another method. They extract the amplitudes directly from the measured yield, taking advantage of the precisely known ratio

$$B(D^{*+} \to D^0\pi^+)/B(D^{*+} \to D^+\pi^0) = 2.21 \pm 0.07$$

The high value of

$$|A_2/A_0| = 0.7 \pm 0.2$$

is a clear evidence that the $I = 2$ amplitude is not suppressed in D meson decays.

3.2 Measurement of the Cabibbo-Suppressed Decay $D^+ \to \pi^0\ell^+\nu_\ell$

CLEO measures the mass difference

$$M_{diff} = M(\pi^0_{slow}\pi^0_{fast}\ell) - M(\pi^0_{fast}\ell)$$

for the process

$$D^{*+} \to D^+\pi^0_{slow}, D^+ \to \pi^0_{fast}\ell^+\nu_\ell$$

and for the process $D^+ \to \bar{K}^0\ell^+\nu_\ell$ [10]. From the measurement of the branching ratios

$$\frac{B(D^+ \to \pi^0\ell^+\nu_\ell)}{B(D^+ \to \bar{K}^0\ell^+\nu_\ell)} = C|V_{cd}/V_{cs}|^2 \frac{|f_+^\pi(0)|^2}{|f_+^K(0)|^2} = (9.0 \pm 1.8 \pm 1.6)\%$$

Table 3: $D^*(2010)$ Branching Ratios

mode	PDG92	CLEO
$D*+$		
$D^0\pi^+$	0.55 ± 0.04	$0.679 \pm 0.011 \pm 0.020$
$D^+\pi^0$	0.272 ± 0.025	$0.310 \pm 0.005 \pm 0.017$
$D^+\gamma$	0.18 ± 0.04	$0.011 \pm 0.014 \pm 0.015$
$D*0$		
$D^0\pi^0$	0.55 ± 0.06	$0.635 \pm 0.023 \pm 0.035$
$D^0\gamma$	0.45 ± 0.06	$0.365 \pm 0.023 \pm 0.035$

CLEO obtains a new estimate of

$$|V_{cd}/V_{cs}|^2 \frac{|f_+^\pi(0)|^2}{|f_+^K(0)|^2} = 0.0452 \pm 0.0090 \pm 0.0080$$

that can be compared with MARK III result[11)]

$$|V_{cd}/V_{cs}|^2 \frac{|f_+^\pi(0)|^2}{|f_+^K(0)|^2} = 0.057^{+0.038}_{-0.015} \pm 0.005$$

The values obtained are in agreement with theory.

3.3 Measurement of the D^* branching ratios

The CLEO measurement of the D* branching ratios [12)] is based on a very high integrated luminosity ($780 pb^{-1}$) and a complete reconstruction of the final states. The branching ratios, given in Table 3, are compared with the 1992 PDG results [13)]. There are significant differences respect to the world average, essentially due to the low value found for $D^{*+} \to D^+\gamma$.

This value, much more in agreement with theoretical predictions, does not request an anomalous magnetic moment for the charm quark [13)].

3.4 Charm Baryons decays

CLEO, due to the improved neutral detection efficiency, has measured many new channels with neutrals. In Table 4 are summarized only the branching ratios of Λ_c decays through the W-exchange diagram mechanism. The values obtained are in good agreement with calculations using only the W-exchange diagram. It seems that there is no need to invoke final state interactions.

4 Conclusions

The impressive results from CLEO are mainly due to the improvement in γ (hence π^0) detection efficiency. A high resolution calorimeter is essential. The E687 and

Table 4: Λ_c^+ Branching Ratios

Mode	Yield	Branching Ratio
$\Lambda_c^+ \to pK^-\pi^+$	5670 ± 210	1.0
$\Lambda_c^+ \to \Sigma^+K^+K^-$	59 ± 10	$0.070 \pm 0.011 \pm 0.011$
$\Lambda_c^+ \to \Xi^0K^+$	56 ± 10	$0.078 \pm 0.013 \pm 0.013$
$\Lambda_c^+ \to \Xi^{*0}K^+$	24 ± 7	$0.053 \pm 0.016 \pm 0.010$

E791 event reconstruction with neutrals is still in the starting stage, but in some time new results will be available.

The recently approved Fermilab experiment E831 should be able to collect in 1995 a sample of more than 100K events with neutrals. This seems to be a quite good opportunity for fixed target experiments to be competitive with e^+e^- colliders.

5 Acknowledgements

I would like to thank the authors of E687 and CLEO collaboration for providing me with their preliminary results.

References

1. **CLEO collaboration**, Y. Kubota et al., Nucl. Instr. and Methods A320, 66 (1992) .

2. J. Wiss (E687), These proceedings.

3. R. Sidwell, "Fermilab E791", presented at DPF meeting, Batavia, Ill., Nov. 10-17, 1992.

4. D. Potter, presented at 1992 DPF meeting, Batavia, Ill., Nov. 10-17, 1992.

5. "Recent Results on Charm Meson Decays involving π^0's", G. P. Grim, American Physical Society, Vol 38, No. 2, 1053, (1993).

6. **A Study of the Mass Differences $D^{*0} - D^0$ and $D^{*+} - D^0$**, S. V. Greene, American Physical Society, Vol 38, No. 2 , 1038 (1993).

7. **Hadron and Photon production of Heavy quarks** , J.N.Butler, Int. Conf. on High Energy Physics, Dallas, Tx, Aug. 6-12, 1992.

8. **Recent Results on Charm Baryon Decays involving Σ^+'s**, B. G. Cheon, American Physical Society, Vol 38, No. 2, 1038 (1993).

9. **The $D \to \pi\pi$ branching fractions**, M. Selen at al., CLNS-93-1225, (1993).

10. **Measurement of the ratio $\frac{B(D^+ \to \pi^0 \ell^+ \nu_\ell)}{B(D^+ \to K^0 \ell^+ \nu_\ell)}$**, M. S. Alam at al., CLNS-93-1227, (1993).

11. J. Adler et al., Phys. Rev. Lett. 62, 1821 (1989).

12. **Measurement of $D^*(2010)$ branching fractions**, F. Butler et al., Phys. Rev. Lett. 69, 2041 (1992).

13. Particle Data Group, Phys. Rev. D45 part II (1992) 1.

14. **Study of the Decays $\Lambda_c^+ \to \Xi^0 K^+$, $\Lambda_c^+ \to \Sigma^+ K^+ K^-$, $\Lambda_c^+ \to \Xi^- K^+ \pi^+$**, P. Avery at al., CLNS-93-1205, (1993).
Measurement of exclusive Λ_c decays with a Σ^+ in the final state, Y. Kubota et al., CLNS-93-1231, (1993).

Frascati Physics Series, Vol. 1 (1993)
HEAVY QUARKS at FIXED TARGET
Frascati, May 31st – June 2nd 1993
(pp. 229–244)

CHARM BARYON DECAYS IN FIXED TARGET EXPERIMENTS

Sergio P. Ratti
Dipartimento di Fisica Nucleare e Teorica dell' Università
and
Sezione INFN Via A.Bassi 6, I–27100 Pavia (ITALIA)

1. Introduction

Although the first discovery goes eighteen years back or so[1], progress in understanding charm baryons has been rather slow if compared to the understanding of charm mesons.

Mesons, being simply quark–antiquark pairs, are somewhat simpler and the number of possible decays is somewhat limited. Charm baryons "are" a three–body system and are far from being investigated in detail. Nonetheless, charm baryon decays provide a pretty nice tool to test theoretical models, in particular the QCD–non–pertubative strong interaction sector.

By now, experimental results on several baryons, expecially the lowest lying (ucd) isosinglet Λ_c^+, are becoming good enough even to challenge quantitative theoretical predictions. The measurement of the lifetimes, which are shorter than the charm meson lifetimes, are becoming accurate enough. Cabibbo suppressed channels are being detected with sizeable statistics; both the discovery of decay channels other than the "golden modes" and the measurement of relative branching ratios of more and more channels are providing interesting hints into the understanding of charm physics. The absence of color suppression as well as of helicity suppression offers a unique possibility to investigate the importance of W–exchange diagrams in the weak decay of the charm quark [2].

Experimentally the data are far from being complete. To give a macroscopic example, information on purely leptonic decays of baryons[3] is almost completely absent and just starting to come to the surface.

In order to remain within the allocated limits, in the present paper I will not tackle specific topics which are either somewhat premature, or have limited evidence for the time being, or would require too much space for a proper coverage, i.e.:

a – the asymmetry in the Ξ_c^+ decay reported by the Excharm experiment[4];
b – the asymmetry parameters in the two body Λ_c^+ weak decays –not done in fixed target experiment but in progress on Cleo–II data[5a];
c – semileptonic decays[5b];
d – spin determination.

I would rather concentrate on an update of the 1992 information delivered at the 1992 Dallas Conference and at the Division of Particle and Fields APS Meeting at

Fermilab[6], restricting the discussion to the data collected in fixed target experiments but finding a constant comparison with the excellent data collected by the experiments performed at the e^+e^- colliders [Cleo II and Argus] unavoidable.

The fixed target experiments considered here range from the relatively old NA–14 and NA–32, to WA–62 and WA89 at CERN; from E400 to E687, E691 and E791 at Fermilab and Excharm at Serpukov.
NA–14, NA–32 and E791 are hadroproduction experiments which use pion beams; E400 ed Excharm ran with a neutron beam, while E691 and E687 used different photon beams at Fermilab.

WA62, performed back in the early eighties, the direct parent of WA89, is somewhat peculiar since the data were taken at CERN with an hyperon (Σ^-) beam[7]. By operating in a strange baryon beam, the charm baryon signal to noise ratio is greatly enhanced; by requiring the presence of an identified proton, or a Λ^o, or a K^o [a similar requirement was used also in Excharm], the trigger rate is kept low, the efficiency for detecting charm mesons is reduced but the charm baryon content in the data is enhanced.

To a large extent, the nature of the non–strange primary beams does not affect significantly the results of hadroproduction. Photoproduction occurs with a smaller cross section but has a lower hadronic background as well[8], while in hadroproduction non–charm hadronic background is larger for a larger charm production cross section.

To study the highest SU(4) supermultiplet states [containing more than 1 charm quark] one has still to wait for experiments of a future generation. In the literature –and even in private communications or knowledge– there is no evidence yet of charmed baryons containing more than one c–quark.

Thus, referring to new data and to the presentations to the Dallas International Conference and to the APS Division of Particles and Fields Conference, held last november in Fermilab, as a starting point[6], I will cover the following specific topics:

1 – new and rare modes, including the Cabibbo suppressed ones, and the relative branching ratios for the most studied isosinglet charm baryon Λ_c^+;
2 – available data on the Σ_c excited states;
3 – heavy baryons containing one c–quark and one or two s–quarks.

The very interesting issue of the charm baryons lifetimes will be addressed in the contribution by L. Cremaldi. For sake of semplicity I'll subdivide the discussion on the basis of the non charm baryon present in the final state.

2. Λ_c^+ decays containing a proton in the final state

Several new decay modes have been discovered including some Cabibbo suppressed channels. In this Section, I will give a review of the actual knowledge. In a recent preprint[9a] NA–32 has presented evidence for several quasi two body decay modes containing a proton or a nucleon isobar, namely Δ^{++} and $\Lambda^o(1520)$, as well as multipion final states, however based on rather limited statistical samples. Their branching ratios relative to the golden mode $\Lambda_c^+ \to pK^-\pi^+$ are reported in Table I.

TABLE I – Summary of the $\Lambda_c^+ \to px$ decay modes. Yields and relative Branching Ratios in fixed target experiments.

BRANCHING RATIOS RELATIVE TO pK^-p^+

	MODE	E687 YIELD	E687	ACCMOR NA-32	E691	D.P.G.
	$pK^-\pi^+$	1340±91	1.0	1.0	1.0	1.0
	$p(K^-\pi^+)_{nr}$			0.57±.08±,05#		
	$pK^{*o}(892)$			0.35±.065±.03#		
	$\Delta(1232)^{++}K^-$			0.12±.045±.05#		
	$\Lambda^o(1520)\pi^+$			0.09±.035±.02#		
	pK^o	150±31	1.05±.33 (very preliminary)		0.55±.17±.14	0.49±.07
CS	$p\phi$	4.1±3.4	[<.58(pKK)] [<0.056]	0.040±.027		ACCMOR
CS	pK^-K^+	35.4±10.3	0.096±.029±.010	0.048±.027		ACCMOR
	$pK^-\pi^+\pi^o$	30±7	seen			
	$p\pi^o(K^-\pi^+)_{nr}$			0.73±.12±.05		
	$pK^-\pi^+2\pi^o$			0.16±.07±.03		
	$pK^-\pi^+3\pi^o$			0.10±.06±.02		
	$pK^o\pi^+\pi^-$	115±27	0.76±.20 (very preliminary)	0.98±.36±.08	< 1.7 %	0.49±.17
CS	$p(4\pi)^o$	40±10*	seen	0.036±.023		ACCMOR
	$\Lambda^o(3\pi)^+$	149±40*	0.55±0.15±0.10	0.94±.41±.13	0.82±.29±.27	0.66±.11

*) – from a partial statistics only. #) – statistical errors symmetrized from ref. 8b.

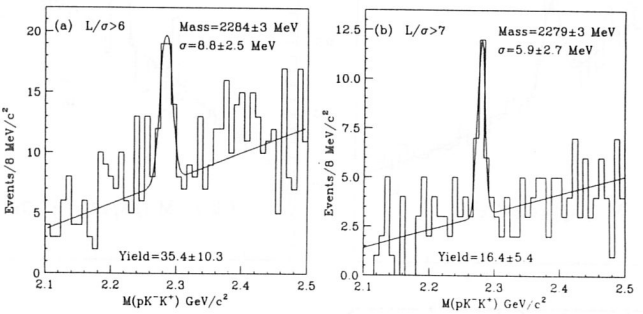

E687[10] has collected evidence for 3 Cabibbo suppressed modes, i.e.: pKK, $p\phi$ and $p(4\pi)$. The data are shown in Fig.s 1. Fig.s 1a,b show the first compelling evidence (35.4±10.3 events) for the pKK decay mode.

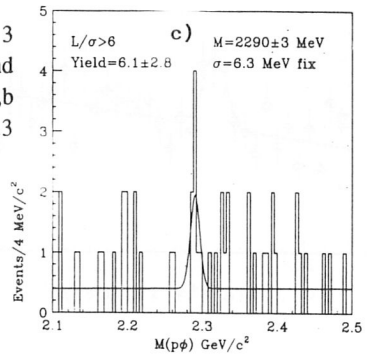

Fig. 1

The signals are selected by two different analysis conditions: Fig. 1a, loose conditions and detachment $l/\sigma > 6.0$; Fig. 1b tight conditions and detachment $l/\sigma > 7.0$. The signal behaves according to the measured lifetimes when increasing l/σ cuts are applied to the initial sample. The mass and width are also in good agreement with both the expected values and the Montecarlo simulations. The branching ratio relative to $pK^-\pi^+$ is $BR[\Lambda_c^+ \to pKK]/[\Lambda^+_c \to pK^-\pi^+] = 0.096 \pm .029 \pm .005$. Weaker is the signal for the $p\phi$ channel (Fig. 1c): a yield of (6.1 ± 2.8) events gives a relative branching ratio $BR[\Lambda_c^+ \to p\phi]/[\Lambda_c^+ \to pKK] = (0.25 \pm .22)$ or, better, an upper limit of .58% with 90% confidence level.

Fig.s 2 show a series of recent results on Cabibbo allowed, but rather rare decay modes containing a neutral strange particle (Fig.s 2a–d). In the channel $\Lambda_c^+ \to pK^o$ of Fig. 2a, more than one hundred events –to begin with– are becoming available in this 2–body channel, so that its relative BR will probably become soon known with adequate accuracy. For the channel $\Lambda_c^+ \to pK^o 2\pi$ (Fig. 2b), only 2 events have been reported so far in the literature[11] by the ACCMOR collaboration.

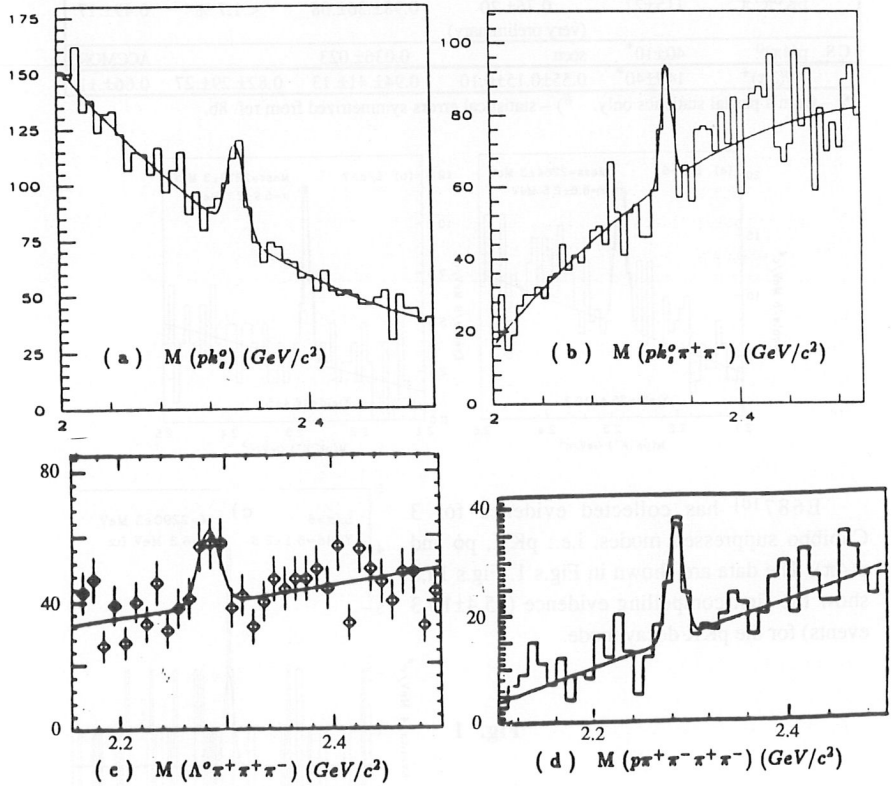

Fig. 2

The data of Fig. 2c, showing the E687 evidence for the channel $\Lambda_c^+ \to \Lambda^o 3\pi$, are still preliminary and come from the 1987–88 run.

The Cleo–II collaboration has recently shown a signal of about 400 events above background. All information concerning channels containing Σ^o's or $\Lambda^o\pi^o$'s have been summarized in ref. [6a]). Fig. 2d, finally, shows the evidence for the Cabibbo suppressed multiparticle channel $\Lambda_c^+ \to p4\pi$, another decay mode very poorly known untill now[11].

The high multiplicity of the final state makes its detection somewhat difficult. Only few events of this channel have been reported so far[11].

The numerical values of the observed yields –as well as the branching ratios relative to the "golden mode" ($\Lambda_c^+ \to pK^-\pi^+$), when measured– are collected in Table 1. The first column reminds if the mode given in column 2 is Cabibbo suppressed (CS); the yields are given in column 3 for the data from E687; in columns 4 to 7 the branching ratios, when given, are reported for the fixed target experiments E687 (col. 4); NA–32 (col. 5); E691 (col. 6) as well as the values reported in the Data Particle Book[11].

3. Λ^+_c decays containing a $\Sigma^\pm$ in the final state

This section will be devoted to the discussion of the channels containing a charged Σ hyperon in the final state. Yields and branching ratios for the Λ_c^+ decays into channels containing $\Sigma^\pm$ hyperons are compared in Table II. The detection of a Σ^-, which has a 100% decay branching ratio into $n\pi^-$ is more difficult than that of the positive counterpart since it requires the use of an hadron calorimeter, a detector which is at work in E687[12].

This experiment presents here the first evidence for two decay modes containing the Σ^- hyperon: i.e.: the decays $\Lambda_c^+ \to \Sigma^-\pi^+\pi^+$ and $\Lambda_c^+ \to \Sigma^-\pi^-\pi^+\pi^+\pi^+$. The decay $\Lambda_c^+ \to \Sigma^-\pi^+\pi^+$ (Fig. 3a) is compared to the decay $\Lambda_c^+ \to \Sigma^+\pi^+\pi^-$ where the Σ^+ is detected in both allowed decay modes: $n\pi^+$ (Fig. 3b) and $p\pi^o$ (Fig.3c). The $\Sigma^\pm$ hyperons are reconstructed as "kinks"; the decay kinematics is applied for both the $n\pi^+$ or the $p\pi^o$ mode. When the $\Sigma^\pm$ hyperon is recognized by the μstrip spectrometer the kinematics is closed. However this happens only in a very small percentage of the candidates. Most of the times the kinematic solution presents a twofold ambiguity.

For the $n\pi^\pm$ case, a selection can be made by imposing that the ratio between the energy released, within a proper cylinder –around the hitting point– of the calorimeters (inner electromagnetic, E_{IE} and hadronic, E_{HC}) and the neutron energy $E_{KinK}(n)$, derived from kinematics lie between the limits:

$$0.3 < [E_{IE}(n)+E_{HC}(n)]/E_{KinK}(n)<1.7.$$

The combinatorial background is larger in the Σ^+ channel than in the Σ^- channel; this justifies the slightly different cut on the l/σ detachment parameter for the two cases. Contrary to the channel $\Lambda_c^+ \to \Sigma^+\pi^+\pi^-$, the channel $\Lambda_c^+ \to \Sigma^-\pi^+\pi^+$ cannot proceed via an exchange diagram. The relative branching ratio $BR[\Lambda^+_c \to \Sigma^+\pi^+\pi^-]/[\Lambda_c^+ \to \Sigma^-\pi^+\pi^+]$ thus provides information on the contribution from the hadronic weak decay diagrams.

The branching ratio BR[$\Lambda_c^+ \to \Sigma^+\pi^+\pi^-$]/[$\Lambda_c^+ \to \Sigma^-\pi^+\pi^+$]=(2.02±0.63±0.08) is measured by E687.

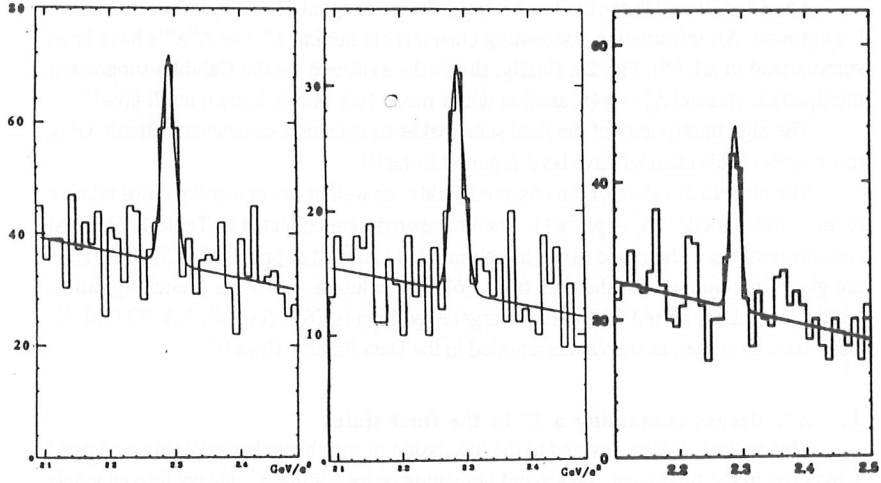

(a) $M(\Sigma^-\pi^+\pi^+)$ (GeV/c^2) (b) $M(\Sigma^-\pi^-\pi^+)$ (GeV/c^2) (c) $M(\Sigma^+\pi^+\pi^-)$ (GeV/c^2)

Fig. 3

This value is intuitively reasonable in view of the fact that the exchange diagram $\Lambda_c^+ \to \Sigma^+$ is available to the Σ^+ but not to the Σ^- channel. The small difference in the phase space volumes, $Q(\Sigma^+)_{LIPS}/Q(\Sigma^-)_{LIPS}$=1.03, due to the Σ^+/Σ^- mass difference is negligible.

In order to measure the branching ratio relative to the golden mode, due to the cut on the energy released into the calorimeters, E687 needs to simulate the hadron showers in the hadron calorimeter. It is well known that this is not a trivial task since the hadronic showers are very irregular mostly at low energies. To avoid this problem they have in progress[13] a systematic investigation of the energy release by about one million protons coming from the Λ^0's detected in the experiment. From these real protons the efficiency curve for the two combined calorimeters can be experimentally measured. The systematics due to this is minimized in the measurement of the quoted $\Sigma^\pm$ ratio.

Assuming BR[$\Lambda_c^+ \to \Sigma^+\pi^+\pi^-$]/[$\Lambda_c^+ \to pK^-\pi^+$] =(0.56±.07±.06), as measured by Cleo–II, I may speculate that the E687 branching ratio relative to the golden mode is: BR[$\Lambda_c^+ \to \Sigma^-\pi^+\pi^+$]/[$\Lambda_c^+ \to pK^-\pi^+$]=(0.28±0.06), given in parenthesis in Table II.

Further interesting channels are $\Lambda_c^+ \to \Sigma\phi$ and $\Lambda_c^+ \to \Sigma KK$. Evidence from Cleo has been recently reported. The evidence of E687 is shown in Fig.s 4. Fig. 4a shows the KK mass spectrum for the ΣK^+K^- candidate events. A signal of 453±33 ϕ mesons above back–ground is selected. Fig. 4b shows the $\Sigma\phi$ mass distribution for a detachment $l/\sigma >$ 2.0. Fig. 4c shows the same distribution for the ΣKK mass when the positive kaon is

definitely recognized by the Cerenkov counters, for the same detachment cut. The relative branching ratio is: $BR[\Lambda_c^+ \to \Sigma\phi]/[\Lambda_c^+ \to \Sigma^+\pi^+\pi^-] = (0.16 \pm .09 \pm .05)$.

TABLE II – Summary of $\Lambda_c^+ \to \Sigma x$ decay modes. Relative B.R. in fixed target experiments.

	MODE	Y	E687 BR/BR(pK^-p^+)	Y	NA-32 BR/BR(pK^-p^+)	Y	CLEO BR/BR(pK^-p^+)
	$\Sigma^+\pi^o$						0.17±.03±.02
	$\Sigma^-\pi^+\pi^+$	103 ± 17	*[0.28±0.06]*				can't measure
	$\Sigma^+\pi^+\pi^-$	97 ± 16	assume CLEO		0.54 +.18 -.15	?	0.56±.07±.06
	$\Sigma^+K^-K^+$	14 ± 6	small	1	0.13 +.18 -.09	59 ± 10	0.070±.011±.011
	$\Sigma^+\phi$	16 ± 4	*[0.089±.049]*	58	0.069±.023±.016		
	$\Sigma^{*+}\pi^+\pi^-$					25	0.30±.09±.07
	$\Sigma^{*-}\pi^+\pi^+$					16	0.21±.07±.05
	$\Sigma^+\omega^o$					–	0.40±.09±.04
CS	$\Sigma^+K^+\pi^-$			2	0.13 +.12 -.07		
	$\Sigma^+(4\pi)^o$			1	0.06 +.08 -.04		
	$\Sigma^-(4\pi)^{++}$	14	(preliminary) (first) (observation)				

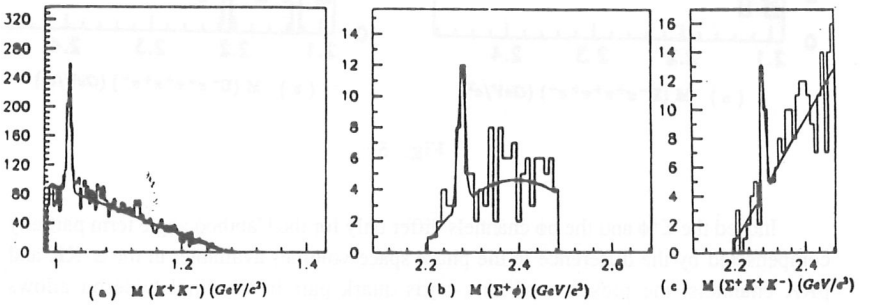

Fig. 4

It is relevant to notice that very little phase space is available for the ΣKK decay and that the KK mass can span only a very small range (0.98–1.09) around the ϕ mass. A preliminary analysis of the mass shows an enhancement, at the Λ_c^+, mass of 14±6 events at the same detachment cut used for the $\Sigma\phi$ channel. The final Montecarlo simulation is still in progress, to account for the slightly different cuts used. If I speculate that the acceptances for the $\Sigma\phi$ and the ΣKK channels are about equal, assuming the measured relative branching ratio $BR[\Lambda_c^+ \rightarrow \rightarrow \Sigma\phi]/[\Lambda_c^+ \rightarrow \Sigma^+\pi^+\pi^-]=(0.16\pm.09\pm.05)$ and, as before the Cleo data, I can estimate the branching ratios relative to the golden mode given in parenthesis in Table II, values that have to be taken as merely speculative (see the conclusions).

The pKK and pϕ channels, discussed in Section 3, as well as the decay $\Lambda_c^+ \rightarrow p\pi^+\pi^-$ [the analysis of this particular channel is still in progress], containing a proton, are interesting in connection with the *similar* channels $\Lambda_c^+ \rightarrow \Sigma^+\pi^+\pi^-$, $\Lambda_c^+ \rightarrow \Sigma^+KK$, $\Lambda_c^+ \rightarrow \Sigma^+\phi$, containing a Σ^+, which are Cabibbo allowed. Indeed the exchange diagrams $\Lambda_c^+ \rightarrow \Sigma^+$ and $\Lambda_c^+ \rightarrow$ p differ only for the cosθ [sinθ] term [and for a different value of the phase space volumes available], thus the internal relative branching ratios should bring experimental information on the Pauli interference which might play a different role in the different decay modes.

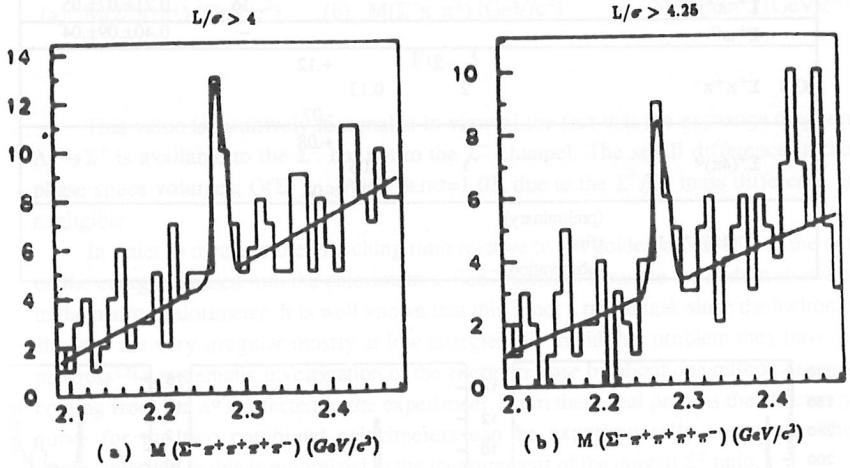

Fig. 5

Indeed the $\Sigma^+\phi$ and the pϕ channels differ only for the Cabibbo angle term partially compensated by the difference in the phase space volumes available; in the Σ^+KK and pKK channels, the presence of an s–antis quark pair in the final hyperon allows interferences which are not present when the proton is included into the final state. As for the $\Sigma^+\pi^+\pi^-$ and $p\pi^+\pi^-$ channels, the possible Pauli interference between s quarks in the

Σ channel are balanced by the interference between u quarks in the p channel. The decay mode $\Lambda_c^+ \rightarrow \Xi^- K^+ \pi^-$ also enters into the game of the decay diagrams.

Finally, in Fig. 5 the M[($\Sigma^-(4\pi)$)] spectrum in the mass region 2.1–2.48 GeV/c^2 is shown, giving the first evidence for an accumulation at the Λ_c^+ mass for different detachment cuts. The five track vertex searching is more contaminated by combinatorial background and requires some tighter confidence level conditions in the analysis which are directly indicated in the Figure.

4. The Σ_c triplet and its isospin mass splitting

Recent measurements have been done also on the Σ_c–Λ_c mass differences $\Delta M(\Sigma_c - \Lambda_c)$. The data comes from E691[14], ARGUS[15], E687[16a] and Cleo–II[6b,17]. The Argus and E691 results appeared already in the literature. Numerical values of the mass difference $\Delta M(\Sigma_c - \Lambda_c)$ are summarized in Table III. For sake of completeness an old measurement in BEBC[18] is also reported in Table III. In Fig.s 6 the results of E687 (Fig. 6a,b) and Cleo–II (Fig. 6c,d,e) are shown. E687 detected (32.5±8.2) Σ_c^0 events (Fig. 6a) and (22.0±6.1) Σ_c^{++} events (Fig. 6b) in a preliminary analysis where the Λ_c channel used is the golden mode. Cleo found very good signals for all 3 members of the triplet. Fig.s 6c,d,e show the Cleo evidence for Σ_c^+, Σ_c^0, Σ_c^{++} respectively. The Cleo collaboration[17] has analysed the isospin mass splitting issue. Among the different theoretical calculations[2,19], that may vary from +18 MeV/c^2 to –6.5 MeV/c^2, the authors are consistent with previous observations[13,14] and favour the predictions of S. Sinha[19f] for $\Delta M(\Sigma_c^{++}-\Sigma_c^0)$, while no theoretical models[19] predict a positive value for the $(\Sigma_c^+-\Sigma_c^0)$ term measured by Cleo–II to be $\Delta M(\Sigma_c^+-\Sigma_c^0)=(1.4\pm0.5\pm0.3)$ MeV/c^2. All the Σ_c issue is still an open question.

There are 2 isotriplets predicted by SU(4): one of spin 1/2 and one having spin 3/2. One of the two multiplets is definitely missing and, in order to make sure of which is which and what is what a check on the spin parity of the detected particles should be performed, just in case something be not so naive as expected.

TABLE III – Summary of $\Delta M(\Sigma_c-\Lambda_c)$ measurements.

Exp.	$\Delta M(\Sigma_c^{++}-\Lambda_c)$	$\Delta M(\Sigma_c^0-\Lambda_c)$	$\Delta M(\Sigma_c^+-\Lambda_c)$
ARGUS	168±0.6±1.6	167±0.3±1.6	---
BEBC	---	---	168±3
CLEO 1.5	167.8±0.4±0.3	167.9±0.5±0.3	
CLEO II	168.2±0.3±0.2	167.1±0.3±0.2	168.5±0.4±0.2
E691	--	168.4±1.0±0.3	---
Excharm	--	---	162±10±15
E687	167.7±0.7±0.9	168.8±1.0±0.9	---

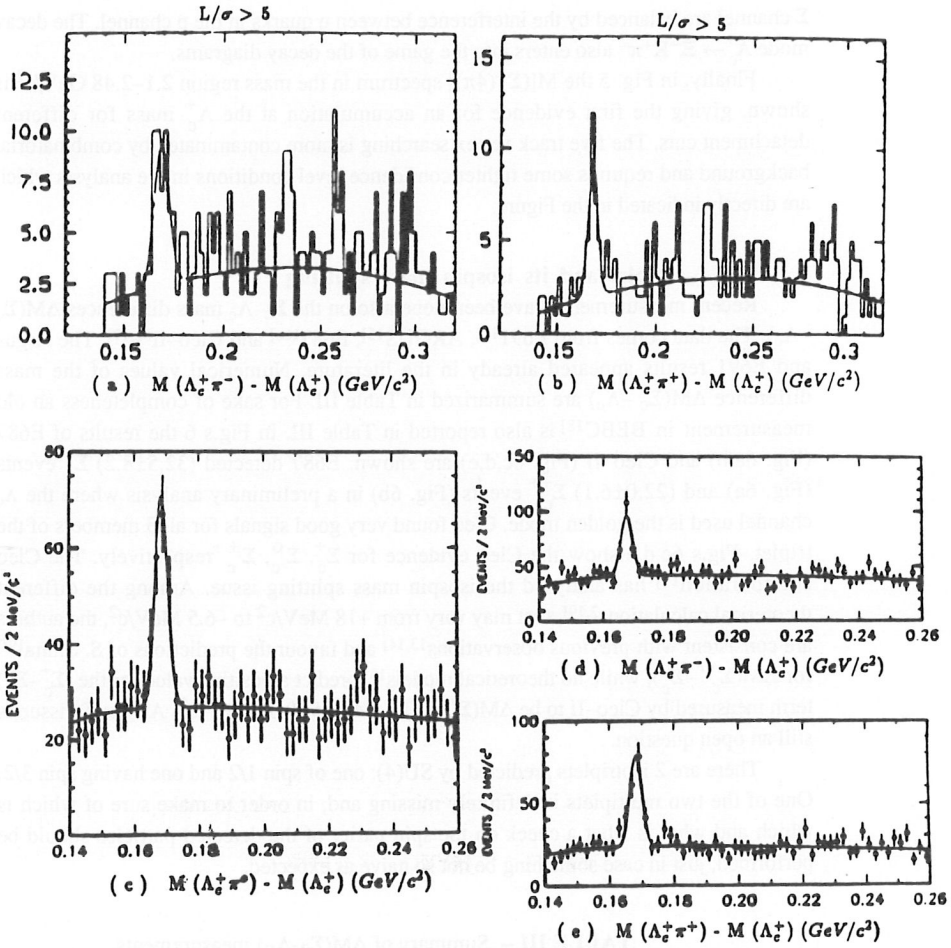
L/σ > 5
(a) M (Λc+π−) - M (Λc+) (GeV/c2)
L/σ > 5
(b) M (Λc+π+) - M (Λc+) (GeV/c2)
EVENTS / 2 MeV/c2
(c) M (Λc+π0) - M (Λc+) (GeV/c2)
EVENTS / 2 MeV/c2
(d) M (Λc+π−) - M (Λc+) (GeV/c2)
EVENTS / 2 MeV/c2
(e) M (Λc+π+) - M (Λc+) (GeV/c2)

Fig. 6

5. Charm Strange Baryons

Recent observations on the charm strange baryons come from Excharm[4], E687[20,21] and Cleo[5,6b]. The yields and masses from known and recent measurements are collected in Table IV. The evidence for the Ξ_c charm baryons decaying into a Σ^+ hyperon from E687 is reported in Fig.s 7.

Fig. 7a shows the preliminary mass spectrum for the new channel $\Xi_c^o \to \Sigma^+ K^-$. A signal of (20±8) events is detected above background; Fig. 7b shows the $\Sigma^+ K^- \pi^+ \pi^-$ mass spectrum, where a signal of (26±9) events is detected above background. In Fig.s 7c and d, the evidence for the channel $\Xi_c^+ \to \Sigma^+ K^- \pi^+$ is given for both the $\Sigma^+ \to p\pi^o$ (Fig. 7c, 26±8 events) and the $\Sigma^+ \to n\pi^+$ channel (Fig. 7d, 14±3 events).

E687 has collected a total of 51,311 fully reconstructed Ξ^- hyperons (where $\Xi^- \to \Lambda\pi^-$; $\Lambda^o \to p\pi^-$) and 1537 fully reconstructed Ω^- hyperons from which several combinations can be constructed to search for several signals at the charm strange baryon masses. Some have been already published[20] and are not shown here but reported in Table IV.

However in Fig.s 8 the evidence from E687[16b] is given for 3 Ξ_c^+ decay modes containing Ξ^- ($\Xi^- \pi^+ \pi^+$, Fig. 8a), π^+ ($\Lambda^o K^- \pi^+ \pi^+$, Fig. 8b), and Ω^- ($\Omega^- K^- \pi^+$, Fig. 8c).

New results on some decay modes of Ξ_c's have been recently reported by the Excharm collaboration[4]. Due to the particular trigger, they have been able to measure some Ξ_c^o branching ratios relative to the decay mode $\Xi_c^o \to \Lambda^o K^- \pi^+ \pi^+$. The results are shown in Fig.s 9: in Fig. 9a the signal of 50/61 events for the channel $\Xi_c^o \to \Lambda^o K^{*o}(892)$; in Fig.9b the signal of 68/248 events for the channel $\Xi_c^+ \to \Lambda^o K^- \pi^+ \pi^+$ and in Fig.9c the signal of 58/144 events for the channel $\Xi_c^+ \to K^- K_s^o \pi^+ \pi^+$.

To conclude the charm strange baryon section, I have collected the available information on the Ω_c^o mass in the bottom part of Table IV. There, the evidence from WA–62[22] and Argus[23] are also reported for completeness. The new mass value provided by E687 for the $\Omega^- \pi^+$ decay mode seems to favour the low value measured by Argus rather than the high value measured by WA–62. In any case, this charm double–strange baryon is not at all well known; only 5 decay modes have been identified so far; therefore the future experiments should be able to provide a lot of new informations.

TABLE IV – Summary of Ξ_c's and Ω_c^o masses.

	Decay Mode	Mass (MeV/c^2)	Yield	Rel. B.R.	Exp.
Ξ_c^o	$\Xi^-\pi^+$	2436.0±3.1	29.2±6.7	1.0[&]	CLEO
	" "	2462.1±3.1±1.4	42±10	1.0	**E687**
	Σ^+K^-	2470.4±3.2	20±8	seen	**E687**
	$\Sigma^+K^-\pi^+\pi^-$	2473.4±3.8	26±9	seen	**E687**
	$\Xi^-\pi^+\pi^o$	2468.2±2.9	45.0±9.5	3.5±1.1	CLEO
	$\Xi^o\pi^+\pi^-$	2471.2±2.6	30.2±8.1	3.6±1.2	CLEO
	pK^-K^{*o}	2473.3±1.9	4	seen	NA-32
	$pK^-K^o_S\pi^o$	--	58±12	seen	Excharm
	$\Xi^-\pi^+\pi^-\pi^+$	2472.1±2.7±1.6	36.2±9.1	~3.3	ARGUS
	$\Lambda^oK^{*o}(892)$	--	50±8	seen	Excharm
Ξ_c^+	$\Xi^-\pi^+\pi^-$	2467.1±2.4	50.3±8.8	1.0	CLEO
	" "	2464.4±2.0±1.4	29.7±7.0	seen	**E687**
	$\Xi^o\pi^+\pi^o$	2469.9±4.6	24.5±7.6	3.2±1.0	CLEO
	$\Xi^o\pi^+$	2470.6±3.0	15.7±4.9	0.61±.23	CLEO
	$pK^-K^o_S\pi^+$	--	--	1.98±.76[#]	Excharm
	$pK^-K^o_S\pi^+$	--	--	<0.08[#]	WA-62
	$pK^{*o}(892)K^o_S$	--	--	0.44±.23[#]	Excharm
	$\Lambda^{*o}(1520)K^o_S\pi^+$	--	--	1.45±.62[#]	Excharm
	$\Sigma^oK^-\pi^+\pi^+$	2460±5±30	26	seen	E400
	$\Sigma^+K^-\pi^+$	2466.5±2.6±1.2	2	seen	NA-32
	$\|\rightarrow(p\pi^o,n\pi^+)$	--	~40±11	seen	**E687**
	$\Lambda^oK^-\pi^+\pi^+$	2460±25	82	seen	WA-62
	" "	--	68±16	seen	Excharm
	$\Lambda^oK^{*o}(892)\pi^+$	--	--	[0.43±.15][#]	Excharm
(*	$\Lambda^oK^-\pi^+\pi^+$		50±12	seen	WA-89
(*	(combined)$\rightarrow$	2450±4±7			WA-89
(*	$\Xi^-\pi^+\pi^-$		11±3	seen	WA-89
Ω_c^o	$\Xi^-K^-\pi^+\pi^+$	2719.0±7.0±2.5	12.2±4.5	seen	ARGUS
	$\Omega^-\pi^+$	2706.0±3.0±5.0	9.6±3.7	seen	**E687**
	$\Omega^-\pi^-\pi^+\pi^+$	2713±5.1	6.5±3.2	[0.26±.16][*]	ARGUS
	$\Omega^-K^+K^o_S$	--	~10	seen	**E687**
	$\Omega^-K^-K^+\pi^+$	2701±4.8	22±6	seen	**E687**

[&]- assumed; [#]- BR relative to $\Lambda^oK^-\pi^+\pi^+$]; [*]BR relative to $\Xi^-K^-\pi^+\pi^+$]

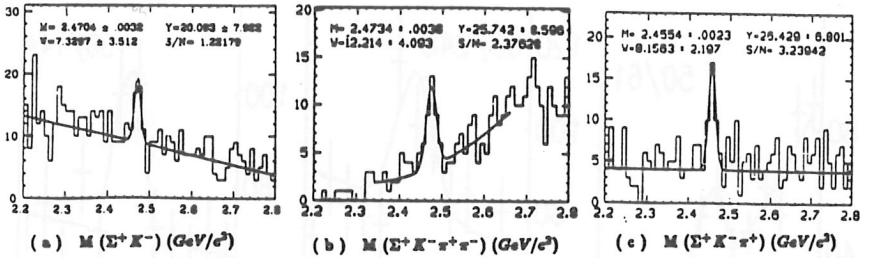
M= 2.4704 ± .0032 Y=30.083 ± 7.982
W=7.3897 ± 3.512 S/N= 1.28179
M= 2.4734 ± .0038 Y=25.742 ± 8.598
W=12.214 ± 4.093 S/N= 2.37628
M= 2.4554 ± .0023 Y=26.429 ± 6.801
W=8.1583 ± 2.197 S/N= 3.23942
(a) M (Σ⁺K⁻) (GeV/c²)
(b) M (Σ⁺K⁻π⁺π⁻) (GeV/c²)
(c) M (Σ⁺K⁻π⁺) (GeV/c²)

Fig. 7

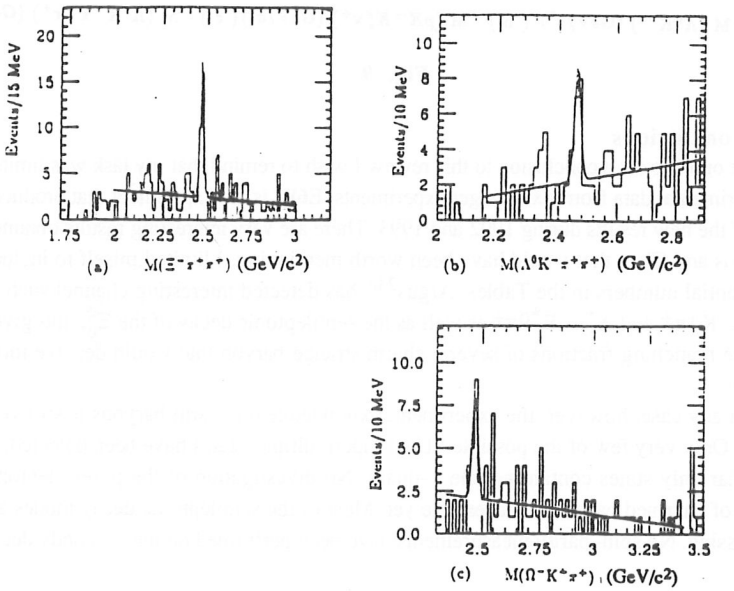
Events/15 MeV
(a) M(Ξ⁻π⁺π⁻) (GeV/c²)
Events/10 MeV
(b) M(Λ⁰K⁻π⁺π⁺) (GeV/c²)
Events/10 MeV
(c) M(Ω⁻K⁺π⁺) (GeV/c²)

Fig. 8

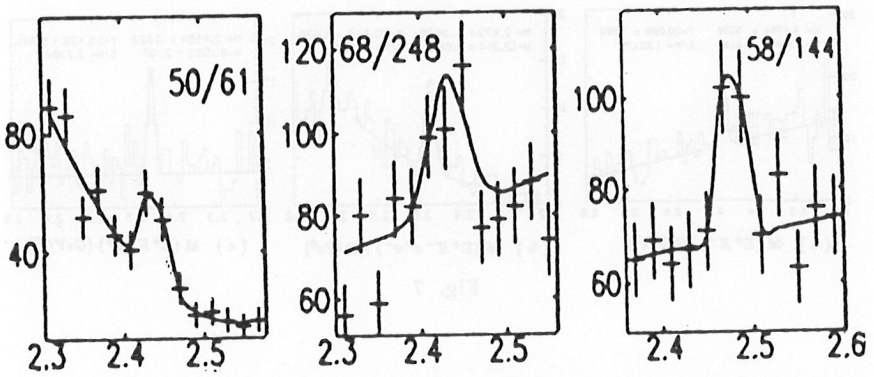

Fig. 9

6. Conclusions

In order to set a conclusion to this review I wish to remind that my task was limited to experimental data from fixed target experiments. E687 is the experiment that produced most of the new results during 1992 and 1993. There are very interesting results obtained by Argus and Cleo, that would have been worth mentioning. I limited miself to include the essential numbers in the Tables. Argus[23b] has detected interesting channel such as $\Lambda_c^+ \rightarrow \Xi^- K^+ \pi^+$ and $\Lambda_c^+ \rightarrow \Xi^{*0} \pi^+$ as well as the semileptonic decay of the Ξ_c^0, and given absolute branching fractions of several charm strange baryon that would deserve more attention.

In any case, however, the experimental knowledge on charm baryons is still very limited.Only very few of the possible SU(4) supermultiplet states have been detected; in particular only states containing one c–quark. No investigation of the purely leptonic decays of charmed baryons is accessible yet. Most of the semileptonic decay modes are still missing. No spin–parity measurements have been performed on the two body decay modes.

Even for the best studied isosinglet Λ_c a lot of possible channels seem to be still missing. I fully share the concern about the absolute branching fraction for the $\Lambda_c^+ \rightarrow pK^- \pi^+$ decay mode. If the value quoted by Cleo–II (4.3±1.0±0.8)% or by Argus[23c] (4.0±.8±.3) are correct, adding all detected modes, including all possible semileptonic decays, we account for no more that 40% of the full decay width. It is unlikely that all what is missing comes from Σ^- or neutron channels. It might be that the measured absolute branching fraction is too low.

7. Acknowledgments

I wish to thank J. Cumalat, M. Procario and S. Squarcia for providing important references. I express my gratitude to the members of the Pavia group for their help in discussing and preparing the data, in particular to P. Vitulo and M.Merlo for the assistance in the preparation of the manuscript and the Figures.

8. References

1. A.Cazzoli et al.: Phys. Rev. Lett. **34**,1125 (1975);
2. a – B.Guberina, R.Ruckl and J.Trampetic: Zeit. Fur Phys. **C33**, 297 (1986);
   b – M.B.Voloshin and M.A.Shifman: Sov. Phys. J.E.T.P. **64**, 698 (1986);
   c – V.Gupta and K.V.L.Sharma: Int. J. Mod. Phys. **A5**, 879 (1990);
3. see E.Meroni: contribution to this Conference;
4. D.Kekelidze: in Proc. XXVIth ICHEP, [J.R.Sanford.Ed., AIP Conf. Proc. n.272, 1993] p. 1066;
5. a)– S.Yang: "Asymmetry Parameters in the Weak Decays $\Lambda_c^+ \rightarrow \Lambda\pi^0$ and $\rightarrow \Sigma^+\pi^0$. Preprint WAPS 93, Moriond '93;
   b) – T.Miao: "Study of $\Lambda_c^+ \rightarrow x\Lambda l^+\nu_l$", DPF '92.
6. a) – J.Cumalat in: "The Fermilab Meeting DPF 92" [C.H.Albright, P.Kasper, R.Raja, and J.Yoh Ed.s, World Sci., 1993] p. 197;
   b) – B.Nemati, in: ibidem, p. 694;
7. The experiment E781, approved at Fermilab in an hyperon beam, is also very promising but didn't take data yet.
8. see contribution to this Conference by J.Wiss;
9. a) – A.Bozek et al.:"A Study of Λ_c^+ Decays into $pK^-\pi^+$,$pK^-\pi^+\pi^0$, $pK^-\pi^+2\pi^0$'s", preprint (1993);
   b) – A.Bozek et al.:"An Observation of Exclusive Λ_c^+ Decays into Σ^+ and Mesons", preprint (1993);
10. P.L.Frabetti et al.: "Evidence of the Cabibbo suppressed decay $\Lambda_c^+ \rightarrow pK^-K^+$", preprint (1993), Phys. Lett.**B314**, 477–481 (1993) ;
11. Data Particle Group: Phys. Rev. **D45**, Part 2 (1992);
12. P.L.Frabetti et al.: Nucl. Instr. Meth.in Phys. Res. A320, 519 (1992);
13. L.Viola, private communication;
14. J.C.Anjos et al.: Phys. Rev. Lett. **62**, 1721 (1989);
15. H.Albrecht et al.: Phys. Lett. **B211**, 489 (1988);
16. a) – H.W.K.Cheung (for E687): "Observation of High Energy Photoproduction of Σ_c^{++} and Σ_c^+ ". E687 internal note (1992);
   b) – H.W.K.Cheung: in Proc. XXVIth ICHEP, [J.R.Sanford.Ed., AIP Conf. Proc. n.272 ,1993] p.1082;
17. P.Wang, C.R.Sun: "Observation of the Charm Baryon Σ^+_c and Measurement of the Isospin Mass Splitting of the Σ_c". Preprint Cleo–93–6A (1993);
18. M.Calicchio et al.: Phys. Lett. **B93**, 521 (1980);

19. a) – S.Capstick: Phys. Rev. **D36**, 2800 (1987); b)– T.Kobayashi and N.Yamazaki: Prog. Theor. Phys. **65**, 775 (1981); c)– L.H.Chan: Phys. Rev. **D31**, 204 (1985); c) – W–Y.P.Hwang and D.B.Lichtenberg: Phys. Rev. **D35**, 3526 (1986); d)– A.C.D.Wright: Phys. Rev. **D17**, 3130 (1978);
e) – N.G.Dehspande: Phys. Rev. **D15**, 1885 (1978); f)– S.Sinha: Phys. Lett. **B218**, 333 (1989);
20. P.L.Frabetti et al.: Phys. Rev. Lett. **70**, 1381, 2058 (1993);
21. P.L.Frabetti et al.: Phys. Lett. **B300**, 190 (1993);
22. S.F.Biagi et al.: Z. Phys. C28, 175 (1985);
23. a) – H.Albrecht et al.: DESY preprint n.92–052;
b) – J.Stiewe: in Proc. XXVIth ICHEP, [J.R.Sanford.Ed., AIP Conf. Proc. n.272, 1993] p. 1076.

Frascati Physics Series, Vol. 1 (1993)
HEAVY QUARKS AT FIXED TARGET
Frascati, May 31st – June 2nd 1993
(pp. 245–262)

STATUS OF HEAVY QUARK LIFETIME MEASUREMENTS

L. M. Cremaldi
University of Mississippi, Department of Physics and Astrnomy
Oxford MS 38677, (USA)

Abstract

A current status of heavy quark lifetime measurements and analysis techniques is presented. This report is highlighted by the latest high statistics results from E687 at Fermilab, where they have reported results from their full data sample on charmed meson and baryon lifetimes.

INTRODUCTION

Elementary particles decay at a rate governed by the interactions of their fundamental constituents. In many cases these decay rates can be calculated within the context our weak interaction theory and QCD [1,2,3,4]. It is of major interest to have precise measurements of particle lifetimes and indeed, particle lifetimes are some of the most accurately measured quantities in all of particle physics.

A number of high statistics charm experiments have recently reported on charmed particle lifetimes, the latest being E687 at Fermilab. They have measured charmed meson and baryon lifetimes to unprecedented levels and have worked to reduce systematic errors to a minimum. Recenty LEP and CDF have provided us with good measurements of b-particle lifetimes. After a brief introduction to heavy quark lifetimes and measurement, we present these latest lifetime measurements.

UNDERSTANDING LIFETIMES

We have found that the lifetimes of charmed and beauty mesons follow a simple picture, that of a heavy quark decaying independently of the spectator light quarks. In this approximation we can calculate the semileptonic decay rate for D mesons as,

$$\Gamma_{SL}(D \to l\nu X) = \frac{G_F m_c^5}{192\pi^3} g(m_s/m_c).$$

Here $g(m_s/m_c)$ is a correction factor involving the finite charm and strange quark masses. This simple scaling from that of muon beta decay indicates that the lifetime of charmed particles is of the order of $10^{-12} - 10^{-13}$ seconds, depending on the quark masses picked. We also know that the purely leptonic decay rates $\Gamma_L \approx 10^{-3} - 10^{-4}$ are very small and don't contribute a much to the total decay rate. This picture has proven to be remarkably accurate, but is violated in the end. Precise measurements of the D^+, D^0, D_s^+ lifetimes [6] yields a hiearchy, $\tau(D^+) : \tau(D^0) : \tau(D_s^+) = 2.5 : 1 : 1$. The ratio of semileptonic branching fractions is measured to be, $BR_{SL}(D^+)/BR_{SL}(D^0) = 2.3^{+0.5}_{-0.4} \pm 0.1$ [5], roughly equal to the ratio of their lifetimes.

Charmed Mesons We can begin to understand charmed meson lifetimes within a simple model. The lifetime will depend on each of above rates as, $\tau = (\Gamma_L + \Gamma_{SL} + \Gamma_{NL})^{-1}$. With the semileptonic decay rates of charmed mesons predicted and measured to be about equal, and the lifetimes differing, we are led to consider the nonleptonic decay rate, Γ_{NL}, for explaining the D^+, D^0, D_s^+ charmed meson lifetime differences.

In addition to the simple spectator decay rate,Figure 1(a), two annihilation graphs Figure 1(b),(c), can contribute to the D^0, D_s^+ decays, an s and t channel w-exchange. The nonperturbed rate is approximately, $\Gamma_{NL}^{annih} \approx G_F^2 m_c^2 |\psi(0)|^2$, roughly $1/m_c^2 \times \Gamma_{NL}^{spect}$ in a naive scaling, indicating the annihilation graphs are helicity suppressed if initial state quarks are in a spin zero state. Various mechanisms for lifting this helicity suppression have been discussed. The size of their actual contribution is experimentally difficult to isolate and therefore somewhat debatable [1,3].

It was quickly pointed out that QCD radiative corrections could dramatically alter the semileptonic and nonleptonic rates helping to explain the lifetimes and semileptonic branching fractions [1,8]. When this is done the simple spectator decay rate is altered not only in magnitude, but also a color misalligned piece is added to the weak hamiltonian, Figure 1(a). These two pieces can be referred to as an external and internal spectator decay, and we denote them by Γ_{NL}^{ext} and Γ_{NL}^{int} respectively. In the case of the D^+ the light quarks in the external and internal w-decays can generate the same final state and the graphs must be added at the amplitude level, thus generating the possibility for destructive interference; which we denote by Γ_{NL}^{int*}. A simple minded picture of D meson lifetimes is then,

$$\begin{aligned}
\tau(D^+) &= (\Gamma_{SL} + \Gamma_{NL}^{ext} + \Gamma_{NL}^{int*})^{-1} \\
\tau(D^0) &= (\Gamma_{SL} + \Gamma_{NL}^{ext} + \Gamma_{NL}^{int} + \Gamma_{NL}^{annih})^{-1} \\
\tau(D_s^+) &= (\Gamma_{SL} + \Gamma_{NL}^{ext} + \Gamma_{NL}^{int} + \Gamma_{NL}^{annih})^{-1}
\end{aligned}$$

Two possibilities for creating a longer D^+ lifetime can be construed; (1) If $\Gamma_{NL}^{annih} \approx \Gamma_{NL}^{ext}$ is large and Γ_{NL}^{int} small, we can increase the D^0, D_s^+ rate, or (2) $\Gamma_{NL}^{annih} \approx \Gamma_{NL}^{ext}$ is small and $\Gamma_{NL}^{int*} \approx \Gamma_{NL}^{ext}$, we decrease the D^+ decay rate. Both explanations can be tolerated by the present models and there is no smoking gun which cleanly points to either. See Bigi's paper [3] for a good discussion of these topics.

The lifetime measurements alone can only guide us in our models. In the end, we must consider measurements of explicit charm decay rates as in the BSW model [8] and others for detailed comparisons.

Charmed Baryons In the case of charmed baryons the extra light quark can lift the helicity suppression of the annihilation graphs, thus we expect w-exchange contributions to play an important role. Indeed, we might interpret the short Λ_c^+ lifetime, $\tau(\Lambda_c) \approx .5 \times \tau(D^0)$, as evidence for strong w-exchange. We also expect interference effects to play a competing role in these decays as they do in D-meson decays.

In a simple analysis of the decays of the lowest lying charmed baryons, we quickly conclude that the charged states will be longer lived than the neutral states. Below I list the contributions from the external and internal spectator decay, annihilation, and destructive interference (*) graphs.

$$\begin{aligned}
\tau(\Xi_c^+(csu)) &= (\Gamma_{SL} + \Gamma_{NL}^{ext} + \Gamma_{NL}^{int*(u)} + \Gamma_{NL}^{int(ss)})^{-1} \\
\tau(\Lambda_c^+(cud)) &= (\Gamma_{SL} + \Gamma_{NL}^{ext} + \Gamma_{NL}^{int*(u)} + \Gamma_{NL}^{annih})^{-1} \\
\tau(\Xi_c^0(csd)) &= (\Gamma_{SL} + \Gamma_{NL}^{ext} + \Gamma_{NL}^{int(ss)} + \Gamma_{NL}^{annih})^{-1} \\
\tau(\Omega_c^0(css)) &= (\Gamma_{SL} + \Gamma_{NL}^{ext} + \Gamma_{NL}^{int(sss)})^{-1}
\end{aligned}$$

We see that the Ξ_c^+ and Λ_c^+ each have light spectator u-quark destructive interference terms (see Figure 1(d)), and w-exchange in the Λ_c case. These widths will be reduced as compared to the Ξ_c^0 and Ω_c^0, where the negative interference graphs are absent. Guberina, Rückl, and Trampetic [9] calculate a lifetime hiearchy as $\tau(\Xi_c^+) > \tau(\Lambda_c^+) > \tau(\Xi_c^0) \approx \tau(\Omega_c^0)$. Voloshin and Shifman calculate [10] $\tau(\Xi_c^+) \approx \tau(\Lambda_c^+) > \tau(\Xi_c^0) > \tau(\Omega_c^0)$. Further discussion of the details of these calculations can be found in a review by Körner and Siebert [11].

B Lifetimes Deviations from the spectator model should not be drastic in B-decays [1]. In a simple scaling one expects that the lifetimes of particles containing a b-quark will be about equal, where $\Gamma_{NL}^{annih}/\Gamma_{NL}^{spec} \approx (m_c/m_b)^3$ [12]. Bigi gives an argument for $\tau(B^+)/\tau(B^0) \approx 1.2$ [3]. Accurate measurements of B^+, B^0, B_s lifetimes are needed for detailed comparisons.

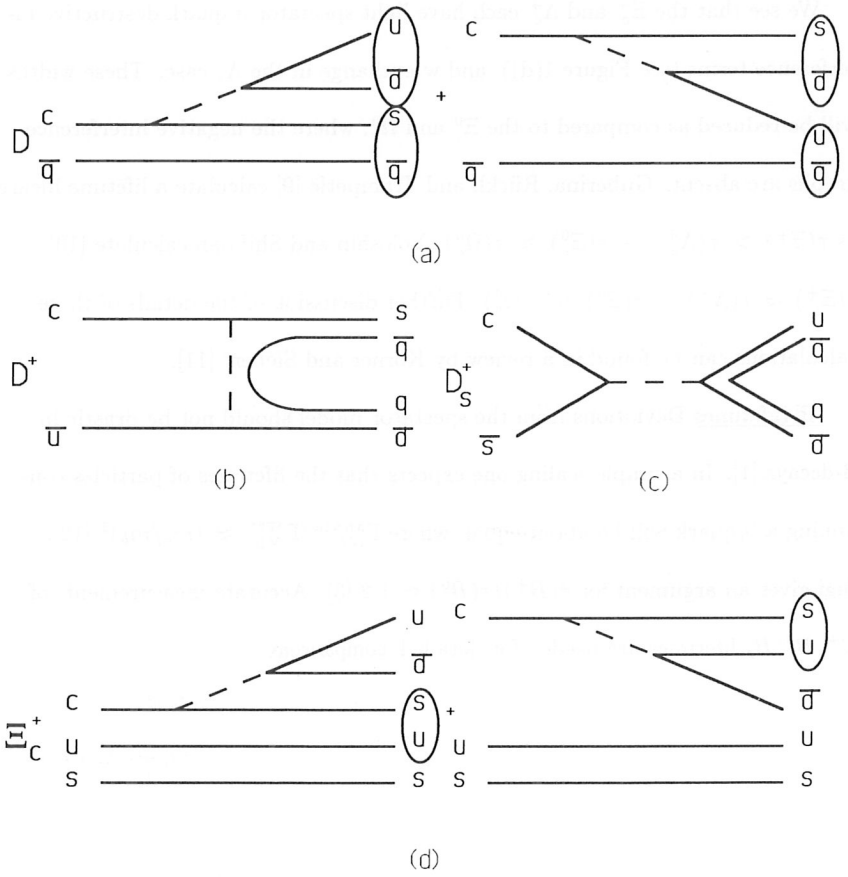

Figure 1: Diagrams contributing to nonleptonic charm decays: (a) External radiation graph and internal radiation (color missaligned) graph, (b) W-exchange mechanism for D^0 decays, (c) s channel annihilation in D_s decays, and (d) Ξ_c^+ external and internal radiation graph with possible negative interference.

LIFETIME MEASUREMENTS

The methods of lifetime measurement are extensively unchanged over time. In the usual technique, the decay distance, ℓ, is measured between the birth and death of a particle. This distance is brought into a proper lorentz frame and converted to time, $t = \ell/\beta\gamma c = (m/pc)\ell$. An accurate measure of the decay length ℓ and momentum, p is required as, the error on the lifetime can be approximated by $\sigma_\tau = \sqrt{(\tau^2 + \delta_t^2)/N_s}$.

Higher precision vertex detection techniques have been introduced over the years to accomodate different dynamic ranges of τ measurements. These techniques have included bubble chambers, emulsion detectors, hybrid spectrometers, and recently silicon microstrip detectors. Most recenly, the silicon microstrip detector is the only capable of recording at high data rates and providing high positional accuracy ($\approx 10\mu m$). Multiparticle spectrometers with silicon vertex detectors have provided the highest precision charmed particle measurements to date.

The proper time resolution δ_t will usually be dominated by measurement of ℓ, but in cases where the momentum, p, is not fully measured, δ_p can make sizeable constributions. In the presence of signal, S, and background,B, $N_s \simeq S^2/\sqrt{S+B}$, yielding the number of background free events. A 10σ Λ_c signal would provide a $\sigma_\tau/\tau = 10$ %. This corresponds to N_s =100 background free events.

For direct measurements of high statistical accuracy generally, $\delta_t \ll \tau$ and we have the familiar $\tau/\sqrt{N_s}$ scaling with increased signal events N_s. Presently, for a high statistics charm experiment with silicon microstrip detector $N_s \simeq 10^5 D^0's$ and $\delta_t \simeq .05ps$, yielding $\sigma_\tau/\tau \approx 1/3$ %. The familiar reconstruction technique is illustrated in Figure 2(a).

In intermediate cases, where the decay length is poorly measured $\delta_t \geq \tau$, or incomplete reconstruction of the charm decay is not possible (eq. semileptonic decays), but for a *pure statistical sample*, a good lifetime measurement can be made with what is called the impact parameter technique. This is illustrated in Figure 2(b). Measurements of better than 10% statistical accuracy can be achieved. Note that in this case $\sigma_\tau/\tau \approx \delta_t/\sqrt{N_s}$ and we are just measuring the displacement of the mean of a gaussian distribution of impact parameters with respect to zero displacement. Early D-meson lifetimes were measured at PEP and DORIS [6] using impact parameter techniques with good accuracy. More recently our b-lifetimes are being measure by variations of this impact parameter technique at LEP. Impact parameter techniques represent a powerful analysis tool when c and b samples are relatively clean.

E687 CHARM LIFETIMES

Fermilab Photoproduction experiment E687 has contributed the the most recent high statistics lifetime measurements. The data was recorded in the 1990-91 running period, approximately 500 million interactions logged. The E687

spectrometer, described in details elsewhere, [13], is a large open geometry multiparticle spectrometer with good detection capability for hadrons and photons. The incident beam is a $\approx$ 220 GeV photon beam striking a 4cm long beryllium target. A 12 plane silicon microstrip vertex detector provided high resolution

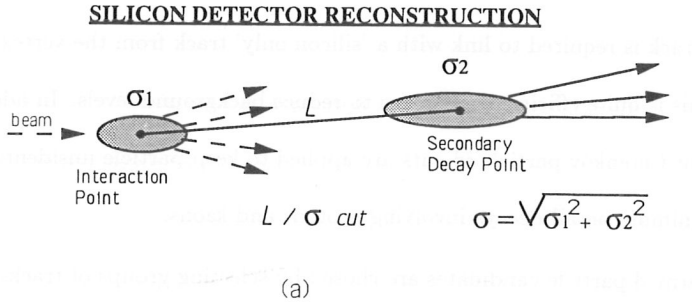

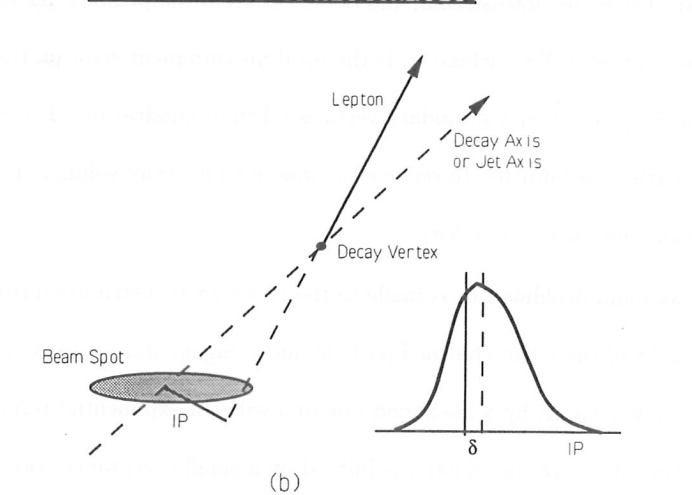

Figure 2: (a) Full silicon vertex detector reconstruction and (b) impact parameter techniques for estimating decay lengths L and δ .

tracking near the target. Particle identification is provided by 3 multicell threshhold Cerenkov counters, calorimetry, and downstream muon detectors. The E687 spectrometer has good acceptance for longlived hyperon decays making it efficient for detecting charmed baryon signals decaying through hyperon channels. In cases where charged hyperon decays are present, the reconstructed hyperon track is required to link with a 'silicon only' track from the vertex detector. This is quite efficient and serves to reduce background levels. In addition, stringent Cerenkov particle id cuts are applied to keep particle misidentification to a minimum on all decays involving protons and kaons.

Charmed particle candidates are chosen by selecting groups of tracks that are consistent with a forming a good secondary vertex and requiring that this secondary vertex be downstream, and detached, from the primary vertex by a distance of at least $N\sigma_z$, where σ_z is the total measurement error on the z position of the primary and secondary vertices taken in quadrature. The actual decay length ,ℓ, is adjusted to remove the inaccessible decay volume, due to the detachment cut, or $\ell^{'} = \ell - N\sigma_z$.

A maximum likelihood fit is made to the $t^{'} = \ell^{'}/\gamma\beta c$ distribution from events within $\approx 2\sigma$ of the mean charmed particle mass. Signal and background events in this window are fit by a likelihood function with an exponential term describing the time decay of the signal, modulated by a small acceptance correction function, $f(t')$, usually derived from a Monte Carlo simulation.

$$\mathcal{L}_i = \exp^{t_i'/\tau} \times f(t_i') + B(t_i')$$

The background events are fit by a time shape $B(t')$ taken from events in the sidebands of the mass plot. Unbinned maximum likelihood fits are generally used for ease of background subtraction. For details and variations of these fitting techniques, please see the noted references.

Charmed Mesons With a sample of about 20K D^0 mesons decaying into $K\pi$ and $K3\pi$ channels, 15K $D^+ \rightarrow K\pi\pi$ decays, and 900 $D_s \rightarrow \phi\pi$ decays, E687 was able to make the best measurements of D-meson lifetimes to date. They have also been able to measure their systematic errors to levels commensurate with their high statistics. Systematic errors when translated into distances are approaching our knowledge of silicon detector positions and further reduction in these errors will be a difficult for future measurements. In Table 1 we give the most recents D-meson lifetime measurements, with the first error being statistical and second systematic. These measurements are further displayed in Figures 3(a),(b), and Figure 4(a), along with past measurements.

Table 1.- E687 D-Meson Lifetime Measurements

Mode	$\tau(ps)$	$\tau_{PDG}(ps)$ [ ]	Reference
D^0	$0.4200 \pm 0.0045 \pm 0.0030$	$.4200 \pm 0.008$	[14]
D^+	$1.049 \pm 0.015 \pm 0.011$	$.455 \pm 0.333$	[14]
D_s^+	$0.475 \pm 0.020 \pm 0.007$	$.450^{+.030}_{-.026}$	[15]

E687 chose to use only the $\phi\pi$ sample for the $\tau(D_s)$ measurement in order to avoid possible contamination from $D^+ \rightarrow K\pi\pi$ events. If we look at the mea-

sured $D_s - D^0$ lifetime difference, $\tau(D_s^+) - \tau(D^0) = 0.051 \pm 0.023 \pm 0.01$ we have our first 2σ indication of the D_s lifetime being somewhat longer than the D^0. It may be possible to discern differences in the D_s, D^0 lifetime models, but probably a difficult job.

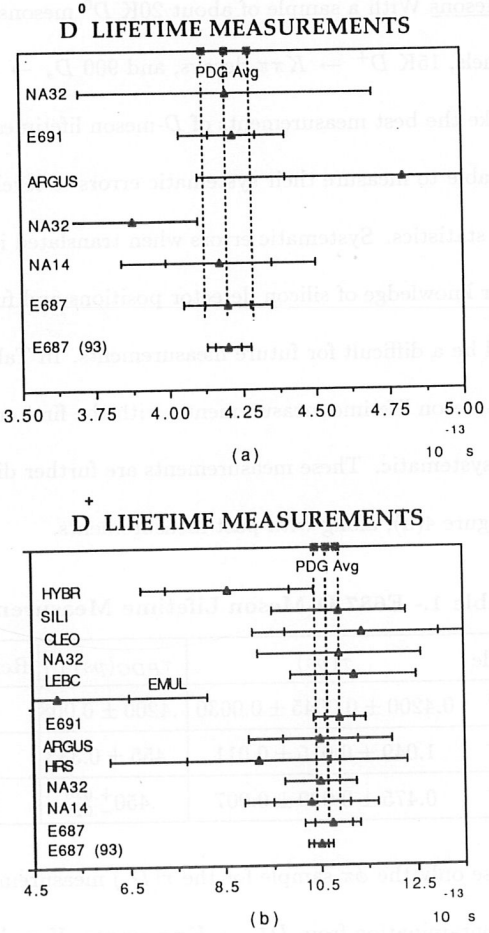

Figure 3: (a) D^0 and (b) D^+ lifetime measurements. The Particle Data Group average [6] is indicated.

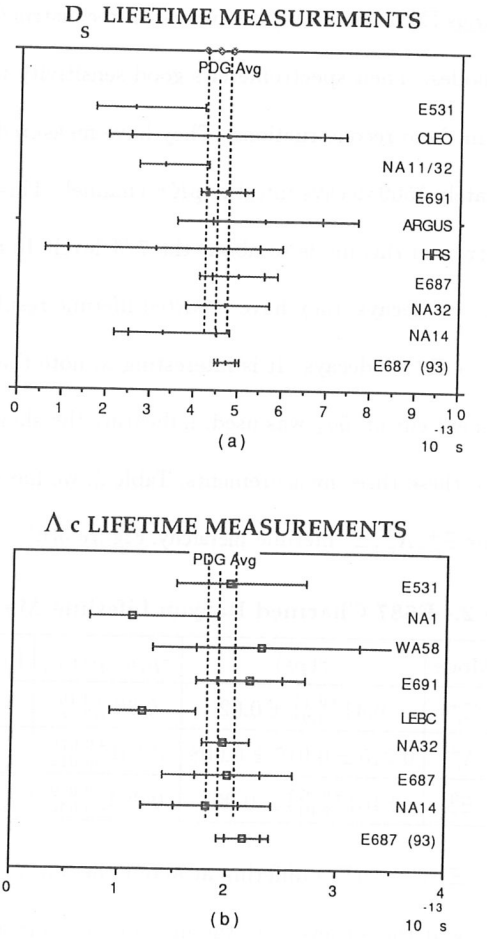

Figure 4: (a) D_s^+ and (b) Λ_c^+ lifetime measurements. The Particle Data Group average [6] is indicated.

Charmed Baryons E687 has had good success in reconstructing many charmed baryon decay modes. Their spectrometer's good sensitivity to Λ, Ξ, and Σ decays has aided in these reconstructions. They have measured the Λ_c lifetime from approximately 1500 decays into the $pK\pi$ channel. This has reduced the measurement error on this mode to about the 7 % level. In addition to the standard $\Lambda_c^+ \to pK^-\pi^+$ decays, they have reported lifetime results for $\Xi_c^0 \to \Xi^-\pi^+\pi^+$ decays and $\Xi_c^0 \to \Xi^-\pi^+$ decays. It is interesting to note that in the Ξ_c^0 decay a small detachment cut of $.5\sigma_z$ was used, indicating the short lived nature of this state. With these three measurements, Table 2, we have for the first time a good look at the $\Xi_c^+, \Lambda_c^+, \Xi_c^0$ lifetime hierarchy, Figure 5(b).

Table 2.- E687 Charmed Baryon Lifetime Measurements

Mode	$\tau(ps)$	$\tau_{PDG}(ps)$ [ ]	Reference
Ξ_c^+	$0.41^{+0.11}_{-0.08} \pm 0.02$	$0.30.^{+0.10}_{-0.06}$	[16]
Λ_c^+	$0.215 \pm 0.016 \pm 0.008$	$0.191^{+0.015}_{-0.012}$	[17]
Ξ_c^0	$0.101^{+0.025}_{-0.017} \pm 0.005$	$0.082^{+0.059}_{-0.030}$	[18]

As predicted, $\tau(\Xi_c^+) > \tau(\Xi_c^0)$ differing at about the 3 σ level, with $\tau(\Lambda_c^+ > \tau(\Xi_c^0)$, separating at the 4σ level. As the measurement error on these decays are reduced, further constraints on the models will be possible. Again, as in the case of charmed mesons, accurate measures of branching ratios will be important in understanding the details of charmed baryon decays.

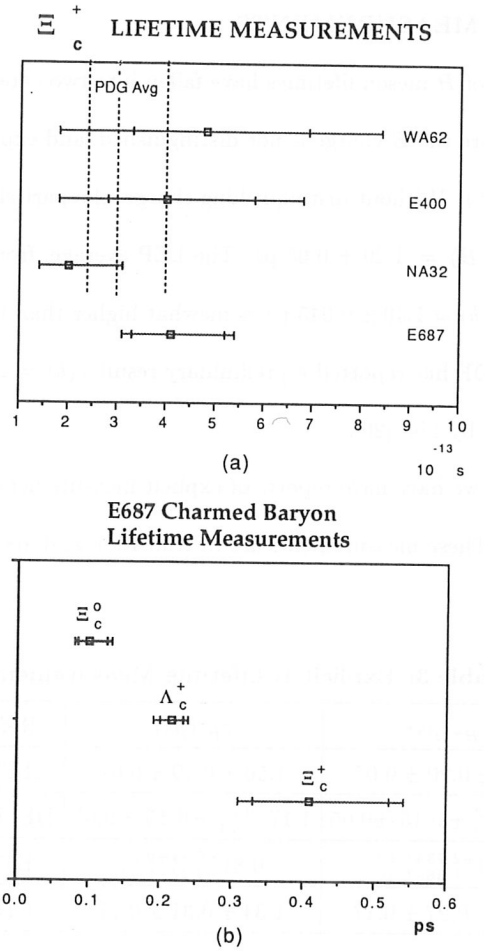

Figure 5: (a) Ξ_c^+ lifetime measurements. The Particle Data Group average [6] is indicated. (b) Comparison of $\Xi_c^+, \Lambda_c^+, \Xi_c^0$ charmed baryon lifetimes from E687.

b-LIFETIME MEASUREMENTS

Measurements of B-meson lifetimes have fallen into two categories, generic measurements where the B charge is not distinguished, and explicit measures of $\tau(B^0)$ and $\tau(B^+)$. Without distinquishing charge, the particle data group [6] report a generic $\tau(B) = 1.29 \pm 0.05$ ps. The LEP average, from a report by Augustin [19] is $\tau(b) = 1.40 \pm 0.045$ ps, somewhat higher than previous pre-LEP measurements. CDF has reported a preliminary result $\tau(b) = 1.48 \pm 0.06 \pm .09$ ps in a recent talk by Liss [20].

More recently, we have have reports of explicit measurements from LEP, CDF, and E653. These measurements are in transition and are presented in Table 3.

Table 3: Explicit B Lifetime Measurements

$\tau_{B^+}(ps)$	$\tau_{B^0}(ps)$	Reference
$1.34 \pm 0.20 \pm 0.07$	$1.56 \pm 0.19 \pm 0.07$	ALEPH [20]
$1.30^{+0.33}_{-0.29} \pm 0.15 \pm 0.05$	$1.17^{+0.29}_{-0.23} \pm 0.15 \pm 0.05$	DELPHI [20]
$3.84^{+2.73+0.80}_{-1.36-0.16}$	$0.81^{+0.34+0.08}_{-0.22-0.02}$	E653 [21]
$1.59 \pm 0.27 \pm 0.17$	$1.34 \pm 0.31 \pm 0.17$	CDF [20]

In addition, ALEPH has presented beautiful measurements of the B_s^+ [21] and Λ_b [24] lifetimes from $B_s \to D_s^+ \ell^- \nu X$ decays and $\Lambda_b \to \Lambda_c^+ \ell^- \nu$ decays. Their recent measurements give $\tau_{B_s} = (1.02 \pm 0.39 \pm 0.10)$ ps and $\tau_{\Lambda_b} = (1.12 \pm 0.30 \pm 0.16)$ ps. We can expect the b-lifetime measurements to be continually improving over the next few years.

CONCLUSION

We can conclude by saying that the D^0 and D^+ lifetime measurements are in very good shape with errors at the 1 % level. It may be difficult for future measurements to improve on the systematic errors. Improvements on the D_s measurement may be needed to make $\tau(D_s) - \tau(D^0)$ interesting. E687 has provided the first good look at the charmed baryon lifetime hierarchy. There is good agreement with existing models. Further work on a measurement of $\tau(\Omega_c)$ is needed.

B lifetime measurements are getting much attention at LEP and the CDF collider experiments. Lifetimes have not differed much from spectator model predictions. We expect these measurements to improve as groups learn to better use the vertex detectors in these experiments.

Acknowledgements

I would like to thank the HQ93 organizers for their generous hospitality and planning. My gratitude to J. Wiss and J. Cumalat for sharing their ideas on recent photoproduction results, and to T. Liss and N. Stanton for their information on b-physics lifetimes for this review.

REFERENCES

[1] J.P. Leveille,'B-Decays', UM HE 81-18, based on a talk given at the Workshop on B decays, Cornell University, March 1981, and references therein.

[2] R.Rückl, Habilitationschrift, Univ. Munich (1983), and references therein.

[3] I.I. Bigi, 'On Our Theoretical Understanding of Charm Decays', SLAC-PUB-4067, August 1986 (T/E), and references therein.

[4] R.J. Morrison and M.S.Witherell, 'D Mesons', Annu. Rev. Nucl. Part. Sci. **39**, 183-230, (1989), and references therein.

[5] R.M. Baltrusaitis et al., Phys. Rev. Lett. **54**,1976 (1985).

[6] Particle Data Group, Review of Particle Properties, Phys. Rev. **D 45** (1992).

[7] See reference 44 of reference [4] cited in this paper.

[8] M.Bauer, B.Stech, M.Wirbel, Z. Phys. **C34**, 103 (1987).

[9] B.Guberina, R.Rückl, J.Trampetić et al., Z. Phys. **C33**, 297 (1986).

[10] M.B.Voloshin and M.A.Shifman, Sov. Phys. JETP **64**(4), 698 (1986).

[11] J.G. Körner and H.W.Siebert, 'Charmed Baryons: Theory and Experiment', Annu. Rev. Nucl. Part. Sci. **41**, 511-545 (1991).

[12] H.D.Politzer, M.B.Wise, Phys. Lett. **B206**, 68 (1988).

[13] P.L.Frabetti et al., Nucl. Instr. and Meth. in Phys. Res. sect A, **320**, 519 (1992).

[14] see E687 review talk by J. Butler at Spring Meeting of American Physical Society, Washington D.C., 1993.

[15] P.L. Frabetti et al., The E697 Collaboration, FERMILAB-Pub-93/030-E (E687), and submitted to Physical Review Letters.

[16] P.L. Frabetti et al., Phys. Rev. Lett. **70**, 1381 (1993).

[17] P.L. Frabetti et al., Phys. Rev. Lett. **70**, 1755 (1993).

[18] P.L. Frabetti et al., Phys. Rev. Lett. **70**, 2058 (1993).

[19] Jean-Eudes Augustin, 'LEP Physics', CERN-PPE/93-83, 46 (1993), Lectures given at the 4th Hellenic School, Elementary Particle Physics, Corfu, September 1992.

[20] see CDF review talk by T. Liss at Spring Meeting of American Physical Society, Washington D.C., 1993.

[21] K. Kodama, et al.,'Measurement of the Lifetimes of Charged and Neutral Beauty Hadrons',Prog. Theo. Phys., April (1993), OHSTPY-HEP-E-92 -019.

[22] DELPHI Collaboration, CERN-PPE/92-174, submitted to Zeit. Phys. C.

[23] Sam C.C. Ting, 'New Results from LEP Experiments', CERN-PPE/93-34, based on a plenary report presented at the DPF 92 meeting at Fermilab.

SESSION VI

- U. Dore
  Status of Tau–Neutrino Physics and its Future at LHC
- K. R. Schubert
  Future B–Meson Experiments in $e^+ e^-$ and Hadron Hadron Collisions
- A. Fridman
  Production and Decay of Beauty–Baryon
- Y. Giomataris
  Perspectives of an Asymmetric Proton Collider with a Crossing Angle for B–Physics
- B. Cox
  Fixed Target Beauty Physics at the SSC and the LHC
- K. Stanfield
  Plans for the Fermilab Fixed Target Program

STATUS OF TAU-NEUTRINO PHYSICS AND ITS FUTURE AT LHC

U. Dore

Università di Roma I, "La Sapienza", Dipartimento di Fisica G. Marconi
Sezione INFN, Piazzale Aldo Moro, 2, I-00185 Roma, (ITALIA)

No written contribution received

Frascati Physics Series, Vol. 1 (1993)
HEAVY QUARKS AT FIXED TARGET
Frascati, May 31st – June 2nd 1993
(pp. 267–283)

FUTURE B–MESON EXPERIMENTS IN e^+e^- AND HADRON HADRON COLLISIONS

K.R. Schubert
Universität Karlsruhe, Institut für Experimentelle Kernphysik
Engesserstraße 7, Postfach 6980, D–76128 Karlsruhe, (GERMANY)

Abstract

Future B-meson experiments are motivated by our aim to understand CP violation. The known CP-violating phenomena in K-meson decays can either be due to the standard weak interaction or due to new physics. Decisive experiments require precision measurements of the Standard Model parameters ϑ_{23}, ϑ_{13}, and δ_{13}. Results can be obtained from CP-conserving B-decay experiments. Observation of CP violation in B-meson decays is an additional future programme point. Whereas precision measurements of the three Standard Model parameters are only expected from future e^+e^- experiments, the observation of CP violation in B decays has good prospects in both e^+e^- annihilation and hadron-hadron collisions.

1. Introduction

Experiments with B mesons are the key for our understanding of CP violation. Up to now, there are only two known violations of the particle - antiparticle symmetry CP in Nature, one (ϵ', not well established) in direct $K^0 \to \pi\pi$ decays [1] and the other (ϵ, very well established) in $K^0\overline{K}^0$ oscillations. The Standard Model is able to explain the latter violation by second order weak interactions, see Fig. 1, with a box diagram containing coherent superpositions of u, c, and t quarks and the pertinent CKM [2] matrix elements V_{ij} (i=u, c, t; j=d, s). This explanation requires a nontrivial phase in the CKM matrix. If all matrix elements were real, $K^0\overline{K}^0$ oscillations would be CP symmetric in the Standard Model.

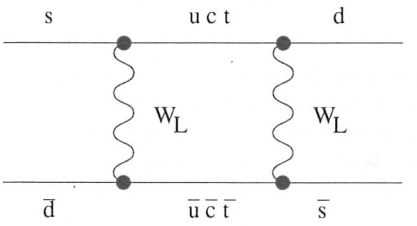

Fig. 1: The standard box graph for $\epsilon(K^0)$.

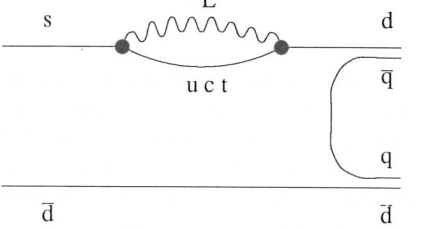

Fig. 2: The standard box graph for $\epsilon'(K^0)$.

As long as our knowledge of the CKM matrix is not sufficient [3], we cannot know if the observed CP violation in the neutral Kaon system is created by the standard weak interaction or by new physics. More precise measurements of ϵ and ϵ' will not change this situation since the contributions of e. g. right-handed W-bosons, supersymmetric Winos or squarks will modify the ϵ-box in Fig. 1 as well as the ϵ'-box in Fig. 2. Progress in constraining our knowledge on the CKM matrix requires experiments with B mesons.

2. Where to do B-meson Physics

The Standard Model explanation for ϵ [4] needs the existence of a third fermion family, now known for 18 years [5], and precise parameter values for m_t, ϑ_{12}, ϑ_{23}, ϑ_{13}, and δ_{13}, where I have used the Particle Data Group notations [6] for the four parameters of the CKM matrix. The angle ϑ_{12} is very well known from Kaon and hyperon decays [7], and the other three CKM parameters can be obtained from CP-conserving B-meson decays.

The angle ϑ_{23} has been obtained from measurements of the B meson life time [8] and of the semileptonic decay fraction of B-mesons [9]. Model-dependent analyses of exclusive and inclusive semileptonic decays lead to $\vartheta_{23} = 0.043 \pm 0.004$. The ratio $\vartheta_{13}/\vartheta_{23}$ is obtained from the high-momentum region of inclusive semileptonic B decays. Only two experiments have seen these $b \to u\ell\nu$ transitions so far, ARGUS [10] at DORIS-II and CLEO [11] at CESR, both in e^+e^- annihilation at $\sqrt{s} = m(\Upsilon 4S) = 10.58$ GeV. Their present average is $\vartheta_{13}/\vartheta_{23} = 0.086 \pm 0.007$ using the model of Altarelli et al [12] and up to a factor of 2 higher for other models. We therefore know $\vartheta_{13} = 0.003 \div 0.006$. There is no information on the phase δ_{13} from B-meson decays so far.

Table 1: Present e^+e^- storage rings for B-meson experiments.

Ring	Location	E_{CM}	$\mathcal{L}_{max}$	$N_{b\bar{b}}$
DORIS-II	DESY	$m(\Upsilon 4S)$	$2 \cdot 10^{31}/cm^2/s$	$\sim 10^5/y$
CESR	Cornell	$m(\Upsilon 4S)$	$2 \cdot 10^{32}/cm^2/s$	$\sim 10^6/y$
LEP	CERN	$m(Z)$	$10^{31}/cm^2/s$	$\sim 3 \cdot 10^5/y$

Most of the present B-meson results originate from the three e^+e^- storage rings shown in Table 1. Progress in precision on the Standard Model parameters ϑ_{13}, ϑ_{23}, and δ_{13} can well be achieved with e^+e^- annihilation but requires about 100 times more B-mesons than available now. The idea to build a new storage ring of the required intensity, a so-called "B-Meson Factory", dates back to 1985. K. Wille showed [13] that luminosities of a few $10^{33}/cm^2/s$ can be reached in a double ring with separate storage of e^+ and e^- in many bunches. Since the double ring technique

can store e^+ and e^- with two different energies, this advantage was soon proposed in order to perform CP-violation experiments on the $\Upsilon(4S)$ resonance. Up to now, there are seven detailed designs of energy-asymmetric B-Meson Factories. Their main properties are given in Table 2, together with those of an upgraded LEP and of some hadron facilities which I will discuss later.

Table 2: Planned B-Meson Factories and other facilities for B meson experiments.

Factory	Location	C[km]	E[GeV]	$\mathcal{L}$[cm^{-2}s^{-1}]	$\dot{N}_{b\bar{b}}[y^{-1}]$	$b\bar{b}$/had
BETA	PSI	0.7	$4+7$	10^{33}	10^7	0.23
VEPP-V	Novosibirsk	0.7	$4+7$	$5\cdot10^{33}$	$5\cdot10^7$	0.23
PEP-II	SLAC	2.0	$3.1+9$	$3\cdot10^{33}$	$3\cdot10^7$	0.23
ISR-B	CERN	1.0	$3.5+8$	$\rightarrow 10^{34}$	$\rightarrow 10^8$	0.23
CESR-B	Cornell	0.8	$3.5+8$	$3\cdot10^{33}$	$3\cdot10^7$	0.23
TRISTAN-3	KEK	3.0	$3.5+8$	$2\cdot10^{33}$	$2\cdot10^7$	0.23
PETRA-B	DESY	2.3	$3+9.3$	$3\cdot10^{33}$	$3\cdot10^7$	0.23
LEP, upgr.	CERN	26.7	2×45.6	$\rightarrow 10^{32}$	$\rightarrow 5\cdot10^6$	0.22
HERA, pA	DESY	6.3	$\sqrt{s}=39$	(30 MHz)	$2\cdot10^8$	$8\cdot10^{-7}$
LHC, pA	CERN	26.7	$=114$	(20 MHz)	10^{10}	$5\cdot10^{-5}$
HERA, pp	DESY	6.3	$=314$	$2\cdot10^{32}$	10^{10}	10^{-4}
TEV-I, $p\bar{p}$	FNAL	6.3	$=1800$	$5\cdot10^{30}$	$2\cdot10^9$	$3\cdot10^{-4}$
LHC, pp	CERN	26.7	$=14000$	$\rightarrow 10^{34}$	$\rightarrow 4\cdot10^{13}$	$3\cdot10^{-3}$

3. The Main Experimental Programme at a B-Meson Factory

The programme at a B-Meson Factory can be divided into four main parts:
a) Precision determination of the weak interaction parameters ϑ_{23}, ϑ_{13}, and δ_{13} including the necessary studies of the strong interaction which influence this determination,
b) search for CP violation in one B-decay mode,
c) systematic investigation of CP violation in a complete set of B-decay modes, and
d) studies of τ-decays, QCD in B-decays, charm spectroscopy and decays, and light meson spectroscopy in jet fragmentation and in photon-photon interactions.
Areas a) and b) require a few years with $\mathcal{L}$ between 10^{33} and $3\cdot10^{33}/\mathrm{cm}^2/\mathrm{s}$ on the $\Upsilon(4S)$ and $\Upsilon(5S)$ resonance. Area c) is a long term programme of about ten years with $\mathcal{L}$ between $3\cdot10^{33}$ and $10^{34}/\mathrm{cm}^2/\mathrm{s}$ on the $\Upsilon(4S)$. All studies in area d) do not require separate runs but are side products during data taking for a) to c).

3.1 Determination of ϑ_{23}

The CKM matrix element $V_{cb}=\sin\vartheta_{23}=s_{23}$ is best obtained from HQET, heavy quark effective theory, [14] and the y distribution of exclusive $B\rightarrow D^*\ell\nu$ events with low background, where y is the product of the four-velocities of the two mesons,

$y = v(\mathrm{B}) \cdot v'(\mathrm{D}^*)$. Using this method, ARGUS [15] obtained [2] $s_{23} = 0.047 \pm 0.006$ from $2 \cdot 10^5$ $\Upsilon(4S)$ decays. A B-Meson Factory detector with $3 \cdot 10^7$ $\Upsilon(4S)$, corresponding to one year with 10^7 s and $3 \cdot 10^{33}/\mathrm{cm}^2/\mathrm{s}$, should reach an error which is ten times smaller, i. e. in the $1 \div 2\%$ region.

For that purpose, also the B-meson life time has to be known with precisions around 1% for B^0 and B^+ separately. At present, $\tau(\mathrm{B})$, $\tau(\mathrm{B}^0)$, and $\tau(\mathrm{B}^+)$ are known to $\pm 2.8\%$, 7.5%, and 9.5%, respectively [8]. The energy asymmetry of a B-Meson Factory produces boosted B. At $8 + 3.5$ GeV, the boost is $\beta\gamma = 0.43$, leading to an average flight path of $\langle \Delta l_{\mathrm{B}} \rangle = \beta\gamma c \langle \Delta t \rangle = 180$ μm. Vertex resolutions with thin Silicon microstrips are around 50 μm or better and lead therefore to a negligible error on the mean life,

$$\sigma_\tau = \sqrt{\frac{\tau^2 + \sigma_{\Delta t}^2}{N}} \; .$$

With $N = 3000$, easily obtainable from $3 \cdot 10^7$ $\Upsilon(4S)$ in backgound-free channels, we obtain $\sigma_\tau / \tau \approx \pm 2\%$, contributing $\pm 1\%$ to the error on ϑ_{23}.

3.2 Determination of ϑ_{13}

The CKM element $|V_{ub}| = \sin\vartheta_{13} = s_{13}$ is now known to be in the range $0.03 \div 0.06$ [10, 11]. Progress requires new methods, the present determination from the high momentum end of the lepton spectrum in inclusive $\mathrm{B} \to \ell\nu\mathrm{X}$ events suffers from the large model-dependent extrapolation over the full momentum range. A promising method is the study of exclusive $\mathrm{B} \to \pi\ell\nu$, $\rho\ell\nu$, $\omega\ell\nu$ decays which has given only upper limits on s_{13} so far [9]. If one is able to tag these decays with fully reconstructed decays of the second B in $\Upsilon(4S) \to \mathrm{B}\overline{\mathrm{B}}$ events, one can obtain a clean sample as shown in the missing mass plot in Fig. 3. For e. g. $\mathrm{B}^+ \to \omega\ell^+\mathrm{X}$, the missing mass M_{X} is obtained from

$$M_{\mathrm{X}}^2 = (E_{\mathrm{B}} - E_\omega - E_\ell)^2 - (\vec{p}_{\mathrm{B}} - \vec{p}_\omega - \vec{p}_\ell)^2 \; ,$$

where $\vec{p}_{\mathrm{B}}$ is known from the reconstructed B tag. The results in Fig. 3 have been obtained in a Monte Carlo study for the ISR B-Meson Factory [16].

A sample of $3 \cdot 10^7$ $\Upsilon(4S)$ would give ≈ 500 $\rho\ell\nu$ and $\omega\ell\nu$ if $\mathcal{B}(\mathrm{B} \to \omega\ell\nu) = 5 \cdot 10^{-5}$. This results in a statistical error of $\pm 2.2\%$ on ϑ_{13}, but theoretical uncertainties will be much larger. However, the measured Dalitz plot density over a wide p_ℓ and q^2 range will allow to reduce this uncertainty, and the remaining error on ϑ_{13} has been estimated to be smaller than 10%.

[2] rescaled for the new B lifetime value.

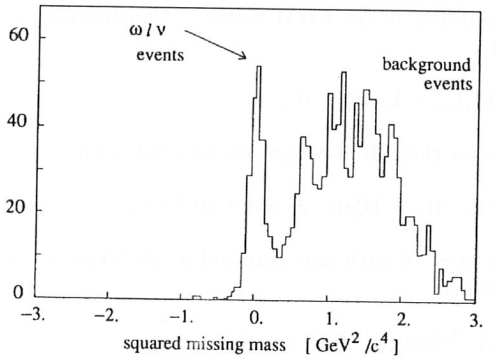

Fig. 3: Missing mass spectrum in tagged $B^+ \to \omega \ell^+ X$ events [16].

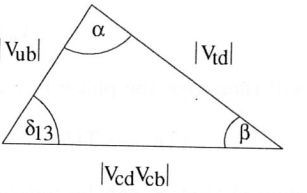

Fig. 4: Unitarity triangle of the CKM matrix.

3.3 Determination of δ_{13} from $B\overline{B}$ Oscillations

There are two oscillating B systems, $B^0\overline{B}^0$ and $B_s\overline{B}_s$. The mass difference of the first one,

$$x_0 = \Delta m(B_H^0 - B_L^0)/\Gamma(B^0) = 0.69 \pm 0.08 \ ,$$

has been directly determined by ARGUS, CLEO, ALEPH, and DELPHI [17], whereas the corresponding difference for the B_s can only be derived from the superposition of B^0 and B_s oscillations as measured by UA1, many PETRA and PEP experiments, and all LEP experiments. The present world average is [17]

$$\chi = f_0 \cdot \frac{x_0}{2 + 2x_0^2} + f_s \cdot \frac{x_s}{2 + 2x_s^2} = 0.121 \pm 0.010 \ ,$$

where f_0 and f_s are the not well known abundancies of B^0 and B_s in b-quark jets. With $f_s < 0.15$ one obtains $x_s < 0.9$ with 90% confidence [17]. A precise measurement of x_s will be of greatest importance for a determination of δ_{13}. This may be seen as follows:

$$x_0 = \frac{G_F^2}{6\pi} \cdot |V_{td}|^2 \cdot m_t^2 \cdot F(m_t/m_W) \cdot f_{B^0}^2 \cdot B_{B^0} \cdot m_{B^0} \cdot \tau_{B^0} \cdot \eta_{QCD} \ ,$$

$$x_s = \frac{G_F^2}{6\pi} \cdot |V_{ts}|^2 \cdot m_t^2 \cdot F(m_t/m_W) \cdot f_{B_s}^2 \cdot B_{B_s} \cdot m_{B_s} \cdot \tau_{B_s} \cdot \eta_{QCD} \ .$$

The ratio x_0/x_s does not depend on m_t, it will depend only on $|V_{td}/V_{ts}|$ when m_{B_s} and τ_{B_s} have been measured. The ratio f_{B^0}/f_{B_s} has to be taken from a lattice calculation but will be much better known than the two decay constants separately. A measurement of x_s within $\pm 15 \div 20$ % will therefore allow to get $|V_{td}|$ within $\pm 10\%$

since V_{ts} is well constrained by the unitarity of the CKM matrix.[3] Construction of the unitarity triangle [18], see Fig. 4,

$$V_{ud}V_{ub}^{*} + V_{cd}V_{cb}^{*} + V_{td}V_{tb}^{*} = 0 \ ,$$

will then give the phase δ_{13}. A study for the ISR B-Meson-Factory [19] with

$$e^{+}e^{-} \rightarrow \Upsilon(5S) \rightarrow B_s^{(*)}\overline{B}_s^{(*)}, \quad B_s \rightarrow D_s^{*}\ell\nu, \quad E = 3 + 10 \text{ GeV},$$

showed that x_s can be measured up to ~ 10 with one year and $3 \cdot 10^{33}/\text{cm}^2/\text{s}$. A more recent study for PEP-II [20] yielded

$$x_s(\max) \approx [2 + 0.5 \cdot {}^{10}\log(\mathcal{L}_{\text{int}} \cdot \text{fb})]\ \beta\gamma c\tau/\sigma_z \ ,$$

where $\mathcal{L}_{\text{int}}$ is the integrated luminosity and σ_z the obtainable resolution for the B_s flight path between production and decay. With one year, $3 \cdot 10^{33}/\text{cm}^2/\text{s}$, and $\sigma_z = 50\ \mu\text{m}$, we may expect to measure x_s within $\pm 20\%$ if it is smaller than 15.

3.4 Search for CP Violation in one B-Decay Mode

There are four classes of expected CP violation in B-meson decay,

- CP violation in B^0 oscillations, described by an ε parameter similar to $\varepsilon(K^0)$ which is expected to be as small as in the Kaon case.
- CP violation in direct decays, e. g. $B^+ \rightarrow K^+\pi^0/B^- \rightarrow K^-\pi^0$. The ϵ' parameter for this asymmetry may be 1000 times larger than in the Kaon case, but is still below the percent region.
- CP violation in the interference between oscillations and decay, requiring a CP eigenstate which can be reached both in B^0 and in $\overline{B}^0$ decays, e. g. $J/\Psi\ K_s^0$ or $\pi^+\pi^-$.
- CP violation in a single event like $\Upsilon(4S) \rightarrow B^0\overline{B}^0 \rightarrow (\pi^+\pi^-)(\pi^+\pi^-)$ which has CP $= +1$ in the initial state and, because of $\ell = 1$, CP $= -1$ in the final state.

Since also the expectations for class 4 are very low, class 3 is by far the most promising one for discovering CP-violating B-decays if the Standard Model is the origin of CP-violating K-decays. The time dependence for decays into these CP eigenmodes is given by

$$\dot{N}(B^0 \rightarrow f) = e^{-t/\tau}(1 + A_f \cdot \sin\Delta m t) \ ,$$

$$\dot{N}(\overline{B}^0 \rightarrow f) = e^{-t/\tau}(1 - A_f \cdot \sin\Delta m t) \ ,$$

[3] It is essentially equal to V_{cb}.

where the first rate describes decays from an initial B^0 and the second one from an initial $\overline{B}^0$. For $\pi^+\pi^-$, the Standard Model predicts $A_{\pi\pi} = -\sin 2\alpha \pm 10\%$, where the angle α is shown in Fig. 4 and the error is an estimate for the theoretical uncertainty originating in the presence of two different decay graphs, a "spectator" (isospin I=0, 2) and a "penguin" (I=0). For $J/\Psi\ K^0_S$, the prediction is $A_{\psi K} = -\sin 2\beta$, see also Fig. 4, with negligible theoretical uncertainty.

3.5 Standard Model Expectations and Luminosity Estimates

What is our present knowledge on the angles α and β? The Standard Model analysis in ref. [3], repeated with 1993 input data, gives the results as shown in Fig. 5. The inputs are $s_{12} = 0.221, s_{23} = 0.043 \pm 0.004$ [9], $s_{13}/s_{23} = 0.086 \pm 0.007$ [10, 11, 12], $\tau_B = 1.44$ ps [8], $|\varepsilon(K^0)| = 0.00226$, $B_K = 0.8 \pm 0.1$, $x(B^0) = 0.69 \pm 0.08$ [17], $m_t = (161 \pm 26)$ GeV [21], and $m_t = (180^{+\infty}_{-14})$ GeV [22]. Since there is a wide

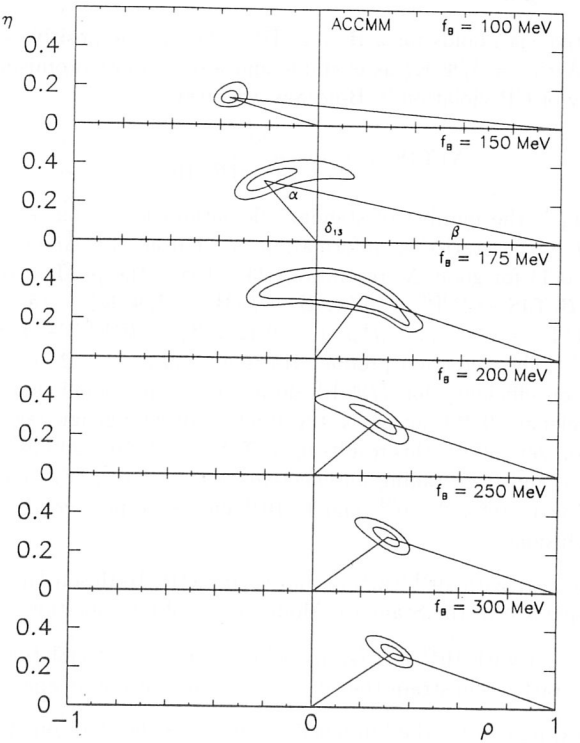

Fig. 5: Results of the updated fit [3] of the unitarity triangle with 1993 input data, using Altarelli et al [12] for s_{13}. The axes use the Wolfenstein parameters $\rho = s_{13}\cos\delta_{13}/s_{12}s_{23}$ and $\eta = s_{13}\sin\delta_{13}/s_{12}s_{23}$. The contours correspond to one and two standard deviations.

spread of theoretical estimates, the parameter $f_B \cdot \sqrt{B_B}$ has been varied between 100 and 300 MeV. There is a good χ^2 value for the fit, i. e. perfect agreement between the data and the Standard Model, for all $f_B\sqrt{B_B}$ values below 250 MeV.

As can be read from Fig. 5, the best fit values for $\sin 2\beta$ vary between 0.20 at 100 MeV and 0.70 at 250 MeV. Though favoured by older QCD sum rule calculations, $f_B\sqrt{B_B}$ values below 150 MeV are very unlikely in present lattice QCD calculations. Between 125 and 250 MeV, $\sin 2\beta$ ranges from 0.20 to 0.80 with 95% confidence. These limits allow an estimate for the number of $\Upsilon(4S)$ mesons which are necessary for measuring A. The CP asymmetry A_f is obtained from reconstructing both decay vertices of $B^0 \to f$ and of the other B meson as flavour tag. With large enough energy asymmetry, we have

$$\Delta t = \frac{z(f) - z(\text{tag})}{\beta\gamma c} \;, \quad \dot{N}(f,\ \text{tag}) = e^{-|\Delta t/\tau|} \cdot (1 \mp A_f \cdot \sin \Delta m \Delta t) \;,$$

where the negative sign holds for a B^0 tag ($\overline{B}^0 \to f$) and the positive sign for a $\overline{B}^0$ tag ($B^0 \to f$). With $f = J/\Psi\ K_S^0$ as example and also as most promising candidate for the discovery of CP-violation in B-decays, we need

$$N(\Upsilon 4S) = \frac{S^2}{2 \cdot I \cdot A^2 \cdot \Pi\mathcal{B} \cdot \Pi\eta} \;,$$

where $S = A/\sigma_A$ is the number of standard deviations for a non-zero observation of $A = A_{\Psi K}$, I is the statistical information on A from the Δt measurement of one event ($I = 0.33$ for good Δt resolution [23]), $\Pi\mathcal{B}$ is the product of four decay fractions, $\mathcal{B}_1 = \mathcal{B}(\Upsilon 4S \to B^0\overline{B}^0) = 0.50$, $\mathcal{B}_2 = \mathcal{B}(B^0 \to J/\Psi\ K_S^0) = (5.2 \pm 0.8) \cdot 10^{-4}$ [24], $\mathcal{B}_3 = \mathcal{B}(J/\Psi \to e^+e^-$ and $\mu^+\mu^-) = 0.122$, $\mathcal{B}_4 = \mathcal{B}(K_S^0 \to \pi^+\pi^-) = 0.69$, $\Pi\mathcal{B} = 2.2 \cdot 10^{-5}$. The detection product $\Pi\eta$ is $\eta_{\text{rec}} \cdot \eta_{\text{tag}} \cdot (1 - 2w)^2$, where η_{rec} is the reconstruction efficiency for $J/\Psi\ K_S^0$ decays (0.55 in a good detector), η_{tag} is the tagging efficiency (0.35), and w is the fraction of wrong-sign tags (0.10). For reaching a 3σ non-zero effect, this results in $N(\Upsilon 4S) = 0.8 \cdot 10^7$, $2.0 \cdot 10^7$, and $1.3 \cdot 10^8$ for $A = 0.8$, 0.5, and 0.2. Taking an effective year with 10^7s, this corresponds to one year and $\mathcal{L} \approx 1 \cdot 10^{33}$, $2 \cdot 10^{33}$, and $1 \cdot 10^{34}/\text{cm}^2/\text{s}$, respectively. This estimate allows two conclusions:

- About one year with $10^{34}/\text{cm}^2/\text{s}$ at an asymmetric B-Meson Factory will lead to a decisive test of the Standard Model origin of CP violation.
- After one year with $10^{33}/\text{cm}^2/\text{s}$, one will either find CP violation in B-meson decays or start to constrain the $(\vartheta_{13}, \delta_{13}, m_t, f_B)$ parameter space.

An equivalent expression for the luminosity estimate is the error on A,

$$\sigma(A_{\Psi K}) = \frac{1}{\sqrt{2 \cdot I \cdot N(\Upsilon 4S) \cdot \Pi\mathcal{B} \cdot \Pi\eta}} = \frac{1.23}{\sqrt{N(\Upsilon 4S) \cdot \Pi\mathcal{B} \cdot \Pi\eta}} \;,$$

which is about 0.14 with $N(\Upsilon 4S) = 3 \cdot 10^7$ and decay fractions and efficiencies as above. Using also $K^0_S \to \pi^0\pi^0$ for reconstruction and a slightly higher tagging efficiency, the PEP-II study group quotes $\sigma(A_{\Psi K_S}) = 0.10$ with $3 \cdot 10^7$ $\Upsilon(4S)$ mesons. Combining decay modes which all have the same asymmetry $\sin 2\beta$ in the Standard Model expectation, the PEP-II group [25] estimates to reach $\sigma(\sin 2\beta) \approx 0.06$ with $N(\Upsilon 4S) = 3 \cdot 10^7$, i. e. with $3 \cdot 10^{33}/\mathrm{cm}^2/\mathrm{s}$ and one year.

4. Detector Requirements

At an asymmetric B-Meson Factory with 3 on 9 GeV, the average particle momentum will be less than 1 GeV/c. Therefore, multiple scattering has to be held to a minimum. Tracking chambers must have low-mass gas and wires. Some particle momenta go up to 4 GeV/c, and particle identification with good $\pi - \mathrm{K}$ separation must extend up to this momentum. For that purpose, a combination of dE/dx and Cerenkov techniques are likely to be required.

Excellent vertex resolution, especially in the boost direction, is of great importance. The vertex detector must have low multiple scattering, high rate capability and radiation hardness.

Photon detection must extend down to very low energies, around 20 MeV, with excellent energy and position resolution. For that purpose, the particle ID system in front of the photon detector must have minimal influence, and the electronic noise performance must be improved compared to present detectors. Radiation hardness is also essential.

Last but not least, the trigger and data acquisition systems must cope with high rates. At $\mathcal{L} = 10^{34}/\mathrm{cm}^2/\mathrm{s}$, the rate for $\mathrm{B\overline{B}}$ events is 10 Hz, and the total rate of good events is around 50 Hz.

5. Decision on B-Meson Factories?

Out of the seven B-Meson Factory projects in Table 2, the three at PSI, CERN, and DESY are no longer pursued. The project at Novosibirsk has found approval three years ago, but the present economic situation in Russia leaves it open when it can be completed.

In the USA, the year 1993 has brought a big step forward. The DOE budget, as proposed by the government this spring, includes construction of a B-Meson Factory with a starting sum of 36 M$ for financial year 94, starting October 93. A site selection between SLAC and Cornell has been prepared by a joint DOE-NSF Committee which worked out its recommendations this June. A site decision by DOE† and final approval by the Parliament is expected before this September. Construction at SLAC would take four to five years, and about the same amount of time is required for setting up an experiment.

† *(Eds.: On October 4th, 1993 the U.S. Department of Energy selected SLAC as the preferred site for construction of a B–Factory).*

In Japan, the government decision process for the B-Meson Factory at KEK is far advanced. Approval by the Parliament is expected near the end of this year and construction could start in April 94.

6. Planned Hadron Experiments in Western Europe

There are six experiments under discussion which plan to do B-meson physics at the CP violation level in hadron-hadron collisions at West-European laboratories. I limit my presentation geographically since other speakers at this Conference cover the plans at the American laboratories [26] and I am not well aware of the situation at UNK [27].

At HERA in DESY there are plans [28] to collide 820 GeV protons in the halo of the existing stored proton beam with an array of wires for an experiment which is specialized for the detection of $B^0 \to J/\Psi K^0_S$ events. At LHC in CERN the two large experiments ATLAS [29] and CMS [30], which have been recommended by the LHCC, have good prospects for $B^0 \to J/\Psi\ K^0_S$ and a few other B physics topics. The LHCC intends to recommend in addition one specialized B-meson experiment with a wider B-physics potential. There are no documents yet, but three groups plan to submit letters of intent until October 93; COBEX, GAJET, and LHB. The three experiments ATLAS, CMS, and COBEX produce B mesons in the pp collider mode, whereas GAJET and LHB intend to use one proton beam of 7 TeV on a fixed target.

6.1 HERA-B

The intended HERA experiment with protons from the beam halo on a fixed internal target like copper has the difficulty of a very low center-of-mass energy, $\sqrt{s} = 39$ GeV, and therefore only a minute $B\overline{B}$ production cross section. This cross section has not yet been measured. A QCD model calculation [31] gives 12 nb at $E_{\rm lab} = 820$ GeV, and 20 nb at 1000 GeV with an uncertainty of about a factor of 2 in both directions. The experiment will be optimized for detection of the $J/\Psi\ K^0_S$ mode and requires a very selective trigger based on J/Ψ recognition and on secondary vertex recognition. The detection product is $\Pi\eta = \eta_{\rm trigger} \cdot \eta_{\rm rec} \cdot \eta_{\rm tag} \cdot (1-2w)^2 \cdot (1-2\chi)^2$ where the additional tag dilution $(1-2\chi)^2$ takes into account wrong-sign tags from $B\overline{B}$ oscillations. The oscillation parameter is measured to be $\chi = 0.12$, see chapter 3.3. The authors of the letter of intent estimate $\eta_{\rm trigger} = 0.70$ and $\eta_{\rm rec} = 0.08$ including vertex cuts. They discuss two different tagging methods, with leptons and with charged Kaons, resulting in

$$\eta_{\rm tag} \cdot (1-2w)^2 = \eta_\ell (1-2w_\ell)^2 + \eta_{\rm K}(1-2w_{\rm K})^2 = 0.15 \cdot 0.68^2 + 0.52 \cdot 0.47^2 = 0.184.$$

The estimate of the statistical error on $A_{\Psi \rm K}$ is the same as in chapter 3.5, $\sigma(A_{\Psi \rm K}) = 1.23/\sqrt{N(b\overline{b}) \cdot \Pi\mathcal{B} \cdot \Pi\eta}$ if the time dependence of $J/\Psi K^0_S$ decays is measured for all decay times. Cutting at $0.7\ \tau_{\rm B}$ increases the information per surviving event by a factor of 2, leading to $\sigma_{\rm stat}(A_{\Psi \rm K}) = 0.87/\sqrt{N(b\overline{b}) \cdot \Pi\mathcal{B} \cdot \Pi\eta}$. Trig-

ger efficiency and radiation damage, which I will not discuss here since the group is still working hard on the estimate of both problems, limits the luminosity to 30 MHz/$\sigma_{\rm inel}$. An advantage of the HERA-B idea is the fact that the luminosity may be kept constant by moving the copper wires in the halo if the halo intensity should vary. This luminosity leads to $\dot{N}(\mathrm{b\overline{b}}) = 30\ \mathrm{MHz} \cdot \sigma(\mathrm{b\overline{b}})/\sigma_{\rm inel} = 2.4 \cdot 10^8/10^7$ s at $E_{\rm lab} = 820$ GeV and to $\sigma_{\rm stat}(A_{\Psi \rm K}) = 0.17$ in one standard year with 10^7 s. For the case that only the $\mu^+\mu^-$ decay of the J/Ψ can be used for an efficient trigger, this error increases from 0.17 to 0.22.

6.2 Faked Asymmetries

In contrast to $\mathrm{e^+e^-}$ experiments, pp and pA experiments have to take care of faked asymmetries because their initial state is not a CP-eigenstate. The observed asymmetry $A_{\rm obs}$ in a CP violation measurement is not only diluted by a factor D but also shifted by a faked asymmetry $A_{\rm f}$,

$$A_{\rm obs} = D \cdot A_{\rm phys} + A_{\rm f}.$$

Three sources of faked asymmetries in pp and pA experiments have been discussed so far,

- $f_0 \neq \overline{f}_0$, i. e. the number of produced $\mathrm{B^0}$ mesons in $\overline{\mathrm{b}}$ jets differs from that of $\overline{\mathrm{B}}^0$ in b jets. One therefore has $N(\mathrm{B^0}) \neq N(\overline{\mathrm{B}}^0)$ in spite of associated production $N(\mathrm{b}) = N(\overline{\mathrm{b}})$,
- $\chi_0 \neq \overline{\chi}_0$, i. e. the oscillation dilution on the tag side is not the same for b and $\overline{\mathrm{b}}$ since $\chi = f_0 \cdot \chi(\mathrm{B^0}) + f_s \cdot \chi(\mathrm{B_s})$ and $f_0 \neq \overline{f}_0$, $f_s \neq \overline{f}_s$,
- $w \neq \overline{w}$, i. e. the tag dilution owing to secondary or misidentified leptons differs for a variety of reasons, misidentification simply because of $N(\pi^+) \neq N(\pi^-)$.

Monte Carlo estimates show that each effect may be in the order of a few percent. Because of the dilution, a total error of $\sigma(A_{\rm f}) = \pm 0.01$ leads to $\sigma(A_{\rm phys}) = \pm 0.01/D$. Since details of the fragmentation process are involved, Monte Carlo estimates of $A_{\rm f}$ are certainly not reliable and control measurements are required. A variety of control measurements has been discussed. An experiment like HERA-B which has to rely on J/Ψ triggers has the possibility to determine $f_0/\overline{f}_0$ from the rates $\mathrm{B^0} \rightarrow \mathrm{J/\Psi\ K^{*0}} \rightarrow \mathrm{J/\Psi\ K^+\pi^-}$ and $\overline{\mathrm{B}}^0 \rightarrow \mathrm{J/\Psi\ \overline{K}^{*0}} \rightarrow \mathrm{J/\Psi\ K^-\pi^+}$ which requires either good $\pi - \mathrm{K}$ identification or very good $\mathrm{K^*}$ mass resolution. Since J/Ψ $\mathrm{K^*}$ with subsequent $\mathrm{K^*}$ decay into charged mesons is not a CP-eigenstate, the direct CP violation in these B-decays is expected to be far below 1 %. The second and third faked asymmetry can be determined from tags of charged B-mesons. Differences in tag efficiencies are determined by $N(\Psi \mathrm{K^+}, \ell^-)/N(\Psi \mathrm{K^+})$ and $N(\Psi \mathrm{K^-}, \ell^+)/N(\Psi \mathrm{K^-})$ and differences in the mistags by $N(\Psi \mathrm{K^+}, \ell^+)/N(\Psi \mathrm{K^+}, \ell^-)$ and $N(\Psi \mathrm{K^-}, \ell^-)/N/\Psi \mathrm{K^-}, \ell^+)$.

The rate of all these control measurements is proportional to that of the asymmetry rates $N(\Psi \mathrm{K^0_S}, \ell^+)$ and $N(\Psi \mathrm{K^0_S}, \ell^-)$. The error on $A_{\rm f}$ is therefore propor-

tional to that on A_{obs} during a wide range of running times. A study for the L3P letter of intent at LHC [32] gave $\sigma_{sys}(A_{\Psi K}) = 0.8 \cdot \sigma_{stat}(A_{\Psi K})$ resulting in $\sigma(A_{\Psi K}) = 1.3 \cdot \sigma_{stat}(A_{\Psi K})$ if both errors are added quadratically. I will use this result in comparing the sensitivities of e^+e^- and pp/pA experiments.

6.3 ATLAS and CMS

The two "universal" LHC experiments are not optimized for CP violation studies in B-decays but offer good prospects nevertheless. Their main handicaps are the limitation to central rapidities, the restricted vertex resolution, and the lack of $\pi - K$ separation. The vertex handicap is not severe since, in contrast to e^+e^- experiments on the $\Upsilon(4S)$, integration over all decay times does not destroy the CP asymmetry. Without any time information, the asymmetry in the $J/\Psi\ K^0_S$ case with only lepton tags is simply given by

$$A_{obs} = \frac{N(J/\Psi K^0_S,\ \ell^-) - N(J/\Psi K^0_S,\ \ell^+)}{N(J/\Psi K^0_S,\ \ell^-) + N(J/\Psi K^0_S,\ \ell^+)}.$$

The integration leads to an additional dilution

$$A_{obs} = (1 - 2\chi) \cdot (1 - 2w) \cdot \frac{x_0}{1 + x_0^2} \cdot A_{\Psi K},$$

where $x_0 = 0.69$, see chapter 3.3, $x_0/(1 + x_0^2) = 0.47$, and to the following error estimate:

$$\sigma(A_{\Psi K}) = \frac{1.50}{\sqrt{N(b\bar{b}) \cdot \Pi\mathcal{B} \cdot \Pi\eta}}.$$

In recent studies for $A_{\Psi K}$, ATLAS quotes $\eta_{trigger} \cdot \eta_{rec} \cdot \eta_{tag} = 4 \cdot 10^{-5}$, and the corresponding product for CMS is estimated to be $1 \cdot 10^{-4}$. Both experiments tag with muons only. The ATLAS estimate for mistags is $1 - 2w = 0.72$. Taking the same value for CMS and assuming a $b\bar{b}$ production cross section of 400 μb and an initial LHC luminosity of $10^{33}/cm^2/s$ leads to $\sigma(A_{\Psi K}) = 1.3 \cdot \sigma_{stat}(A_{\Psi K}) = 0.070$ (ATLAS) and 0.062 (CMS) in 10^7 s.

In addition to measuring the CP asymmetry in $B^0 \to J/\Psi\ K^0_S$ decays, the two universal LHC detectors have good prospects for seeing the B_c meson and to look for $B^0 \to \mu^+\mu^-$ with sensitivities of $\sigma(\mathcal{B}) \sim 10^{-9}$. The CP asymmetry for $B^0 \to \pi^+\pi^-$ can probably not be measured because of too high background and missing $\pi - K$ separation.

6.4 COBEX, GAJET, and LHB

Since letters of intent for the three specialized B-meson experiments are only expected for October 93, I do not want to discuss details of them here. All three intend to measure $B_s\overline{B}_s$ oscillations and CP asymmetries in both $J/\Psi\ K^0_S$ and $\pi^+\pi^-$. They are therefore all equipped with good vertex resolution and good particle identification.

COBEX wants to work in the LHC collider mode (7+7 TeV), with reduced luminosity of about $10^{32}/\mathrm{cm}^2/\mathrm{s}$ for not confusing secondary vertices with multiple pp interactions at the trigger level. The spectrometer covers one forward region up to about 600 mrad which contains two orders of magnitude more B mesons than the central region of ATLAS/CMS. Figures of merit for the pilot quantity $A_{\Psi K}$ will be shown in Table 3.

The two fixed target experiments GAJET and LHB have similar spectrometer geometries but completely different beam-target philosophies. GAJET wants to collide the full intensity of one circulating proton beam with a thin hydrogen gas jet. Some of the very forward decay products and tags are therefore lost in the beam pipe which runs through the spectrometer like in a collider experiment. LHB wants to work with an extracted proton beam and its interactions with a Cu target of $5 \div 10$ mm thickness. This geometry allows a spectrometer without beam tube, $\vartheta_{\min}$ is only defined by minute blind regions in the center of all detector elements.

Proton extraction for LHB is planned with the help of a bent crystal in the halo of one proton beam. Due to channeling, the quartz crystal bends about 10 % of the halo protons into an angle of 0.7 mrad, and subsequent septum and bending magnets enlarge the bend to about 20 mrad. It is still open if the extracted proton beam should be sent into a new experiment hall for LHB or if an extraction place can be found in such a way that LHB could be mounted into an existing LEP hall. In April 93 tests at the CERN-SPS have reached $(12 \pm 3)\%$ extraction efficiency with the bent crystal method. See Table 3 for $\sigma(A_{\Psi K})$ estimates.

6.5 A New Idea

During this conference I got confronted [33] with an idea which looks extremely interesting at a first glance. $B\overline{B}$ production in hadron-hadron collisions requires high luminosity and high centre-of-mass energy. Proton - antiproton collisions do not yet give enough luminosity for CP violation studies. LHC will offer good luminosity and comfortable $b\overline{b}$ fractions both in the collider ($\sigma_{b\overline{b}}/\sigma_{\mathrm{inel}} \sim 3 \cdot 10^{-3}$) and in the fixed target mode ($\sim 5 \cdot 10^{-5}$). On the other hand, experiments at LHC are not expected to start before the end of this century.

The highest energy hadron beam which is available in Europe now is the 820 GeV proton beam in HERA. If collided with a fixed target, the centre-of-mass energy is very low, $\sqrt{s} = 39$ GeV with $\sigma_{b\overline{b}}/\sigma_{\mathrm{inel}}(\mathrm{pCu}) \sim 8 \cdot 10^{-7}$. This energy, together with the limiting luminosity of about 30 MHz/σ_{inel}, is on the very low side for a successful experiment. A fascinating possibility is offered by the fact that HERA consists of two storage rings. If one could fill the 30 GeV electron ring with protons between 10 and 40 GeV ($\sqrt{s} = 180 \div 360$ GeV), this would change the conditions for the HERA-B proposal drastically. Second condition: the luminosity should reach a few $10^{32}/\mathrm{cm}^2/\mathrm{s}$ in order to be competitive with an e^+e^- B-Meson Factory.

7. Conclusions

Finding the origin of CP violation is, together with understanding the origin of mass, one of the two big remaining puzzles in particle physics. In the Standard Model, these two problems are even intimately connected with each other. Experimental progress will come from finding or excluding the Higgs scalar, determining its mass, and well determining the remaining Standard Model parameters ϑ_{23}, ϑ_{13}, and δ_{13}. The latter three are a domain of B-meson decays, and the necessary experiments involve both CP-conserving (a, b, and c below) and CP-violating (d and e below) observations. Five measured quantities will overconstrain the unitarity triangle in Fig. 4 and thereby both determine ϑ_{23}, ϑ_{13}, δ_{13} and test the completeness of the Standard Model in the CP sector.

These experiments can be done in e^+e^- annihilation at threshold, in e^+e^- annihilation at high energies (e. g. at m_Z), or in high-energy hadron-hadron collisions. Since there are no prospects for obtaining an e^+e^- luminosity at $\sqrt{s} = m_Z$ which is two orders of magnitude above that of LEP, I have discussed only the two other routes. How do they compare with each other?

Qualitatively, out of the five key observations

a) $b \to c\ell\nu$, preferentially $d\Gamma(B \to D^*\ell\nu)/d(vv')$,

b) $b \to u\ell\nu$, preferentially $d^2\Gamma(B \to \rho,\omega\ell\nu)/dp_\ell dq^2$,

c) $x(B_s \leftrightarrow \overline{B}_s)/x(B^0 \leftrightarrow \overline{B}^0)$,

d) $A(B^0, \overline{B}^0 \to J/\Psi K_S^0)$, and

e) $A(B^0, \overline{B}^0 \to \pi^+\pi^-)$,

I see clear advantages for a), b) and e) in e^+e^- annihilation, requiring boosted $\Upsilon(4S)$ meson production with luminosities of some $10^{33}/cm^2/s$. Hadron-hadron collisions and e^+e^- annihilation may give comparable results for c) and d) in the beginning. Since hadron-hadron collisions offer the higher B-meson rates at long term, an increase of precision in c) and d) is probably easier to obtain there.

Quantitatively, I want to limit my comparison to only d) since this has been used as "pilot reaction" in essentially all B-decay proposals during the last years. Table 3 summarizes the relevant figures of merit for equal amounts of running time, $T = 10^7 s$. All mentioned experiments have good prospects for observing a CP asymmetry in $B^0, \overline{B}^0 \to J/\Psi\ K_S^0$ if Standard Model physics is the only or the dominant origin of CP violation. We should keep in mind, however, that the so often repeated look onto this Table sees only one side of the CP medal and that the other side, increasing precision on ϑ_{23}, ϑ_{13}, and δ_{13}, is as important for the progress of Physics.

Table 3: Figures of merit for proposed and discussed experiments to measure the CP asymmetry in the decay modes $B^0, \overline{B}^0 \to J/\Psi\ K^0_S$. $f_0 = N(B^0)/N(\overline{b})$. The decay fraction product $\Pi\mathcal{B}$ is not always the same since some experiments reconstruct J/Ψ with only $\mu^+\mu^-$ and PEP-II may be able to reconstruct K^0_S also with $\pi^0\pi^0$. I is the information per reconstructed and tagged decay. The total error σ is the quadratic sum of statistical (σ_{stat}) and systematic error, for a data taking time of 10^7 s. The last line stresses the fact that e^+e^- experiments may combine several decay modes which is hardly possible in hadronic experiments.

	PEP-II [1]	ATLAS	CMS	COBEX	GAJET	LHB	HERA-B
$\mathcal{L}[cm^{-2}s^{-1}]$	$3 \cdot 10^{33}$	10^{33}	10^{33}	10^{32}	20 MHz	10 MHz	30 MHz
$\sigma(b\overline{b})$	1 nb	400 μb	400 μb	400 μb	1 μb	1 μb	12 nb
f_0	0.50	0.38	0.38	0.38	0.38	0.38	0.38
tag	e+μ+K	μ	μ	e+μ+K	e+μ+K	e+μ [2]	e+μ+K
J/Ψ rec.	e+μ	e+μ	μ	μ	e+μ	e+μ	μ or e+μ
$\Pi\mathcal{B}$ $[10^{-5}]$	2.2, 3.2	1.7	0.8	0.8	1.7	1.7	0.8, 1.7
$\eta_{trigger}$	1.0	↓	↓	↓	↓	↓	0.7
η_{rec}	0.55	↓	↓	↓	↓	↓	0.08
η_{tag}	0.35	↓	↓	↓	↓	↓	0.67
$\eta_{tr}.\eta_{rec}\eta_{tag}$	0.193	$4 \cdot 10^{-5}$	10^{-4}	$5 \cdot 10^{-3}$	0.024	0.030	0.038
w	0.10	0.14	0.14	0.24	0.16	0.12	0.24
$1 - 2\chi$	1.0 [3]	0.76	0.76	0.76	0.76	0.76	0.76
I	0.33 [4]	0.22 [5]	0.22 [5]	~ 0.6 [6]	~ 0.6 [6]	0.33 [4]	0.66 [6]
$\sigma_{stat}(A_{\Psi K})$	0.14, 0.10	0.054	0.048	0.018	0.027	0.038	0.24, 0.17
$\sigma(A_{\Psi K})$	0.14, 0.10	0.07	0.062	0.023	0.035	0.05	0.31, 0.22
$\sigma(\sin 2\beta)$	$\to 0.06$	dto.	dto.	dto.	dto.	dto.	dto.

1) The figures for CESR-B and TRISTAN-3 are essentially the same as for PEP-II. 2) LHB may well be able to tag also with Kaons. 3) Owing to the $B\overline{B}$ coherence on the $\Upsilon(4S)$, a background-free tag defines the flavour of the other B-meson at the moment of the tagging decay irrespective of $B^0\overline{B}^0$ oscillations. 4) from the full decay vertex distribution. 5) integrated over all decay times. 6) with vertex cuts; information per remaining event.

References

[1] S. Palestini, these Proceedings
[2] N. Cabibbo, Phys. Rev. Lett. 10 (1963) 531
M. Kobayashi and T. Maskawa, Progr. Theor. Phys. 49 (1973) 652
[3] M. Schmidtler and K. R. Schubert, Z. Physik C 53 (1992) 347
[4] G. Buchalla, A. J. Buras, and M. K. Harlander, Nucl. Phys. B 349 (1991) 1, and references therein
[5] M. Perl et al. (SLAC-LBL), Phys. Rev. Lett. 35 (1975) 1489
[6] Review of Particle Properties, Particle Data Group, Phys. Rev. D 45 (1992) S1
[7] H. Leutwyler and M. Roos, Z. Physik C 25 (1984) 91
[8] D. Karlen, review talk at the 6th Int. Symp. on Heavy Flavour Physics, Montreal (Canada), July 1993
[9] R. Poling, review talk at the 6th Int. Symp. on Heavy Flavour Physics, Montreal (Canada), July 1993
[10] H. Albrecht et al. (ARGUS), Phys. Lett. B 234 (1990) 409, B 255 (1991) 297
[11] R. Fulton et al. (CLEO), Phys. Rev. Lett. 64 (1990) 16 and ref. 9
[12] G. Altarelli et al., Nucl. Phys. B 208 (1982) 365
[13] K. Wille, Proc. Int. Symp. on Production and Decay of Heavy Hadrons, Heidelberg (Germany) 1986, ed. by K. R. Schubert and R. Waldi, p. 473,
R. Eichler et al. SIN-PR-86-13 (1986), and
Proposal PSI-PR-88-09 (1988),
updated for energy-asymmetry in PSI-PR-88-22 (1988)
[14] N. Isgur and M. B. Wise, Phys. Lett. B 232 (1989) 113 and B 237 (1990) 527
[15] H. Albrecht et al. (ARGUS), Z. Physik C 57 (1993) 533
[16] CERN yellow report 90-02 (1990), ed. by T. Nakada, p. 26
[17] H. G. Moser, review talk at the 6th Int. Symp. on Heavy Flavour Physics, Montreal (Canada), July 1993
[18] J. D. Bjorken, presented in discussions at the Workshop on Experiments, Detectors, and Experimental Areas for the SSC, Berkeley, July 1987 ;
C. Jarlskog and R. Stora, Phys. Lett. B 208 (1988) 268, and references therein
[19] CERN yellow report 90-02 (1990), ed. by T. Nakada, p. 24
[20] J. E. Bartelt, SLAC BaBar note 103 (1993), unpublished
[21] J. Lefrançois (LEP), plenary talk at the Int. Europhysics Conf. on High Energy Physics, Marseille (France), July 1993
[22] D. Amidei (CDF), invited talk at the 6th Int. Symp. on Heavy Flavour Physics, Montreal (Canada), July 1993
[23] T. Nakada, Int. Symp. on Heavy Quark Physics, Ithaca (NY, USA) 1989, AIP Conference Proc. 196 (1989) 385
[24] S. Stone, review talk at the 6th Int. Symp. on Heavy Flavour Physics, Montreal (Canada), July 1993
[25] P. J. Oddone, SLAC-400 (1992) 1

[26] B. Cox and K. Stanfield, theses Proceedings
[27] see e. g. Proc. Int. Workshop on B-Physics at Hadron Machines, ed. by P. Schlein, Liblice (Czech Republic) 1993, Nucl. Instr. Meth. A 333 (1993)
[28] H. Albrecht et al., Letter of Intent DESY-PRC 92/04 (1992)
[29] D. Gingrich et al., Letter of Intent CERN/LHCC/92-4 (1992)
[30] M. Markytan et al., Letter of Intent CERN/LHCC/92-3 (1992)
[31] P. Nason, S. Dawson, and R. K. Ellis, Nucl. Phys. B 303 (1988) 607, B 327 (1989) 49, and B 335 (1990) 260
[32] V. Shoutko (L3P), private communication
[33] Y. Giomataris and D. Kaplan, private communication

Frascati Physics Series, Vol. 1 (1993)
HEAVY QUARKS AT FIXED TARGET
Frascati, May 31st – June 2nd 1993
(pp. 285–294)

PRODUCTION AND DECAY OF BEAUTY–BARYON

A. Fridman+
INFN, Sezione di Trieste
Strada Costiera, 11 Miramare, I-34014 Trieste, (ITALIA)

ABSTRACT

We estimate the beauty-baryon production in pN interactions at c.m. energies relevant to the LHC and SSC projects. The possibilities of searching for the CP violation effects in the beauty baryon are discussed. Measurements of special decay channels are suggested in order to estimate $|V_{ub}/V_{cb}|$ with good precision.

1 - Introduction

Recently, the reasons for studying the beauty baryon produced in pN interactions have been presented[1,2]. Here we will summarize some of these aspects. We will discuss the interest in searching for CP violation in beauty-baryon decay as well as the measurements of some CKM matrix elements. A list of beauty baryons (N_b) with their charge and quark content is given in Table 1. We use the following notation[1]. The baryon with isospin $I = 1$ will be denoted by Σ, whereas Ξ will be used for baryons having $I = 1/2$. For $I = 0$, we use Λ unless each quark forming a baryon has $I = 0$. In this case the notation will be Ω. The subscripts of Σ, Ξ, Λ, and Ω indicate the number and the type of the heavy quarks ($Q \equiv b, c$) contained in the considered baryon (the light quarks are represented by $q \equiv u, d, s$). The masses given in the table are those used in the PYTHIA Monte Carlo program[3].

We estimate the $N_b = bq_1q_2$ production cross-section, $\sigma(bq_1q_2)$, from the ratio $R = \sigma(bq_1q_2)/\sigma(b\bar{b})$ calculated with PYTHIA at the c.m. energies of $\sqrt{s} = 0.12, 0.19, 16$ and 40 TeV, corresponding to the LHC and SSC projects (beam fixed-target and collider experiments). Here $\sigma(b\bar{b})$ is the $pN \to b\bar{b}X$ cross-section (X meaning anything) at the corresponding c.m. energy. Using the $\sigma(b\bar{b})$ cross-sections[4] given in Table 2, we obtain the cross-sections indicated[5] by Table 3.

Estimates of $\sigma(bcq)$ are based on the fact that the momentum of the light quark will be negligible with respect to the momentum of the b or c quark. The kinematics as well as the QCD interactions in the final state will thus depend essentially on the bc system. Therefore a rough estimate of $\sigma(bcq)$ could be written as[2]

+ LPNHE, Université de Paris VI et VII

Table 1 - Various beauty baryons using the notation explained above. The charge and the quarks forming the baryons are also given. The mass values are those used in the PYTHIA Monte Carlo program.

	Quarks	Charge	Mass (GeV)
Λ_b	bud	0	5.62
Σ_b	buu	+1	5.80
	bdu	0	"
	bdd	−1	"
Ξ_b	bsu	0	5.84
	bsd	−1	"
Ξ_{bc}	bcu	+1	7.01
	bcd	0	"
Ξ_{2b}	bbu	0	10.42
	bbd	−1	"
Ω_b	bss	−1	6.12
Ω_{bc}	bcs	0	7.19
Ω_{b2c}	bcc	+1	8.31
Ω_{2b}	bbs	−1	10.60
Ω_{2bc}	bbc	0	11.71
Ω_{3b}	bbb	−1	15.11

$$\sigma(bcq) \simeq \sigma(\bar{B}_c)\, G \times \eta_q \,, \tag{1}$$

($\bar{B}_c \equiv b\bar{c}$) where $G = 1/2$ is a color factor comparing the bcq color singlet with the $b\bar{c}$ one and where $\sigma(\bar{B}_c)$ is the $pp \to \bar{B}_c X$ cross-section[6,7]. The estimate of η_q is obtained from the probability of producing a given q quark using the following ratio[2]:

$$bu : bd : bs : bqq = 0.38 : 0.38 : 0.14 : 0.10 \,. \tag{2}$$

The $\sigma(bcq)$ values are then obtained (Table 3), taking the $\sigma(\bar{B}_c)$ from Ref. 7. Table 3 indicates also the number of N_b events expected in one year (10^7 s) of running.

Table 2 - The cross-section values utilized to determine $\sigma(bq_1q_2)$ and $\sigma(bcq)$.

σ	Ref.	0.12 TeV	0.19 TeV	16 TeV	40 TeV
$\sigma(b\bar{b})$	4	~ 2 μb	~ 2.5 μb	~ 200 μb	~ 500 μb
$\sigma(\bar{B}_c)$	6	$\sim$1 nb	–	$\sim$180 nb	–
$\sigma(\bar{B}_c$ or $\bar{B}_c^*)$	7	$\sim$27 pb	~ 100 pb	~ 60 nb	~ 147 nb

Table 3 - Cross-section estimates of the $pN \to N_bX$ reactions for various c.m. energies corresponding to fixed-target and collider experiments. Estimates of the number of N_bX events produced in one year (10^7 s) of running are also given. For the beam target experiments a Cu target was considered with a length of 5 mm along the beam direction and a beam of 10^8 p/s. A luminosity of L=10^{32} cm^{-2}s^{-1} was taken for the colliders.

N_b	0.12 TeV	0.19 TeV	16 TeV	40 TeV
Λ_b	$(1.7 \pm 0.3)\ 10^{-1}$ μb $\sim 4.6\ 10^8$/year	$(1.78 \pm 0.01)\ 10^{-1}$ μb $\sim 4.8\ 10^8$/year	17.0 ± 0.1 μb $\sim 2\ 10^{10}$/year	43.4 ± 0.4 μb $\sim 4\ 10^{10}$/year
Σ_b	$(1.84 \pm 0.02)\ 10^{-2}$ μb $\sim 5\ 10^7$/year	$(2.75 \pm 0.05)\ 10^{-2}$ μb $\sim 7.4\ 10^7$/year	2.9 ± 0.1 μb $\sim 3\ 10^9$/year	7.3 ± 0.2 μb $\sim 7\ 10^9$/year
Ξ_b	$(1.70 \pm 0.02)\ 10^{-2}$ μb $\sim 4.6\ 10^7$/year	$(2.45 \pm 0.05)\ 10^{-2}$ μb $\sim 6.6\ 10^7$/year	2.4 ± 0.1 μb $\sim 2\ 10^9$/year	5.8 ± 0.2 μb $6\ 10^9$/year
Ω_b	$(2.0 \pm 0.4)\ 10^{-4}$ μb $\sim 5.4\ 10^5$/year	$(2.5 \pm 0.5)\ 10^{-4}$ μb $\sim 6.8\ 10^6$/year	$(2.0 \pm 0.4)\ 10^{-2}$ μb $\sim 2\ 10^7$/year	$(10 \pm 2)\ 10^{-2}$ μb $\sim 10^8$/year
Ξ_{bc}	~ 6 pb $\sim 1.6\ 10^4$/year	~ 21 pb $\sim 5.7\ 10^4$/year	~ 13 nb $\sim 10^7$/year	~ 31 nb $3\ 10^7$/year
Ω_{bc}	~ 2 pb $\sim 5.4\ 10^3$/year	~ 8 pb $\sim 2.2\ 10^4$/year	~ 5 nb $\sim 5\ 10^6$/year	~ 12 nb $\sim 10^7$/year

For the collider we use a luminosity of $L = 10^{32}$ cm^{-2}s^{-1}, whereas for the beam-target interactions we consider a beam of 10^8 p/s and a Cu target having a length of 5 mm along the beam direction.

The present estimates indicate that both collider projects (LHC and SSC) lead to similar statistics. With the present fixed-target example the statistics are lower by a factor of $\sim$ 100 with respect to the collider experiments where $L = 10^{32}$cm^{-2}s^{-1}. The choice of longer targets as well as larger luminosities could certainly be envisaged. Within the present estimates, the search for *bcq* baryons could be carried out with the collider experiments.

2 - Comments about the search for CP violation

Similarly to the search for CP violation in the $B^{\pm}$ decay, the study of beauty-baryon decays does not need tagging processes of the associated beauty hadron produced in the same event. However, the search for an asymmetry in the B^+/B^- decay or in one of the cases, $\Lambda_b/\bar{\Lambda}_b$, $\Sigma_b/\bar{\Sigma}_b$, $\Xi_b/\bar{\Xi}_b$, etc., would, in principle, depend on final-state interactions[8].

In the present discussion, let us consider a beauty baryon of spin 1/2 decaying into two hadrons having spin 0 and 1/2 (this situation is similar to $\Lambda \to p\pi$ and $\Xi \to \Lambda\pi$ studied about 30 years ago[9]). The weak decay in these cases will be described by S and P waves (corresponding to relative orbital momenta of $l = 0, 1$, respectively). The partial width Γ and the decay parameters α, β and γ of N_b ($\alpha^2 + \beta^2 + \gamma^2 = 1$) as well as those related to $\bar{N}_b$ (having a bar sign on the parameters) can be used to search for CP violation by testing the non-zero values of the following ratios[9,10]:

$$\Delta = \frac{\Gamma - \bar{\Gamma}}{\Gamma + \bar{\Gamma}} , \tag{3a}$$

$$A = \frac{\Gamma\alpha + \bar{\Gamma}\bar{\alpha}}{\Gamma\alpha - \bar{\Gamma}\bar{\alpha}} \simeq \frac{\alpha + \bar{\alpha}}{\alpha - \bar{\alpha}} , \tag{3b}$$

$$B = \frac{\Gamma\beta + \bar{\Gamma}\bar{\beta}}{\Gamma\beta - \bar{\Gamma}\bar{\beta}} \simeq \frac{\beta + \bar{\beta}}{\beta - \bar{\beta}} . \tag{3c}$$

Note that for a given CP violation effect we expect[10] that $|B| \gg |A| \gg |\Delta|$, indicating that the measurements of β and $\bar{\beta}$ might be very useful. In fact, even with CP violation, $\Delta \neq 0$ can only occur when more than one isospin transition (between the initial and final state) is present (see for instance Ref. 1).

The relations between the various parameters are given in Table 4 for CP conservation or violation in the beauty-baryon decay[1]. For each case we consider

Table 4 - The Γ, α and β relations between the N_b and $\bar{N}_b$ decays for CP conservation or violation. In each case final-state interactions (FSI) were assumed or neglected.

CP conservation		CP violation	
FSI	No FSI	FSI	No FSI
$\Gamma = \bar{\Gamma}$	$\Gamma = \bar{\Gamma}$	$\Gamma \neq \bar{\Gamma}^*$	$\Gamma = \bar{\Gamma}$
$\alpha = -\bar{\alpha}$	$\alpha = -\bar{\alpha}$	$\alpha \neq -\bar{\alpha}$	$\alpha = -\bar{\alpha}$
$\beta = -\bar{\beta}$	$\beta, \bar{\beta} = 0$	$\beta \neq -\bar{\beta}$	$\beta = \bar{\beta}$

* With only one isospin transition, $\Gamma = \bar{\Gamma}$ (see text).

the presence of final-state interactions or decay processes where the final state could be neglected. Note that non-zero values of the β or $\bar{\beta}$ parameters are related to the violation of the time reversal (T) applied to the considered decay process, and hence to the CP violation (CPT rule). However, final-state interactions can also lead to $\beta, \bar{\beta} \neq 0$. Table 4 indicates the relations between β and $\bar{\beta}$ that could indicate the violation of time reversal.

To clarify the discussion, we consider the $pp \to \Lambda_b X$ reaction with the weak decays of $\Lambda_b \to \Lambda\pi^0$ and $\Lambda \to p\pi^-$. Let us now see how to measure the $\alpha \equiv \alpha(\Lambda_b)$ and $\beta \equiv \beta(\Lambda_b)$ parameters [$\bar{\alpha} \equiv \bar{\alpha}(\bar{\Lambda}_b)$ and $\bar{\beta} \equiv \bar{\beta}(\bar{\Lambda}_b)$]. To this end we consider the angular distributions of the proton in the Λ rest frame with respect to the coordinate system shown in Fig. 1 and given by (see Appendix B in Ref. 1):

$$I(\theta_3) \propto 1 + \alpha(\Lambda_b)\alpha(\Lambda)\cos\theta_3 \ . \tag{4}$$

$$I(\theta_2) \propto 1 - \frac{\pi}{4} P(\Lambda_b)\beta(\Lambda_b)\alpha(\Lambda)\cos\theta_2 \ , \tag{5}$$

$$I(\theta_1) \propto 1 - \frac{\pi}{4} P(\Lambda_b)\gamma(\Lambda_b)\alpha(\Lambda)\cos\theta_1 \ . \tag{6}$$

The Λ distribution with respect to the Λ_b polarization [$\vec{P}(\Lambda_b)$, modulus $P(\Lambda_b)$] in the Λ_b rest frame is (see Fig. 1):

$$I(\Theta) \propto 1 + \alpha(\Lambda_b)P(\Lambda_b)\cos\Theta \ . \tag{7}$$

The $\alpha(\Lambda_b)$ decay parameter can be measured with the distribution given by formula (4). Thus a measurement of $P(\Lambda_b)$ would be possible with distribution (7) valid in the Λ_b rest frame. If $P(\Lambda_b) \neq 0$, one could determine $\beta(\Lambda_b)$ and $\gamma(\Lambda_b)$ [formulae (5) and (6)].

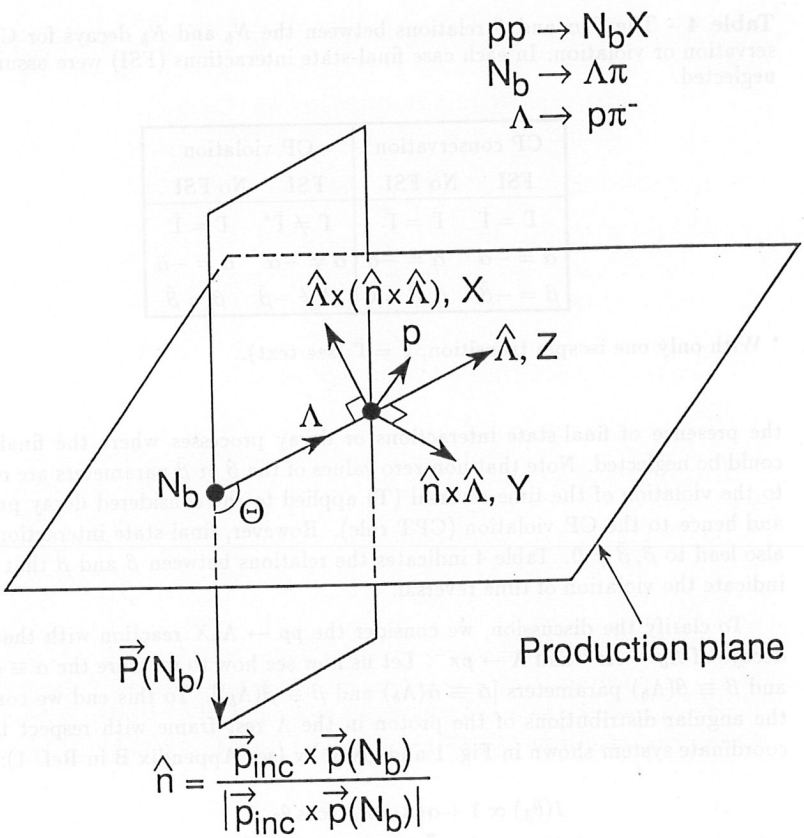

Fig. 1 - The production plane of the $pp \to N_b X$ reaction and the $\vec{P}(N_b)$ polarization normal to this plane. The X, Y, Z represent the coordinate system used in the Λ rest frame for defining the p angular (θ_{1-3}) distributions coming from the $\Lambda \to p\pi$ decay. Here Θ is the Λ emission angle with respect to the $P(N_b)$ direction in the N_b rest frame.

Finally, we summarize the suggestions for measurements related to beauty baryons as follows

- production rates and branching ratios of N_b or/and $\bar{N}_b$,
- existence of baryons having more than one heavy quark,
- measurement of $\alpha(N_b)$ and $\bar{\alpha}(\bar{N}_b)$ for given decay channels.
- measurement of the polarization $P(N_b)$ and $P(\bar{N}_b)$,
- search for CP violation in the N_b, $\bar{N}_b$ decay by comparing their partial decay widths as well as $\alpha(N_b)$ with $\bar{\alpha}(\bar{N}_b)$,
- search for T reversal violation for beauty baryons decaying into two particles having $J = 0$ and $1/2$ if $P(N_b), P(\bar{N}_b) \neq 0$.

3 - CKM matrix elements

The lifetime of beauty baryons is expected to be shorter than that of the B mesons, similarly to the case of charmed hadrons[2]. The Λ_c, Ξ_c^0 are shorter than D^0 (which have similar non-spectator contributions) and Ξ_c^+ shorter than $D^\pm$ (which have less substantial non-spectator contributions). The argument is that QCD color factors make the meson lifetimes longer, basically due to the stronger binding of the light quarks. This difference in QCD effects could facilitate the determination of the CKM matrix elements (V_{ij}) in the beauty-baryon decays. In fact, the QCD effects are expected to be similar for the decay of $N_b \to D^0 X'$, $\bar{D}^0 X'$ (X' representing here either a nucleon, hyperon, charmed or beauty baryon). This is because the spectator graphs yield similar amplitudes. Note, however, that the non-spectator diagrams are different for $N_b \to D^0 X'$ and $N_b \to \bar{D}^0 X'$. This can be seen from Fig. 2, which shows the example of $\Lambda_b \to D^0\Lambda$, $\bar{D}^0\Lambda$ decay. Assuming that the spectator model (factorization process) is dominant in the decay process, the measurement of branching ratios (BR) with $X' \equiv \Lambda, p$ (see Fig. 2) leads to:

$$\frac{BR(\Lambda_b \to \bar{D}^0 \Lambda)}{BR(\Lambda_b \to D^0 \Lambda)} = \frac{|V_{ub}\, V_{cs}|^2}{|V_{cb}\, V_{us}|^2}\,, \tag{8}$$

$$\frac{BR(\Lambda_b \to \bar{D}^0 p)}{BR(\Lambda_b \to D^0 p)} = \frac{|V_{ub}\, V_{cd}|^2}{|V_{cb}\, V_{ud}|^2}\,. \tag{9}$$

The errors in the measured $|V_{cs}|, |V_{us}|, |V_{cd}|, |V_{ud}|$ values are small[2], and will introduce in formulae (8) and (9), only a small systematic error on the $|V_{ub}/V_{cb}|$ measurement, of the order of 10^{-2}.

The decay $B^\pm \to D^0 K^\pm, \bar{D}^0 K^\pm$ could also be used to estimate CKM matrix

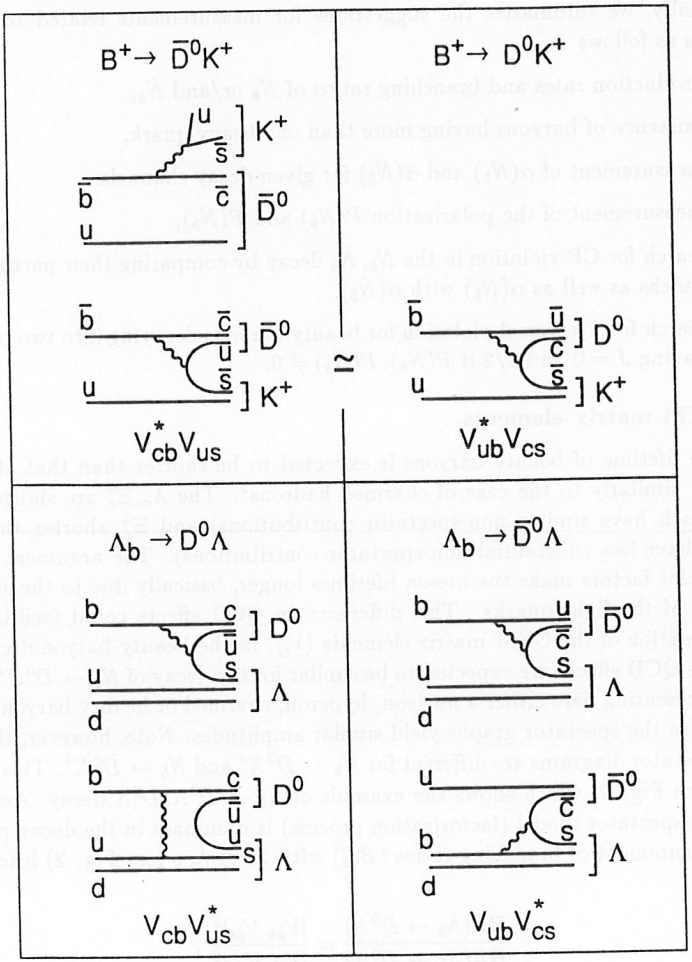

Fig. 2 - Diagrams for the $B^+ \to \bar{D}^0 K^+, D^0 K^+$ (top) and $\Lambda_b \to D^0\Lambda, \bar{D}^0\Lambda$ (bottom) decay channels (see also Ref. 4). The CKM matrix elements entering in the diagrams are indicated. Note that the same kind of diagrams apply for the charge conjugated reactions but where $V_{ij} \leftrightarrow V^*_{ij}$.

Table 5 - Examples of N_b decays having final states that could be easily detected. The Λ decay is not shown as we always consider the $\Lambda \to \pi^- p$ process.

$b \to q$	Baryon decay	Final state
$b \to u$	$\Omega_b^- \to \pi^- \Xi^0, \quad \Xi^0 \to \Lambda\pi^0$	$\pi^-\pi^0\Lambda$
$b \to c$	$\Omega_b^- \to \pi^- \Omega_c^0, \quad \Omega_c^0 \to \pi^+\Omega^-, \quad \Omega^- \to K^-\Lambda$	$\pi^-\pi^+K^-\Lambda$
$b \to u$	$\Xi_b^0 \to \pi^- \Sigma^+, \quad \Sigma^+ \to p\pi^0$	$\pi^-\pi^0 p$
$b \to c$	$\Xi_b^0 \to \pi^- \Xi_c^+, \quad \Xi_c^+ \to \pi^+\Xi^0, \quad \Xi^0 \to \pi^0\Lambda$	$\pi^-\pi^+\pi^0\Lambda$
$b \to u$	$\Xi_b^- \to \pi^- \Lambda,$	$\pi^-\Lambda$
$b \to c$	$\Xi_b^- \to \pi^- \Xi_c^0, \quad \Xi_c^0 \to \pi^+\Xi^-, \quad \Xi^- \to \pi^-\Lambda$	$\pi^-\pi^-\pi^+\Lambda$
$b \to u$	$\Lambda_b^0 \to \pi^- p,$	$\pi^- p$
$b \to c$	$\Lambda_b^0 \to \pi^- \Lambda_c^+, \quad \Lambda_c^+ \to \pi^+\Lambda$	$\pi^-\pi^+\Lambda$

elements. Two spectator diagrams will, however, contribute to the $B^+ \to \bar{D}^0 K^+$ ($B^- \to D^0 K^-$) processes (Fig. 2). This will complicate the extraction of the CKM matrix elements relations. In addition, there will be stronger QCD effects, as already stated above.

We present in Table 5 some beauty-baryon decays that could be measured easily. Here the $b \to c$ and $b \to u$ transitions lead to different final states. The QCD effects could then be different in each diagram. Nevertheless, comparison of the following measured ratios,

$$\frac{BR(\Omega_b^- \to \pi^- \Xi^0)}{BR(\Omega_b^- \to \pi^- \Omega_c^0)} \simeq \frac{|V_{ub}|^2}{|V_{cb}|^2} \frac{\phi(u)}{\phi(c)}$$

$$\frac{BR(\Xi_b^0 \to \pi^- \Sigma^+)}{BR(\Xi_b^0 \to \pi^- \Sigma_c^+)} \simeq \frac{|V_{ub}|^2}{|V_{cb}|^2} \frac{\phi(u)}{\phi(c)}$$

$$\frac{BR(\Xi_b^0 \to \pi^- \Lambda)}{BR(\Xi_b^0 \to \pi^- \Xi_c^0)} \simeq \frac{|V_{ub}|^2}{|V_{cb}|^2} \frac{\phi(u)}{\phi(c)}$$

$$\frac{BR(\Lambda_b \to \pi^- p)}{BR(\Lambda_b \to \pi^- \Lambda_c)} \simeq \frac{|V_{ub}|^2}{|V_{cb}|^2} \frac{\phi(u)}{\phi(c)}$$

with formulae (8) and (9) will allow the comparison of QCD effects in beauty-baryon decays. Here $\phi(u)$ $[\phi(b)]$ is the phase-space factor corresponding to the $b \to u$ $[b \to c]$ transition for a specific final state.

References

1) A. Fridman and R. Kinnunen, Comments on Beauty Baryon Decays and CP-Violation Effects, preprint CERN-PPE/93-61 (1993).

2) A. Fridman and B. Margolis, Beauty Baryon Production and Decays, and CKM Matrix Elements, preprint CERN-TH.6878/93 (1993).

3) H.-U. Bengtsson and T. Sjöstrand, Comput. Phys. Commun. 46 (1987) 43; T. Sjöstrand, preprint CERN-TH.6488/92 (1992).

4) K.J. Foley et al., Proc. Workshop on Experiments, Detectors, and Experimental Areas for the Supercollider, Berkeley, 7-17 July (1987).

5) A. Fridman and R. Kinnunen, Estimates of Beauty Cross-Sections in pN collisions, preprint HU-SEFT, R 1993-03 (1993)

6) M. Lusignoli, M. Masetti and S. Petrarca, Phys. Lett. B266 (1991) 142 .

7) Chao-Hsi Chang and Yu-Qi Chen, The Hadronic Production of the B_c Meson at Tevatron, LHC and SSC, AS-ITP-92-74 Preprint (1992).

8) I.I. Bigi and A.I. Sanda, Nucl. Phys. B281 (1987) 41.

9) See, for instance:
T.D. Lee and C.N. Yang, Phys. Rev. 108 (1957) 1645;
J.W. Cronin and O.E Overseth, Phys. Rev. 129 (1963) 1795;
G. Källen, Elementary Particle Physics, Addison-Wesley Company Inc., Reading, Massachusetts, 1964;
T.D. Lee, Prelude in Theoretical Physics, North-Holland Publishing Company, Amsterdam, 1966;
P. Eberhard, J. Button-Shafer and D.W. Merril, UCRL-11427 Berkeley
P.M. Dauber et al., Phys. Rev. 179 (1969) 1261.

10) J.F. Donoghue and Sandip Pakvasa, Phys. Rev. Lett. 55 (1985) 162;
J.F. Donoghue, Xiao-Gang He and Sandip Pakvasa, Phys. Rev. D34 (1986) 833.

Frascati Physics Series, Vol. 1 (1993)
HEAVY QUARKS AT FIXED TARGET
Frascati, May 31st – June 2nd 1993
(pp. 295–304)

PERSPECTIVES OF AN ASYMMETRIC PROTON COLLIDER WITH A CROSSING ANGLE FOR B–PHYSICS

Y. Giomataris
Lausanne University
CH-1015 Lausanne, (SWITZERLAND)

Abstract

Proton accelerators are abundant B-meson factories in both fixed-target and collider mode. Both can produce 10^{10} B-meson pairs per year, but suffer from high background and require high selective triggers to cope with a many orders of magnitude higher interaction rate. A third approach, the Asymmetric Proton Collider, seems to be an ideal configuration combining the qualities of the two modes. The performances of this approach in the present high-energy accelerators, SPS, Tevatron, and HERA, are evaluated. Such asymmetric collision is adequate to produce a large amount of B-meson pairs and could lead to an ambitious low-cost beauty physics program in the intermediate LEP–LHC(SSC) era. Compared to the electron–positron machine it produces a factor of 1000 higher number of $b\bar{b}$ pairs per year.

1 Introduction

A major experimental goal of contemporary high-energy physics is the observation of CP violation in the B-meson system. The produced asymmetries in rare decays of some promising decay channels of the neutral B-meson ($B_d \to \pi\pi$, $B_d \to J/\psi K_s$, $B_s \to \rho K_s$, D_sK) have to be measured and their flavour tagged. These experimental observations can provide valuable information on the validity of the Standard Model and it is a decisive test of the Kobayashi–Maskawa model which describes CP violation.

In order to fully reconstruct and tag some 1000 B mesons decaying in these modes, a total production of 10^9–10^{10} $b\bar{b}$ pairs is required, taking into account the low branching ratios, the tagging efficiency, reconstruction efficiencies, dilution factors, etc. This is a very demanding experimental goal for which the high-energy physics community will need new ideas and some creativity.

The choice of the accelerator is of paramount importance: an important effort has been made the last few years to study the performances of an electron–positron accelerator, the so-called B-factory. This machine is designed at a centre-of-mass energy ($\sqrt{s}$ = 10.6 GeV) tuned to the mass of the $\Upsilon(4S)$ resonance. In spite of a superior signal-to-background ratio, since most of the events contain $b\bar{b}$ pairs, these machines suffer from a chronic disease: total production cross-section is quite low (1.1 nb) and therefore the

*) Visitor at CERN, Geneva, Switzerland

required luminosity to reach CP-violation sensitivity has to be pushed to its extreme limit ($L = 10^{34}$ cm^{-2} s^{-1}) by two orders of magnitude beyond the highest luminosity achieved at these machines.

In proton high-energy accelerators the B-meson production is copious, with a $b\bar{b}$ pair production cross-section 3–4 orders of magnitude higher (50 μb at the Tevatron). Then the advocated total number of 10^{10} $b\bar{b}$ pairs required to achieve CP-violation sensitivity can be obtained with a moderate luminosity ($L = 10^{32}$–10^{33} cm^{-2} s^{-1}). The total interaction cross-section is 3–5 orders of magnitude higher and B-meson pairs have to be selected inside high backgrounds [1]. A particular effort has been made during the last few years to develop fast and efficient trigger systems in order to reject background events. Therefore hadron machines seem suitable for such studies and the question arises as to the mode in which it is best to perform the experiment: collider or fixed-target mode? In the following section, the two modes are compared. A third approach, the Asymmetric Proton Collider (ASC) with a small crossing angle, appears to be quite attractive [2, 3]. The question of the feasibility of such a machine in existing high-energy proton facilities is addressed.

2 Comparison of fixed-target and collider modes

The main motivation to perform B-meson experiments at a proton collider relies on the high centre-of-mass energy that can be obtained and thus the high B-meson pair production. As an example, the cross-section at the $p\bar{p}$ Tevatron collider is 50 μb while at the fixed target (FT) it is only about 20 nb. There is a significant factor of 2500 in favour of the collider experiment. At higher energies (i.e. at the LHC) the gap decreases, but $b\bar{b}$ production is still significantly higher at the collider centre-of-mass energy. Although the future LHC and SSC machines are adequate for ambitious B-meson experimental studies, we will concentrate our study on the existing proton machines: Tevatron at FNAL, SPS at CERN, and HERA at DESY. The total sensitivity of a collider experiment for B-meson pairs is limited by some important constraints:

- The peak luminosity in present hadron colliders does not exceed 10^{31}cm^{-2}s^{-1}, a limitation mainly due to the weak antiproton beam. In the actual highest energy proton–antiproton collider, the Fermilab Tevatron machine, the average luminosity per year of operation is of the order of 3×10^{30}cm^{-2}s^{-1}. At the end of this decade, there is a hope to improve its luminosity by an order of magnitude with the addition of a main injector. Moreover, at higher collider luminosity, there is an additional obstacle due to the pile-up, especially if a secondary vertex trigger is used. The probability of having two interactions inside the same burst increases with the luminosity, and pile-up events give B-meson faking candidates at the trigger level since the longitudinal dispersion of the two events produces a B-meson topology, i.e a primary plus a secondary-like vertex. In the FT mode the luminosity can be much higher ($\gg10^{33}$cm^{-2}s^{-1}) and a very small target can be used, which facilitates the search for secondary vertices: the pile-up of many background events appears as a high multiplicity event, since these events occur within a well-localized and fixed interaction region.

- Event multiplicity. Particle multiplicity is higher in the collider mode because of the larger centre-of-mass energy.
- Lorentz boost. The effect of the Lorentz boost, in the FT mode, is quite beneficial. Particles are more energetic and the effect of multiple scattering, causing damage especially in the secondary vertex finding procedure, is reduced. It is also welcome for efficient calorimetry and detection. Low-energy particles are difficult to detect with a calorimeter and the resolution is poor. Low-momentum muons are difficult to detect and identify, since they lose an important fraction of their energy in the absorber and their trajectory is disturbed by the multiple scattering effect. This effect is more pronounced in the central region of a collider experiment. Another important point has to do with the acceptance of the experiment: beauty particles are produced up to large rapidities ($\eta = 1$–5) and therefore a full acceptance collider experiment is hard to design, unless a full 4π geometry is adopted. High Lorentz boost in the FT mode helps in the design of a full-acceptance and low-cost forward beauty spectrometer. More than 50% of the decay products of B-meson pairs are contained in a 150 mrad aperture forward detector.
- Trigger at high interaction rates
  i) A high-p_t lepton trigger is the most common trigger used by experiments in high-energy proton colliders and it is efficient for high-p_t processes. To select B-meson pairs efficiently, a relatively low p_t threshold of the order of 1 GeV is required. Lowering the p_t threshold at the 1 GeV level in the collider mode is difficult, especially in the central region because of low-momentum particles. Low-momentum muons lose a big fraction of their energy in the absorber and low-energy electrons are hard to detect and identify. Thanks to the Lorentz boost at the FT experiment high-momentum particles are produced. In addition, in the FT experiment the minimum-bias event exhibits low mean p_t distribution (300 MeV) and it is efficiently rejected with 1 GeV p_t cut-off. The same cut-off at the collider, owing to the higher average p_t (600 MeV), gives poor minimum-bias event rejection. The effect is illustrated in Fig. 1, where the efficiency to select $b\bar{b}$ or minimum-bias events after a p_t threshold is shown for both collider and FT mode. For 1–3 GeV cut-off the efficiency for beauty event selection is comparable in the two modes. The minimum-bias efficiency falls faster in the FT mode. Figure 2 illustrates the effect of different applied p_t thresholds in the two modes: the rejection factor of the minimum-bias event is plotted as a function of the efficiency of the B-meson event. It turns out that a large rejection factor of the minimum-bias event can be obtained in the FT mode. In the collider mode the rejection factor is lower by two orders of magnitude for the same B-meson event selection efficiency.

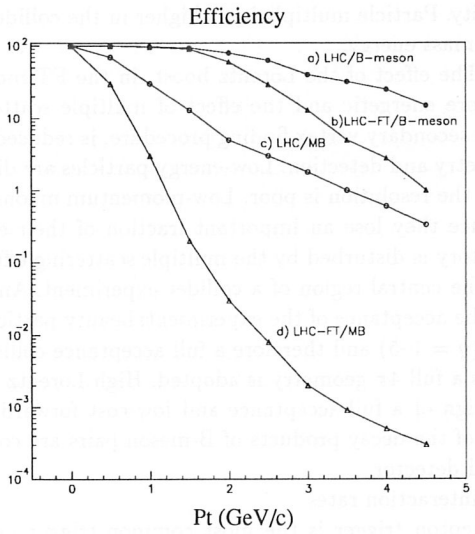

Figure 1: Efficiency for selection of B-meson events as a function of the maximum charged-particle p_t threshold applied in each event. The events are $B^0 \to \pi^+\pi^-$ decays at LHC energies and are simulated using the PYTHIA program: a,c) LHC collider for B-meson pair events and minimum-bias event respectively; b,d) LHC fixed-target mode.

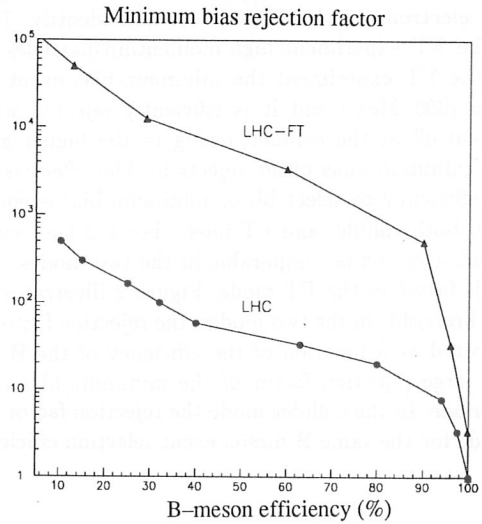

Figure 2: Rejection factor obtained for the minimum-bias event as a function of the efficiency of the B-meson event, after various p_t cut-offs applied in both events.

ii) If a secondary vertex finding procedure is used as a first trigger level, an appreciable dead time is needed to perform a complex algorithm, since the primary vertex position is variable, and both primary and secondary vertex identification is required. Furthermore, in the collider mode, the higher multiplicity of charged particles and their relatively low momentum enhances the probability of fake secondaries because of the multiple scattering on the silicon microvertex or unwanted secondaries from K^0, hyperons, etc.

In the FT experiment the primary vertex is known and can be quite small (100 μm), which facilitates the fast trigger procedure: a first level trigger can be applied using the optical trigger at the highest luminosity (which partially compensates for the lower B-meson production cross-section) [4, 5]. The secondary vertex finding, based on a silicon microvertex, is now easier and faster since the primary vertex is known and only a secondary vertex has to be identified [6, 7, 8]. In addition, as has been mentioned, an efficient rejection of the minimum-bias events can be obtained with high-p_t lepton cut-off.

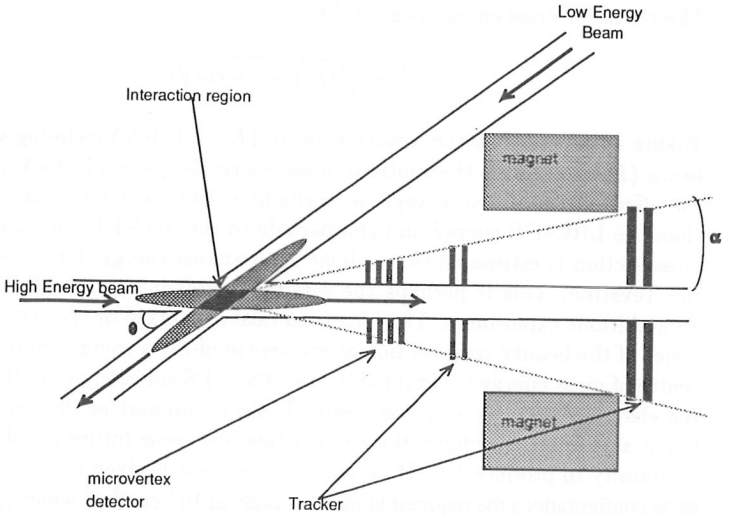

Figure 3: Schematic of an asymmetric collision between a high-energy and a low-energy beam at θ crossing angle.

3 The principle of the Asymmetric Proton Collider mode

It turns out from the previous analysis that the requirements for an optimized B-physics experiment are: high luminosity, the highest possible centre-of-mass energy, Lorentz boost, and if possible a small interaction region in both the transverse and the longitudinal direction. A simple way to achieve this is the use of a slightly tilted asymmetric collider [2]. The high-energy E_1 proton beam of a proton collider machine collides

with a lower momentum E_2 proton beam (e.g. from the booster) at a crossing angle θ, as is shown in Fig. 3. Preliminary discussions with accelerator physicists indicate that such a scheme may be feasible [9]. The boost of the high-energy beams pushes most of the produced particles into the high-energy beam direction. Monte Carlo simulations show that the mean of the polar angle of the B-meson decays in the $\pi\pi$ mode angle in the case of a 1 TeV beam colliding with an 8 GeV beam is about 130 mrad. The mean momentum of each pion is 35 GeV, an ideal value for momentum reconstruction and particle identification. It is clear that a FT-like experiment covering about 200–300 mrad around the z axis towards the 1 TeV beam direction could be suitable.

Such collisions were already studied in 1978 at CERN: the Merging of the Intersecting Storage Rings (MISR) for a collision between a 60 GeV storage ring with the 400 GeV SPS proton beam [10]. Another asymmetric configuration is the HERA electron–proton collider.

The characteristics of this configuration are summarized as follows:

- The centre-of-mass energy is given by

$$\sqrt{s} = \sqrt{2E_1E_2(1+\cos\theta)}\ . \tag{1}$$

Taking as an example the Tevatron beam ($E_1 = 1$ TeV) colliding with the booster beam ($E_2 = 8$ GeV), the centre-of-mass energy is $\sqrt{s} = 178$ GeV (for small angles the effect of the crossing angle is negligible). This centre-of-mass energy is higher than the LHC–FT energy and comparable to the SSC–FT one. The $b\bar{b}$ production cross-section is estimated to be about 2 μb at this energy, 100 times the FT one at the Tevatron. This is perhaps the safe factor missing in the FT mode to perform an ambitious experiment. The idea is to take advantage of the strong energy dependence of the beauty cross-section at low centre-of-mass energy. Similar or even higher centre of mass energy is obtained in the SPS + PS collision or at HERA by replacing the electron beam by a proton beam. Table 1 summarizes the performances of different asymmetric configurations in existing and some future colliders. The required luminosity to produce 10^{10} B-meson pairs per year is given in the last column. In all these configurations the required luminosity is about $10^{32}\text{cm}^{-2}\text{s}^{-1}$ which can, in principle, be obtained in such proton–proton machines.

- The required luminosity, in the range of 10^{32} $\text{cm}^{-2}\text{s}^{-1}$, seems to be achievable with present technologies. The disadvantage of the low-energy beam is compensated by the use of the intense proton beam (instead of the antiproton beam). It can be obtained by increasing the number of bunches in the high-energy proton ring and reducing the beam dimension at the interaction point by inserting low-beta quadrupoles. Detailed studies are necessary to design the interaction region and study the maximum luminosity performances of this machine. An optimistic message comes from some old low-energy proton–proton projects. In 1982, at the ISR, the maximum luminosity achieved was

Table 1

	Beam energy	$\sqrt{s}$ (GeV)	Cross–Section $b\bar{b}$ (μb)	Required luminosity ($cm^{-2}s^{-1}$, @ 10^{10} $b\bar{b}$/year)
Tevatron ASC I	1 TeV + 120 GeV	690	10	1×10^{32}
Tevatron ASC II	1 TeV + 8 GeV	178	2	5×10^{32}
HERA ASC	820 GeV + 26 GeV	292	3	3×10^{32}
SSC ASC I	2 TeV + 200 GeV	1265	30	3×10^{31}
SSC ASC II	2 TeV + 11 GeV	297	3	3×10^{32}
UNK ASC	3 TeV + 400 GeV	2190	60	1.5×10^{31}
SPS + PS ASC	450 GeV + 30 GeV	232	2	4×10^{32}
Tevatron FT	1 TeV	45	0.020	5×10^{34}
SPS FT	450 GeV	30	0.004	3×10^{35}
HERA FT	800 GeV	40	0.010	1×10^{35}
LCH FT	8 TeV	126	1	1×10^{33}
SSC FT	20 TeV	200	3	3×10^{32}

1.4×10^{32} $cm^{-2}s^{-1}$, with 14.7° crossing angle. New ideas were proposed to increase the luminosity to the level of $10^{33} cm^{-2}s^{-1}$ by reduction of the crossing angle, combined with low–beta function and momentum compaction at the intersection [11]. At that time other ambitious projects were studied: the MISR and the ep facility in the SPS (CHEEP) [12]. The idea was to collide the SPS proton beam with a proton (electron) beam in a new low-energy storage ring. Both projects were claiming luminosities of the same order of magnitude as is required fot the ASC project.

The luminosity in head-on bunched-beam accelerators is given by

$$L_0 = N_1 N_2 f/(4\pi\sigma_x^2) \ , \tag{2}$$

where N_1,N_2 is the number of protons per bunch in each colliding beam, f is the bunch frequency, and σ_x is the beam radius at the interaction region. A reasonable assumption for these parameters is: $f = 50$ MHz, $N_1 = 10^{11}$, and an equal number of protons $N_2 = N_1$ for the low–energy beam. Taking σ_x=100 μm the luminosity becomes L_0=5×10^{32} $cm^{-2}s^{-1}$, close to the value we want to reach. Further investigations by machine experts are needed to give an estimation of the radius of the low-energy beam at the interaction region, since its emittance is worse. This effect can be compensated by lowering the beta function of the low-energy beam, using low-beta insertions, but other effects such as beam–beam can limit the performance.

An ideal configuration is to collide the two beams with small crossing angle in order to reduce the interaction region. Large crossing angle helps in the design of an optimal detector, since the interaction region is small and B-meson decays are boosted outside the beam pipe. We should note that very large crossing angle was proposed [13] for an

asymmetric ϕ factory. This new concept uses a collinear collisions between a storage electron and a positron linac. In our case the luminosity is given by

$$L = L_0/\sqrt{1 + ((\sigma_z/\sigma_y)\tan\theta/2)^2}\ , \tag{3}$$

where L_0 is the luminosity obtained in a head-on proton–proton collision, θ is the crossing angle, and σ_z, σ_y are respectively the longitudinal and transverse beam dimensions. There is clearly an undesirable drop of the luminosity inversely proportional to the crossing angle, unless the loss is compensated by other effects. In principle, there are two ways to obtain such a performance:

- Reduce the longitudinal bunch dimension by an order of magnitude as is currently done in electron machines.
- Use a crossing angle. The loss of the luminosity can be compensated by increasing the intensity of the proton beam, since long-range beam–beam effects are suppressed. Other space-charge effects can, however, limit the maximum proton current. The effect of a degradation of the luminosity due to beam–beam interaction on the coherent motion of the barycentres of the colliding bunches in asymmetric collisions should also be considered [14]. If a large crossing angle is used there is free space along the low-energy beam pipe since the experiment is developed along the second beam pipe. In that case the low-beta quadrupoles of the low-momentum beam can be moved closer to the interaction region: a strong focusing can then reduce the low-beta parameter and compensate for the loss of the luminosity.

The detector is a forward spectrometer located around the outgoing beam pipe of the high-energy beam. A sketch of a compact spectrometer is shown in Fig. 4. The silicon microvertex detector is extended over a longitudinal length of about 2 m to allow secondary vertex reconstruction. It is, at the same time, used to assure a precise upstream tracking; the downstream tracking is performed by microstrip gaseous detectors. In this case a modest and short magnet is needed to assure a good momentum resolution with the spectrometer. Further compaction of the full apparatus can be obtained by inserting the Cherenkov counter inside the magnet. Such a compact apparatus could facilitate the design of the interaction region, especially if low-beta insertions close to the interaction point are necessary to ensure a high luminosity. The calorimeter, the muon absorber, and the muon detector are less sensitive to the presence of some material owing to the fact that low-beta quadrupoles are needed for an optimum beam-focusing system.

4 Discussion and outlook

The Asymmetric Proton Collider combines many virtues of the collider and fixed-target mode. This collision configuration could be performed in the existing proton colliders: at CERN, DESY, and FNAL. The high-energy beam (E_1 = 400–900 GeV) of these machines colliding with an intense low-energy proton beam provided by the booster (E_2 = 8–26 GeV) gives quite a high centre-of-mass energy and a comfortable B-meson

production cross-section (a few microbarns). The experiment has a fixed-target like shape along the high-energy beam direction. Preliminary simulations show that a small angular coverage ($\approx$ 300 mrad) spectrometer provides good acceptance and can be designed with a modest cost. The acceptance, however, is a function of the collider boost.

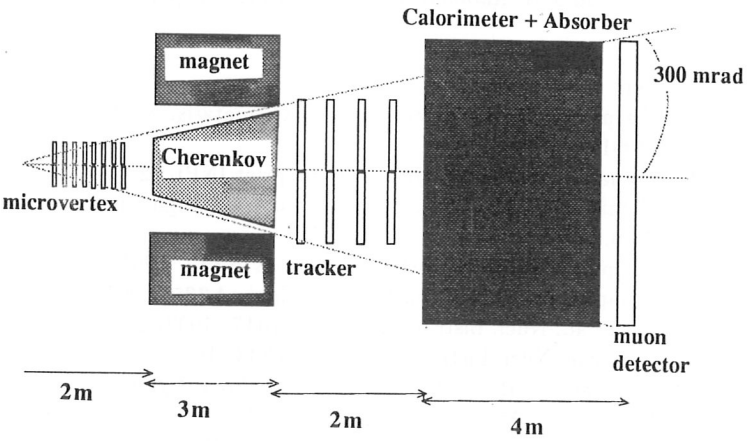

Figure 4: Design of a compact forward spectrometer: silicon microvertex detector, dipole magnet with the Cherenkov counter inside, upstream tracking, a calorimeter, a muon absorber, and a muon detector.

A first idea is to build a new storage ring [9] for the low-energy beam, crossing the high-energy beam with a small angle. By using high-magnetic-field superconductive magnets, the size of the ring can be reduced to the level of a few tens of metres and there is hope for a moderate total cost. A second option, to use an intense low-energy linac to collide with the high-energy beam, is considered as a challenge, but it is necessary to study it and in particular new acceleration and beam-focusing techniques under development. Such collisions were considered [15] for an electron–positron machine and luminosities ($\sim 10^{34}\ cm^{-2}\ s^{-1}$) beyond those achievable in pure storage-ring colliders were claimed.

The bench luminosity varies slightly in the different configurations and is of the order of L_0=5 $\times$ 10^{32} $cm^{-2}s^{-1}$. There is no proof that such luminosity is possible. Some crude calculations and results from other lower energy proton machine indicate that it is perhaps achievable. The value of the beam crossing angle is an important constraint for the peak luminosity. We need to explore, in more detail, the various asymmetric–collider configurations to see if there is an optimum asymmetry or crossing angle.

Acknowledgements

I would like to thank G. Charpak and L. Lederman for critical remarks and very encouraging comments about the Asymmetric Tilted Proton Collider idea. I am indebted for many discussions with my colleagues J. Derre, A. Gougas, D. Kaplan, C. Kochowski, Y. Lemoigne, S. Loucatos, J.P. Perroud and P. Petroff. Thanks are also due to M. Jouhet, C. Rambaldi and J.M. Rabbinowitz for preparing this paper.

References

[1] G. Charpak, L. M. Lederman, and Y. Giomataris, Nucl. Instrum. Methods **A306**, 439 (1991).
[2] Y. Giomataris, Lausanne University preprint INPL 92-4 (1992).
[3] Y. Giomataris et al., Proc. 26th Int. Conf. on High Energy Physics, Dallas, 1992, Vol. 2, p. 1738.
[4] G. Charpak *et al.*, Nucl. Instrum. Methods **A332** (1993) 91.
[5] D.M. Kaplan *et al.*, Nucl. Instrum. Methods **A330** (1993) 33.
[6] J. Ellet et al., Nucl. Instrum. Methods **A317** (1992) 28.
[7] Y. Lemoigne, Nucl. Instrum. Methods **A333** (1993) 113.
[8] G. Darbo and L. Rossi, Nucl. Instrum. Methods **A289** (1990) 584.
[9] P. Martin, B.W. Montague, B. Zotter and P. Lefevre, private discussion.
[10] B.W. Montague and B. Zotter, CERN/ISR–TH/73–23.
B.W. Montague and B. Zotter, CERN/ISR–TH/73–47.
[11] E. Appel et al., MISR group, CERN/78–01 (1978).
[12] J. Ellis et al., CHEEP study groups, CERN/78–02 (1978).
[13] D.B. Cline, Dallas High Energy Conference, p. 1960.
[14] K. Hirata et al., Nucl. Instrum. Methods **A292** (1990) 156.
[15] P. Grosse Wiesmann, Nucl. Phys. **A532** (1991) 545c.

Frascati Physics Series, Vol. 1 (1993)
HEAVY QUARKS AT FIXED TARGET
Frascati, May 31st – June 2nd 1993
(pp. 305–323)

FIXED TARGET BEAUTY PHYSICS AT THE SSC AND THE LHC

B. Cox
University of Virginia, Physics Department
McCormick Road, Charlottesville VA 22901, (USA)

Abstract

The prospects for observing CP violation asymmetries and performing precision measurements of the phase of the CKM matrix in fixed target B experiments at the SSC or LHC are very promising. The yields of reconstructed and tagged B decays and the various factors which minimize the dilution factors make measurements of CP asymmetries in fixed target experiments more than competitive with much more expensive hadron collider experiments and significantly better than asymmetric e^+e^- B factories. In addition, the superior time resolution possible in fixed target experiments allows measurements of mixing and time dependent CP violation effects in B_s decays that are possible with no other option. The sensitivity of the SSC fixed target option (the SFT) is presented for specific modes.

1. Introduction

The fixed target experimental configuration has many technical advantages in the measurement of CP violating asymmetries compared to e^+e^- or hadron collider experiments and is more economical to implement. This is true for both internal (gas jet) and external target (extracted beam/live target) fixed target B options, versions of which have been proposed at the SSC[1] and the LHC[2], although the two types of fixed target B experiments differ considerably in their relative merits and implementation. As will be shown, the technical advantages of the fixed target experiments, in particular, the extracted beam/live target option, are more than enough to offset the larger B cross sections available at collider energies.

Among the technical advantages of the SSC and LHC fixed target experiments generated by the Lorentz boost are the higher momentum of B hadrons resulting in longer B decay lengths and higher momentum of the B decay products and consequentially lower multiple scattering and better vertex resolutions plus greater acceptance for B's. In addition, the relatively low multiplicity of the SSC and LHC fixed target events coupled with the better vertex resolution and longer decay lengths leads to better vertex recognition and reconstruction efficiencies for both the tagging and CP B decays. Moreover, the long decay lengths of the Lorentz boosted B's combined with superior vertex resolution ($c\tau/L$ for B decays $\approx$ 380!) make possible very good time resolution measurements of the CP asymmetries in both B^0_d and B^0_s decay distributions, minimizing "dilution" effects due to mixing and minimum decay length criteria. The superior ratio of resolution to decay length of fixed target experiments also significantly decrease the dilution effects due to mistagging

by allowing association of the tagging particle with a given secondary or tertiary vertex. The overall effect is to make possible more precise measurements of the angles of the unitarity triangle. The very good time resolution also make possible measurements using the rapidly oscillating B^0_S and allows use of more complex analysis procedures using decays into CP non conjugate final states where analysis of the time distributions are essential.

Finally, the fact that a fixed target spectrometer need cover only a relatively small solid angle compared to a forward collider experiment, let alone a 4π hadron or e^+e^- experiment, leads to undeniable economies in detector construction. All of these features, which are addressed quantitatively in the following sections, more than overcome the higher BB production per interaction of the hadron collider configuration and will be shown to result in better asymmetry measurements in the well known CP self conjugate B decays. In addition, these features both allow the option of CP measurements in more complicated modes where tertiary as well as secondary vertices must be detected for both tag and CP B decays and permit extraction of physics information from partially reconstructed B decays. A qualitative summary of the relative merits of collider verses fixed target (either internal or external target) are summarized in Table 1.

Table 1
Fixed Target Vs Hadron Collider B Physic Options

Cross Sections	-
Difficult Extraction*	-
Higher Acceptance	+
External Experimental Area*	+/-
No Beam Pipe*	+
Higher Momentum Secondaries	+/-
Lower Track Multiplicity	+
Active Target*	+
Higher Reconstruction Efficiencies	+
Vertexing Efficiencies/Resolutions*	+
Track Resolutions	+
Radiation Damage*	+
Triggering Efficiency/Flexibility	+
Time Resolution	+
Smaller Detectors/Lower Cost	+

* The factors in favor of fixed target options ≡ +; Starred items are advantages/disadvantages peculiar to the external (extracted beam/live target) option in distinction to the internal (gas jet) option.

For comparison of collider and fixed target B production parameters, a short summary of the features of hadroproduction of B's in the SSC fixed target (SFT) and SSC collider configurations is presented in Table 2.

Table 2
B Production Parameters for the SSC Fixed Target Compared to SSC Collider

	SSC Collider	SSC Fixed Target (SFT)
Interaction Rate	10^7 Int./sec	10^7 Int./sec
σ_T (pN or pSi)	100 mb	356 mb
σ_{BB} (pN or pSi)	1000μb	56μb
σ_{BB}/σ_T	1/100	1/6300
Event Charged Multiplicity	"few" hundred	≈ 20
‹ pB ›	43 GeV/c	445 GeV/c
‹ plepton ›	36 GeV/c	280 GeV/c
Median B Decay Length	3 mm	42 mm
Mean B Decay Length	13 mm	95 mm

In Table 2, we have taken 10^7 interactions per second as a limit for high rate B physics fixed target or collider detector to avoid the problem of multiple high multiplicity events per bucket. The heavy target enhancement of the pN B production and total cross sections is taken to be $A^{0.72}$ and A^1 respectively for the fixed target experiment.

2. The Physics of CP Violation in B Decays

The unitarity of the CKM matrix[3] when expressed either in the Kobayashi-Maskawa representation

$$\begin{pmatrix} d' \\ s' \\ b' \end{pmatrix} = \begin{pmatrix} V_{ud} V_{us} V_{ub} \\ V_{cd} V_{cs} V_{cb} \\ V_{td} V_{ts} V_{tb} \end{pmatrix} \cdot \begin{pmatrix} d \\ s \\ b \end{pmatrix}$$

or the Wolfenstein approximation[4]

$$\begin{pmatrix} d' \\ s' \\ b' \end{pmatrix} = \begin{pmatrix} 1-\lambda^2/2 & \lambda & A\lambda^3(\rho-i\eta) \\ -\lambda & 1-\lambda^2/2 & A\lambda^2 \\ A\lambda^3(1-\rho-i\eta) & -A\lambda^2 & 1 \end{pmatrix} \cdot \begin{pmatrix} d \\ s \\ b \end{pmatrix}$$

results in the relationship $V_{ud} V^*_{ub} + V_{cd} V^*_{cb} + V_{td} V^*_{tb} = 0$. This relationship is one of six such CKM matrix unitarity relationships[5] which contain information about the weak phases of the CKM matrix. This particular relationship can be approximated by $V^*_{ub} + V_{td} = |V_{cd} V^*_{cb}|$. By using the experimentally observed values, $V_{ud} \approx 1$, $V_{tb} \approx 1$, $V_{cd} \approx -0.22$ (and real). Inspection of the Wolfenstein approximation shows that each of the terms in this complex equation is of order λ^3 (where $\lambda = V_{us} = \sin\theta_C \approx 0.22$). This relationship is most often presented geometrically as the unitarity triangle.

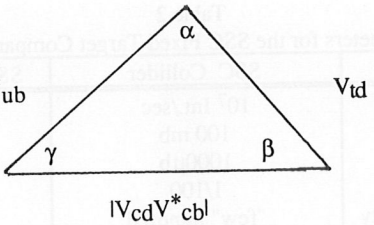

Determination of the three angles of the unitarity triangle can be made by measuring asymmetries between B and B rates for decays of B^0_d and B^0_s into CP. Alternatively, the sides of the triangle can be found by determining the various CKM matrix elements or any combination of two sides and two angles.

There are measurable manifestations of the complex phase of the CKM matrix in several types of B decays. By suitable measurements of these decays, the three angles of the CKM triangle can be determined. These processes include the following types of measurements. "γ" indicates that, in most cases, the measurement proposed does not determine γ directly.

I. Measurement of time dependent asymmetries between B^0->f and $\bar{B}^0$-> $\bar{f}$ decays where f= $\bar{f}$, i.e.. decays of neutral B mesons into CP eigenstates: Decay modes belonging to this class that have been considered for determination of the α, β and γ angles of the unitarity triangle are

B^0_d-> $\pi^+\pi^-$	sin 2α
B^0_d-> ψK^0_s	sin 2β
B^0_d->D^+D^-	sin 2β
B^0_s-> ρK^0_s	sin 2"γ"

II. Measurement of time dependent asymmetries between B^0->f and $\bar{B}^0$-> $\bar{f}$ where $f \neq \bar{f}$. In the modes considered the final states f and $\bar{f}$ are "almost" CP eigenstates, i.e. they are eigenstates at the quark level: Examples of such decays are

B^0_d->$a^+\pi^-$ and/or B^0_d->$a^-\pi^+$	sin2α
B^0_s->D^+K^- and/or B^0_s->D^-K^+	sin2"γ"

III. Measurement of the six rates for B decays:

B -> $\bar{D}^0$ + X	$\bar{B}$ -> $\bar{D}^0$ +$\bar{X}$	
B -> D^0 + X	$\bar{B}$ -> D^0 + $\bar{X}$	$X \neq \bar{X}$
B -> D^0_1 +X	$\bar{B}$ -> D^0_1+$\bar{X}$	

By using suitable combinations of the six indicated decay rates, a specific angle of the unitarity triangle can be determined. No time dependent measurements or tagging are

required for measurements of this class. Examples of decays modes suitable for this type of CP study are

$B^+ \rightarrow \bar{D}^0 K^+$ sin 2"γ'
$B^0_d \rightarrow \bar{D}^0 K^{0*}$ sin 2"γ'

IV. Measurement of the six rates for B decays:

$B \rightarrow \bar{D}^0 + X$ $\bar{B} \rightarrow \bar{D}^0 + \bar{X}$
$B \rightarrow D^0 + X$ $\bar{B} \rightarrow D^0 + \bar{X}$ $X=\bar{X}$
$B \rightarrow D^0_{1,2} + X$ $\bar{B} \rightarrow D^0_{1,2} + \bar{X}$

Once again, by suitable combinations of the six decay rates, a specific angle of the unitarity triangle can be determined. Examples of decays modes of this sort are

$B^0_d \rightarrow D^0 K^0_S$ sin 2"γ'
$B^0_S \rightarrow D^0 \Phi$ sin 2"γ'

There are more complicated methods of extraction of the angles of the CKM triangle but for the purposes of this paper we will concentrate on examples of class I and II to demonstrate the sensitivity of the fixed target B physics technique.

Following the development of Aleksan et al[6] for particular class I or II type B decays where only one amplitude dominates the decay, the CP violating asymmetries resulting from interference between the dominate amplitude can be written as

$$\Gamma(B^0 \rightarrow f) + \Gamma(B^0 \rightarrow \bar{f}) \cong A^2 e^{-\tau} \cdot \left\{1 - d_\rho \cdot \cos\Delta\alpha \cdot \sin\left(2\phi_M + \phi_f + \phi_f'\right) \cdot \sin x_{d,s}\tau\right\} \quad (1)$$

$$\Gamma(\bar{B}^0 \rightarrow f) + \Gamma(\bar{B}^0 \rightarrow \bar{f}) \cong A^2 e^{-\tau} \cdot \left\{1 + d_\rho \cdot \cos\Delta\alpha \cdot \sin\left(2\phi_M + \phi_f + \phi_f'\right) \cdot \sin x_{d,s}\tau\right\} \quad (2)$$

where

$$x_{d,s} = \frac{\Delta m}{\gamma} \; ; \; \tau = \gamma t$$

Δm = difference of the mass of CP light and heavy eigenstates

γ = average lifetimes of the CP light and heavy eigenstates

$$A^2 = \left|\langle f|T|\overline{B^0}\rangle\right|^2 + \left|\langle f|T|B^0\rangle\right|^2$$

$$d_\rho = \frac{2\rho}{1+\rho^2} \text{ with } \rho = \frac{\left|\langle f|T|\overline{B^0}\rangle\right|}{\left|\langle f|T|B^0\rangle\right|}$$

$\Delta\alpha = \alpha - \alpha' \equiv$ difference of the strong interaction phases for $\bar{B}^0 \rightarrow f$ and $B^0 \rightarrow f$

$$\phi_M = B^0 \Leftrightarrow \overline{B^0} \text{ mixing phase}$$

$$\phi_f = CKM \text{ weak phase appropriate to } \bar{B}^0 \rightarrow f$$

$$\phi_f' = CKM \text{ weak phase appropriate to } B^0 \rightarrow f$$

CP violation is indicated by the difference between (1) and (2). As shown by (1) and (2), the decays of B^0 into f and $\bar{f}$ can be added and compared to the $\bar{B}^0$ into f and $\bar{f}$ in order to increase statistics for observing the asymmetry between the particle and antiparticle decays. The special case of (1) and (2) for decays into CP eigenstates (f= $\bar{f}$) requires that $\phi=\phi'$, $\rho=1$ and $\alpha=\alpha'+n\pi$ where n=0,1.

For Class I and II decays dominated by a single amplitude, the unitarity triangle angle under study can be determined up to a four fold ambiguity by fitting (1) and (2) to the data and obtaining the coefficients S and $\bar{S}$ of the sine oscillation of the B^0->f and $\bar{B}^0$-> $\bar{f}$ time distributions. In terms of S and $\bar{S}$', the fitted coefficients,

$$\sin 2\phi = \pm\frac{1}{\sqrt{2}}\left[1 + S\bar{S} \pm \sqrt{(1-S^2)(1-\bar{S}^2)}\right]^{\frac{1}{2}} \quad (3)$$

where

$$2\phi = 2\phi_M + \phi_f + \phi_f'$$

The CP eigenstate modes are preferred because of the ease of interpretation due to the absence of the complications of strong interaction phases ($\Delta\alpha=0$) in the extraction of the weak phases. However, high statistics measurements of the CP asymmetries using these CP eigenstate decay modes may not be feasible because of inadequate statistics due to the small cumulative branching ratios ($\approx 10^{-5}$ to 10^{-7}) into final states that can be detected experimentally. In addition, the relatively undistinguished nature of some of the CP eigenstate modes may lead to problems of backgrounds. Indeed, the low branching ratio and large backgrounds for B^0_S->ρK^0_S have lead us to consider alternative ways of measuring γ using the decays of class II.

Class I and II modes require tagging of the particle or antiparticle nature of the B_{CP} decay at t=0 by use of the decay of the "other" B in the event. This is most usually accomplished by detecting the charge of the lepton from the semileptonic decay or the charge of a $K^{\pm}$ from the D decay product of the other B. This extra requirement of a tag generates a requirement for more statistics and the possibility of mistagging further increasing the need for data to sort out the problems.

For a time dependent measurements of events of Class I or II which have a finite time resolution, the error in sin (2ϕ) is given by

$$\delta(\sin 2\phi) \cong \frac{1}{d_{tag}} \cdot \frac{1}{d_{CP}} \cdot \frac{1}{d_\rho} \cdot \frac{1}{d_{Bkg}} \cdot \frac{1}{d_{mistag}} \cdot \frac{1}{d_{res}} \cdot \frac{1}{\sqrt{N_{recon}}} \quad (4)$$

where N_{recon} is the sum of the reconstructed and tagged B^0 and $\bar{B}^0$ decays in the selected mode for which a measurement of CP asymmetries is being analyzed.

The various ":dilution" factors in the error are

d_{tag} = dilution of B_{tag} mixing $= [p_{\pm} + p_{\Lambda}] + \frac{p_s * x_s}{[1+x_s^2]} + \frac{p_d * x_d}{[1+x_{d,s}^2]}$

where $p_{\pm}, p_d, p_s, p_{\Lambda}$ are the hadronization fractions for $B_u^{\pm}$, B_d^0, B_s^0, Λ_b

d_{CP} = dilution due to CP decay statistics

$$= e^{-\tau_{cut}} * \left[1 + \frac{2x_{d,s}\sin 2x_{d,s}\tau_{cut} - \cos 2x_{d,s}\tau_{cut}}{1+4x_{d,s}^2}\right] \xrightarrow{\tau_{cut} \Rightarrow 0} \sqrt{\frac{2x_{d,s}^2}{1+4x_{d,s}^2}}$$

d_{ρ} = dilution due to deviation of final state from a CP eigenstate

$$= \frac{2\rho}{1+\rho^2} \xrightarrow{f \Rightarrow CP\ eigenstate} 1$$

d_{bkg} = dilution due to background $= \sqrt{\frac{S}{S+B}}$

d_{mistag} = dilution due to mistagging $= (1-2w)$

d_{res} = dilution due to time resolution $= e^{-\sigma_t^2(x^2+\frac{1}{2})}$

Several things should be noted about the various dilution factors. First, the error, $\delta\sin 2\phi$, is inversely proportional to the square root of the number of reconstructed, tagged events and inversely proportional to the dilution factor. Therefore, if a choice is to be made, it is better to sacrifice events in order to improve the composite dilution factor rather than try to improve the statistics in a particular decay channel. It should also be noted that all terms are positive in the expression for d_{tag} so this factor is minimized if all possible species of the other B are used for tagging. In addition, we note that with $x_d \approx 0.7$ and $x_s \geq 5.0$, the B_S decays contribute very little to a time independent asymmetry measurement. In effect, asymmetries due to B_S decays are washed out.

However, it should be cautioned that the doubly damaging dilution d_{mistag} due to mistagging may be less bothersome if a particular B species is selected for the tagging B. The mistagging can arise from several sources

1. b->c->μ,e decay: This source of mistags is minimized by p_t cuts on leptons and can be eliminated completely if the complete event topology including all secondary and tertiary vertices is reconstructed. In fact, mistags can be identified and changed to proper tags if the leptons and K's can be assigned to the proper vertices. A capability for complete vertex topology is a strength of the SFT live target experimental configuration.

2. π,K->μ,e decays: This source is minimized by association of the lepton with the primary vertex. It is also minimized in the trigger sample by p_t cuts on lepton imposed by the trigger.

3. Punchthrough of hadrons through the muon shield: This is not a serious problem for the SFT fixed target muon detector since, as shown below, the shield can be very thick because of the high momentum of the Lorentz boosted fixed target muons from B decay.

4. γ->e conversions This source is minimized by p_t and momentum cuts on e^+e^- pair since the conversion electrons from the π^0 decay photons are relatively low in energy. This will be quantitatively discussed in the triggering section below.

We have attempted to estimate the dilution factors for the various combinations of B^0_d and B^0_s decays even though important information about the various modes (such as hadronization factors, backgrounds, values of physics parameters such as ρ, x_s, etc.) are poorly known or completely unknown at this time. We describe below the assumptions we have made in the estimation of the dilution factors.

First, we have used hadronization factors $p\pm/pd/ps/p\Lambda$ = 0.38 / 0.38 / 0.14 / 0.10 and mixing parameters x_d=0.7 and x_s=10 to calculate $1/d_{tag}$=1.49. We have used the same mixing parameters and a $15\sigma_z \approx 3.75$mm minimum path length criterion (leading to a $\tau_{cut} = 15\sigma_z/L_{decay}$ of 0.039 for the SFT silicon vertex detector) to calculate $1/dCP \approx 1.77$ and 1.40 for B^0_d and B^0_s respectively. We have used $\sigma_\tau \approx \sigma_z/L_{decay}$ = 0.0026 to show the effect of the excellent fixed target time resolution which leads to $1/d_{res} \approx 1$ even for B^0_s decays. We point out that the minimum time cut and the effect of the finite time resolution are much more devastating for the collider configurations (especially the central collider configuration) since the ratio of resolution to path length is much poorer than for the fixed target configuration. In particular, measurements of B^0_s time distributions are very difficult in collider experiments. Next, since little is know about the ρ for the non CP eigenstate modes, we have followed the lead of Aleksan et al[6] and assumed a value of 1/2 for the ratio of the rates for $\bar{B}^0$->f to B^0->f for the non CP eigenstate modes. This results in $1/d_\rho$=1.03 for such modes as compared to 1 for the decays into true CP eigenstates. Finally, while the backgrounds considered so far for the various modes have been negligible, this work is still in progress. Accordingly, we have made what seems to us a conservative assumption that a minimum signal to background ratio of 5/1 can be achieved for most modes. This assumption leads to $1/d_{bkg}$ = 1.12.

Table 3 below gives an evaluation of the dilution factors appropriate to Class I and II decays of neutral B's that we are considering.

Table 3
Dilution Factors

B_{CP}	B_{tag}	$1/d_{tag}$	$1/dCP$	$1/d_\rho$	$1/d_{bkg}$	$1/d_{mistag}$	$1/d_{res}$	$1/d_{total}$
B^0_d	$\mu^\pm$	1.49	1.77	1.0,1.03	1.12	1.075	≈1	3.17,3.27
	$e^\pm$					1.18		3.48,3.59
	$K^\pm$					1.33		3.93,4.05
B^0_d	$\mu^\pm$	1.49	1.40	1.0,1.03	1.12	1.075	1.001	2.51,2.59
	$e^\pm$					1.18		2.76,2.84
	$K^\pm$					1.33		3.11,3.20

These dilution factors are used in what follows to weight properly the various CP decays that are tagged using the three possible tagging methods listed in Table 3.

The final number necessary for the estimates of the error in the determination of sin2ϕ is the number of reconstructed and tagged events, N_{recon}.

$$N_{recon} = N_B \cdot f_B \cdot BR_{CP} \cdot BR_{tag} \cdot A_{accep} \cdot \varepsilon$$
$$\varepsilon = \varepsilon CP \cdot \varepsilon tag \cdot \varepsilon trig$$

N_B ≡ Number of B's produced per year of operation in the SFT
BR_{CP} ≡ Composite Branching ratio for the CP decay
BR_{tag} ≡ Composite Branching ratio for the tag decay
f_B ≡ Hadronization ratio for specific CP and tagging B configuration
Accp ≡ Composite acceptance for the B_{CP}, B_{tag} and trigger particles.
ε_{CP} ≡ Composite detector and reconstruction efficiencies for CP B decay
ε_{tag} ≡ Composite detector and reconstruction efficiency for tagging B decay
ε_{trig} ≡ Composite detector efficiency for trigger

In the following sections, we will evaluate Nrecon for specific modes.

3. Beauty Production at the SSC

The cross section for pp-> $B\bar{B}$ production as a function of $\sqrt{s}$ has been calculated to third order by Nason, Dawson and Ellis[7]. These calculations have been further refined by Berger and Ming[8]. Based on these calculations, a B hadroproduction cross sections for pN interactions of 2 μb and 0.5 to 1μb at SSC and LHC fixed target energies respectively are expected. In addition, to estimate the production of B's by protons on silicon for the SFT live target, an A dependence of $A^{1.0}$ has been assumed resulting in a pSi cross section of 56 μb for B production at 193 GeV. To estimate the number of the various B species, the hadronization fractions $p\pm/pd/ps/p\Lambda$ = 0.38 / 0.38 / 0.14 / 0.10 have been used.

Using a total inelastic cross section of 32 mb for pN interactions at 193 GeV and an atomic number dependence of $A^{0.72}$, the total cross section for pSi interactions at 193 Gev/c at the SFT is calculated to be 352 mb. This leads to the expectation of one $B\bar{B}$ pair for every 6300 interactions in pSi interactions at 193 GeV (compared to ≈1/100 at $\sqrt{s}$=40 TeV, a factor of 60). Using the crystal extracted beam with intensity 2.5×10^8 protons/second producing 10^7 interactions per second in the SFT live target region 4.0% of an interaction length) operated for 10^7 seconds, 10^{14} interaction will be produced in one year of operation. The average number of interactions per beam bucket (16 ns spacing) will be 0.1 to 0.2 at this intensity. As a result, we expect cleaner interactions compared to other options such as gas jet and wire experiments which plan for 2 to 4 interactions per bucket. The $B\bar{B}$ production together with the hadronization fractions given above results in the expected yields of the various B species per year in the SFT given Table 4 below:

Table 4
Production per Year (10^7 sec) of B Pairs in SFT

B Pair Cross Section for pN	2 μb
B Pair Production Cross Section for pSi	56 μb
Number of B Pairs	1.6×10^{10}
Number of $B^{\pm}_u$	1.2×10^{10}
Number of B^0_d	1.2×10^{10}
Number of B^0_s	4.5×10^{9}
Number of B^0_c	3.2×10^{7}
Number of Λ_b	3.2×10^{9}

Given these species of B's, the numbers of interesting B decays which are useful for triggering, tagging or CP studies themselves can be estimated. Table 5 tabulates the production per year in the SFT of these decays. Table 5 also includes yields of combinations of CP and lepton/kaon tagging or lepton triggering using the other B decays where tagging is needed

Table 5
Production per Year of Interesting B Decays in the SFT

∠	Class	B_{CP}	Tag	BR*	#/year	Trig	Requirements
		$B\to l^{\pm}$	-	0.21	6.7×10^{9}		
		$B\to K^{\pm}$	-	0.85	2.7×10^{10}		
α	I	$B^0_d\to\pi^+\pi^-$	$B\to l^{\pm}$	2.1×10^{-6}	2.5×10^{4}	$l^{\pm}$	Time/Tag
		$B^0_d\to\pi^+\pi^-$	$B\to K^{\pm}$	8.5×10^{-6}	1.0×10^{5}	h^+h^-	
	II	$B^0_d\to a^+\pi^-$	$B\to l^{\pm}$	3.2×10^{-6}	3.8×10^{4}	$l^{\pm}$	Time/Tag
		$B^0_d\to a^+\pi^-$	$B\to K^{\pm}$	1.3×10^{-5}	1.6×10^{5}	h^+h^-	
		$\bar{B}^0_d\to a^-\pi^+$	$B\to l^{\pm}$	7.8×10^{-7}	9.4×10^{3}	$l^{\pm}$	
		$\bar{B}^0_d\to a^-\pi^+$	$B\to K^{\pm}$	3.1×10^{-6}	3.7×10^{4}	h^+h^-	
β	I	$B^0_d\to J/\Psi K^0_S$	$B\to l^{\pm}$	5.7×10^{-6}	6.8×10^{4}	l^+l^-	Time/Tag
		$B^0_d\to J/\Psi K^0_S$	$B\to K^{\pm}$	2.3×10^{-5}	2.8×10^{5}	l^+l^-	
	I	$B^0_d\to D^+D^-$	$B\to l^{\pm}$	2.3×10^{-6}	2.8×10^{4}	$l^{\pm}$	Time/Tag
"γ"	I	$B^0_s\to\rho K^0_S$	$B\to l^{\pm}$	1.1×10^{-7}	5.0×10^{2}	$l^{\pm}$	Time/Tag
	I	$B^0_s\to D^+_s D^-_s$	$B\to l^{\pm}$	1.4×10^{-5}	6.4×10^{4}	$l^{\pm}$	Time/Tag
	II	$B^0_s\to D^+_s K^-$	$B\to l^{\pm}$	3.2×10^{-6}	1.4×10^{4}	$l^{\pm}$	Time/Tag
		$\bar{B}^0_s\to D^+_s K^-$	$B\to l^{\pm}$	2.3×10^{-6}	1.0×10^{4}	$l^{\pm}$	
	III	$B^0_d\to\bar{D}^0K^{0*}$	self	2.7×10^{-5}	3.2×10^{5}	$l^{\pm}$	
		$B^0_d\to D^0K^{0*}$		2.7×10^{-6}	3.2×10^{4}		
		$B^0_d\to D^0_1K^{0*}$		0.6×10^{-6}	0.6×10^{3}		
	III	$B^+\to\bar{D}^0K^+$	self	5.5×10^{-6}	3.8×10^{5}	$l^{\pm}$	
		$B^+\to D^0K^+$		5.5×10^{-7}	5.1×10^{3}		
		$B^+\to D^0_1K^+$		1.2×10^{-7}	1.4×10^{3}		
	I	$B^0_d\to\Psi\rho^0$	$B\to l^{\pm}$	1.2×10^{-6}	5.4×10^{3}	l^+l^-	Time/Tag
		$B^0_d\to\Psi\rho^0$	$B\to K^{\pm}$	5.2×10^{-6}	2.3×10^{4}	l^+l^-	
	I	$B^0_s\to\Psi\phi$	$B\to l^{\pm}$	2.6×10^{-5}	1.2×10^{5}	l^+l^-	Time/Tag
		$B^0_s\to\Psi\phi$	$B\to K^{\pm}$	1.0×10^{-4}	4.7×10^{5}	l^+l^-	

The branching ratios of Table 5 are composite branching ratios for the required B decay configuration. They include branching ratios for all secondary decays such as K^0_S->$\pi\pi$, J/Ψ->$\mu\mu$, ϕ->K^+K^- required to produce an experimentally detectable final state. The composite branching ratio also contains the branching ratios for the tagging and trigger decays of the "other" B where required. For B->D decay composite branching ratios of Table 5, we have used only the experimentally accessible D modes into all charged decay products given in Table 6 in our determination of the yields of B decays suitable for CP violation measurements. These all charged decays result in 2, 3, 4 or 5 charged particles in the final state in a variety of topologies (one prong, two prong and three prong vertices in one or two vertex topologies with the incoming neutral or charged B sometimes observed in the SFT live target). The geometric acceptances of each of the modes in Table 5 that have a $D^{\pm}$ or D^0 in the final state have been determined from a Monte Carlo which includes the 3 and 5 body final states or the 2 and 4 body for the charged D's and neutral D mesons respectively, properly weighted with the BR's for the individual channels. In the final yield calculations, the tracking, particle ID and vertexing efficiencies for the D's are also included using the weighted average of the product of these factors for the various modes taking into account the various vertex topologies of the modes.

Table 6
Major All Charged $D^{\pm}_d$, D^0, D^0_{CP}, $D^{\pm}_s$ Decay Modes

D Meson	Mode	BR	Total
$D^{\pm}_d$	$K^{\pm}\pi^+\pi^-$	9.6×10^{-2}	10.5×10^{-2}
	$K^{\pm}\pi^+\pi^-\pi^+\pi^-$	6.1×10^{-3}	
	$\pi^+\pi^-\pi^{\pm}$	2.8×10^{-3}	
$D^{\pm}_s$	$K^+K^-\pi^{\pm}$	3.9×10^{-2}	6.7×10^{-2}
	$\pi^+\pi^-\pi^{\pm}$	1.2×10^{-2}	
	$K^+K^-\pi^+\pi^-\pi^{\pm}$	1.4×10^{-2}	
	$\pi^{\pm}\pi^+\pi^-\pi^+\pi^-$	0.2×10^{-2}	
	$K^{\pm}\pi^+\pi^-$	1.4×10^{-3}	
D^0_d	$K^-\pi^+$	3.7×10^{-2}	12.8×10^{-2}
	$K^-\pi^+\pi^-\pi^+$	7.5×10^{-2}	
	K^+K^-	4.1×10^{-3}	
	$K^+K^-\pi^+\pi^-$	2.4×10^{-3}	
	$\pi^+\pi^-$	1.6×10^{-3}	
	$\pi^+\pi^-\pi^+\pi^-$	7.5×10^{-3}	
	$\pi^+\pi^-\pi^+\pi^-\pi^+\pi^-$	4.0×10^{-4}	
D^0_{CP}	$\pi^+\pi^-$	1.6×10^{-3}	5.6×10^{-3}
	K^+K^-	4.1×10^{-3}	

4. Triggering in a B Fixed Target Environment

The flexible three level triggering strategy adopted for the SFT detector is based on detection of high p_t leptons and hadrons. To reduce the Level I 10^7 interaction/sec rate to a level sufficient for a second level trigger ($\approx10^4$ /sec), we plan to adopt a strategy similar to

the one successfully employed for muon triggers in Fermilab Experiment E771 to both hadrons and leptons in the SFT. The SFT triggers will impose at level I both p_t and momentum requirements on hadrons and leptons within the angular range 2 mrad to 75 mrad as given below:

• opposite charge dilepton trigger
max. p_t lepton >1.0 GeV/c, min. p_t lepton>0.5 GeV/c
Plepton >20 GeV/c

• opposite charge dihadron trigger
max. p_t >3.0 GeV/c, min. p_t >1.0 GeV/c

• lepton -hadron trigger
p_t lepton >1.5 GeV/c, p_t hadron >1.0 GeV/c
Plepton >20 GeV/c

This ensemble of triggers allows us to trigger on semileptonic and kaon decays from tagging B decays or on the various CP decay topologies of interest (B^0_d->$\pi^+\pi^-$, B^0_d->$J/\Psi K^0_S$, $B^{\pm}$->$D^0K^{\pm}$, B^0_S->D^0K^{*0}, etc.).

Level I

The Level I p_t requirement is imposed by forming coincidences of collections of pads in several planes of wire chambers which encompass all possible trajectories of tracks above a given p_t threshold. The lepton ID for the high p_t μ or e are imposed on this tracking trigger at Level I by requiring an additional coincidence to be satisfied by a signal from the region of the muon detector or electromagnetic calorimeter which is pointed at by the high p_t charged particle trajectory formed by the pad coincidences. In the case of the RICH/TRD, as discussed below, the requirement of the particle ID is imposed at Level II because of the additional complications of extracting information from the RICH. Any particle not receiving a e or μ ID at level I is considered to be a hadron. The minimum momentum requirement for muons is imposed by the thickness of the muon detector. The minimum momentum requirement for the $e^{\pm}$ is set by imposing a threshold on the electromagnetic detector elements indicated by the high p_t track trajectory. This trigger, which can be implemented with Programmable Logic Array chips, will require approximately 150 ns to form, similar to the high p_t muon trigger of E771. A latency period of approximately 1 μsec will be required to collect all signals necessary for this trigger from the spectrometer.

The dielectron, dimuon, dihadron and hadron lepton triggers have inefficiencies due to the various detector components required to form them. Intrinsic to each of these triggers is the tracking trigger formed using the pad chamber signals. In order to minimize pad chamber inefficiencies, five planes of pad chambers will be used and each plane signal will be formed from the OR of signals from a double gas gap. To form the pad coincidence which defines the track, any three out of five will be required. This should effectively

eliminate inefficiencies at this stage of the tracking trigger. We expect to achieve better than 98% efficiency for each track pair with this system.

A second component of the inefficiency will be present due to in efficiency in track ID for the electron and the muon. We will identify the muon using Resistive Plate Chambers (RPC's) similar to those used in E771. Requiring any three of five chambers to define a muon, we expect to achieve efficiencies better than 99% per muon. The situation with electrons may be worse since the electron is tagged by a coincidence of the TRD and the EM calorimeter. To be conservative, we assume this can be formed with greater than 95% efficiency per electron or 90% per electron pair. Overall, we estimate the detector efficiencies for the single electron, single muon, dihadron, dielectron, dimuon, electron hadron and muon hadron triggers to be 95%, 99%, 98%, 90%, 98%, 94% and 98% respectively.

The major contributions to the muon and electron trigger rates are due to π,K semimuonic decays, hadron punch through and charm meson decay in the case of the muon trigger and π^0 photon conversions in the case of the electron trigger. The major contributors to the dihadron trigger rates are direct production of charged hadrons in the primary interaction and charm meson decays into charged kaons. The p_t cut eliminates much of the π,K->μ decay triggers for the muon trigger and a substantial fraction of the π^0->$\gamma\gamma$->e^+e^- conversion triggers for the electrons. The μ,e triggers due to punch through hadrons in the case of the muon trigger and conversion electrons from π^0 photons in the case of the electron trigger are further reduced by the 20 GeV/c minimum momentum cut on the electron and muon candidates in Level I

The SFT trigger rate has been estimated using PYTHIA simulations for minimum bias and charm production. The retention of B signals for the modes of interest have also been estimated using PYTHIA. The trigger rates for each Level I trigger are summarized in Tables 7.

Table 7
Level I Interaction Rate Suppressions of Trigger Backgrounds

Trigger Type (p_t max, p_t min)	Level I π,K->μ,e Suppression	Level I γ->e$\pm$ Suppression	Level I Charm->μ,e Suppression
High P_t $\mu^{\pm}$ (1.5)	4.4×10^{-4}	-	2.1×10^{-5}
High P_t $e^{\pm}$ (1.5)	-	1.6×10^{-3}	2.1×10^{-5}
e^+e^- (1.0,0.5)	-	7.6×10^{-4}	8.8×10^{-7}
$\mu^+\mu^-$ (1.0,0.5)	8.4×10^{-5}	-	2.1×10^{-6}
h^+h^- (3.0,1.0)	1.0×10^{-3}	-	6.6×10^{-5}
μ-hadron (1.5,1.0)	2.5×10^{-4}	-	2.7×10^{-7}
e-hadron (1.5,1.0)	-	9.7×10^{-4}	2.7×10^{-7}
Total Suppression	3.1×10^{-3}		

We estimate that we can achieve at Level I an overall suppression of 5×10^{-3} taking into account the finite p_t resolution for p_t cuts required by the various triggers. This would result in 50 KHz of triggers passed on to Level II for further filtering.

For those events triggered on decay products from the B_{CP} decays themselves, both lepton and kaon tagging using the other B decay are possible. For those events in which the other B decay provides the trigger, only the given decay product (high p_t lepton or kaon) is normally available for tagging purposes. This will be further discussed in the tagging section.

SFT Level II

As discussed above, the various level I SFT triggers result in a composite Level I trigger rate of approximately 5×10^4 triggers per second. An additional level of triggering is required to reduce the trigger rate to the goal of $<10^4$ events per second feeding Level III. This additional global trigger rejection of a factor of ≥ 5 for all modes can be provided by a relatively loose requirement for presence of secondary vertices in the silicon detector.

The Level II trigger is based on use of associative memories for fast tracking in the silicon detector. Associative memories are inverse memories that can be programmed with all possible valid track trajectories. When hit information from the silicon detector is provided to the associative memories, the data patterns are compared with the stored configurations. Providing there are matches between data hit patterns and valid track possibilities, the associative memories return the location of the correspondence which can be used as an index for track slopes and intercepts. Once tracks are reconstructed in this manner, a post associative memory processor will process the tracks, evaluating a function of the impact parameters which indicates the likelihood of the presence of secondary vertices in the event. Using this algorithm, Monte Carlos estimates indicate that the required factor of ten suppression of trigger rate can be achieved with a B retention of 90%. Thus, we expect a trigger rate of 5000 triggers/second surviving Level II.

SFT Level III

Level III of the SFT data acquisition system is provided by an online farm of relatively modest proportions, not markedly larger than those already in operation or proposed for the Fermilab fixed target program. We expect to be able to easily achieve a reduction of a factor of five for events selected for offline analysis by this farm. Finally, we estimate that composite SFT trigger and data acquisition system would have less that 10% dead time and pass approximately 1000 20 KByte events/second to storage at 10^7 interactions per second. Therefore, a relatively modest data storage capacity is required for the SFT (<20 MBytes/second).

B Signal Retention

Level I, II, and III of the data acquisition system necessarily result in loss of B signal in the various decay modes. We have investigated the signal loss using PYTHIA and simulations of the SFT detector. Preliminary results for acceptances and trigger efficiencies and the trigger level retention factors are given in Table 8 for both CP decay products and the tagging particles if required.

Table 8
Level I Signal Retention for B_{CP} and "Other" Tagging B Decays

B Decay Topology	Accp. charged tracks	Eff_{trig} Level I	Eff_{trig} Level II	Overall Fraction A*Trig	Trigger/ Threshold GeV/c
$B->\mu^{\pm}$	0.82	0.45•0.99	0.81	0.30	High P_t μ (1.5)
$B->e^{\pm}$	0.82	0.45•0.95	0.81	0.28	High P_t e (1.5)
$B^0_d->\pi^+\pi^-$ • $B->l^{\pm},K^{\pm}$	0.55, 0.50	0.57•0.98	0.81	0.25,0.23	h^+h^- (3.0,1.0)
$B^0_d->\pi^+\pi^-$ • $B->l^{\pm}$	0.74	0.45•0.96	0.81	0.26	$\mu/e•h^{\pm}$ 1.5,1)
$B^0_d->a^+\pi^-$ • $B->l^{\pm}$	0.50	0.45•.96	0.81	0.22	$\mu/e•h^{\pm}$ 1.5,1)
$B^0_d->J/\Psi K^0_S$•$B->l^{\pm},K^{\pm}$	0.30 , 0.25	0.91•0.97	0.81	0.21,0.19	l^+l^- (1,.5)
$B^0_d->D^+D^-$ • $B->l^{\pm}$	0.40	0.45•.96	0.81	0.17	$\mu/e•h^{\pm}$ 1.5,1)
$B^0_S->\rho K^0_S$ • $B->l^{\pm}$	0.28	0.45•0.96	0.81	0.10	$\mu/e•h^{\pm}$ (1.5,1)
$B^0_S->D^+_sD^-_s$• $B->l^{\pm}$	0.40	0.45•0.96	0.81	0.17	$\mu/e•h^{\pm}$ (1.5,1)
$B^0_S->D^+_sK^-$ • $B->l^{\pm}$	0.50	0.45•0.96	0.81	0.22	$\mu/e•h^{\pm}$ (1.5,1)
$B^+->D^0K^+$ • $B->l^{\pm}$	0.50	0.45•0.96	0.81	0.17	$\mu/e•h^{\pm}$ (1.5,1)
$B^0_d->J/\Psi\rho$ •$B->l^{\pm},K^{\pm}$	0.56,.51	0.91•0.97	0.81	0.40,0.36	l^+l^- (1,.5)
$B^0_d->J/\Psi\phi$ •$B->l^{\pm},K^{\pm}$	0.60,.51	0.91•0.97	0.81	0.43,0.36	l^+l^- (1,.5)

The acceptance factors in Table 8 include all the charged decay products of the B_{CP} and $B_{trig/tag}$. For some triggers, both lepton and kaon tagging are used. In these cases the first number in the acceptance column is for lepton tagging and the second number for kaon tagging. The second factor in the Eff_{trig} is the efficiency due to detector inefficiencies. Global second level trigger time live time. If the lepton from the other B decay provide the trigger, then pions from the B decays are not required to have Θ>2mrad.

5. Yields of Reconstructed/Tagged Events

All the acceptance and efficiency factors contributing to the yield of reconstructed and tagged events in the SFT are collected and the expected numbers of events in potentially interesting modes have been summarized in Table 9 below. All branching ratios for the various interesting B decay configurations have been included in the estimates of the numbers of B_{CP} decays produced per year in the SFT. The estimates include the branching ratios for the tagging and triggering particles as well as for the CP decay and the decays of secondary D's, K^0_S, ϕ, etc..

The acceptances listed in Table 9 are the overall acceptances for every component of the B event that must be reconstructed in order for the event to be useful in the extraction of a particular angle of the unitarity triangle. For example, for B decays where triggering or tagging is required, the acceptance of the triggering or tagging particle are included in the acceptance.

The efficiency estimates in Table 8 include estimates of ε_{trig}, ε_{tag} and ε_{CP}. ε_{trig}, the trigger efficiency, includes both the effect of trigger settings such as minimum p_t and p of the triggering tracks as well as the estimated efficiency of the detector components which generate the trigger. In addition, the trigger efficiency includes a factor of 0.9 to account

for a live time goal of 90%. ε_{tag} is the efficiency for tagging the event. This quantity does not contain branching ratios or acceptances but reflects only the efficiency with which the process of tagging the event can be accomplished. This process requires several steps which vary from mode to mode but generally includes some particle ID for the tagging particle, the reconstruction efficiency for the tagging particles, the vertex association efficiency among other factors. Similarly, the ε_{CP} factor contains no branching ratios or acceptances. It only reflects the efficiency with the charged decay products of the BCP decay can be reconstructed and form a vertex distinguishable from other vertices in the event. The product of the three efficiency factors is the efficiency for triggering on, reconstructing and tagging a particular $B_{CP} \cdot B_{tag}$ event topology for events where the necessary decay products of both B's are in the acceptance of the spectrometer. N_{recon}, the final entry in Table 8, is the total number of accepted, triggered, tagged and reconstructed B events of each given topology which are available for use in either time independent or dependent extraction of the angles α, β and γ of the unitarity triangle.

Finally, the various event samples which are tagged with both a lepton or a kaon must be corrected for overlaps between the two kinds of tags. The sum of the two tagged samples is greater than the actual number of K or lepton tagged events because of the events which contain both a lepton and a K from the decay of the other B. Kaons are present in 85% and leptons in 21% of the B decays. If we make the assumption that the tags completely overlap, then every B->l decay will also have a kaon tag if we ignoring losses of either K's or leptons due to inefficiencies. With this assumption, we can have no more than the number of kaon tagged events as the total number of tagged decays and the lepton tag does little except corroborate the kaon tag. The opposite assumption would be that they are maximally uncorrelated would lead to 100% of the events tagged by one or the other with a 7% overlap. We adopt the average position that there is a 15% overlap. Therefore, a total of 85% +6% =91% of the sum of the kaon and lepton tag samples will have one or the other or both types of tags.

In addition, a correction must be made, in the case of the event topologies such as $B->\pi\pi$ which are collected by two different triggers to account for events which satisfy both triggers. If we assume the two triggers are completely independent, then the number of dipion triggers will also have a lepton trigger = 0.74•0.38 = 0.30. This fraction must be subtracted from the dipion trigger sample (after correcting for tag overlaps), and the resulting number of events uniquely triggered by the dipion must be added to the lepton trigger sample to get the true number of dipion events obtained from the sum of both triggers. The number of events after corrections for both trigger and tag overlaps is shown in the column listed as $N_{corr.}$

Table 9
Reconstructed/Tagged B Topologies in the SFT Per Year

B (CP • tag • trig)	Prod.	Accp	ε_{trig}	ε_{tag}	ε_{CP}	N_{recon}	N_{corr}
$B->\mu^{\pm}$	3.4×10^{9}	0.82	0.37	0.89	-	8.6×10^{8}	
$B->e^{\pm}$	3.3×10^{9}	0.82	0.34	0.82	-	6.9×0^{8}	-
$B->K^{\pm}$	2.7×10^{10}	0.82	-	0.77	-	1.7×10^{10}	
$B^0_d->\pi^+\pi^-$ • $B->l^{\pm}$ (tag)	2.5×10^{4}	0.55	0.45	0.85	0.73	3,900	
$B^0_d->\pi^+\pi^-$ • $B->K^{\pm}$(tag)	1.0×10^{5}	0.55	0.45	0.77	0.73	13900	15200
$B^0_d->\pi^+\pi^-$ • $B->l^{\pm}$(trig/tag)	2.5×10^{4}	0.74	0.36	0.85	0.73	4,200	
$B^0_d->a^+\pi^-$ • $B->l^{\pm}$(trig/tag)	3.8×10^{4}	0.50	0.37	0.85	0.60	3700	3700
$B^0_d->a^-\pi^+$ • $B->l^{\pm}$(trig/tag)	9.4×10^{3}	0.50	0.37	0.85	0.60	9200	9200
$B^0_d->J/\Psi K^0_S$ • $B->l^{\pm}$(tag)	6.8×10^{4}	0.30	0.70	0.85	0.66	8200	33000
$B^0_d->J/\Psi K^0_S$ • $B->K^{\pm}$(tag)	2.8×10^{5}	0.30	0.70	0.77	0.66	27400	
$B^0_d->D^+D^-$ • $B->l^{\pm}$(trig/tag)	2.8×10^{4}	0.40	0.37	0.85	0.35	1300	1300
$B^0_S->\rho K^0_S$ • $B->l^{\pm}$(trig/tag)	5.0×10^{2}	0.28	0.37	0.85	0.60	30	30
$B^0_S->D^+_sD^-_s$ • $B->l^{\pm}$(trig/tag)	6.4×10^{4}	0.40	0.37	0.85	0.35	2900	2900
$B^0_S->D^+_sK^-$ • $B->l^{\pm}$(trig/tag)	1.4×10^{4}	0.50	0.37	0.85	0.40	900	900
$\bar{B}^0_S->D^+_sK^-$ • $B->l^{\pm}$(trig/tag)	1.0×10^{4}	0.50	0.37	0.85	0.40	640	640
$B^0_d->\bar{D}^0_dK^{0*}$ • $B->l^{\pm}$(trig/tag)	3.2×10^{5}	0.45	0.37	0.85	0.38	17600	17600
$B^0_d->D^0K^{0*}$ • $B->l^{\pm}$(trig/tag)	3.2×10^{4}	0.45	0.37	0.85	0.38	1760	1760
$B^0_d->D^0_1K^{0*}$ • $B->l^{\pm}$(trig/tag)	0.6×10^{3}	0.45	0.37	0.85	0.42	370	370
$B^+->\bar{D}^0_dK^+$ • $B->l^{\pm}$(trig)	3.8×10^{5}	0.50	0.37	0.85	0.42	25800	25800
$B^+->D^0K^+$ • $B->l^{\pm}$(trig)	5.1×10^{3}	0.50	0.37	0.85	0.42	350	350
$B^+->D^0_1K^+$ • $B->l^{\pm}$(trig)	1.4×10^{3}	0.50	0.37	0.85	0.47	110	110
$B^0_d->\Psi\rho^0$ • $B->l^{\pm}$(tag)	5.4×10^{3}	0.56	0.70	0.85	0.60	1,100	4600
$B^0_d->\Psi\rho^0$ • $B->K^{\pm}$(tag)	2.3×10^{4}	0.51	0.70	0.77	0.60	3900	
$B^0_S->\Psi\phi$ • $B->l^{\pm}$(tag)	1.2×10^{5}	0.60	0.70	0.85	0.54	24000	94700
$B^0_S->\Psi\phi$ • $B->K^{\pm}$(tag)	4.7×10^{5}	0.55	0.70	0.77	0.54	80000	

6. Estimated Errors in α, β and 'γ' per year of SFT Operation

Collecting all the factors which contribute to the error in ϕ as given in equation (4), we have made estimates of the errors in α, β and 'γ' per year of SFT operation using several B-> CP eigenstate modes. These errors are preliminary and incorporate only a portion of the CP•tag topologies that can be used for measurements of CP violation in B decays in fixed target experiments. Therefore, they should be considered as upper limits on the errors that can be achieved in the determination of each angle. The results are given in Table 10 below.

Table 10
Expected Errors in α, β and 'γ' per Year of SFT Operation
From Time Dependent Measurements of BCP-> CP Eigenstates

∠	B (CP • tag • trig)	Prod.	Accp	ε_{tot}	N_{recon}	$1/d_{tot}$*	δsin2φ	δφ
α	B^0_d->$\pi^+\pi^-$ • B->$l^\pm$ (tag)	7.1×10^4	0.55	0.29	15200	3.71	0.030	0.9°
	B^0_d->$\pi^+\pi^-$•B->$K^\pm$(tag)	2.9×10^5	0.55	0.27				
	B^0_d->$\pi^+\pi^-$•B->$l^\pm$(trig/tag)	7.1×10^4	0.74	0.26				
β	B^0_d->J/ΨK^0_S•B->$l^\pm$(tag)	6.8×10^4	0.30	0.40	33000	3.80	0.021	0.6°
	B^0_d->J/ΨK^0_S•B->$K^\pm$(tag)	2.8×10^5	0.30	0.37				
	B^0_d->D^+D^-•B->$l^\pm$(trig/tag)	2.8×10^4	0.40	0.11	1300	3.33	0.097	2.8°
'γ'	B^0_S->ρK^0_S•B->$l^\pm$(trig/tag)	5.0×10^2	0.28	0.19	30	2.64	0.242	7.0°
	B^0_S->$D^+_S D^-_S$•B>$l^\pm$(trigtag)	6.4×10^4	0.40	0.11	2900	2.64	0.050	1.4°
	B^0_d->Ψρ^0•B->$l^\pm$(tag)	5.4×10^3	0.56	0.36	4600	3.00	0.045	1.3°
	B^0_d->Ψρ^0•B->$K^\pm$(tag)	2.3×10^4	0.50	0.34				
	B^0_S->Ψφ•B->$l^\pm$(tag)	1.2×10^5	0.60	0.33	94700	3.00	0.010	0.3°
	B^0_S->Ψφ•B->$K^\pm$(tag)	4.7×10^5	0.55	0.31				

*Weighted by the proportion of the μ, e and K tags

7. Summary

In conclusion, the fixed target method as demonstrated by the evaluation of the SFT live target/extracted beam configuration has potential as great as if not greater than the competing e^+e^- and collider configurations for precision measurements of CP violation and extraction of the angles of the unitarity triangle and, therefore, the phases of CKM matrix. Based on the $43.5M cost estimate of EOI-14[1] and the $117M and >$200M estimates for a forward collider[10] and e^+e^- options[11] respectively, the fixed target option appears to be the most economical method of performing measurements of CP violation.

8. References

[1] B. Cox et al, EOI-14, SSC Laboratory (May, 1990); G. Carboni et al, LHB Collaboration, INFN PI/AE91/04, (1991)
[2] Y.Lemoigne, GAJET Collaboration, Nucl. Instr. Meth. **A333**, 13(1993); J. Rosen EOI-13, SSC Laboratory (May, 1990).
[3] M. Kobayashi and T.Maskawa, Prog. Theor. Phys. 49, 652(1973).
[4] L. Wolfenstein, Phys. Rev. Lett. 51, 1945(1983).
[5] I. Bigi, UND-HEP-92-BIG01, (1992).
[6] R. Aleksan, I.Dunietz, B. Kayser and F. Le Diberder, Nuclear Physics B361, 141(1991).
[7] P.Nason, S. Dawson and R.K. Ellis, Nucl. Phys. B303, 607(1988).
[8] E.L. Berger and R. Ming, ANL-HEP-PR-92-11, (1992).
[9] S.N. Zhang et al, A High Pt Muon Trigger Processor, IEEE Transactions on Nuclear Science, **NS39**, No. 4, 814(1992).
[10] K. Foley et al., "Experiments, Detectors and Experimental Areas for the Super Collider", eds. R. Donaldson and M.G.D. Gilchriese, 701(1987).
[11] A Feasibility Study for Asymmetric B Factory Based on PEP, SLAC-353

PLANS FOR THE FERMILAB FIXED TARGET PROGRAM

K. Stanfield

Fermi National Accelerator Laboratory, FERMILAB
P.O.Box 500, Batavia IL 60510, (USA)

No written contribution received

PARTICIPANTS

Baldini R.	Laboratori Nazionali di Frascati, Italia	baldini@vaxlnf.lnf.infn.it
Barberis D.	Univ. di Genova, Italia	dario@vaxgea.ge.infn.it
Bellini G.	Univ. di Milano, Italia	vaxmi::bellini
Benhar O.	INFN – Sanità, Italia	vaxsan::benhar
Bertani M.	Laboratori Nazionali di Frascati, Italia	bertani@vaxlnf.lnf.infn.it
Bettoni D.	INFN – Ferrara, Italia	vaxfe::bettoni
Bianco S.	Laboratori Nazionali di Frascati, Italia	bianco@vaxlnf.lnf.infn.it
Bigongiari A.	CAEN, Viareggio, Italia	caen@vm.cnuce.cnr.it
Biino C.	INFN – Torino, Italia	vaxto::biino
Brons S.	Max–Planck–Inst. für Kernph., Germany	ste@vsnhd1.cern.ch
Campana P.	Laboratori Nazionali di Frascati, Italia	campana@vaxlnf.lnf.infn.it
Capitani G.P.	Laboratori Nazionali di Frascati, Italia	gpc@vaxlnf.lnf.infn.it
Ceradini F.	Univ. di Roma I "La Sapienza", Italia	vaxrom::ceradini
Cester R.	Univ. di Torino, Italia	vaxto::cester
Conetti S.	University of Virginia, USA	sergio@fnalv.fnal.gov
Cox B.	University of Virginia, USA	cox@fnalv.fnal.gov
Cremaldi L. M.	University of Mississippi, USA	cremaldi@fnalv.fnal.gov
Dameri M.	INFN – Genova, Italia	dameri@vaxgea.ge.infn.it
Dore U.	Univ. di Roma I, Italia	vaxrom::dore
Elia V.	Univ. di Lecce, Italia	valerio@lecce.infn.it
Fabbri F.L.	Laboratori Nazionali di Frascati, Italia	flf@vaxlnf.lnf.infn.it
Flaminio V.	INFN – Pisa, Italia	vaxpi::flaminio
Fridman A.	INFN – Trieste, Italia	fridman@cernvm.cern.ch
Gianini G.	Univ. di Pavia, Italia	vaxpv::gianini
Giomataris Y.	Lausanne University, Switzerland	ioa@cernvm.cern.ch
Gorini E.	Univ. di Lecce, Italia	vaxle::gorini
Grammatico A.	POL.HI.TECH., Carsoli (AQ), Italia	
Grancagnolo F.	Univ. di Lecce, Italia	vaxle::grancagnolo
Greco M.	Laboratori Nazionali di Frascati, Italia	greco@vaxlnf.lnf.infn.it
Introzzi G.	Univ. di Pavia, Italia	vaxpv::introzzi
Kaplan D. M.	Northern Illinois University, USA	kaplan@fnalv.fnal.gov

Lach J.	FERMILAB, Batavia , USA	lach@fnalv.fnal.gov
Leveraro F.	Univ. di Milano, Italia	vaxmi::leveraro
Liguori G.	Univ. di Pavia, Italia	vaxpv::liguori
Lusignoli M.	Univ. di Roma I, Italia	vaxrom::lusignoli
Mariotti C.	INFN – Sanità, Roma, Italia	vaxsan::mariotti
Martellotti G.	INFN – Roma I, Italia	40808::martellotti
Martinengo P.	Univ. di Genova, Italia	vaxge::martinen
McManus A.P.	Univ. of Virginia, USA	mcmanus@fnalv.fnal.gov
Meoni M.	POL.HI.TECH., Carsoli (AQ), Italia	
Meroni E.	Univ. di Genova, Italia	vaxmi::emeroni
Netchaeva P.	Univ. di Genova, Italia	vaxge::netchaeva
Orestano D.	Univ. di Roma I, Italia	
Osculati B.	Univ. di Genova, Italia	vaxge::osculati
Palestini S.	INFN – Torino, Italia	vaxto::palestini
Pallavicini M.	Univ. di Genova, Italia	vaxge::pallavicini
Panareo M.	Univ. di Lecce, Italia	vaxle::panareo
Pancheri G.	Laboratori Nazionali di Frascati, Italia	pancheri@vaxlnf.lnf.infn.it
Pastrone N.	INFN – Torino, Italia	vaxto::pastrone
Paver N.	Univ. di Trieste, Italia	38428::nello
Piccolo M.	Laboratori Nazionali di Frascati, Italia	mxp@vaxlnf.lnf.infn.it
Primavera M.	Univ. di Lecce, Italia	primavera@lecce.infn.it
Purohit M.V.	Princeton Univ. USA	puphep::purohit
Ratti S.P.	Univ. di Pavia e Sezione INFN, Italia	39275::ratti
Ridolfi G.	CERN, Switzerland	ridolfi@vxcern.cern.ch
Rossi L.	Univ. di Genova, Italia	vaxge::rossi
Sansoni A.	Laboratori Nazionali di Frascati, Italia	sansoni@vaxlnf.lnf.infn.it
Sarwar S.	Laboratori Nazionali di Frascati, Italia	sarwar@vaxlnf.lnf.infn.it
Satta L.	Univ. di Roma I, Italia	satta@vaxlnf.lnf.infn.it
Schubert K.R.	Univ.of Karlsruhe, Germany	bd13@dkauni2.bitnet
Smith R. P.	FERMILAB, USA	rpsmith@fnalv.fnal.gov
Stanfield K.	FERMILAB, USA	fnalv::michelle

Strolin P.	Univ. di Napoli, Italia	strolin@napoli.infn.it
Valente V.	Laboratori Nazionali di Frascati, Italia	valente@vaxlnf.lnf.infn.it
Verzocchi M.	INFN – Roma I, Italia	vaxrom::verzocchi
Viola L.	Univ. di Pavia, Italia	vaxpv::viola
Vitulo P.	Univ. di Pavia, Italia	vaxpv::vitulo
Vivaldi F.	CAEN, Viareggio (LU), Italia	caen@vm.cnuce.cnr.it
Votano L.	Laboratori Nazionali di Frascati, Italia	votano@vaxlnf.lnf.infn.it
Wah Yau W.	Univ. of Chicago, USA	uchep::wah
Wiss J.	Univ. of Illinois at Urbana (U–C), USA	uihep::jew
Zallo A.	Laboratori Nazionali di Frascati, Italia	zallo@vaxlnf.lnf.infn.it